Symmetry & Nonlinear Compensation in Fiber-Optic Transmissions

Haiqing Wei
Department of Electrical and Computer Engineering
McGill University, Montreal, Canada

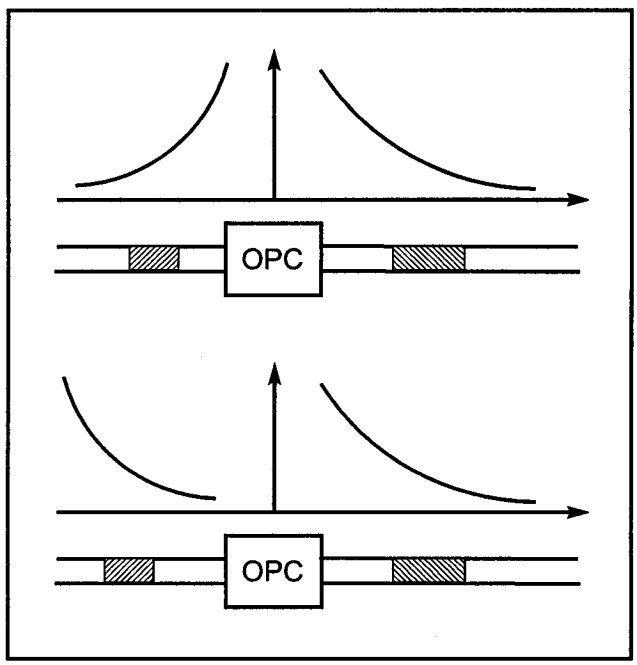

A thesis submitted to the
Faculty of Graduate Studies and Research
in partial fulfillment of the requirements for the degree of
Doctor of Philosophy

© Haiqing Wei 2006

Library and Archives Canada

Published Heritage Branch

395 Wellington Street
Ottawa ON K1A 0N4
Canada

Bibliothèque et Archives Canada

Direction du Patrimoine de l'édition

395, rue Wellington
Ottawa ON K1A 0N4
Canada

Your file Votre référence
ISBN: 978-0-494-27857-4
Our file Notre référence
ISBN: 978-0-494-27857-4

NOTICE:
The author has granted a non-exclusive license allowing Library and Archives Canada to reproduce, publish, archive, preserve, conserve, communicate to the public by telecommunication or on the Internet, loan, distribute and sell theses worldwide, for commercial or non-commercial purposes, in microform, paper, electronic and/or any other formats.

The author retains copyright ownership and moral rights in this thesis. Neither the thesis nor substantial extracts from it may be printed or otherwise reproduced without the author's permission.

AVIS:
L'auteur a accordé une licence non exclusive permettant à la Bibliothèque et Archives Canada de reproduire, publier, archiver, sauvegarder, conserver, transmettre au public par télécommunication ou par l'Internet, prêter, distribuer et vendre des thèses partout dans le monde, à des fins commerciales ou autres, sur support microforme, papier, électronique et/ou autres formats.

L'auteur conserve la propriété du droit d'auteur et des droits moraux qui protège cette thèse. Ni la thèse ni des extraits substantiels de celle-ci ne doivent être imprimés ou autrement reproduits sans son autorisation.

In compliance with the Canadian Privacy Act some supporting forms may have been removed from this thesis.

While these forms may be included in the document page count, their removal does not represent any loss of content from the thesis.

Conformément à la loi canadienne sur la protection de la vie privée, quelques formulaires secondaires ont été enlevés de cette thèse.

Bien que ces formulaires aient inclus dans la pagination, il n'y aura aucun contenu manquant.

Canada

Contents

Abstract iv

Résumé v

Acknowledgments vi

List of Acronyms viii

List of Figures xvi

1 Introduction and Statement of Originality 1

1.1 Introduction 1

1.2 Previous Methods for Suppressing Nonlinear Signal Distortions 3

1.3 Our Solutions and Similar Schemes of Others 5

1.4 Originality and Contributions 7

1.5 Outline of Thesis 9

2 Optical Fiber as Nonlinear Dispersive Channel 14

2.1 Amplifier Noise, Signal Power, and Transmission Distance 14

2.2 Fiber Nonlinearity and Nonlinear Impairments to Optical Signals . . 20

3 Fundamental Equations of Fiber Nonlinearity 24

4 Scaled Symmetries and Nonlinear Compensations 32

4.1 Dispersion and Nonlinear Compensations Using SMS 34

4.1.1 Theory of nonlinear compensation using OPC and SMS 36

4.1.2 A numerical example 38

4.2 Dispersion and Nonlinear Compensations Using STS 40

4.2.1 Basics of dispersive and nonlinear wave propagation in fibers . 40

4.2.2 Principles of dispersion compensation using OPC 43

4.2.3 Principles of nonlinear compensation using OPC and STS . . 44

4.3 Dispersion and Nonlinear Compensations w/o OPC 51

5 Advantages, Limitations, Other Technologies 57

5.1 Advantages and Limitations, Comparison to Other Technologies . . . 57

5.2 Polarization Effects and Vectorial Nonlinear Schrödinger Equations 61
5.3 Effectiveness of Nonlinear Compensations under Stochastic Polarization Variations 64

6 PRACTICAL NONLINEAR COMPENSATION USING STS 69
6.1 Optimal STS Setups of Fiber Transmission Lines 69
6.2 Practical Examples of STS Designs Using Commercial Fibers 75
6.3 Simulation Results and Discussions 78

7 PRACTICAL NONLINEAR SUPPRESSION WITHOUT OPC 91
7.1 Optimal STS Setups for Intra-channel Nonlinear Compensation . . . 91
7.2 Simulation Results and Discussions 96
7.3 Reversing intra-channel ghost-pulse generation by mid-way self-phase modulation 103

8 PRACTICAL IMPLEMENTATIONS: OPC, DCM, & MORE 111
8.1 Inter-channel Crosstalk in FWM-based Phase Conjugators 112
8.1.1 Mathematical analysis 113
8.1.2 Computer simulations 118
8.2 Optimal packaging of dispersion compensating fibers for matched nonlinear compensation and reduced optical noise 120
8.3 Linearity of nonlinear perturbations in fiber transmission lines and its applications to nonlinear compensations 129
8.3.1 Linearity of nonlinear perturbations and one-for-many nonlinear compensations 131
8.3.2 Simulation results and discussions 135

9 CONCLUSIONS AND PERSPECTIVES 143

A QUANTUM NOISE IN OPTICAL COMMUNICATIONS 147
A.1 Introductory Quantum Fiber Optics 147
A.2 Interaction with the Environment 151
A.3 A Classical Markovian Model 153
A.4 Applications and a Numerical Example 156

B FUNDAMENTALS OF NONLINEAR FIBER OPTICS 159

C FIBER PARAMETERS 168

REFERENCES 170

Abstract

This thesis presents methods and practical implementations for compensating or suppressing signal distortions induced by fiber nonlinearity in long-distance transmissions. Our methods take advantage of the availability and already wide deployment of dispersion-compensating fibers with various choices of dispersions and dispersion slopes. The basic principle behind the methods is to choose suitable fibers and to arrange them properly into transmission lines manifesting scaled symmetries. Based on the nonlinear Schrödinger equation which describes the nonlinear and dispersive signal propagation in optical fibers, we have shown analytically that a scaled symmetry renders the nonlinear signal distortion by the first part of a transmission line to be largely undone by the second part, when an optical phase conjugator is installed in the middle of the line. Without a phase conjugator, the most detrimental nonlinear interactions among pulses within a wavelength channel may be significantly suppressed in a scaled symmetric line. We have identified two types of scaled symmetries: mirror and translation. Although mirror-symmetric systems have been discussed by other authors before, our own proposals and designs using high-dispersion fibers in conjunction with distributive Raman or erbium-doped amplification could make practical transmission systems manifesting nearly perfect mirror symmetries in the scaled sense and hence excellent nonlinear compensations. Firstly noted and investigated thoroughly by us, the concept of scaled translation symmetries in transmission lines may well spur the adoption of nonlinear compensation methods in practical transmission systems, since distributive amplifiers are no longer necessary for translation symmetries. To support our mathematical analyses, extensive computer simulations have been carried out to validate the effectiveness of our proposed systems, most of which assume practical system setups and parameters and could therefore serve as paradigms for real system designs.

Résumé

Méthodes et réalisations pratiques pour compenser ou supprimer des déformations de signal induites par la non-linéarité de fibre dans les transmissions de longue distance sont présentés dans cette thèse. Nos méthodes se réalisent pour la disponibilité et le déploiement des fibres dispersion-compensatrices ayant une variété de dispersions et de pentes de dispersion. Le principe de base derrière ces méthodes est de choisir les fibres appropriées et de les arranger de manière exacte en lignes de transmission manifestant des symétries mesurées. Basé sur l'équation de Schrödinger non-linéaire qui décrit la propagation non-linéaire et dispersive de signal dans les fibres optiques, nous avons démontrée de manière analytique qu'une symétrie mesurée rend la déformation non-linéaire de signal de la première partie d'une ligne de transmission d'être annulé en grande partie par la deuxième partie, quand un conjugateur optique de phase est installé au centre de la ligne. Sans conjugateur de phase, les interactions non-linéaires les plus nuisibles parmi des impulsions dans un canal de longueur d'onde peuvent être sensiblement supprimées dans une ligne symétrique mesurée. Nous avons identifié deux types de symétries mesurées: miroir et traduction. Bien que des systèmes miroir-symétriques sont déjà discutés par différents auteurs, nos propositions et conceptions utilisant des fibres de haut dispersion en même temps que Raman distributif ou amplification dopée à l'erbium pourraient faire les systèmes pratiques de transmission manifestant des symétries de miroir presque parfaites dans le sens mesuré et par conséquence les excellentes compensations non-linéaires. Nous étions les premiers à observer et investiguer à fond le concept de symétries mesurées de traduction dans des lignes de transmission qui peut causer l'adoption des méthodes non-linéaires de compensation dans les systèmes pratiques de transmission, puisque les amplificateurs distributifs ne sont plus nécessaires pour des symétries de traduction. Pour prouver nos analyses mathématiques, des simulations extensives sur ordinateur ont été effectuées pour valider l'efficacité de nos systèmes proposés. Ces systèmes assument des installations et des paramètres pratiques de système et pourraient donc fonctionner comme paradigmes pour des conceptions de systèmes actuels.

ACKNOWLEDGMENTS

I am deeply indebted to my supervisor, Prof. David V. Plant, whose inspiration, guidance, support, and encouragement have been indispensable during the course of my Ph.D. study, and will surely continue to be so for a long time to come. When I started the study of nonlinear compensation, its possibility in realistic transmission systems using practically available components was not so clear; some of the concepts and techniques in my approach, especially nonlinear compensation using scaled translation symmetry, were not well-aligned with conventional wisdom and not immediately accepted by the fiber-optic community. Prof. Plant's trust in my methods and his continuous supports have been constant sources of energy fuelling my quest for a systematic theory and practically relevant means of nonlinear compensation. Nowadays, methods for compensating fiber nonlinearities, especially those using translation symmetries, are better understood and accepted, thanks to related works of other research groups, many of which are similar to and often independent of ours. I would like to thank members of my thesis advisory committee, Profs. Jose Azana, Lawrence Chen, and David V. Plant, who provided guidance in choosing the right topic, properly addressing the important questions, and nicely presenting the essential results. Many thanks go to members of the thesis examination committee, Profs. John Cartledge, Benoit Champagne, Lawrence Chen, Fabrice Labeau, and David V. Plant. The final revision of this thesis has benefited a great deal from their careful readings and constructive comments. Special thanks go to Ms. Carrie Serban for helping rendering the French abstract.

I would like to thank the faculties and general communities at Peking University (PKU) and McGill University, where I have acquired the necessary knowledge and training for pursuing scientific research and engineering development. I have enjoyed the intellectual stimulations and friendships of many great scholars and bright fellow students at the two prestigious institutions. The golden years at PKU and McGill will be treasured in my lifelong memory. In particular, I am deeply indebted to Prof. Rushan Han of PKU for bringing me to the door, and then the joy, of scientific research for the very first time, and Prof. Hong Guo of McGill for furthering my interest and strengthening my skills in theoretical and computational physics. I am grateful to Profs. Peter Grütter, Hong Guo, Mark Sutton, Louis Taillefer, Peter Russell, John C. Taylor, Peter E. Caines, Andrew G. Kirk, and David V. Plant, for

their illuminating courses in solid state physics, pure and applied mathematics, optics and photonics.

Thanks go to Gazillion Bits, Inc. and Allambda Technologies, Inc. for supporting my pursuit of continued graduate study while being employed as an R&D engineer.

List of Acronyms

ASE	amplified spontaneous emission
BER	bit-error rate
CDCF	conventional DCF
CDCM	conventional DCM
DCF	dispersion-compensating fiber
DCM	dispersion-compensating module
DGD	differential group delay
DLR	dispersion-to-loss ratio
DSF	dispersion-shifted fiber
DSP	digital signal processing
EDFA	erbium-doped fiber amplifier
FBG	fiber Bragg grating
FFT	fast Fourier transform
FWM	four-wave mixing
GVD	group-velocity dispersion
HD	high dispersion
IFWM	intra-channel four-wave mixing
IXPM	intra-channel cross-phase modulation
LP	linearly polarized
MFD	modal field diameter
NLSE	nonlinear Schrödinger equation
NOLM	nonlinear optical loop mirror
NZDSF	nonzero dispersion-shifted fiber
+NZDSF	positive NZDSF
-NZDSF	negative NZDSF
ODCF	optimized DCF
ODCM	optimized DCM
OOK	ON/OFF keying
OPC	optical phase conjugation
OSNR	optical signal-to-noise ratio
OTDM	optical time-division multiplexed(ing)

PDL	polarization-dependent loss
PGF	probability generating function
PM	polarization-maintaining
PMD	polarization mode dispersion
PSR	pump-power to signal-power ratio
PZD	point of zero dispersion
RDF	reverse dispersion fiber
RZ	return-to-zero
SBS	stimulated Brilliouin scattering
SMF	standard single-mode fiber
SMS	scaled mirror symmetry
SNR	signal-to-noise ratio
SPM	self-phase modulation
SRS	stimulated Raman scattering
STS	scaled translation symmetry
TF	transmission fiber
WDM	wavelength-division multiplexed(ing)
XPM	cross-phase modulation

List of Figures

2.1 The variation of $M(G-1)$ as M increases. 18

4.1 Two types of system configurations for nonlinear compensation with OPC: mirror-symmetric (top) and translation-symmetric (bottom). . 33
4.2 A mirror-symmetric transmission line using -NZDSF and DCF. 38
4.3 Received signals at the end of the simulated SMS link. Top: only the dispersion of the transmission fiber is pre-compensated by the HD fiber. Bottom: both dispersion and nonlinearity are pre-compensated. 39
4.4 The cascade of two fiber lines with opposite nonlinear coefficients but identical linear parameters of dispersion and loss/gain. DCG: dispersion compensation and gain. 46
4.5 The signal power and dispersion maps for a series of two fiber lines with opposite nonlinear coefficients but identical linear parameters of dispersion and loss/gain. 46
4.6 The functionality of a fictitious fiber with negative nonlinearities may be realized equivalently by a conventional fiber with positive nonlinearities with the help of OPC. 47
4.7 The signal power and dispersion maps for a cascade of two fiber spans in scaled translation symmetry with scaling ratio $R = 1$. Top: the variation of signal power along the propagation distance. Bottom: the dispersion map, namely, the variation of accumulated dispersion along the propagation distance. 52

5.1 Degree of parallelism between $\mathbf{E}_{\text{non}}$ and $\mathbf{E}_{\text{lin}}$ as θ varies. 67

6.1 A mirror-symmetric configuration of pairs of fiber spans in scaled translational symmetry, with the dispersion in each span compensated to zero. Top: schematic arrangement of fibers and amplifiers with respect to OPC. Middle: map of signal power $P(z)$ along the propagation distance z. Bottom: map of accumulated dispersion $b_2(z)$ along the propagation distance z. 73

6.2 A mirror-symmetric configuration of pairs of fiber spans in scaled translational symmetry, with non-zero residual dispersion in the spans. There are pre- and post-dispersion compensators (DCs), as well as a dispersion conditioner immediately after OPC. Top: schematic arrangement of fibers and amplifiers with respect to OPC. Middle: map of signal power $P(z)$ along the propagation distance z. Bottom: map of accumulated dispersion $b_2(z)$ along the propagation distance z. . . 74
6.3 A mirror-symmetric configuration of pairs of fiber spans in scaled translational symmetry, with non-zero residual dispersion in the spans. There are pre- and post-dispersion compensators (DCs) but no dispersion conditioner at the site of OPC. Top: schematic arrangement of fibers and amplifiers with respect to OPC. Middle: map of signal power $P(z)$ along the propagation distance z. Bottom: map of accumulated dispersion $b_2(z)$ along the propagation distance z. 75
6.4 A transmission line consisting of SMFs and slope-matching DCFs. . . 78
6.5 Received eye diagrams of the 2nd DEMUX channel using the setup of Fig. 6.4. Top: fiber nonlinearity is OFF, the signal is only impaired by amplifier noise. Bottom: fiber nonlinearity is ON, the signal distortion is only increased slightly. 79
6.6 Received eye diagrams of the 2nd DEMUX channel when the setup of Fig. 6.4 is modified, and the fiber nonlinearity is always ON. Top: fiber lengths of and input powers to the two types of spans are exactly the same. Bottom: all fiber spans are identical in length and input signal power as well as the ordering of fibers (SMF followed by DCF). 80
6.7 The Q value versus transmission distance in number of 180km spans for three system setups: squares - baseline system without fiber nonlinearity; circles - optimized system with STS and OPC; triangles - conventional system without STS and OPC. The solid horizontal line marks the level of $Q = 6$ for BER $\leq 10^{-9}$. 81
6.8 A transmission line consisting of +NZDSFs, -NZDSFs, and DCFs compensating the dispersion slope. 82
6.9 Received eye diagrams of the 2nd DEMUX channel using the setup of Fig. 6.8. Top: fiber nonlinearity is OFF, the signal is only impaired by amplifier noise. Bottom: fiber nonlinearity is ON, no extra penalty is visible. 83

6.10 Received eye diagrams of the 2nd DEMUX channel when all -NZDSFs are replaced by +NZDSFs in the setup of Fig. 6.8. Top: with OPC. Bottom: without OPC. 84
6.11 Scalability and cascadability of the nonlinearity-suppressed NZDSF transmission line in Fig. 6.8. Top: the number of circulations on each side of OPC is doubled to ten times and the signal power is increased by 3 dB. Bottom: two identical transmission lines as in Fig. 6.8 are in cascade all-optically and the signal power is increased by 3 dB. The eye diagrams are still of the 2nd DEMUX channel. 85
6.12 The Q value versus transmission distance in number of 200km spans for three system setups: squares - baseline system without fiber nonlinearity; circles - optimized system with STS and OPC; triangles - conventional system without STS and OPC. The solid horizontal line marks the level of $Q = 6$ for BER $\leq 10^{-9}$. 86
6.13 A transmission line consisting of ten fiber spans on each side of OPC, each span has 50 km DSF and a slope-compensating DCF. 87
6.14 Received eye diagrams of the 2nd DEMUX channel using the setup of Fig. 6.13. Top: fiber nonlinearity is OFF, the signal is only impaired by amplifier noise. Bottom: fiber nonlinearity is ON. 89
6.15 Received eye diagrams of the 2nd DEMUX channel when the setup of Fig. 6.13 is modified by setting $D = 0$ ps/nm/km for the DCFs while keeping the dispersion slope. Top: with OPC in the middle of the link. Bottom: when OPC is removed. 90

7.1 The signal power and dispersion maps for a cascade of two fiber spans in STS with lumped dispersion compensators. Top: the variation of signal power along the propagation distance. Bottom: the dispersion map, namely, the variation of accumulated dispersion along the propagation distance. 92
7.2 A transmission line consists of 6 pairs of fiber spans, with the first span in each pair having 50 km SMF followed by 50 km RDF then 16 dB EDFA gain, and the second span having 40 km RDF followed by 40 km SMF then 20 dB EDFA gain. 96
7.3 A transmission line consists of 6 pairs of fiber spans, with the first span in each pair having 50 km SMF followed by 50 km RDF then 16 dB EDFA gain, and the second span having 40 km SMF followed by 40 km RDF then 20 dB EDFA gain. 96

7.4 The transmission results of the 3rd DEMUX channel with $\delta D = 0$ and amplifier noise turned off to signify the nonlinear effects. Top: received optical eye diagram of the scaled translation-symmetric setup in Fig. 7.2. Bottom: received optical eye diagram of the setup in Fig. 7.3 without STS. 97
7.5 The transmission results of the 3rd DEMUX channel with $\delta D = 0$ and amplifier noise turned on. Top: received optical eye diagram of the scaled translation-symmetric setup in Fig. 7.2. Bottom: received optical eye diagram of the setup in Fig. 7.3 without STS. 98
7.6 The transmission results of the 3rd DEMUX channel with $\delta D = 0.2$ ps/nm/km and amplifier noise turned on. Top: received optical eye diagram of the scaled translation-symmetric setup in Fig. 7.2. Bottom: received optical eye diagram of the setup in Fig. 7.3 without STS. . . 99
7.7 The transmission results of the 3rd DEMUX channel with $\delta D = 0.6$ ps/nm/km and amplifier noise turned on. Top: received optical eye diagram of the scaled translation-symmetric setup in Fig. 7.2. Bottom: received optical eye diagram of the setup in Fig. 7.3 without STS. . . 100
7.8 A conventional system transmitting multiple NRZ-modulated WDM channels. 101
7.9 Received optical eye diagrams by the 9th channel of the system in Fig. 7.8. Top: after 2 recirculating loops; Bottom: after 3 recirculating loops. 101
7.10 A scaled translation-symmetric system transmitting multiple NRZ-modulated WDM channels. 102
7.11 Received optical eye diagrams by the 9th channel of the system in Fig. 7.10. Top: after 2 recirculating loops; Bottom: after 3 recirculating loops. 102
7.12 Received eye diagram by the 9th channel of 16 RZ-modulated channels after 6 recirculating loops. 103
7.13 Two transmission lines with channelized self-phase modulation in the middle. TSTL: scaled translation-symmetric transmission line. DSF: dispersion-shifted fiber for self-phase modulation. 106
7.14 Optical eye diagrams of the 3rd channel at the end of transmissions. Top: of a conventional design without STS. Middle: of a system with STS. Bottom: of a system with STS and mid-way SPM. 108

7.15 The Q value versus transmission distance in number of 180km spans for three system setups: squares - optimized system with STS and mid-way SPM; circles - translation-symmetric system without mid-way SPM; triangles - conventional system without STS nor mid-way SPM. The solid horizontal line marks the level of $Q = 6$ for BER $\leq 10^{-9}$. . 109

8.1 The simulation setup of FWM-based OPC. 116
8.2 The input 10Gb/s NRZ optical signal. 116
8.3 The phase-conjugated signals of channel 1, when it is 100 GHz away from the pump frequency. 117
8.4 The phase-conjugated signals of channel 1, when it is 200 GHz away from the pump frequency. 118
8.5 The phase-conjugated signals of channel 1, when it is 300 GHz away from the pump frequency. 119
8.6 Two portions of dispersion-compensating fiber packaged into a compact module or cabled into a transmission line, where the first portion may have an intentionally increased loss coefficient to form an STS with a transmission fiber, while the second portion could have the lowest possible loss coefficient and does not need to satisfy any scaling rule. . 121
8.7 The power map and M-type dispersion map over the transmission distance of two traditional fiber spans. 122
8.8 The power map and N-type dispersion map over the transmission distance of two matched fiber spans for an STS. 123
8.9 Three configurations of transmission lines with different dispersion maps and DCMs. Top: an M-type dispersion map using conventional DCMs; Middle: an N-type dispersion map using conventional DCMs; Bottom: an N-type dispersion map using optimized DCMs. Acronyms: CDCF - conventional DCF, ODCF - optimized DCF, CDCM_M - conventional DCM in an M-type dispersion map, CDCM_N - conventional DCM in an N-type dispersion map, ODCM - optimized DCM. 125
8.10 A test transmission system consisting of 6 recirculating loops with an M-type dispersion map on the left side, an optical phase conjugator in the middle, then on the right side another 6 loops identical to the ones on the left. Each recirculating loop consists of two identical spans of 100 km SMF followed by a CDCM_M, as shown on the top of Fig. 8.9. 126

8.11 A test transmission system consisting of 6 recirculating loops with an N-type dispersion map on the left side, an optical phase conjugator in the middle, then on the right side another 6 loops identical to the ones on the left. Each recirculating loop has 100 km SMF followed by a CDCM_N, then 100 km SMF followed by a 20dB EDFA, as shown in the middle of Fig. 8.9. 127
8.12 A test transmission system consisting of 6 recirculating loops with an optimized N-type dispersion map on the left side, an optical phase conjugator in the middle, then on the right side another 6 loops identical to the ones on the left. Each recirculating loop consists of 100 km SMF followed by an ODCM, then 100 km SMF followed by a 20dB EDFA, as shown at the bottom of Fig. 8.9. 127
8.13 Optical eye diagrams of the 3rd DEMUX channel at the end of transmissions. Top: of a conventional line with the M-type dispersion map. Middle: of a line with conventional DCMs in the N-type dispersion map. Bottom: of a system using optimized DCMs and STS. 128
8.14 A system in one-for-many STS between (RDF + SMF) and (SMF + RDF) spans with OPC in the middle. 134
8.15 Optical eye diagram of the 3rd DEMUX channel received at the end of the one-for-many scaled translation-symmetric system shown in Fig. 8.14. 134
8.16 A comparative system with no one-for-many STS but with OPC in the middle. 136
8.17 Optical eye diagrams of the 3rd DEMUX channel for the two comparative systems. Top: the system with OPC in the middle; Bottom: the system without OPC. 137
8.18 An optimized system using SMF+RDF and RDF+SMF spans configured into a one-for-many STS. 138
8.19 A comparative system using all SMF+RDF spans without one-for-many STS. 138
8.20 Optical eye diagrams of the 3rd channel at the mid-point of transmissions. Top: of the optimized system; Bottom: of the comparative system. 139
8.21 Optical eye diagrams of the 3rd channel at the end of transmissions. Top: of the optimized system; Bottom: of the comparative system. . 140
8.22 An optimized system with one-for-many STS and mid-way SPM. . . . 141

8.23 Optical eye diagram of the 3rd channel received at the end of the optimized system with one-for-many STS and mid-way SPM. 141
8.24 The Q value versus transmission distance in number of 320km spans for three system setups: squares - optimized system with one-for-many STS and mid-way SPM; circles - one-for-many translation-symmetric system without mid-way SPM; triangles - conventional system without STS nor mid-way SPM. The solid horizontal line marks the level of $Q = 6$ for BER $\leq 10^{-9}$. 142

A.1 A signal pulse interacting with an interaction center. 153
A.2 Probability distribution of the number of photons after 100km fiber transmission. 158

1

Introduction and Statement of Originality

1.1 Introduction

The capability of transmitting high-power optical signals over long-distances with little distortion is an essential element to the realization of high-capacity optical networks that are widely connected over long distances (thousands of kilometers) and switched in most places by all-optical means. However, group-velocity dispersion (GVD) and optical nonlinearity impose limits to the transmission distance, or more precisely, the product of data capacity and transmission distance [1, 2]. Coming from the material dispersion and the nonlinear dependence of waveguide propagation constant on the signal frequency, fiber GVD leads to different group-velocities for different frequency components of a signal pulse, and eventually pulse broadening and chirping [1]. The problem of GVD has basically been solved by the development of dispersion-compensating fibers (DCFs) with oppositely signed dispersions to offset the dispersion effects of transmission fibers over a wide frequency band. The most advanced DCFs are even capable of slope-matching compensation, namely, compensating the dispersion and the dispersion slope of the transmission fibers simultaneously [3, 4]. A fiber-optic transmission line is a nonlinear channel because of the nonlinear response of glass materials to signal electric fields, namely, the nonlinear dependence of the induced electric polarization to external excitations [5, 6]. In state-of-the-art transmission systems, single-mode fibers may carry tens even more wavelength channels, each wavelength carries $\geq$10 Gb/s worth of data with over mW optical power, and the signals may travel several thousands of kilometers in the fibers. The optical nonlinearity of fibers becomes significant with such long transmission distance at such high data rate. Indeed, fiber nonlinearity has become one of the major limiting

factors in practical transmission systems. Unlike the GVD effect, fiber nonlinearity is a much more difficult problem to overcome, because oppositely signed nonlinearity is not readily found in natural waveguide materials. That is, there exists no long waveguide with opposite nonlinearity to compensate that of a transmission fiber.

Fortunately, the use of optical phase conjugation (OPC) makes it possible for one fiber to compensate the dispersion as well as the nonlinearity of another transmission fiber [7, 8]. The basic principle is that OPC enables one fiber transmission line to propagate inversely (thus to restore) an optical signal that is dispersively and nonlinearly distorted by the other, when the two fiber lines are mirror-symmetric about the OPC. However, a strict mirror symmetry is rather difficult to realize in practice, as it requires opposite loss/gain coefficients for each pair of fiber segments in conjugation. In other words, it takes an unusual amplifying waveguide to compensate a conventional fiber with loss. Although amplifying fibers are obtainable through distributed Raman pumping [9] or distributed Er-doped fiber amplifiers (EDFAs) [10], the loss of pump power makes it difficult to maintain a constant gain over an extended fiber length. This difficulty may seriously undermine the effectiveness of nonlinearity compensation in mirror-symmetric systems. We have noted and emphasized the importance of scaled mirror symmetry (SMS), in particular, the significance and feasibility of scaling the dispersion slopes of fibers together with their dispersions, loss/gain and nonlinear coefficients [11, 12, 13]. We have shown analytically and verified with computer simulations that practical transmission systems using commercially available fibers may be arranged into nearly perfect mirror symmetries in the scaled sense and hence enjoy excellent nonlinear compensations.

A more interesting discovery made by us is that nonlinearity compensation is also possible in a transmission system manifesting a translation symmetry in the scaled sense [12, 13]. Better yet, we have demonstrated that scaled translation symmetry (STS) and OPC enable simultaneous compensations of fiber nonlinearities and dispersions up to the third-order in dispersion-managed fiber transmission lines employing slope-compensating fibers [14]. One great advantage of using STS is that a pair of conjugating fiber segments are required to have the same sign for the loss/gain coefficients, opposite second-order dispersions, and the same sign for the third-order

dispersions. Such conditions are naturally satisfied, at least approximately, in conventional fiber transmission systems, where, for example, a standard single-mode fiber (SMF) may be paired with a DCF as conjugating counterparts. Another discovery of ours is the capability of STS, as well as SMS, to suppress the intra-channel nonlinear effects even in the absence of OPC [15]. We are able to explain such suppression of intra-channel nonlinearities by a unified theory, which uses rather simple mathematical derivations and points to the heart of the physical mechanism.

1.2 *Previous Methods for Suppressing Nonlinear Signal Distortions*

It has been known for some time that the nonlinearity of one fiber line may be compensated by that of another with the help of OPC. However, previous demonstrations and proposals [8, 16, 17, 18, 19, 20] do or would perform unsatisfiably in suppressing fiber nonlinearities. They either are tailored to work on only one special aspect of the nonlinear effects, or fail to cope with the dispersion slope and even higher-order dispersion effects. In reference [8], it is proposed that OPC may be employed in the middle of a long transmission line, not only to compensate the fiber dispersion, but also to cancel the integrated self-phase modulation (SPM) in the transmission fibers on the two sides of OPC. Then reference [16], among others, demonstrates experimentally the compensation of dispersion and integrated SPM using OPC. However, signal distortions induced by fiber nonlinearities are distributive in nature, due to the interplay between the fiber dispersion and the Kerr (and Raman) nonlinearities. Compensating the integrated SPM merely removes the path-averaged nonlinear effects within a single wavelength channel, and the removal of such path-averaged nonlinearities represents a rather limited improvement. In reference [17], a lumped nonlinear compensator is proposed using a specially designed fiber consisting of many segments. The method achieves better suppression to the SPM impairments, but it fails to take account of the effect of higher-order dispersions, in particular the dispersion slope. Consequently, the method would not work with high-capacity wavelength-division multiplexing (WDM) systems. The proposed nonlinear compensator is an integrated device installed at either the transmission or the receiving end of a point-

to-point link, which has to be tailor-made for the specific transmission line. The result is a lack of flexibility: an installed nonlinear compensator may cease to work when the corresponding transmission line is altered; it may be prohibitively costly and labor-intensive to design and optimize a special nonlinear compensator for each transmission line. Moreover, an optical lumped nonlinear compensator may be difficult to fabricate, as it requires many fiber segments spliced together to approximate the distributive dispersions and nonlinearities in the transmission fibers. Ironically, due to the other uncooperative aspect of optical nonlinearity, it becomes a challenge to generate enough nonlinearities in a lumped nonlinear compensator using short segments of fibers. In accordance with the periodic power map in a transmission line, a lumped nonlinear compensator may need many optical amplifiers between its fiber segments, or the fiber segments have to be with changing dispersions or nonlinear coefficients. Neither condition is readily fulfilled with even today's technology. Indeed, it has only been possible to apply and test the proposal to transmission systems using dispersion-shifted fibers (DSFs), and still the method only compensates Kerr nonlinearities in the path-averaged sense [17, 18]. Reference [19] suggests to compensate the stimulated Raman scattering (SRS) effect using spectral inversion, *i.e.* OPC, which again, is a compensation method based upon path average. The distributive nature of fiber nonlinearity defies once more such scheme of path-averaged compensation. Indeed, the proposed method of SRS compensation is severely limited by the pulse walk-off under an asymmetric profile of signal power about the spectral inverter [21]. Finally, the experimental demonstration reported in [20] represents the state-of-the-art of nonlinearity compensation using mirror symmetries. The experiment tries to make a fiber line symmetric about the point of OPC. In particular, it uses backward Raman pumping to approximate a symmetric power map. The paper reported evidences of suppressed four-wave mixing (FWM), SPM, and cross-phase modulation (XPM) individually, only within a narrow system bandwidth. However, the Raman pumped fibers are the same as the transmission fibers, which are often too long for the Raman pump power to stay at a useful level so to maintain a constant gain. In other words, it is difficult to achieve a symmetric power map by Raman-pumping transmission fibers. Furthermore, higher-order dispersions are

not compensated by OPC, which could turn into a significant limitation in systems with wider bandwidths. Originally unnoticed by us, but brought into our attention by a manuscript reviewer during the process of our work being published, Marhic *et al.* in reference [22] noted that two fibers having opposite dispersions and with OPC in the middle may compensate each other's Kerr nonlinear effects. That may be the first attempt of nonlinear compensation using OPC and fibers with opposite dispersions that does not require mirror-symmetric power maps. However, Marhic *et al.*'s analysis was restricted to FWM and XPM in two fiber spans with OPC in the middle, and overlooked the effect of dispersion-slope as well as the importance of scaling fiber dispersions and nonlinearities. Their proposal did not address the practical question of how to optimally design a multi-span transmission line for best nonlinear compensations. Furthermore, the assumed pairs of fibers with the same loss and nonlinear coefficients but exactly opposite dispersions are not commonly found in practical transmission systems.

1.3 Our Solutions and Similar Schemes of Others

To overcome the difficulties that have plagued previous schemes, we have proposed methods of nonlinear compensations using scaled symmetries [11, 12, 13, 14, 15]. Basically, our methods suggest to use recently available specialty fibers with high dispersion (HD) values such that a shorter piece of specialty fiber may compensate a long transmission fiber. The dispersion, dispersion slope or higher order-dispersions of the specialty fiber are set in proportion to those of the transmission fiber, and for a mirror symmetry in the scaled sense the specialty fiber may be erbium-doped or Raman pumped to have a gain coefficient proportional to the loss of the transmission fiber. We have shown both analytically and through computer simulations that in the presence of OPC and SMS, an HD fiber could reverse the dispersive and nonlinear signal propagation in a transmission fiber and vice versa. A distinctive feature of our proposals is that the mathematical derivations are always made as general as possible, while the physical implementations are restricted to using fiber components and technologies that are either already commercially available, practically installed, or at least becoming available soon, namely, the proposed implementations are kept

as close as possible to practice.

Along the same line of thought, we have researched and discovered the possibility of nonlinear compensations using OPC in a transmission system manifesting a translation symmetry in the scaled sense [12, 13, 14], which no longer requires an amplifying fiber as conjugate to each lossy transmission fiber. One advantage of using STS is to eliminate the necessity of distributive amplification, so that the methods of nonlinear compensations are directly applicable to conventional transmission systems consisting of transmission fibers and DCFs. We have also discovered the capability of STS, as well as SMS, to suppress the nonlinear effects due to the overlap of dispersed pulses within a single wavelength channel, even in the absence of OPC [15]. Independent of and no earlier than our investigations, Kaewplung *et al.* proposed an OPC-based method for simultaneous suppression of dispersion-slope and sideband instability induced by Kerr nonlinearity in single-channel transmissions [23]. Their proposal considered transmission systems using SMFs and the so-called reverse dispersion fibers (RDFs) whose dispersion value is approximately -17 ps/nm/km at 1550 nm (close to the exact opposite of that of the SMFs), and suggested using two types of spans with SMFs and RDFs differently ordered on the two sides of OPC respectively. In a theoretical analysis [24] and an experimental demonstration [25], Chowdhury *et al.* studied the suppression of intra-channel nonlinearities using OPC in the middle of conventionally configured transmission systems in the so-called pseudo-linear regime. In the direction of compensating intra-channel nonlinearities without OPC, Striegler and Schmauss discussed a "symmetric fiber link" consisting of two types of fiber spans using SMFs and RDFs, one type having an SMF followed by an RDF while the other having an RDF before an SMF [26]. They also proposed a method of fiber-based compensation of timing jitter due to intra-channel XPM, using an extra DCF module and a fiber Bragg grating (FBG) [26, 27]. All references [23, 24, 25, 26, 27] noted the possibility of reducing nonlinear penalties even in systems without a mirror-symmetric power map, using either what is dubbed "symmetric dispersion maps", or OPC in the middle, or both. However, none of these contributions has achieved sufficient generality and obtained the optimal while practical parameter settings for best nonlinear compensations in their discussed systems.

The discussion in reference [23] was limited to a single-channel system, considered only the suppression of sideband instability as an intra-channel nonlinear effect, and did not recognize the importance of scaling the nonlinearity (especially the signal power) in different fibers. References [24, 25] did not configure the transmission systems according to and then take advantage of the STS to improve the performance of OPC-based nonlinear compensations. References [26, 27] too, failed to configure the transmission systems in compliance with the scaling rules for an STS to the fullest extent. In particular, the signal power in fibers is not carefully adjusted according to the scaling rules. The suppression of intra-channel nonlinearities is not optimal as a consequence. Indeed, the sub-optimality of the system configuration may be responsible for the finding that the condition for best compensation of amplitude jitter differs from that for optimal compensation of timing jitter [26]. Also without using OPC, there have been proposals for suppressing amplitude and timing jitters due to intra-channel nonlinearities in Raman-pumped transmission lines manifesting a lossless or mirror-symmetric map of signal power [28, 29]. However, the loss of pump power makes it difficult to maintain a constant gain in a long transmission fiber, and the significant deviation of signal power map from a desired mirror-symmetric profile degrades the result of intra-channel nonlinear compensations [30].

1.4 *Originality and Contributions*

As mentioned in the introduction section, this thesis concerns problems of nonlinear signal propagation in fiber-optic transmission lines and methods of compensating nonlinear distortions to optical signals so to increase the transmission distance or system capacity. Listed below are some of the published and to be published contributions as results of this thesis research.

1) Ref. [13] carefully re-derived the nonlinear Schrödinger equation (NLSE) from the first principles, retaining the mathematical exactitude down to details; justified each approximation and discussed the scope of its applicability;

2) Refs. [11, 12, 13] proposed methods of compensating fiber nonlinearities using OPC and scaled mirror-symmetric configurations of fiber transmission lines; tested the methods using computer simulations for systems using negative nonzero dispersion-

shifted fibers (NZDSFs) and DCFs with high negative dispersions;

3) Ref. [14] proposed methods of compensating fiber nonlinearities using OPC and scaled translation-symmetric configurations of fiber transmission lines; tested the methods using computer simulations for several practical systems using deployed or commercially available transmission fibers and DCFs;

4) Ref. [15] proposed and computer-simulated methods of compensating nonlinear distortions to signals within a single wavelength channel by using STS without OPC;

5) Ref. [31] proposed and tested methods of using mid-way SPM to suppress the generation of "ghost pulses" in scaled symmetric systems without OPC, where ghost pulses are generated through intra-channel nonlinear interactions that are not suppressed by scaled symmetries;

6) Ref. [32] proposed and tested methods of packaging DCFs to optimally compensate the nonlinear effects of transmission fibers and to minimize the signal loss at the same time (such method should be well suited for translation-symmetric systems using lumped dispersion-compensating modules (DCMs), with or without OPC);

7) Generalized the methods of nonlinearity compensation using scaled symmetries to "one-for-many" configurations, where a transmission line may consist of two (or more) types of fiber spans, one type has stronger nonlinearity and the other weaker, each span of stronger nonlinearity compensates multiple spans of weaker nonlinearity; an article on such generalization has been submitted for journal publication [33];

8) Analyzed the effect of random fiber birefringence on the effectiveness of nonlinear compensations using a method of orthogonal projection of nonlinearly generated fields onto the Jones vectors of unperturbed signal fields; our analysis confirms the effectiveness of distributed nonlinear compensations under stochastic polarization variations in practical transmission lines using non-polarization-maintaining (non-PM) fibers, so long as the time spread due to polarization mode dispersion (PMD) is kept small comparing to the width of signal pulses; a short paper on such method of orthogonal projection and applications is in preparation for journal publication [34].

1.5 Outline of Thesis

The main body of this thesis is organized into three parts. Part I, Motivation and Preparation: The Physics and Mathematics of Fiber Nonlinearity, discusses the basic physics and mathematical formulations of fiber nonlinearity. Part II. Theory: Scaled Symmetries and Nonlinear Compensations, presents theoretical derivations for nonlinear compensations using mirror and translation symmetries in the scaled sense. Part III, Practice: Applications, Implementations, and Verifications, describes practical implementations of scaled symmetric transmission systems for nonlinear compensations, verifies the system implementations by numerical simulations, and discusses practical realizations of optical phase conjugators as well as optimal packaging of DCMs.

Part I consists of Chapters 2 and 3. Chapter 2 discusses the basic physics of fiber nonlinearity and its manifestations, and explains from an engineering point of view how optical nonlinearity in fibers could become a limiting factor to the design and performance of transmission systems. Chapter 3 derives the NLSE from the first principles, namely, from the Maxwell equations and the material responses to electromagnetic excitations. The NLSE shall serve as a fundamental mathematical tool in our theoretical analyses, and guide us in searching for suitable designs of transmission lines with nonlinear compensations. The derivation retains the mathematical exactitude down to details. Still in compact and convenient forms, the final equations include the effect of group-velocity dispersion down to an arbitrary order, and take into account the frequency variations of the optical loss as well as the transverse modal function. The chapter also establishes a new formulation of multi-component nonlinear differential equations, which is especially suitable for the study of wide-band wavelength-division multiplexed systems of optical communications.

Part II includes Chapters 4 and 5. Using the mathematical formulations established in Part I, Chapter 4 presents theories on methods of distributed nonlinear compensations using two types of fiber arrangements with respect to an optical phase conjugator or a point of zero dispersion (PZD) in a transmission line. In one type of arrangement, the fiber parameters and the signal intensity are mirror-symmetric in the scaled sense about the phase conjugator or PZD. While the other type is char-

acterized by a translation symmetry in the scaled sense. It will be shown that OPC and a scaled symmetry, either mirror or translation, could reverse the dispersive and nonlinear signal propagation, so to undo the distortions due to signal-signal nonlinear interactions in a long-distance transmission line. It is argued that not only the dispersion, but also the slope and even higher-order dispersions should be carefully chosen, in order for one fiber to compensate the nonlinearity of the other across a wide optical bandwidth containing many WDM channels. In particular, the possibility of nonlinear compensation between two translation-symmetric fiber lines in the scaled sense is our new discovery, which could be a rather interesting method in practice, because two fibers do not have to have opposite gain/loss coefficients to form an STS: a lossy waveguide can be used to compensate a lossy transmission fiber, or the two fibers can be both amplifying. The chapter goes on to demonstrate that, without a phase conjugator, the most detrimental nonlinear interactions among pulses within one wavelength channel may be significantly suppressed in a scaled mirror- or translation-symmetric line. Chapter 5 discusses the advantages and limitations of distributed nonlinear compensations using scaled symmetries, and compares them with other technologies that deal with nonlinear signal distortions, including lumped nonlinear compensation using fibers and other optical components, and digital signal processing using semiconductor integrated circuits to compensate dispersion and nonlinear distortions. The chapter also addresses the question of how effective distributed nonlinear compensations may be in the presence of stochastic polarization variations.

Part III consists of Chapters 6, 7, and 8. Chapter 6 discusses practical nonlinear compensations using STS. The chapter shows how to optimally configure dispersion-managed fiber transmission lines employing slope-compensating fibers, such that OPC may be used to achieve simultaneous wide-band compensations of fiber nonlinearities and residual dispersions, without the need of distributive amplification in transmission fibers. It is demonstrated that when the dispersion slope of transmission fibers is equalized by slope-compensating fibers, the residual dispersion and the slope of dispersion slope are compensated by mid-way OPC. More importantly, fiber nonlinearity may be largely suppressed by arranging the fibers into conjugate pairs about the

phase conjugator, where fiber segments of each pair form an STS. The STS is responsible for canceling optical nonlinearities of fibers within each pair up to the first-order perturbations, then a mirror-symmetric ordering of the fiber pairs about the conjugator linearizes a long transmission line effectively. The chapter discusses practical designs of fiber systems for long-distance transmissions, using realistic (commercially available) transmission fibers and slope-compensating fibers, where the transmission fibers may be standard SMFs, NZDSFs, or even DSFs with dispersion crossing the zero point, and the slope-compensating fibers may be any DCFs with dispersion slopes opposite to that of the transmission fibers. In addition to analytical derivations, the chapter presents numerical simulations to demonstrate simultaneous nonlinearity and dispersion compensations over a wide optical band, via mid-way OPC in long-distance transmission lines using any of the listed type of transmission fibers.

Chapter 7 discusses practical nonlinear suppression without OPC. The chapter presents detailed design and optimization criteria for constructing a transmission line in STS using commercially available fibers, and provides examples of transmission systems so-designed, then presents numerical simulations to demonstrate that two fiber spans in an STS could indeed cancel out their intra-channel nonlinear effects to a large extent without using OPC, and significant reduction of intra-channel nonlinear effects may be achieved in a long-distance transmission line consisting of multiple pairs of translation-symmetric spans. It is also shown that scaled symmetries are insufficient to suppress ghost-pulse generation into empty data slots when ON/OFF keying (OOK) is used for data modulation. The chapter proposes a method using mid-way SPM to reverse the generation of ghost pulses due to intra-channel four-wave mixing (IFWM), and presents computer simulations to demonstrate significant improvement of signal quality by the combination of scaled symmetries and mid-way SPM.

Chapter 8 discusses practical implementations of OPC and DCMs, as well as methods of one-for-many nonlinear compensations using STS. For implementations of OPC, the chapter showcases an example of a Kerr medium pumped by a strong laser beam, where the nonlinear process of FWM mixes the pump laser and a weak signal to generate a phase-conjugated version of the signal. However, it is noted that

the same FWM effect results in parasitic processes by generating inter-mixing terms among the WDM signals. The center frequency of such unwanted mixing terms may coincide with some of the original or conjugated WDM signals to cause significant interference. The chapter studies such interference effect by means of theoretical calculation and computer simulations, and shows that the coherent interference effect decreases as the pump-power to signal-power ratio (PSR) increases. Unfortunately, there could still be strong interference even with a PSR of 20 dB. Some guard-band in the frequency domain may be necessary to avoid such coherent interference. For implementations of DCMs used in scaled translation-symmetric systems, the chapter discusses a method of packaging DCFs achieving optimal nonlinear compensation and good optical signal-to-noise ratio (OSNR) simultaneously. An optimally packaged DCM may consist of portions of DCFs with higher and lower loss coefficients. Such optimized DCMs may be paired with transmission fibers to form lines with STS, so to effectively compensate signal distortions due to dispersion and nonlinearity, with or without OPC. The remaining of the chapter proposes and tests methods of one-for-many nonlinear compensations using STS, which realize simultaneous compensations of both dispersion and nonlinearity over a wide optical band. When OPC is employed, a transmission line may consist of many pairs of compensating fiber spans mirror-symmetrically ordered about the phase conjugator, where each pair may include one fiber span of stronger nonlinearity and several conjugating fiber spans of weaker nonlinearity. First-order nonlinearities are well compensated between spans within each pair, and the mirror-symmetric ordering of conjugating pairs about the phase conjugator helps to prevent the accumulation of nonlinearities over a long transmission distance. When there is no OPC in the middle, a transmission line configured into a one-for-many STS may still suppress the intra-channel nonlinear effects.

At the end, Chapter 9 draws conclusions and discusses perspectives of distributed nonlinear compensations.

Part I. Motivation and Preparation: The Physics and Mathematics of Fiber Nonlinearity

2

Optical Fiber as Nonlinear Dispersive Channel

GVD and optical nonlinearity are two major limiting factors in high-speed long-distance fiber-optic transmissions [1, 2]. DCFs have been developed to offset the dispersion effects of transmission fibers over a wide frequency band. The most advanced DCFs are even capable of slope-matching compensation, namely, compensating the dispersion and the dispersion slope of the transmission fiber simultaneously. Unlike the GVD effect, fiber nonlinearity is a much more difficult problem to overcome, because oppositely signed nonlinearity is not readily found in natural waveguide materials. That is, there exists no long waveguide with opposite nonlinearity to compensate that of a transmission fiber. In the past, there wasn't an effective means to control fiber nonlinearity other than passively dodging it by lowering the signal power, thus shortening the span distance between optical amplifiers, or using distributive Raman amplification. Here we are concerned with active methods to suppress or compensate fiber nonlinearity using OPC and/or scaled symmetries. But firstly, let's try to understand where the nonlinearity comes from and how it becomes a serious limitation. In the traditional subject of nonlinear optics, optical nonlinearity has been notoriously known as weak and hard to get. Indeed, classical nonlinear optics has a lot to do with the search of materials with high nonlinearities and clever designs to enhance nonlinear effects. Still, it is often the case that desired nonlinear products are far weaker than pump signals. How could, then, optical nonlinearity "suddenly" become so strong and turn into a limiting factor in fiber-optic transmission lines? It has to do with the small fiber core area, the long distance optical pulses may travel along a transmission line, and the high-power needed to battle optical noise accumulated over the transmission distance.

2.1 Amplifier Noise, Signal Power, and Transmission Distance

Optical communication systems are actually quieter, that is less noisy, than electronic circuits and the radio-frequency counterparts, because of the inherent immunity of

fiber-optic components to electromagnetic interferences and the thermal noise that plagues electronic circuits, and because of the large energy gap involved in optical transitions in the communications infrared band, $h\nu \sim 0.8$ eV at $\lambda \sim 1.55$ μm, comparing to the thermal energy $kT \sim 0.026$ eV at the room temperature $T \sim 300$ K. However, the large value of $h\nu$ enhances the quantum nature of light. As a consequence, the optical systems are susceptible to photon shot noise, and quantum noise whenever there is gain or/and loss [35, 36, 37, 38, 39, 40]. Interested readers are referred to Appendix A for detailed discussions about quantum noise in optical communications. High-loss fiber links without optical amplifiers are fundamentally constrained by the quantum (shot-noise) limit of photo-detection, although the performance of practical photo-detectors are severely degraded by thermal noise [39, 41]. By contrast, fiber transmission systems with an optical amplifier before the photo-detector, and perhaps many optical amplifiers periodically repeating the signals along the transmission lines, are mostly limited by the quantum noise generated by the gain or/and loss processes. One of the manifestations is the familiar amplified spontaneous emission (ASE) noise generated by optical amplifiers [10]. The quantum nature of the electromagnetic field, in particular the Heisenberg uncertainty principle between the in-phase ($\cos\omega t$) and the quadrature ($\sin\omega t$) components of any mode of electromagnetic oscillation, forces any phase-insensitive linear high-gain amplifier to add at least a half-photon worth of field fluctuation, namely noise, to each mode of the input signal field [35, 39]. When the input signal is in a coherent state [37, 39], which has the minimum amount of uncertainty imposed by quantum mechanics, that is again a half-photon worth of noise, in both the in-phase and the quadrature fields, the best phase-insensitive amplifier adds another half-photon worth of uncertainty to each quadrature component of the input signal so to degrade the signal-to-noise ratio (SNR) by a factor of two, hence the familiar 3-dB lower bound for the noise figure of phase-insensitive linear amplifiers with a high gain. On the other hand, phase-sensitive amplifiers which may amplify the in-phase component while de-amplify the quadrature component, are not limited by the 3-dB noise figure [35, 39]. They may actually realize noiseless amplification to the in-phase component of a signal with high gain, at the price of de-amplification and a great deal of quantum noise dumped to the quadrature component. Lab experiments have demonstrated phase-sensitive amplification with sub-3-dB noise figures in parametric processes with second- or third-order optical nonlinearities [42, 43, 44, 45, 46, 47], and great performance improvements have been predicted when using phase-sensitive amplifiers in fiber-optic transmission systems [48, 49]. However, phase-sensitive amplifiers are still in their infancy, as their operation often involves a complicated optical system and lacks the

stability required by practical field deployment. By contrast, EDFAs, as the most common phase-insensitive amplifiers in fiber-optic systems, enjoy a much simpler and rugged design with exceptional stability, and their noise performance in practice is very close to the 3-dB quantum limit, thanks to the inherent physical characteristics of erbium ions in glass, and the large amount of capital and research invested by the fiber-optic industry. It is rather common to have commercial EDFAs with a noise figure of 4 dB, merely one dB away from the quantum limit.

It should be pointed out though, that phase-insensitive amplifiers do not always degrade the SNR of any input signal by 3 dB and more. They do so only when the input signal is quantum-limited, having the least possible field fluctuations permitted by the uncertainty principle. Practical signals usually carry far more noise than electromagnetic coherent states do. Even if the original signal is indeed at a coherent state, it will acquire significantly more noise after several EDFA spans with loss and gain. No matter how noisy the input signal may be, a quantum-limited phase-insensitive amplifier always contributes the same amount of ASE noise, that is equivalent to the quantum-limited uncertainty carried by a coherent state. It is the ASE noise, not the SNR degradation in dB, that is additively accumulated along a transmission line of many EDFA spans with periodic losses and gains. That is why $M \geq 20$ EDFA spans are often cascaded in practical long-distance transmission lines without degrading the SNR by $3M \geq 60$ dB. Independent of the input signal, each EDFA actually adds a fixed amount of ASE noise whose power totals [10, 50],

$$P_{\text{ASE}} = 2n_{\text{sp}}(G-1)h\nu B_{\text{o}}, \tag{2.1}$$

where the factor 2 is due to the presence of two quadrature components, n_{sp} is the so-called spontaneous emission factor, G is the amplifier gain in linear scale, $h\nu$ is the photon energy, and B_{o} is the optical bandwidth. For an active medium with two atomic states relevant to the optical transition, n_{sp} may be calculated as [10],

$$n_{\text{sp}} = \frac{N_2\sigma_{\text{e}}}{N_2\sigma_{\text{e}} - N_1\sigma_{\text{a}}}, \tag{2.2}$$

where N_1, N_2 are the population densities of the lower and higher energy states, and σ_{a}, σ_{e} are the absorption and emission cross sections respectively. Note that n_{sp} is minimized to 1 when $N_1 = 0$, namely the state population is fully inverted. Also note that $\text{NF} = 2n_{\text{sp}}$ is just the noise figure in linear scale at a large amplifier gain. It is convenient to define an optical SNR, or OSNR in short, as the ratio of the average signal power over the total power of ASE noise,

$$\text{OSNR} = \frac{P_0}{M\text{NF}(G-1)h\nu B_{\text{o}}}, \tag{2.3}$$

where P_0 is the average signal power out of each EDFA, and M is the number of EDFA spans. More convenience is often sought in practice by using the Gaussian approximation for the distribution of the received optical signal, and it is customary to measure the signal quality by the so-called Q factor [41, 50, 51], $Q = |\mu_1 - \mu_0|/(\sigma_1 + \sigma_0)$, where $\mu_{0,1}$ and $\sigma_{0,1}$ are the means and variances of the 0 and 1 levels respectively. The Q factor gives an estimate to the bit-error rate (BER), BER $= \frac{1}{2}\mathrm{Erfc}(Q/\sqrt{2})$, if the threshold is set optimally. $Q \geq 6$ is required to get the standard BER $\leq 10^{-9}$. When ASE is the dominating noise source, which is the case for systems with EDFAs, especially an optical pre-amplifier before photo-detection, and the system is free of other penalties due to GVD and PMD *etc.*, the Q factor is directly related to the OSNR as [52, 53],

$$Q = \frac{2\mathrm{OSNR}}{1 + \sqrt{1 + 4\mathrm{OSNR}}}\sqrt{\frac{B_\mathrm{o}}{B_\mathrm{e}}}, \tag{2.4}$$

where B_o and B_e are respectively the optical and electrical bandwidths of the receiver for each wavelength channel. Equation (2.4) can be solved analytically to get,

$$\mathrm{OSNR} = Q\sqrt{\frac{B_\mathrm{e}}{B_\mathrm{o}}}\left(1 + Q\sqrt{\frac{B_\mathrm{e}}{B_\mathrm{o}}}\right), \tag{2.5}$$

and

$$\frac{P_0}{M(G-1)} = Q\sqrt{\frac{B_\mathrm{e}}{B_\mathrm{o}}}\left(1 + Q\sqrt{\frac{B_\mathrm{e}}{B_\mathrm{o}}}\right)\mathrm{NF}h\nu B_\mathrm{o}, \tag{2.6}$$

by combining (2.3) and (2.5).

With the Q factor being lower-bounded to ensure a desired low BER, and the amplifier NF, $h\nu$, B_o, B_e all being constants, the essence of transmission-line design is to maximize the ratio $P_0/M(G-1)$, necessarily beyond the lower limit defined by the right side of (2.6), of course under the practical constraints of cost and complexity. Given a total transmission distance L in kilometers and the number of EDFA spans M, the amplifier gain G should compensate the loss of each fiber span, that is $G = 10^{0.1\alpha L/M}$, with α being the loss coefficient of the fiber in dB/km. Besides increasing the average signal power P_0, minimizing the factor $M(G-1)$ is desired in order to improve the signal quality. As $M(10^{0.1\alpha L/M} - 1)$ is a monotonically decreasing function for $M \geq 1$, the more amplifiers, or the shorter the length of each EDFA span, the better signal quality. The factor $M(G-1)$ is minimized to $0.1\alpha L \log 10$ when $M \to \infty$. The only (but serious) problem is that EDFAs are expensive devices to install and to operate. For terrestrial transmission systems, repeater hubs are needed to accommodate and shield the optical amplifiers from harsh weather conditions, as well as to provide constant power supply and to air-condition the equipments. The

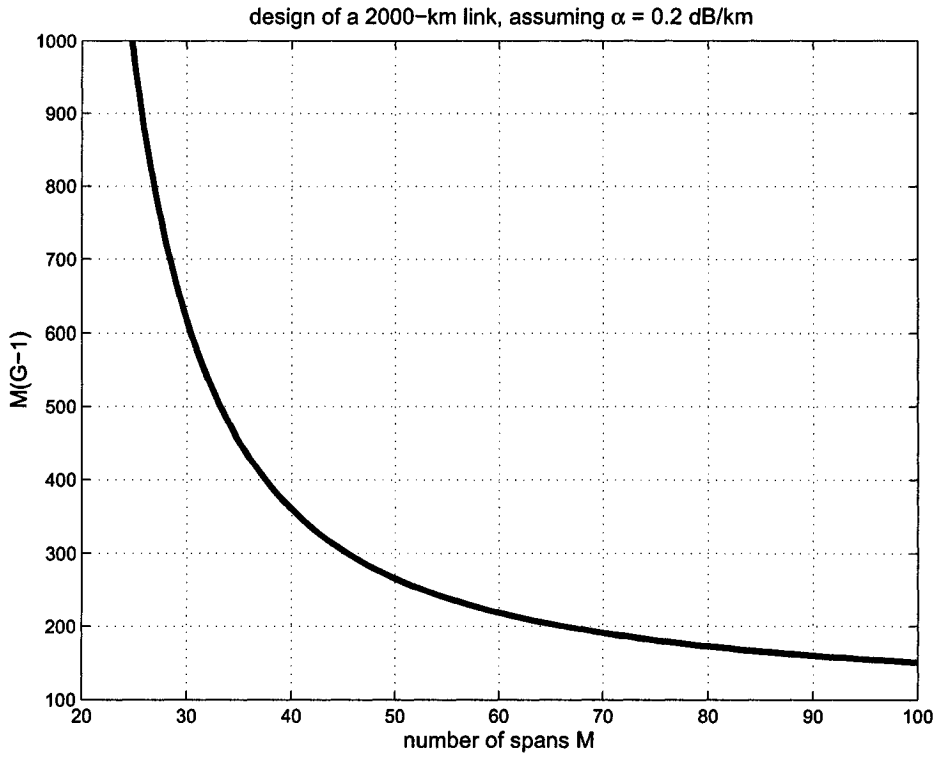

Figure 2.1: The variation of $M(G-1)$ as M increases.

cost only goes higher for submarine systems, where EDFAs are accommodated by hermetically sealed pressure vessels, and high voltage electricity is carried by a thick copper sheath running in parallel to the fibers. The limited amount of space in the pressure vessels limit the number of EDFAs, thus the number of fibers in one cable to about 10, in contrast to terrestrial cables which often have up to 100 fibers inside. There is also practical limitation in transmitting the electrical power along the cable [54], so the power consumption of each EDFA and the number of EDFA spans should be planned carefully. Furthermore, as the number of EDFAs increases to a certain point, or the length of each EDFA span decreases to a certain value, the factor $M(G-1)$ tends to saturate and manifests little further improvement. For example, in a 2000-km link, assuming $\alpha = 0.2$ dB/km, $M(G-1) = M(10^{40/M}-1)$, which reaches its minimal $40 \log 10 \approx 92$ when $M \to \infty$. Fig. 2.1 shows the variation of $M(G-1)$ as M increases. It is clearly seen that the variation becomes rather slow after $M > 40$, namely, when the per-span length becomes less than 50 km. With $M = 80$, so per EDFA span length $L/M = 25$ km, $M(G-1)$ is about 173, which is within a factor of 2 of the minimal. Therefore, it does not make much practical sense to have amplifier spans shorter than 25 km, even it could be done as in deploying

new fiber cables. Mostly limited by the cost and complexity, practical fiber plants usually have amplifiers separated by $\sim$ 50 km for submarine systems and $\sim$ 100 km for terrestrial ones.

Fiber Raman amplifiers [41] may also be employed to repeat the optical signals. Such amplifiers take advantage of the fiber nonlinear effect of SRS, that is stimulated Raman scattering, between pump lasers and the optical signals. The physics of SRS, how its effect among WDM channels may distort the signals (besides its good deed in Raman amplification), and how the impairments may be avoided, shall be discussed later in details. In essence, SRS is an inelastic scattering process between light and material molecules, where photons of the pump laser collide with the molecules, lose some of their energy to excite the molecules, and turn themselves into photons of another frequencies. Recently, the advancement of compact high-power diode lasers makes Raman amplification a practical technology for applications in fiber-optic communications [9, 55, 56]. Unlike EDFAs, Raman amplification does not require special materials, and can take place in regular fibers. In particular, the transmission fibers may be Raman pumped to amplify signals in a distributed manner, in which lies another advantage of Raman amplification, besides the unrestricted bandwidth so long as a suitable pump laser is available. A distributed fiber amplifier, EDFA or Raman, may be considered as a chain of amplets with tiny gains to compensate the fiber loss. Indeed, by carefully arranging the Raman pumps and the length as well as the type of fibers, the distributed Raman gain may be adjusted to compensate the local fiber loss almost exactly, such that a fiber transmission line appears lossless [57]. It should be noted though, that the Raman amplifiers are still phase-insensitive ones, which are bound to induce noise to the optical signals. Lossless the total optical power may appear to be in a Raman-pumped fiber, the signals are still impaired gradually by the accumulation of noise, although the distributed configuration leads to a lower noise figure than a similar span of the same length of transmission fiber followed by a lumped amplifier [9, 10]. The best that distributed amplification can do is to materialize the performance limit $P_0/0.1\alpha L \log 10$ for the left side of equation (2.6). Furthermore, the distributed Raman gain enhances the effect of coherent multi-path interference of an optical signal to itself due to Rayleigh back-scattering [58, 59], which may become a dominating noise source over the ASE. Indeed, the so-called double Rayleigh scattering effect limits the optimal OSNR improvement to merely 6 $\sim$ 7 dB when distributed Raman amplification is introduced to normally EDFA-repeated transmission systems [9, 58]. Apart from the fundamental physics limitations, Raman amplifiers are currently higher in cost, lower in reliability, and less mature than the EDFAs.

Either in a new deployment limited by cost, or an installed fiber plant whose performance (in bit-rate per channel or transmission distance) is to be upgraded, the span distance, the amplifier type and gain are often fixed or constrained, so raising the optical power P_0 is the only other way to increase the performance factor in equation (2.6). In fact, it is a rather efficient means to upgrade the line rate or transmission distance by increasing the signal power P_0. A 3-dB increase of power will enable a previous transmission system to double the bit-rate per channel (thus the total capacity), or let the signals to reach twice as long a transmission distance without ever leaving the optical domain. The latter is especially meaningful for the envisioned all-optical networking technology, where optical signals may hop through several point-to-point transmission links without being terminated by any O/E converter. The optical power has to be raised for the signals to travel a prolonged distance due to all-optical switching. By contrast, it looks less efficient to buy an extra fiber distance for each amplifier span with a margin from increased signal power. A 3-dB margin would only extend 100-km terrestrial amplifier spans to 115 km, so to save about 13% of the amplifiers. Extending submarine spans from 50 km to 65 km would save about 23% of the amplifiers.

Were the fiber transmission lines linear media, increasing the power of the signals may not be much of a problem. Unfortunately, reality is not so simple. A fiber-optic transmission line is a nonlinear channel due to the material nonlinear effects. In fact, fiber nonlinearity has become one of the major limiting factors in modern optical transmission systems [2, 60]. Not only the transmission fibers, but also the EDFAs and Raman amplifiers may induce and sometimes enhance the nonlinear impairments [61, 62, 63]. Our goal is to understand the physics of fiber nonlinearities, mathematically formulate the theory of fiber nonlinear optics, and seek possible means to suppress, even compensate the nonlinear effects of fiber transmission lines.

2.2 *Fiber Nonlinearity and Nonlinear Impairments to Optical Signals*

Researchers of nonlinear optics know only too well the notoriety of optical nonlinearities in that they are usually difficult to observe and exploit, because the optical response of a material deviates significantly from linearity only when the electrical field of the optical excitation becomes close to the atomic Coulomb field, which is on the order of 10^8 V/cm. Such strong field corresponds to an extreme optical intensity on the order of 10^{13} W/cm^2, according to the formula $I = \frac{1}{2} n \epsilon_0 |E|^2$, n is the refractive index of the medium. Under usual conditions with normal optical in-

tensities, almost all materials manifest dominating linear responses, their nonlinear responses are nothing but weak. For example, in the optical Kerr effect, which is a third-order nonlinearity, the refractive index n of a material depends upon the optical intensity I, as $n = n_0 + n_2 I$, where n_0 is the nominal refractive index, and n_2 is the Kerr coefficient. Materials that manifest strong third-order nonlinearity, such as semiconductors and some polymers, have a Kerr coefficient $n_2 = 10^{-14} \sim 10^{-12}$ m^2/W [64]. The silica glass fibers, with $n_2 = 2 \sim 3 \times 10^{-20}$ m^2/W [2, 6], have a rather weak Kerr nonlinearity. How could, then, fiber nonlinearity become a limiting factor to the optical communication systems? The answer lies in the small core area of the fibers and the extremely long-distance of nonlinear interaction in long-distance all-optical transmissions. The effective mode area of single-mode transmission fibers is usually around or below 80 $\mu\mathrm{m}^2$, and the average power of each WDM channel is typically 1 mW, so the optical intensity of just one WDM channel may peak at $I_{\mathrm{peak}} \sim 2\mathrm{mW}/80\mu\mathrm{m}^2 = 2.5 \times 10^7$ W/m^2 in the transmission fiber. Due to the attenuation of the optical power, the full length of a 50 or 100 km fiber span does not experience the same strength of nonlinear interaction, but the effective length of nonlinear interaction can be as long as $(1 - e^{-\alpha L_{\mathrm{span}}})/\alpha \sim 20$ km because of the extremely low loss coefficient $\alpha = 0.02 \log 10 \sim 0.5$ [2]. A typical long-distance transmission line of thousands of kilometers may have 20 fiber spans and more, where the signal power is repeated periodically by optical amplifiers. So the effective length of nonlinear interaction can total $L_{\mathrm{nlin}} = 400$ km. During the propagation of such a long distance, a pulse of one WDM channel may modulate the phase of other signals of other channels or itself via the Kerr effect by as much as $2\pi n_2 I_{\mathrm{peak}} L_{\mathrm{nlin}}/\lambda \approx \pi/3$ (if taking $n_2 = 2.6 \times 10^{-20}$ m^2/W, $\lambda = 1.55$ μm), which may cause substantial distortions to the signals. Certainly, the above is a worst-case example. In reality, pulse walk-off between the WDM channels may reduce the interaction length of any two colliding pulses, but make the pulse collision a random process and more difficult to deal with. In any case, the nonlinear signal interaction in transmission fibers is indeed sufficiently strong to limit the system performance.

By the underlying physical mechanisms, three nonlinear effects usually take place in optical fibers when the signal power is high. The three are stimulated Brilliouin scattering (SBS), SRS, and the optical Kerr effects. SBS happens when the beat between two counter-propagating optical signals, separated by about 10 GHz in frequency, excites acoustic waves at the beat frequency, which in turn forms a dynamic optical grating to scatter the optical signals from one frequency and one direction to the other. Fortunately, SBS has a low effective bandwidth, of 10 MHz approximately, and a sizable threshold about 1 mW. It is easy to make sure that the spectral

power density never reaches the threshold in any frequency interval of 10 MHz, by simply imposing on the optical signals a phase modulation at hundreds of MHz or higher. Furthermore, optical isolators are usually deployed along fiber transmission lines to block the backward propagating signals. As a result, SBS is almost surely prevented in modern optical transmission systems. However, it is much more difficult to suppress the SRS and optical Kerr effects.

In a picture of quantum mechanics, the SRS effect refers to the scattering of a photon by material molecules, in which process the incident photon is annihilated, while a new photon with lower frequency is created, together with the generation of an optical phonon taking up the energy difference. Unlike the SBS effect, the SRS process has a very wide bandwidth, well in excess of 10 THz, and it can take place efficiently with co-propagating signals. SRS induces cross-talk among wide-band WDM channels co-propagated for a long distance, where a given channel experiences random loss or gain that depends upon the intensity of the other channels at lower or higher frequencies. The optical Kerr effect originates from the dependence of the material refractive index on the optical intensity. The bandwidth of the Kerr effect is extremely wide, on the same order of the optical frequency. Within a single channel, the Kerr effect manifests as SPM, that is self-phase modulation, which may broaden the signal spectrum, and in the presence of group-velocity dispersion, could lead to timing jitter and amplitude fluctuation to the optical pulses. When many WDM signals are transmitted in a single fiber, the Kerr effect can mediate inter-channel cross-talks through nonlinear processes called FWM, *i.e.* four-wave mixing, and XPM, *i.e.* cross-phase modulation. FWM refers to the generation of the fourth wave as the product of three waves, while XPM manifests itself as random frequency shifts experienced by one channel due to the variation of the total intensity of other channels. The random frequency shift is translated into pulse timing jitter by the GVD of the transmission line. For WDM channels spaced equally in frequency, the fourth wave of FWM may overlap another channel exactly in frequency, so to cause amplitude fluctuation in that channel. Fortunately, efficient FWM requires tight phase-matching among the waves, which is spoiled in fibers with non-zero GVD. By contrast, XPM is not easily dismissed by dispersion. This is probably the reason that XPM is taken as the fundamental mechanism limiting the capacity of fiber-optic channels [60]. Recently, a lot of interests have been generated by the so-called "pseudo-linear transmissions" of high-speed short return-to-zero (RZ) pulses [65]. Such pseudo-linear transmissions using short RZ pulses may alleviate the nonlinear interactions among WDM channels, especially the inter-channel XPM effect, however, they are still subject to the limitation of fiber nonlinearity, which now manifests as

various intra-channel nonlinear effects [65].

It is interesting to note that the difficulty in the study of nonlinear fiber channels lies actually in the interplay between the group-velocity dispersion and the fiber nonlinearity. If nonlinearity is absent and there is only dispersion, which does nothing other than inducing a nonlinear frequency-dependent phase shift to the signals, a phase equalizer could compensate the effect of dispersion and conventional coding schemes may be employed to utilize the Shannon capacity of the channel. In practice, DCFs are excellent wide-band phase equalizers. On the other hand, if there is only Kerr nonlinearity and no dispersion in the transmission fibers, then a transmission system may employ the constant-power modulation formats of phase-shift keying or frequency modulation, which do not suffer from any degradation from the Kerr nonlinearity. Theoretically, the simpleness of a dispersionless nonlinear channel is reflected by the existence of analytical formulas for the channel input output transfer function, which may be employed to compute or estimate the channel capacity [66, 67, 68] (although it should be cautioned that some specific results in references [66] and [67] may be incorrect).

3

Fundamental Equations of Fiber Nonlinearity

To understand the dispersive and nonlinear signal propagation in optical fibers and consider methods of nonlinearity compensation, it is firstly necessary to establish a mathematical formulism that is sufficiently accurate and generic to grasp the essential physics of signal dispersion and nonlinear interactions, and at the same time is concise and simple enough to facilitate convenient mathematical analyses and derivations. For this purpose, the present chapter shall outline the fundamental physics, model assumptions, mathematical approximations, and essential logic steps to derive NLSEs, namely, nonlinear Schrödinger equations, from the first-principle Maxwell's equations. The outline is meant to emphasize the assumptions and approximations that are made for the derivations, so to highlight the applicability and limitations of the NLSEs in describing the dispersive and nonlinear signal propagation in optical fibers, without diving into great mathematical details. Interested readers are referred to Appendix B for complete derivations that provide every mathematical step in details.

To start, it is firstly necessary to understand the propagation of optical signals inside a nonlinear and dispersive waveguide. In dielectric optical waveguides, *e.g.* silica glass fibers, there is no source of electric charge, nor source of current, that is able to excite electromagnetic waves at the optical frequency. The magnetic response of most dielectrics is negligible at optical frequencies. The optics of dielectric waveguides is governed by Maxwell's equations [69, 70, 71],

$$\nabla \times \mathbf{E} = -\mu_0 \frac{\partial \mathbf{H}}{\partial t}, \tag{3.1}$$

$$\nabla \times \mathbf{H} = \epsilon_0 \frac{\partial \mathbf{E}}{\partial t} + \frac{\partial \mathbf{P}}{\partial t}, \tag{3.2}$$

$$\nabla \cdot (\epsilon_0 \mathbf{E} + \mathbf{P}) = 0, \tag{3.3}$$

$$\nabla \cdot \mathbf{H} = 0, \tag{3.4}$$

and the material equation [5, 6],

$$\begin{aligned} \mathbf{P}(\mathbf{r}, t) = \epsilon_0 \int \chi^{(1)}(\mathbf{r}, s) \mathbf{E}(\mathbf{r}, t-s) ds \\ + \epsilon_0 \int \chi^{(3)}(\mathbf{r}, t_1, t_2, t_3) \vdots \mathbf{E}(\mathbf{r}, t-t_1) \mathbf{E}(\mathbf{r}, t-t_2) \mathbf{E}(\mathbf{r}, t-t_3) dt_1 dt_2 dt_3, \end{aligned} \tag{3.5}$$

where $\chi^{(1)}$ and $\chi^{(3)}$ are the linear and the third-order nonlinear susceptibilities of the dielectric material respectively. In general, $\chi^{(3)}$ is a tensor and $\vdots$ denotes tensor product. Although Maxwell's equations describe all optical phenomena with the most generality and highest accuracy, they appear to be overly complicated if directly applied to optical fibers, in which optical signals are usually weakly guided because the index difference between the core and cladding regions is only small [69, 70]. It turns out that the weakly guided eigen modes in fibers are well approximated by linearly polarized (LP) modes [69, 70]. With an LP representation $\mathbf{E}(\mathbf{r},t) = E(\mathbf{r},t)\hat{\mathbf{e}}$, $\hat{\mathbf{e}}$ being a unit vector of electric field polarization, equations (3.1-3.5) may be simplified and combined into a single differential equation of a scalar quantity,

$$\nabla^2 E - \frac{1}{c^2}\frac{\partial^2 E}{\partial t^2} - \frac{1}{c^2}\frac{\partial^2}{\partial t^2}\int \mathrm{Re}[\chi^{(1)}(s)]E(t-s)ds = \frac{i}{c^2}\mathrm{Im}[\chi^{(1)}]\frac{\partial^2}{\partial t^2}E + \frac{1}{c^2}\chi_K^{(3)}\frac{\partial^2}{\partial t^2}E^3 + \frac{1}{c^2}\frac{\partial^2}{\partial t^2}\int \chi_R^{(3)}(s)E^2(t-s)E(t)ds, \quad (3.6)$$

from which and with suitable approximations, a single- and a multi-component NLSEs may be derived in even simpler forms to describe the dispersive and nonlinear propagation of optical signals in fibers.

Details of the mathematical derivations have been published in reference [13] and are reproduced in Appendix B. This present chapter shall not go to such mathematical details. However, it may be beneficial to highlight the theoretical model and analytical tools by recapping the assumptions and mathematical approximations being made in the derivations. Such highlight should help to identify the applicability of the NLSEs as well as their limitations.

Assumptions

1) First of all, the optical field is believed to obey Maxwell's equations (3.1-3.4);

2) The waveguide material is assumed to display third-order nonlinearity, with the electric response given by (3.5);

3) The waveguide material is step-wise uniform and isotropic; Namely, the waveguide consists of domains of uniform and isotropic materials, such that the polarization $\mathbf{P}$ (linear response) is always a scalar constant times the electric field $\mathbf{E}$ within each domain;

4) The third-order nonlinearity consists of an instantaneous (Kerr) response and a time-delayed (Raman) scattering effect;

5) All signals are assumed co-linearly polarized when entering an optical fiber, and coupled into one polarization eigen state when the fiber is polarization maintaining;

6) The fiber parameters may be z-dependent, but their derivatives with respect to z are always negligible.

The above assumptions are responsible for distilling the first-principle equations (3.1-3.4) and the material property (3.5) into the single scalar equation (3.6). Note that no approximation has been made so far, (3.6) is still mathematically rigorous up to the validity of the above assumptions about the physics of optical waves and dielectric waveguides. The equation may be further simplified with a few reasonable approximations.

Firstly, when the total signal bandwidth W is not much more than a few THz, it satisfies the "narrow band" condition $W \ll \omega_0$, as the carrier frequency $\omega_0 \approx 193$ THz for lasers in the 1550nm communication window. The frequency dependence of the transverse modal function may be neglected, so that a trial solution,

$$E(\mathbf{r},t) = \mathrm{Re}\left\{F(x,y,z)A(z,t)\exp\left[i\int^z \beta_0(\zeta)d\zeta - i\omega_0 t\right]\right\}, \tag{3.7}$$

with $\beta_0(z)$ being the optical propagation constant at ω_0 and position z, may be substituted into (3.6) to derive a differential equation for the envelope function $A(z,t)$. Since the fast variation is absorbed by the factor $\exp[i\int^z \beta_0(\zeta)d\zeta - i\omega_0 t]$, the signal envelope $A(z,t)$ is expected to be slow-varying in both z and t. Bear in mind Assumption 6) that the z-dependence of fiber parameters are always slow, or usually change only stepwise and remain constant for tens to hundreds of kilometers, so that their derivatives with respect to z are always negligible. The transverse modal function $F(x,y,z)$ is determined by substituting $F(x,y,z)A(z,\omega-\omega_0)\exp[i\int^z \beta_0(\zeta)d\zeta]$ into the Fourier transform of (3.6) with the right side set to zero. Then $F(x,y,z)$ is found to solve the eigen-value equation,

$$\left(\frac{\partial^2}{\partial x^2}+\frac{\partial^2}{\partial y^2}\right)F(x,y,z)+\frac{\omega^2}{c^2}F(x,y,z)+\frac{\omega^2}{c^2}\mathrm{Re}[\chi^{(1)}(x,y,z,\omega)]F(x,y,z) = \beta^2(z,\omega)F(x,y,z). \tag{3.8}$$

Note that the eigen-value β^2 is ω-dependent, which may be expanded into a Taylor series,

$$\beta^2(z,\omega) = \beta_0^2(z) + 2\beta_0(z)\sum_{k=1}^{+\infty}\frac{\beta_k(z)}{k!}(\omega-\omega_0)^k, \quad \forall\, z\in\mathbf{R}, \tag{3.9}$$

with

$$\beta_k(z) \stackrel{\mathrm{def}}{=} \frac{1}{2\beta_0(z)}\left.\frac{d^k\beta^2(z,\omega)}{d\omega^k}\right|_{\omega=\omega_0}, \quad \forall\, k\geq 1, \quad \forall\, z\in\mathbf{R}. \tag{3.10}$$

Substituting equations (3.7), (3.8), and (3.9) into (3.6), and using the following:

Approximations

S1) The optical loss or gain in the materials is regarded as frequency-independent;

S2) The two-photon absorption effect is neglected in fibers of silica glass;

S3) The frequency dependence is neglected for the transverse modal function;

S4) The guided modes are treated as linearly polarized;

S5) Nonlinear products out of the signal band are neglected;

S6) The Raman term involving $A^2(z,t-s)A^*(z,t)$ is dropped because of a large phase-mismatch;

S7) The term $\partial^2 A/\partial z^2$ is neglected in view of the slow-varying nature of $A(z,t)$ in z;

S8) Also neglected are terms involving time-derivatives of $A(z,t)$ multiplied by $\mathrm{Im}[\chi^{(1)}]$ and the nonlinear coefficients $\chi_K^{(3)}$, $\chi_R^{(3)}$;

one obtains an NLSE in the so-called retarded frame [6, 13],

$$\frac{\partial A}{\partial z} - i\mathsf{D}(z)A + \frac{\alpha(z)}{2}A = i\gamma(z)|A|^2A + i\left[g(z,\tau)\otimes|A|^2\right]A, \tag{3.11}$$

where

$$\mathsf{D}(z) \stackrel{\text{def}}{=} \sum_{k=2}^{+\infty} \frac{\beta_k(z)}{k!}\left(i\frac{\partial}{\partial t}\right)^k, \tag{3.12}$$

$$\alpha(z) \stackrel{\text{def}}{=} \frac{\omega_0^2}{c^2\beta_0(z)}\int \mathrm{Im}[\chi^{(1)}(x,y,z)]|F(x,y,z)|^2dxdy, \tag{3.13}$$

$$\gamma(z) \stackrel{\text{def}}{=} \frac{3\omega_0^2}{8c^2\beta_0(z)}\int \chi_K^{(3)}(x,y,z)|F(x,y,z)|^4dxdy, \tag{3.14}$$

$$g(z,\tau) \stackrel{\text{def}}{=} \frac{\omega_0^2}{4c^2\beta_0(z)}\int \chi_R^{(3)}(x,y,z,\tau)|F(x,y,z)|^4dxdy, \tag{3.15}$$

$F(x,y,z)$ is assumed to be normalized, and $\otimes$ denotes the convolution operator such that,

$$\left[g\otimes|A|^2\right](z,t) \stackrel{\text{def}}{=} \int g(z,\tau)|A(z,t-\tau)|^2d\tau. \tag{3.16}$$

When the bandwidth of the optical signals becomes too large, it may violate the ω-independent assumptions for the transverse modal function $F(x,y,z)$ and the

loss or gain coefficient $\mathrm{Im}[\chi^{(1)}]$. However, the huge bandwidth is usually shared by many WDM channels, each of which, labeled by $n \in \mathbf{Z}$, is narrow-band around its own center frequency ω_n. Within each WDM channel, the transverse modal function $F_n(x, y, z)$ and the loss or gain coefficient $\mathrm{Im}[\chi_n^{(1)}]$, both subscripted by n, are regarded as frequency-independent and valued at ω_n. In which case, a channelized representation may be used for the optical signals,

$$E(\mathbf{r}, t) = \mathrm{Re}\left\{\sum_n F_n(x, y, z) A_n(z, t) \exp\left[i \int^z \beta_{n0}(\zeta) d\zeta - i\omega_n t\right]\right\}, \tag{3.17}$$

where $\beta_{n0}(z) \stackrel{\mathrm{def}}{=} \beta(z, \omega_n)$ is the optical propagation constant at frequency ω_n and position z, A_n is naturally the slow-varying envelope of the nth channel, and $F_n(x, y, z)$ is the transverse modal function, $\forall\, n \in \mathbf{Z}$. A multi-component NLSE may be derived to describe the dynamics of signal propagation using the following approximations [13]:

Approximations

M1) The optical loss or gain in the materials may vary for different channels, however they are treated as frequency-independent within each channel;

M2) The two-photon absorption effect is again neglected in fibers of silica glass;

M3) The transverse modal function may depend on the center frequency of the channels, however no frequency dependence is considered within each channel;

M4) The guided modes are treated again as linearly polarized;

M5) Nonlinear products out of the total signal band are neglected;

M6) The Raman terms involving $A_m^2(z, t-s)A_n^*(z, t)$, $\forall\, m, n \in \mathbf{Z}$ are dropped due to large phase-mismatches;

M7) The terms $\partial^2 A_n/\partial z^2$, $\forall\, n \in \mathbf{Z}$, are neglected in view of the slow-varying nature of $A_n(z, t)$ in z;

M8) Also neglected are terms involving the time-derivatives of $A_n(z, t)$, $\forall n \in \mathbf{Z}$, multiplied by $\mathrm{Im}[\chi^{(1)}]$, $\chi_K^{(3)}$, or $\chi_R^{(3)}$.

The transverse modes $F_n(x, y, z)$, $n \in \mathbf{Z}$, are determined by the eigen-value equations,

$$\left(\frac{\partial^2}{\partial x^2} + \frac{\partial^2}{\partial y^2}\right) F_n(x, y, z) + \frac{\omega_n^2}{c^2} F_n(x, y, z) + \frac{\omega_n^2}{c^2} \mathrm{Re}[\chi^{(1)}(x, y, z, \omega_n)] F_n(x, y, z)$$
$$= \beta^2(\omega) F_n(x, y, z), \quad \forall\, n \in \mathbf{Z}. \tag{3.18}$$

Substituting (3.17) and (3.18) into (3.6), projecting the field into individual transverse modes $F_n(x,y)$, $n \in \mathbf{Z}$, and similarly, dropping the nonlinear products suffering from large phase-mismatches, neglecting $\partial^2 A/\partial z^2$ and the terms involving the time-derivatives of $A(z,t)$ multiplied by $\mathrm{Im}[\chi^{(1)}]$, $\chi_K^{(3)}$, or $\chi_R^{(3)}$, disregarding the z-derivatives of the fiber parameters and F_n, $\forall\, n \in \mathbf{Z}$, a multi-component NLSE is obtained [13],

$$\frac{\partial A_n}{\partial z} - i\mathsf{D}_n(z)A_n + \frac{\alpha_n(z)}{2}A_n = i\sum_l \sum_m \gamma_{lmn}(z)A_l A_m A_p^* \exp[i\theta_{lmn}(z)] - \sum_l \sum_m g_{lmn}(z)A_l A_m A_p^* \exp[i\theta_{lmn}(z)], \quad \forall\, n \in \mathbf{Z}, \tag{3.19}$$

where p is determined by the condition $\omega_p = \omega_l + \omega_m - \omega_n$, and

$$\mathsf{D}_n(z) \stackrel{\text{def}}{=} \sum_{k=1}^{+\infty} \frac{\beta_{nk}(z)}{k!}\left(i\frac{\partial}{\partial t}\right)^k - \beta_{01}(z)\left(i\frac{\partial}{\partial t}\right), \tag{3.20}$$

$$\alpha_n(z) \stackrel{\text{def}}{=} \frac{\omega_n^2}{\beta_{n0}(z)c^2}\int \mathrm{Im}[\chi_n^{(1)}(\mathbf{r})]|F_n(x,y)|^2 dxdy, \tag{3.21}$$

$$\gamma_{lmn}(z) \stackrel{\text{def}}{=} \frac{\omega_n^2}{8\beta_{n0}(z)c^2}\int [3\chi_K^{(3)}(\mathbf{r}) + 2G_r(\mathbf{r}, \omega_n - \omega_l)]F_l F_m F_n^* F_p^* dxdy, \tag{3.22}$$

$$\theta_{lmn}(z) \stackrel{\text{def}}{=} \int^z [\beta_{l0}(\zeta) + \beta_{m0}(\zeta) - \beta_{n0}(\zeta) - \beta_{p0}(\zeta)]d\zeta, \tag{3.23}$$

$$g_{lmn}(z) \stackrel{\text{def}}{=} \frac{\omega_n^2}{4\beta_{n0}(z)c^2}\int G_i(\mathbf{r}, \omega_n - \omega_l)F_l F_m F_n^* F_p^* dxdy, \tag{3.24}$$

$\forall\, l, m, n \in \mathbf{Z}$, with

$$\beta_{nk}(z) \stackrel{\text{def}}{=} \frac{1}{2\beta_{n0}(z)}\left.\frac{\partial^k \beta^2(z,\omega)}{\partial \omega^k}\right|_{\omega=\omega_n}, \quad \forall\, k \geq 1,\ \forall\, n \in \mathbf{Z}, \tag{3.25}$$

$$G_r(\mathbf{r}, \omega) \stackrel{\text{def}}{=} \mathrm{Re}\left[\int \chi_R^{(3)}(\mathbf{r}, t)\exp(\omega s)dt\right], \tag{3.26}$$

$$G_i(\mathbf{r}, \omega) \stackrel{\text{def}}{=} \mathrm{Im}\left[\int \chi_R^{(3)}(\mathbf{r}, t)\exp(\omega s)dt\right]. \tag{3.27}$$

As the Fourier transform of $\chi_R^{(3)}(t)$, $G_r(\omega) + iG_i(\omega)$ is basically the Raman gain spectrum. Because $\chi_R^{(3)}$ is real valued, G_r and G_i are even and odd functions of ω respectively, namely, $G_r(-\omega) = G_r(\omega)$, $G_i(-\omega) = -G_i(\omega)$. Except for being applicable to a wider bandwidth, the multi-component NLSE (3.19) reflects essentially the same physics, shares a similar mathematical structure, and predicts mostly the same phenomena as equation (3.11).

For a fiber link stretching from $z = 0$ to $z = L$ with given input signal $A(0,t)$, the NLSE (3.11) or (3.19) may be integrated to obtain the output signal $A(L,t)$. Unfortunately, the simultaneous presence of dispersion and nonlinearity makes it

difficult to obtain a closed-form analytical solution for either NLSE. So far, an NLSE can only be integrated by numerical means. Such theoretical difficulty may be blamed for the poor understanding of the dispersive and nonlinear communication channels, and consequently the lacking of an effective counter measure to the fiber nonlinearity up to date.

Part II. Theory: Scaled Symmetries and Nonlinear Compensations

4

Scaled Symmetries and Nonlinear Compensations

The ability of transmitting high-power optical signals over long-distances with low distortion is an essential element to the realization of high-capacity optical networks that are widely connected over long distances (thousands of kilometers) and switched in most places by all-optical means. However, GVD and optical nonlinearity impose limits to the transmission distance, or more precisely, the product of data capacity and transmission distance [1, 2]. The problem of GVD has basically been solved by the development of DCFs with oppositely signed dispersions to offset the dispersion effects of transmission fibers over a wide frequency band. The most advanced DCFs are even capable of slope-matching compensation, namely, compensating the dispersion and the dispersion slope of the transmission fibers simultaneously [3, 4]. Unlike the GVD effect, fiber nonlinearity is a much more difficult problem to overcome, because oppositely signed nonlinearity is not readily found in natural waveguide materials. That is, there exists no long waveguide with opposite nonlinearity to compensate that of a transmission fiber.

Using the mathematical formulations established in Chapter 3, we shall discuss nonlinear compensation using two types of fiber arrangements with respect to the OPC, as shown in Fig. 4.1. In one type of arrangement, the fiber parameters and the signal intensity are in SMS, that is scaled mirror symmetry, about the OPC. While the other type is characterized by STS, that is scaled translation symmetry. We argue that not only the dispersion, but also the slope and even higher-order dispersions should be carefully chosen, in order for one fiber to compensate the nonlinearity of the other, across a wide optical bandwidth containing many WDM channels. We also emphasize the important notions of scaled nonlinearity and scaled symmetry. Scaled nonlinearities and symmetries enable two fibers with a wide range of parameters to compensate each other's nonlinearity, as long as their parameters satisfy a set of proportional rules. In particular, a short piece of specialty fiber with very high dispersion may be used to compensate both the dispersion and the nonlinearity of a long transmission fiber. The dispersion, dispersion slope or higher order-dispersions are set in proportion to the parameters of the transmission fiber, and the specialty fiber may

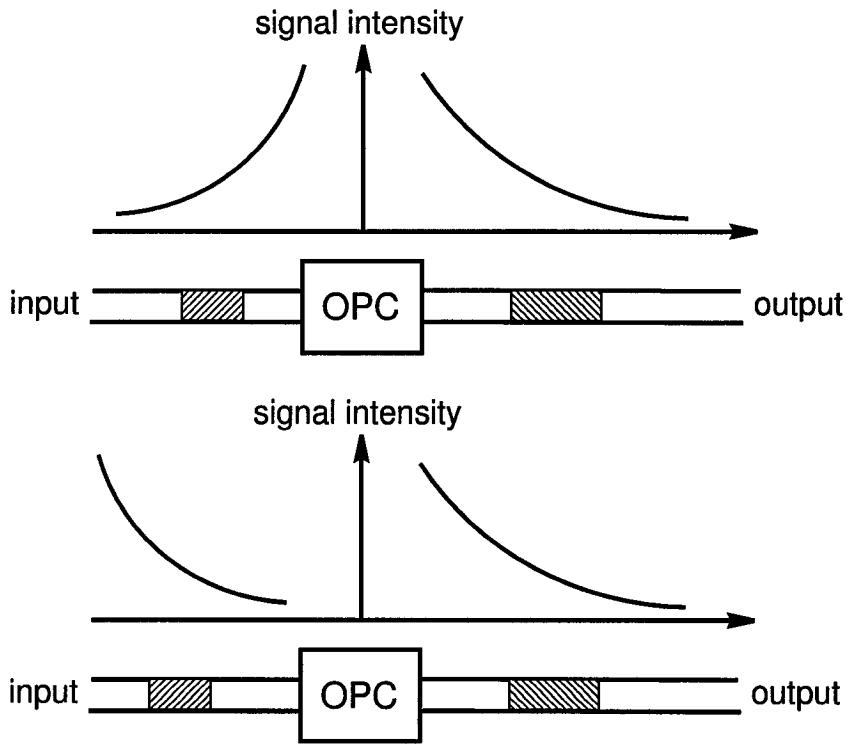

Figure 4.1: Two types of system configurations for nonlinear compensation with OPC: mirror-symmetric (top) and translation-symmetric (bottom).

be erbium-doped or Raman pumped to have a gain proportional to the loss of the transmission fiber. In a mirror-symmetric setup, such specialty fibers may perfectly linearize fiber transmission lines. Besides practical applications in fiber transmission systems, the method of scaling nonlinearity and nonlinear compensation has a deep implication to a fundamental question in information theory. That is, fiber nonlinearity does not necessarily impose a limit to the channel capacity. In practice, there could be errors in scaling the fiber parameters, so that the nonlinear compensation may not be perfect. Nevertheless, excellent performance would still be achieved by choosing the parameters carefully according to the scaling rules. The possibility of nonlinearity compensation between two translation-symmetric fiber lines is the first of such discovery as far as we are aware. It is also a rather interesting scheme, in that the two fibers do not have to have opposite gain/loss coefficients: a lossy waveguide can be used to compensate a lossy transmission fiber, or the two fibers can be both amplifying. Although the STS setup is only capable of compensating local and weak nonlinearity up to the first-order perturbation, it may find wide applications in practical transmission systems, especially long-distance ones, where the nonlinearity

of each fiber span is indeed only a perturbation, but the accumulation of nonlinearity along the distance can significantly distort the signals.

4.1 Dispersion and Nonlinear Compensations Using SMS

The use of OPC has been know to enable one fiber compensating the dispersion as well as the nonlinearity of another transmission fiber [7, 8]. The basic principle is that OPC enables one fiber transmission line to propagate inversely (thus to restore) an optical signal that is dispersively and nonlinearly distorted by the other, when the two fiber lines are mirror-symmetric about the OPC. However, a mirror symmetry may be difficult to realize in practice, as it requires opposite loss/gain coefficients for each pair of fiber segments in conjugation. In other words, it takes an unusual amplifying waveguide to compensate a conventional fiber with loss. Although amplifying fibers are obtainable through distributed Raman pumping [9] or distributed EDFAs [10], the loss of pump power makes it difficult to maintain a constant gain over an extended fiber length. This difficulty may seriously undermine the effectiveness of nonlinearity compensation in mirror-symmetric systems [20, 30]. For a possible solution, we have noted the importance of mirror symmetries in the scaled sense, in particular, the significance and feasibility of scaling the dispersion slopes of fibers together with their dispersions, loss/gain and nonlinear coefficients [11, 12, 13]. Starting from the nonlinear Schrödinger equation, it may be shown analytically that the dispersive and nonlinear evolution of optical signals may be scaled, such that a short piece of fiber with suitably scaled parameters could subject optical signals to the same dispersive and nonlinear propagation as a long fiber. Therefore, it is possible to form a mirror symmetry, albeit in the scaled sense, between a short specialty fiber and a long transmission fiber. Based on this principle, we propose methods of nonlinear compensation using SMSs to overcome the difficulties that have plagued previous schemes. Another guiding principle for our proposals is that the mathematical derivations should be made as general as possible, while the physical implementations should be restricted to using fiber components and technologies that are either already commercially available, practically installed, or at least becoming available soon. In other words, the proposed implementations should be kept as close as possible to industrial practice.

Basically, we suggest to use recently available specialty fibers with high dispersion values, such that a short piece of HD fiber may compensate a long transmission fiber. For a mirror symmetry in the scaled sense, the dispersion, dispersion-slope and higher order-dispersions of the HD fiber are set in proportion to those of the transmission fiber, then the HD fiber may be erbium-doped or Raman pumped to have

a gain coefficient proportional to the loss of the transmission fiber. Because of their shorter length and usually being packaged compactly at the transmitting/receiving ends or the power repeater sites, it could be much easier to maintain and control the distributive gain profile in the HD fibers. Indeed, it is noted that practical transmission systems using commercially available fibers might be arranged into nearly perfect mirror symmetries in the scaled sense and hence enjoy excellent nonlinearity compensation. In particular, a pair of commercially available fiber types are identified for nonlinear compensation with SMS, which is between a negative (in dispersion) NZDSF (-NZDSF) and a conventional DCF with high negative dispersion. In a transmission line with transmission and HD fibers arranged into scaled mirror-symmetric pairs about an optical phase conjugator in the middle, an SMS about the phase conjugator is formed for both the dispersion and the signal power maps, which ensures that the two parts, before and after OPC, would propagate and distort optical signals reversely with respect to each other, so that distortions to signals due to nonlinear interactions among them would be undone at the end of the transmission line.

It should be noted that the basic idea of scaling fiber parameters for nonlinear compensation using mirror symmetry has been explored before by Watanabe *et al.* [17]. However, the analysis in reference [17] fails to take account of the effect of higher-order dispersions, in particular the dispersion slope. Consequently, the methods may not work well with high-capacity WDM systems. Also the proposed implementations in reference [17] are limited to transmission lines based on dispersion-shifted fibers, and using lumped nonlinear compensators to compensate Kerr nonlinearities in the path-averaged sense. The proposed nonlinear compensator is an integrated device installed at either the transmission or the receiving end of a point-to-point link, uses a specially designed fiber consisting of many segments, and has to be tailor-made for the specific transmission line. The result is a lack of flexibility: an installed nonlinear compensator may cease to work when the corresponding transmission line is altered; it may be prohibitively costly and labor-intensive to design and optimize a special nonlinear compensator for each transmission line. Moreover, an optical lumped nonlinear compensator may be difficult to fabricate, as it requires many fiber segments spliced together to approximate the distributive dispersions and nonlinearities in the transmission fibers. Ironically, due to the other uncooperative aspect of optical nonlinearity, it becomes a challenge to generate enough nonlinearities in a lumped nonlinear compensator using short segments of fibers. In accordance with the periodic power map in a transmission line, a lumped nonlinear compensator may need many optical amplifiers between its fiber segments, or the fiber segments have to be with changing dispersions or nonlinear coefficients. Neither condition is readily fulfilled with even

today's technology.

4.1.1 *Theory of nonlinear compensation using OPC and SMS*

A simple scaled mirror-symmetric system may be depicted as in Fig. 4.1, top graph, where the curves of signal power form a mirror symmetry in the scaled sense about the OPC. It will be shown below that the scaling rules, namely, conditions for optimal nonlinear compensation, require that the curves of fiber dispersion and gain/loss coefficients also follow the same mirror symmetry as the curves of signal power do. Such a scaled mirror-symmetric system may consist of a fiber line on the left stretching from $z = -L/R$ to $z = 0$, $L > 0$, $R > 0$, followed by OPC, then a fiber line on the right stretching from $z = 0$ to $z = L$. The two fiber lines may carry WDM or optical time-division multiplexed (OTDM) signals. So long as the total optical bandwidth is not much more than a few THz, the combined optical signals may be represented by,

$$E(z,t) = A(z,t)\exp\left[i\int^z \beta(\zeta,\omega_0)d\zeta - i\omega_0 t\right], \quad \forall\ z \le 0, \tag{4.1}$$

$$E'(z,t) = A'(z,t)\exp\left[i\int^z \beta'(\zeta,\omega_0')d\zeta - i\omega_0' t\right], \quad \forall\ z \ge 0, \tag{4.2}$$

on the two sides of OPC respectively, where ω_0 and ω_0' are center frequencies that are not necessarily the same due to a possible shift of center frequency by OPC, $A(z,t)$ and $A'(z,t)$ are slow-varying envelopes, while $\beta(z,\omega)$ and $\beta'(z,\omega)$ are the z- and ω-dependent propagation constants on the two sides. Being omitted is the transverse modal function. For mathematical simplicity, all optical signals are assumed co-linearly polarized. The dynamics of signal propagation in the two fiber lines is governed by two NLSEs respectively,

$$\frac{\partial A}{\partial z} - i\mathsf{D}(z)A + \frac{\alpha(z)}{2}A = i\gamma(z)|A|^2A + i\left[g(z)\otimes|A|^2\right]A, \quad -L/R \le z \le 0, \tag{4.3}$$

$$\frac{\partial A'}{\partial z} - i\mathsf{D}'(z)A' + \frac{\alpha'(z)}{2}A' = i\gamma'(z)|A'|^2A' + i\left[g'(z)\otimes|A'|^2\right]A', \quad 0 \le z \le L, \tag{4.4}$$

where for the first fiber line, $\alpha(z)$ is the gain/loss coefficient, $\gamma(z)$ and $g(z)$ are the Kerr and Raman nonlinear coefficients respectively, and the functional operator $\mathsf{D}(z)$ is defined as in equation (3.12). The parameters $\alpha'(z)$, $\{\beta_k'(z)\}_{k\ge2}$, $\gamma'(z)$, $g'(z)$, and the operator $\mathsf{D}'(z)$ are similarly defined for the second fiber line. It is an easy exercise to show that the complex conjugate of (4.3) reduces to (4.4), when the parameters satisfy the following scaling rules,

$$\alpha(-z) = -R\alpha'(Rz), \tag{4.5}$$

$$\beta_k(-z) = (-1)^k R\beta_k'(Rz), \quad \forall\ k \ge 2, \tag{4.6}$$

$$\gamma(-z) = R\gamma'(Rz)|C|^{-2}, \tag{4.7}$$

$$g(-z) = Rg'(Rz)|C|^{-2}, \tag{4.8}$$

and the envelope functions are related as,

$$A(-z,t) = CA'^{*}(Rz,t), \tag{4.9}$$

for all $z \in [0, L/R]$, where $R > 0$ and $C \neq 0$ are scaling constants. Physically, it says that the two fiber lines compensate each other for both dispersions and nonlinearities. An optical signal $A(-L/R,t)$ entering the first fiber line may be dispersed and nonlinearly distorted to become $A(0,t)$, which are converted into $A'(0,t) = A^{*}(0,t)/C^{*}$ by the OPC. The second fiber line will then propagate the optical signal in a reversed (mirror-symmetric) manner with respect to the first. The final output signal $A'(L,t) = A^{*}(-L/R,t)/C^{*}$ is an exact replica of the initial signal up to complex conjugation. It is noted that parts of one fiber line would have to provide gain in correspondence to attenuation in parts of the other, and vice versa. An HD fiber may be chosen with parameters satisfying equations (4.6-4.8) to be the scaled mirror image of a transmission fiber which usually attenuates light. At the same time, erbium doping or Raman pumping should be employed to obtain the proper gain specified by equation (4.5). It is noted that the requirements for the third- and higher-order dispersions may be relaxed in the scaling rules of equation (4.6), then the two fibers may be no longer in strict mirror symmetry across a wide optical band, rather the symmetry and nonlinear compensation between them become approximate. Nevertheless, such approximation is often a good one when the values of $|\beta_k/\beta_2|$, $k \geq 3$, are quite small, so that the percentage change of β_2 is insignificant across the signal band, which is exactly the case for standard single-mode fibers in the 1550-nm band.

Therefore, OPC and a specialty fiber with parameters designed according to (4.5-4.9) could perfectly compensate the nonlinearity of a transmission fiber, if not for the ever-existing noise, especially that incurred when the signal amplitude is low, destroying the mirror symmetry. In Fig. 4.1, top graph, for fiber locations not too far from the OPC, the signal power is relatively high to minimize the effect of the optical noise, which usually originates from ASE and quantum photon statistics. However at the two ends of the link, the effect of the optical noise could become substantial. A simple but fairly accurate model may assume that optical noise is incurred exclusively at the two extreme ends of the link, dispersive and nonlinear signal propagation is the only effect of the inner part of the link. In this model, the nonlinearity of a segment of transmission fiber with $z_1 \leq z \leq z_2$ is fully compensated by the portion of the specialty fiber with $-z_2/R \leq z \leq -z_1/R$, $\forall\ z_1, z_2 \in [0, L]$. In particular,

the entire link from $z = -L/R$ to $z = L$ is equivalent to a linear channel impaired by additive noise at the two ends. If W is the total optical bandwidth of the input WDM channels, then the OPC should have a bandwidth wider than W to cover the extra frequency components generated through wave mixing in the specialty fiber. With nonzero dispersion fibers, however, the extra bandwidth due to wave mixing may hardly exceed 100 GHz, which is often negligible in comparison to the total bandwidth W of several, even tens of THz. Thus the linearized link may be assumed to have the same bandwidth limit W throughout, applicable to which is Shannon's formula for channel capacity [72], $C = W \log_2(1 + S/N)$. Obviously, many of such linearized links may be cascaded to reach a longer transmission distance, and the entire transmission line is still linear end-to-end in spite of the nonlinearity existing locally in the fibers.

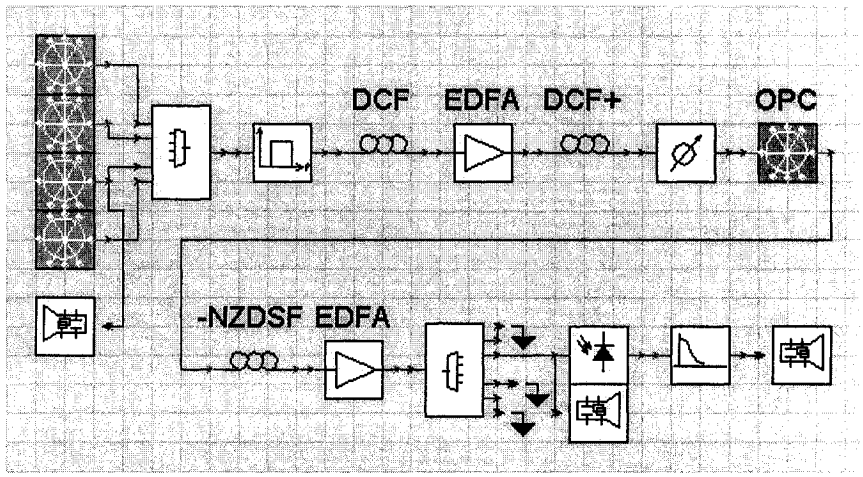

Figure 4.2: A mirror-symmetric transmission line using -NZDSF and DCF.

4.1.2 A numerical example

For a numerical example, we have simulated a scaled mirror-symmetric link as shown in Fig. 4.2, which consists of two pieces of DCF, an optical phase conjugator, and a 200km long -NZDSF as the transmission fiber with loss coefficient $\alpha' = 0.2$ dB/km, dispersion $D' = -8$ ps/nm/km, dispersion slope $S' = 0.08$ ps/nm^2/km, effective mode area $A'_{\text{eff}} = 50$ μm^2, Kerr nonlinear index $n'_2 = 2.6 \times 10^{-20}$ m^2/W. The DCFs are also made of silica glass with the same Kerr nonlinear index, but with parameters $(D, S) = 20 \times (D', -S')$ and $A_{\text{eff}} = 12.5$ μm^2. One piece of DCF, 5 km in length and labeled by DCF+ in Fig. 4.2, is erbium-doped or Raman-pumped to maintain a constant gain, so that its "loss coefficient" α is negative, $\alpha = -20\alpha' = -4.0$ dB/km,

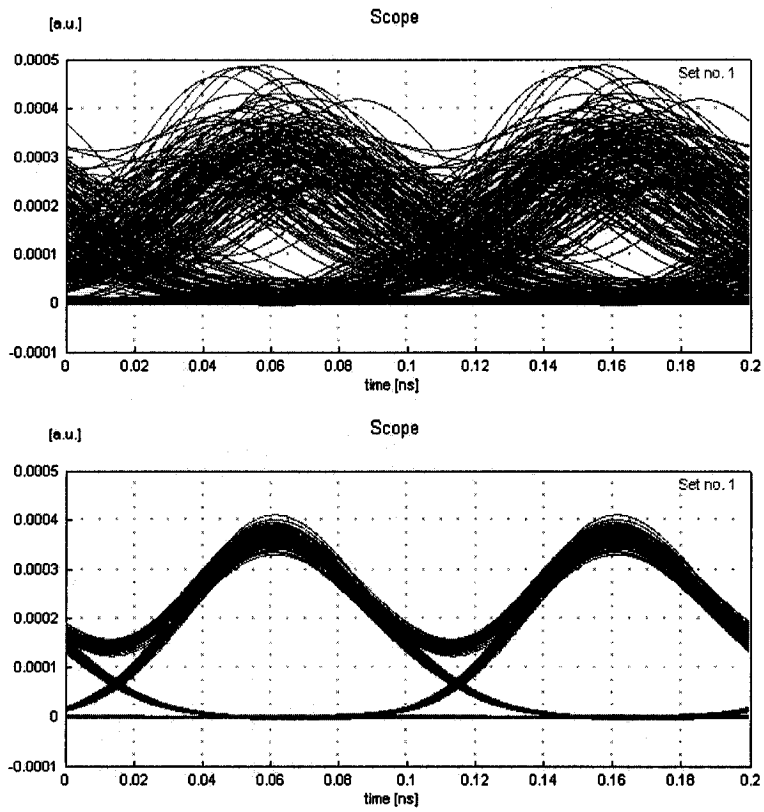

Figure 4.3: Received signals at the end of the simulated SMS link. Top: only the dispersion of the transmission fiber is pre-compensated by the HD fiber. Bottom: both dispersion and nonlinearity are pre-compensated.

in order to form a scaled mirror symmetry with respect to the first 100km -NZDSF. The other piece of DCF, also 5 km in length, is used to balance the dispersion, which has no gain but a loss coefficient of 1.0 dB/km. The nonlinearity of the DCFs (as HD fibers in the system) can be switched on and off. The input consists of four WDM channels at 100 GHz spacing, co-polarized, all RZ modulated at 10 Gb/s. Each RZ pulse generator consists of a continuous-wave laser followed by a zero-chirp modulator, which is over-driven to produce a pulse train with the amplitude proportional to $\cos\left(\frac{\pi}{2}\sin\pi\Omega t\right)$, where Ω is the bit rate. Therefore the duty cycle of the pulses is 33%, if defined as the ratio of pulse full-width-half-maximum to the time interval between adjacent bits. The power of all optical pulses is peaked at 100 mW when entering the transmission fiber. ASE noise from amplifiers is added at the two ends of the link. More specifically, each optical transmitter sends RZ pulses with peak power of 5.0 mW into the first 5km DCF with loss coefficient 1.0 dB/km, followed by a 5dB EDFA; then the signals propagate through the 5km DCF+ with gain coefficient 4.0

dB/km; after being attenuated by a factor of 5.0 in power and phase conjugated, the signals are transmitted through the 200km -NZDSF, and finally boosted by a 20dB EDFA before being demultiplexed and photo-detected. The noise figure is 4.0 dB for both EDFAs. The photo-detector is with responsivity 1.0 A/W and thermal noise 10.0 pA/$\sqrt{\text{Hz}}$. The center frequency is 193.1 THz for the optical band. MUX/DEMUX filters are 7th order Bessel with 3dB bandwidth 25 GHz. The electrical filter is 3rd order Bessel with 3dB bandwidth 7.0 GHz. Fig. 4.3 shows the received signals of the 3rd transmitted channel, with the DCF nonlinearity off and on respectively. The eye diagram on the top shows the overwhelming nonlinear distortions in the received signals, when the DCF has no nonlinearity, but only pre-compensates the dispersion of the transmission fiber. When the nonlinearity of the DCF is turned on, the eye diagram at the bottom shows no visible nonlinear degradation, but only the effect of ASE noise, which clearly demonstrates the effect of nonlinear compensation due to OPC and SMS.

4.2 Dispersion and Nonlinear Compensations Using STS

4.2.1 Basics of dispersive and nonlinear wave propagation in fibers

As discussed in Chapter 3, the eigenvalue solution of Maxwell's equations in a single-mode fiber determines its transverse modal function and propagation constant $\beta(\omega)$ as a function of the optical frequency ω [41, 69, 70]. When a fiber transmission line is heterogeneous along its length, the propagation constant could also depend on the longitudinal position z in the line, and may be denoted as $\beta(z,\omega)$. Using the slow-varying envelope form,

$$E(z,t) = A(z,t)\exp\left[i\int^{z}\beta_0(\zeta)d\zeta - i\omega_0 t\right], \tag{4.10}$$

with $\beta_0(z) \stackrel{\text{def}}{=} \beta(\omega_0, z)$, to represent an optical signal, which may be of a single time-division multiplexed channel or a superposition of multiple WDM channels, the evolution of the envelope $A(z,t)$ in an optical fiber of length L is governed by the following nonlinear NLSE [6, 13],

$$\frac{\partial A(z,t)}{\partial z} + \sum_{k=2}^{+\infty}\frac{i^{k-1}\beta_k(z)}{k!}\left(\frac{\partial}{\partial t}\right)^k A(z,t) + \frac{\alpha(z)}{2}A(z,t) = i\gamma(z)|A(z,t)|^2 A(z,t) + i\left[g(z,t)\otimes|A(z,t)|^2\right]A(z,t), \tag{4.11}$$

$\forall\ z \in [0, L]$, in the retarded reference frame with the origin $z = 0$ moving along the fiber at the signal group-velocity. In the above equation, $\alpha(z)$ is the loss/gain

coefficient,

$$\beta_k(z) \stackrel{\text{def}}{=} \frac{1}{2\beta_0(z)} \left. \frac{\partial^k \left[\beta^2(\omega, z)\right]}{\partial \omega^k} \right|_{\omega=\omega_0}, \quad \forall\, k \geq 2, \tag{4.12}$$

are the z-dependent dispersion coefficients of various orders [13], $\gamma(z)$ is the Kerr nonlinear coefficient of the fiber, $g(z,t)$ is the impulse response of the Raman gain spectrum, and $\otimes$ denotes the convolution operation [13]. It may be noted that all fiber parameters are allowed to be z-dependent, that is, they may vary along the length of the fiber. Because of the definition in terms of derivatives, β_2 may be called the second-order dispersion (often simply dispersion in short), while β_3 may be called the third-order dispersion, so on and so forth. The engineering community has used the term dispersion for the parameter $D = dv_g^{-1}/d\lambda$, namely, the derivative of the inverse of group-velocity with respect to the optical wavelength, and dispersion slope for $S = dD/d\lambda$ [1]. Although β_2 and D are directly proportional to each other, the relationship between β_3 and S is more complicated. More details and numerical examples are provided in Appendix C. To avoid confusion, we adopt the convention that dispersion and second-order dispersion are synonyms for the β_2 parameter, while dispersion slope and third-order dispersion refer to the same β_3 parameter, and similarly the slope of dispersion slope is the same thing as the fourth-order dispersion β_4.

Had there been no nonlinearity, namely $\gamma(z) = g(z,t) \equiv 0$, equation (4.11) would reduce to,

$$\frac{\partial A(z,t)}{\partial z} + \sum_{k=2}^{+\infty} \frac{i^{k-1}\beta_k(z)}{k!} \left(\frac{\partial}{\partial t}\right)^k A(z,t) + \frac{\alpha(z)}{2} A(z,t) = 0, \tag{4.13}$$

which could be solved analytically using, for example, the method of Fourier transform. Let F denote the linear operator of Fourier transform, a signal $A(z,t)$ in the time domain can be represented equivalently in the frequency domain by,

$$\tilde{A}(z,\omega) \stackrel{\text{def}}{=} \mathsf{F}A(z,t) = \int A(z,t)\exp(i\omega t)dt = \int E(z,t)\exp[i(\omega_0+\omega)t]dt. \tag{4.14}$$

Through a linear fiber, an optical signal $\tilde{A}(z_1,\omega)$ at $z = z_1$ would be transformed into $\tilde{A}(z_2,\omega) = H(z_1,z_2,\omega)\tilde{A}(z_1,\omega)$ at $z_2 \geq z_1$, where the transfer function $H(z_1,z_2,\omega)$ is defined as,

$$H(z_1,z_2,\omega) \stackrel{\text{def}}{=} \exp\left[i\sum_{k=2}^{+\infty} \frac{\omega^k}{k!} \int_{z_1}^{z_2} \beta_k(z)dz - \frac{1}{2}\int_{z_1}^{z_2} \alpha(z)dz\right]. \tag{4.15}$$

In the time domain, the signals are related linearly as $A(z_2,t) = \mathsf{P}(z_1,z_2)A(z_1,t)$, with the linear operator $\mathsf{P}(z_1,z_2)$ given by,

$$\mathsf{P}(z_1,z_2) \stackrel{\text{def}}{=} \mathsf{F}^{-1}H(z_1,z_2,\omega)\mathsf{F}. \tag{4.16}$$

Namely, $\mathsf{P}(z_1, z_2)$ is the concatenation of three linear operations: firstly Fourier transform is applied to convert a temporal signal into a frequency signal, which is then multiplied by the transfer function $H(z_1, z_2, \omega)$, finally the resulted signal is inverse Fourier transformed back into the time domain. In terms of an impulse response,

$$h(z_1, z_2, t) \stackrel{\text{def}}{=} \mathsf{F}^{-1}[H(z_1, z_2, \omega)], \tag{4.17}$$

$\mathsf{P}(z_1, z_2)$ may also be represented as,

$$\mathsf{P}(z_1, z_2) = h(z_1, z_2, t)\otimes, \tag{4.18}$$

where $\otimes$ denotes functional convolution. That is, the action of $\mathsf{P}(z_1, z_2)$ on a time-dependent function is to convolve the function with the impulse response. All linear operators $\mathsf{P}(z_1, z_2)$ with $z_1 \leq z_2$, also known as propagators, form a semigroup [73] for the linear evolution governed by equation (4.13).

However, the existence of nonlinear terms in equation (4.11) makes the equation much more difficult to solve. Fortunately, when the signal power is not very high so that the nonlinearity is weak and may be treated as perturbation, the output from a nonlinear fiber line may be represented by a linearly dispersed version of the input, plus nonlinear distortions expanded in power series of the nonlinear coefficients [74]. Such representation falls into the general theory of Volterra series expansion for nonlinear systems [75, 76]. In practical transmission lines, although the end-to-end response of a long link may be highly nonlinear due to the accumulation of nonlinearity through many fiber spans, the nonlinear perturbation terms of higher orders than the first are usually negligibly small within each fiber span. Up to the first-order perturbation, the signal $A(z_2, t)$ as a result of nonlinear propagation of a signal $A(z_1, t)$ from z_1 to $z_2 \geq z_1$, may be approximated using,

$$A_0(z_2, t) = \mathsf{P}(z_1, z_2)A(z_1, t), \tag{4.19}$$

$$\begin{aligned} A_1(z_2, t) = \int_{z_1}^{z_2} \mathsf{P}(z, z_2) \Big\{ & i\gamma(z)|A_0(z, t)|^2 A_0(z, t) \\ & + i \left[g(z, t) \otimes |A_0(z, t)|^2 \right] A_0(z, t) \Big\} dz, \end{aligned} \tag{4.20}$$

where $A(z_2, t) \approx A_0(z_2, t)$ amounts to a zeroth-order approximation which neglects the fiber nonlinearity completely, whereas the result of first-order approximation $A(z_2, t) \approx A_0(z_2, t) + A_1(z_2, t)$ accounts in addition for the lowest-order nonlinear products integrated over the fiber length. The term $A_1(\cdot, t)$ may be called the first-order perturbation because it is linearly proportional to the nonlinear coefficients $\gamma(\cdot)$ and $g(\cdot, t)$. As an empirical rule, such approximation of first-order perturbation is

generally applicable to a single fiber span of several tens to 100 kilometers with optical power per WDM channel not much higher than 10 mW. For systems that consist of tens of spans to reach thousands of kilometers, the nonlinearity within each span has to be controlled at a low level in order to avoid large accumulated nonlinearity of the whole system corrupting optical signals. Indeed, such long-distance transmission systems are often constructed with spans of tens to 100 kilometers in length and carrying approximately 10 mW or less per WDM channel. Even when methods of nonlinear compensation/suppression discussed in this thesis are employed to increase the permissable power by a factor of $2 \sim 5$, the nonlinearity of each fiber span may still be reasonably approximated by the first-order perturbation theory.

4.2.2 *Principles of dispersion compensation using OPC*

Dispersion equalization by OPC may be explained nicely using transfer functions in the frequency domain [77]. Optical signals at a fixed position in a fiber, possibly of many channels wavelength-division multiplexed together, may be described by a total electrical field $E(t) = A(t)\exp(-i\omega_0 t)$, with the parameter z of location omitted. The signals are fully represented by the slow-varying envelope $A(t)$, or equivalently, by the Fourier transform of the envelope $\tilde{A}(\omega) = \mathsf{F}A(t)$. Leaving aside the loss/gain and neglecting the nonlinearities, the linear dispersive effect of a fiber transmission line is described by a multiplicative transfer function,

$$H(\omega) = \exp\left(i\sum_{k=2}^{+\infty}\frac{b_k\omega^k}{k!}\right), \tag{4.21}$$

with

$$b_k = \int \beta_k(z)dz, \quad \forall\, k \geq 2, \tag{4.22}$$

being the dispersions accumulated along the fiber length, and the dispersion parameters $\{\beta_k\}_{k\geq 2}$ being defined as in equation (4.12). A fiber line with such dispersion parameters transforms a signal $\tilde{A}(\omega)$ into $H(\omega)\tilde{A}(\omega)$, while OPC acts as a linear operator that changes the same signal into $\mathsf{OPC}[\tilde{A}(\omega)] = \tilde{A}^*(-\omega)$. Consider two fiber transmission lines that are not necessarily identical, but nevertheless have accumulated dispersions satisfying the conditions,

$$b_k^R = (-1)^k b_k^L, \quad \forall\, k \geq 2, \tag{4.23}$$

so that $H_R(\omega) = H_L(-\omega)$, where the super- and sub-scripts L, R are used to distinguish the two fiber lines on the left and right respectively. When OPC is performed in the middle of the two fiber lines, the entire setup transforms an input signal $\tilde{A}(\omega)$

into,

$$H_R(\omega)\mathrm{OPC}[H_L(\omega)\tilde{A}(\omega)] = H_R(\omega)H_L^*(-\omega)\tilde{A}^*(-\omega) = \tilde{A}^*(-\omega). \qquad (4.24)$$

If $\tilde{A}(\omega)$ is the Fourier transform of $A(t)$, then the output signal $\tilde{A}^*(-\omega)$ corresponds to $A^*(t)$ in the time domain, which is an undistorted replica of the input signal $A(t)$ up to complex conjugation. This proves that the dispersion of a transmission line with OPC in the middle may be compensated over a wide bandwidth, when the dispersion coefficients of the odd orders on the two sides of OPC, b_{2k+1}^L and b_{2k+1}^R with $k \geq 1$, in particular the third-order dispersions b_3^L and b_3^R, are both compensated to zero, or they are exactly opposite to each other, while the even-order dispersion coefficients are the same on both sides. If a link has $b_3^R = -b_3^L$, or even $b_3^R = b_3^L = 0$, then it is compensated at least up to and including the fourth-order dispersion b_4. It is worth pointing out that the center frequency of the signal band may be shifted by the OPC from ω_0^L on the left side to ω_0^R on the right side, $\omega_0^L \neq \omega_0^R$, and the dispersion parameters on the two sides of OPC are defined with respect to the corresponding center frequencies.

4.2.3 *Principles of nonlinear compensation using OPC and STS*

To compensate the nonlinearity of transmission fibers, our method of using STS [12, 13] requires that the conjugating fiber segments have the same sign for the loss/gain coefficients, opposite second-order dispersions, and the same sign for the third-order dispersions. Such conditions are naturally satisfied, at least approximately, in conventional fiber transmission systems, where, for example, an SMF may be paired with a DCF as conjugating counterparts. The symmetry is in the scaled sense, because the lengths of the fibers and the corresponding fiber parameters, including the fiber loss coefficients and dispersions, as well as the Kerr and Raman nonlinear coefficients, are all in proportion, and the proportional ratio may not be 1. The symmetry is translation, because the curves of signal power variation along the fiber keep the similar shape, albeit scaled, when translated from the left to the right side of OPC, as depicted in the bottom graph of Fig. 4.1, so do the curves of any above-mentioned fiber parameter if plotted against the fiber length. The shaded areas in the graph represent two typical fiber segments that are in STS about the phase conjugator. The fundamental discovery is that two fiber lines translation-symmetric about the OPC are able to cancel each other's nonlinearities up to the first-order perturbation. To understand the principle, imagine two fiber lines with opposite nonlinear coefficients but identical linear parameters of dispersion and loss/gain. It turns out that the nonlinear effects of the two are compensated up to the first-order perturbation, when they are used in cascade as shown in Fig. 4.4. The first fiber stretching

from $z = -L$ to $z = 0$ is a real, physical one with parameters $\alpha(z)$, $\{\beta_k(z)\}_{k\geq 2}$, $\gamma(z)$, $g(z,\cdot)$, so that the signal propagation in which is governed by,

$$\frac{\partial A(z,t)}{\partial z} + \sum_{k=2}^{+\infty} \frac{i^{k-1}\beta_k(z)}{k!}\left(\frac{\partial}{\partial t}\right)^k A(z,t) + \frac{\alpha(z)}{2}A(z,t) = i\gamma(z)|A(z,t)|^2 A(z,t) + i\left[g(z,t)\otimes|A(z,t)|^2\right]A(z,t), \tag{4.25}$$

$-L \leq z \leq 0$. The other is a fictitious fiber stretching from $z = 0$ to $z = L$, with parameters $\alpha'(z)$, $\{\beta'_k(z)\}_{k\geq 2}$, $\gamma'(z)$, $g'(z,\cdot)$ satisfying,

$$\alpha'(z) = \alpha(z-L), \tag{4.26}$$

$$\beta'_k(z) = \beta_k(z-L), \quad \forall\, k \geq 2, \tag{4.27}$$

$$\gamma'(z) = -\gamma(z-L), \tag{4.28}$$

$$g'(z,t) = -g(z-L,t), \quad \forall\, t \in (-\infty,+\infty), \tag{4.29}$$

$\forall\, z \in [0,L]$. Note that the fictitious fiber may be unphysical because of the oppositely signed nonlinear coefficients γ' and g' [78, 79]. The signal propagation in this fictitious fiber obeys the following NLSE,

$$\frac{\partial A'(z,t)}{\partial z} + \sum_{k=2}^{+\infty} \frac{i^{k-1}\beta'_k(z)}{k!}\left(\frac{\partial}{\partial t}\right)^k A'(z,t) + \frac{\alpha'(z)}{2}A'(z,t) = i\gamma'(z)|A'(z,t)|^2 A'(z,t) + i\left[g'(z,t)\otimes|A'(z,t)|^2\right]A'(z,t), \tag{4.30}$$

$0 \leq z \leq L$. Fig. 4.5 shows the signal power and dispersion maps in the series of two fiber lines. It is obvious from equations (4.15-4.20) and (4.26-4.29) that the two fiber lines would induce opposite first-order nonlinear distortions to otherwise the same linear signal propagation (zeroth-order approximation), because the two linear propagators $\mathsf{P}(z_1-L, z_2-L)$ and $\mathsf{P}(z_1,z_2)$ are exactly the same, for all $z_1 \in [0,L]$ and all $z_2 \in [z_1,L]$, while the Kerr nonlinear coefficients $\gamma(z-L)$ and $\gamma'(z)$, as well as the Raman coefficients $g(z-L,\cdot)$ and $g'(z,\cdot)$, are exactly opposite-valued, for all $z \in [0,L]$. If the overall dispersion of each fiber line is compensated to zero and the signal loss is made up by linear optical amplifiers, then the same perturbation argument may be applied to the two lines in cascade to show that the fiber nonlinearity is annihilated up to the first-order perturbation. The problem is that an optical fiber with negative nonlinear coefficients may be only fictitious. It does not exist naturally.

For a fictitious fiber of length L and with parameters as those in equation (4.30), the Kerr nonlinear coefficient γ' is negative-valued, and the Raman gain g is reversed, or called "negative" as well [78], in the sense that it induces optical power flow from

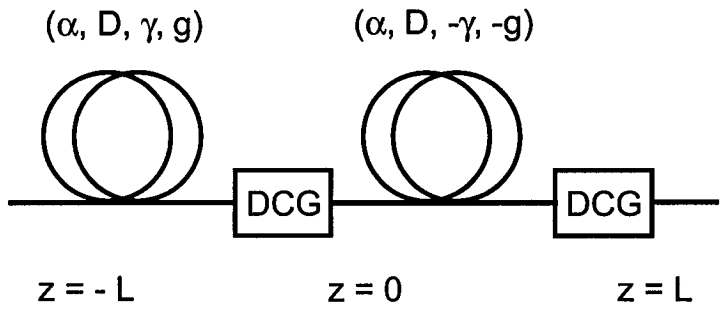

Figure 4.4: The cascade of two fiber lines with opposite nonlinear coefficients but identical linear parameters of dispersion and loss/gain. DCG: dispersion compensation and gain.

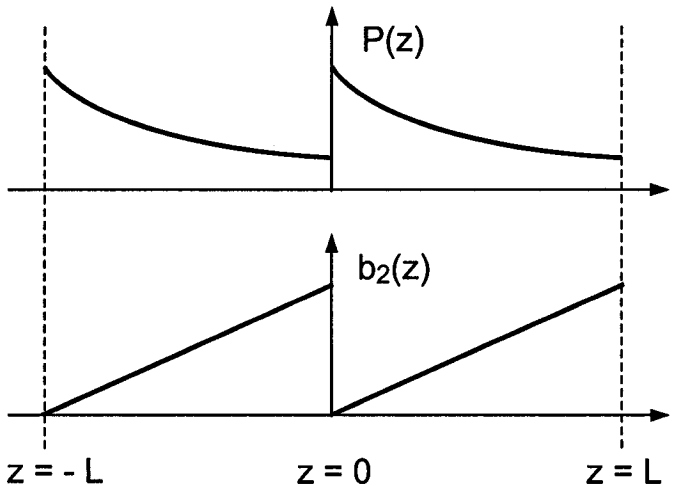

Figure 4.5: The signal power and dispersion maps for a series of two fiber lines with opposite nonlinear coefficients but identical linear parameters of dispersion and loss/gain.

lower to higher frequencies, which obviously will not happen normally. Fortunately, such fictitious fiber may be simulated by an ordinary fiber with the help of OPC, as depicted in Fig. 4.6. An ordinary fiber of length L/R may be found with parameters α'', $\{\beta_k''\}_{k\geq 2}$, γ'', g'' satisfying the following rules of scaling,

$$\alpha''(z) = R\alpha'(Rz), \tag{4.31}$$

$$\beta_k''(z) = (-1)^{k-1} R\beta_k'(Rz), \quad \forall\, k \geq 2, \tag{4.32}$$

$$\gamma''(z) = -Q\gamma'(Rz), \tag{4.33}$$

$$g''(z,t) = -Qg'(Rz,t), \quad \forall\, t \in (-\infty, +\infty), \tag{4.34}$$

$\forall\, z \in [0, L/R]$, where $R > 0$, $Q > 0$ are scaling factors. In this ordinary fiber, the

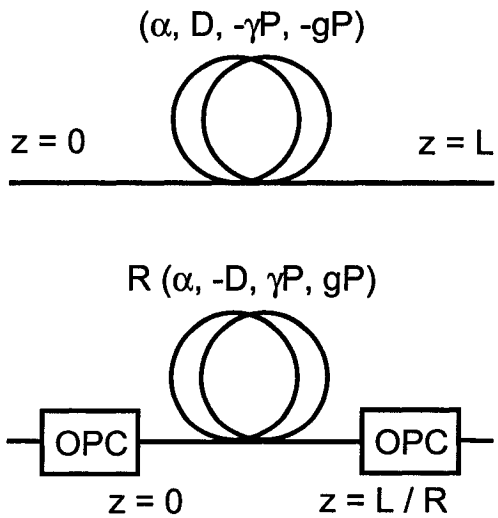

Figure 4.6: The functionality of a fictitious fiber with negative nonlinearities may be realized equivalently by a conventional fiber with positive nonlinearities with the help of OPC.

NLSE of signal propagation is,

$$\frac{\partial A''(z,t)}{\partial z} + \sum_{k=2}^{+\infty} \frac{i^{k-1}\beta_k''(z)}{k!}\left(\frac{\partial}{\partial t}\right)^k A''(z,t) + \frac{\alpha''(z)}{2}A''(z,t) = i\gamma''(z)|A''(z,t)|^2 A''(z,t) + i\left[g''(z,t) \otimes |A''(z,t)|^2\right] A''(z,t), \tag{4.35}$$

$\forall\, z \in [0, L/R]$. That is, with the substitution of parameters according to equations (4.31-4.34),

$$\frac{\partial A''(z,t)}{R\partial z} + \sum_{k=2}^{+\infty} \frac{(-i)^{k-1}\beta_k'(Rz)}{k!}\left(\frac{\partial}{\partial t}\right)^k A''(z,t) + \frac{\alpha'(Rz)}{2}A''(z,t) = - iQR^{-1}\gamma'(Rz)|A''(z,t)|^2 A''(z,t) - iQR^{-1}\left[g'(Rz,t) \otimes |A''(z,t)|^2\right] A''(z,t), \tag{4.36}$$

$\forall\, z \in [0, L/R]$. After a further substitution,

$$A''(z,t) = e^{i\theta}(R/Q)^{1/2}[A'(Rz,t)]^*, \tag{4.37}$$

with $\theta \in \mathbf{R}$ being an arbitrary phase, then a change of variable $Rz \rightarrow z$, and finally taking the complex conjugate of the whole equation, equation (4.36) becomes mathematically identical to equation (4.30). Equation (4.37) is actually the scaling rule for the signal amplitudes. The physical implication is that, if a signal $A'(0,t)$ is injected into the fictitious fiber and the complex conjugate signal $e^{i\theta}(R/Q)^{1/2}[A'(0,t)]^*$

is fed to the ordinary fiber, then the signal at any point $z \in [0, L/R]$ in the ordinary fiber is $e^{i\theta}(R/Q)^{1/2}[A'(Rz,t)]^*$, which is $e^{i\theta}(R/Q)^{1/2}$ times the complex conjugate of the signal at the scaled position Rz in the fictitious fiber. In particular, the output signals are $A'(L,t)$ and $e^{i\theta}(R/Q)^{1/2}[A'(L,t)]^*$ from the fictitious and the ordinary fibers respectively. Except for scaling the signal power by a factor R/Q, the ordinary fiber with two phase conjugators installed at its two ends performs exactly the same dispersive and nonlinear signal transformation as the fictitious fiber. Such equivalence is illustrated in Fig. 4.6. In practice, the phase conjugator at the output end of the ordinary fiber may be omitted, as most applications would not differentiate between a signal and its complex conjugate. Replacing the fictitious fiber with negative nonlinearities in Fig. 4.4 by such scaled ordinary fiber with OPC attached at the input end, one arrives at a nonlinearity-compensating setup using all physical components/devices: an optical phase conjugator in the middle, an ordinary fiber on the left side stretching from $z = -L$ to $z = 0$ with parameters $\alpha(z)$, $\{\beta_k(z)\}_{k\geq 2}$, $\gamma(z)$, $g(z,\cdot)$, and an ordinary fiber on the right side stretching from $z = 0$ to $z = L/R$ with parameters $\alpha''(z)$, $\{\beta_k''(z)\}_{k\geq 2}$, $\gamma''(z)$, $g''(z,\cdot)$. It follows from equations (4.26-4.29) and (4.31-4.34) that the parameters of the two fibers are related as,

$$\alpha''(z) = R\alpha(Rz - L), \tag{4.38}$$

$$\beta_k''(z) = (-1)^{k-1}R\beta_k(Rz - L), \quad \forall\ k \geq 2, \tag{4.39}$$

$$\gamma''(z) = Q\gamma(Rz - L), \tag{4.40}$$

$$g''(z,t) = Qg(Rz - L, t), \quad \forall\ t \in (-\infty, +\infty), \tag{4.41}$$

$\forall\ z \in [0, L/R]$. Equations (4.38-4.41) are called the scaling rules for two fibers to form a translation symmetry in the scaled sense about an optical phase conjugator [12, 13]. In order for two fiber lines in STS to compensate their nonlinearities up to the first-order perturbation, it is further required that the input signals $A(-L,t)$ and $A''(0,t)$ at the beginning of the two fiber lines satisfy the following,

$$A''(0,t) = e^{i\theta}(R/Q)^{1/2}[A(-L,t)]^*, \tag{4.42}$$

where $\theta \in \mathbf{R}$ is an arbitrary phase. Equation (4.42) may be regarded as the scaling rule for the input signals to the fibers.

The analysis suggests that OPC may help to compensate fiber nonlinearities between two transmission lines that are in STS. It should be emphasized that the fiber line on each side of OPC does not necessarily consist of only one fiber span, and the signal intensity does not have to evolve monotonically either. The simple setup used above should only be regarded as an example for illustration and mathematical

convenience. The proposed method of nonlinear compensation works fine when each side of the OPC consists of multiple fiber spans with optical amplifiers in between repeating the signal power. In which case, each fiber on one side should be paired with a scaled translation-symmetric counterpart on the other side, with the parameters and input signals of the fiber pair satisfying the similar scaling rules as in equations (4.38-4.42). Because most fibers do not start or end at $z = 0$ in a transmission line consisting of many spans, the scaling rules for them would be similar to equations (4.38-4.42) but with the position coordinates suitably adjusted. Furthermore, the scaling ratios may vary from one pair of fibers to another. Put in words, *the scaling rules for STSs between pairs of fiber segments require that each pair of fiber segments have the same sign for the loss/gain coefficients, opposite second-order dispersions, the same sign for the third-order dispersions, and the same positive-valued nonlinear coefficients [78]. Moreover, a fiber may have its linear parameters scaled by a common factor and its nonlinear coefficients scaled by another factor, then the length of the fiber may be scaled inversely proportional to the linear parameters, and the signal power may be adjusted accordingly to yield the same strength of nonlinear interactions.* The conditions of "the same sign for loss coefficients and opposite signs for the second-order dispersions" are naturally satisfied by the transmission fibers and DCFs used in conventional transmission systems. Another fact, simple but crucially important for practical applications, is that nonlinear effects are significant only in portions of fibers where the signal power is high. *When scaling fiber parameters and signal amplitudes to have two fiber spans inducing the same or compensating nonlinear effects, it is only necessary to make sure that the scaling rules of equations (4.38-4.41) and (4.42) are fulfilled in portions of fibers experiencing high levels of signal power. Elsewhere, the scaling rules may be loosened or neglected when the signal power is low.* Relaxing the scaling rules in portions of fibers carrying low-power signals makes it much easier to find practical and commercially available fibers with suitable dispersion characteristics to manage the accumulated dispersions of individual spans.

With such scaling of nonlinearities [12, 13], both the Kerr and Raman nonlinearities may be suppressed simultaneously if a proportional relation is maintained between the γ and g parameters as in the scaling rules of equations (4.40) and (4.41). When equations (4.40) and (4.41) can not be fulfilled simultaneously, either the Kerr or the Raman nonlinearity may be primarily targeted for compensation depending upon the actual application. For a translation symmetry between two fibers with opposite dispersions, the scaling rule of equation (4.38) requires the same sign for the loss/gain coefficients of the two fibers, which is a convenient condition to meet by the natural fiber losses. This is in contrast to the mirror symmetry between two fiber segments

that requires an amplifying segment correspond to a lossy one and vice versa. Fibers may be designed and fabricated with the requirements of scaled symmetry taken into consideration. For a given piece of fiber, the loss coefficient may need to be intentionally increased to meet the scaling rule. The extra loss may be induced by, for example, doping the fiber preform with erbium, or transition metals, or other impurities [80, 81], macro-bending [70] the fiber or writing long-period Bragg gratings into the fiber for scattering losses. Macro-bending may be built in a lumped fiber module having the fiber coiled tightly with a suitable radius. Also discrete fiber coils or Bragg gratings for light attenuation may be implemented periodically along the length of a fiber to approximate a continuous uniform loss coefficient. More sophisticatedly, Raman pumps may be employed to induce gain or loss to the optical signals depending upon the pump frequencies being higher or lower than the signal band, so to alter the effective gain/loss coefficient of the fiber. Even though it is rather difficult to change the dispersion of a given fiber, OPC is capable of shifting the center frequency of the signal band, which can fine-tune the effective dispersion at the center of the signal band, so long as the fiber has a non-zero dispersion slope. Even though most fibers are made of similar materials with similar nonlinear susceptibilities, their guided-wave nonlinear coefficients measured in $W^{-1}km^{-1}$ could be quite different due to the wide variation of modal sizes. Unless the ratio of nonlinear coefficients matches the ratio of dispersions, the signal powers in two conjugate fibers may have to differ by several dB as required by the scaling rule of equation (4.42) for STS. Alternatively, by taking advantage of the additivity of the first-order nonlinear perturbations, it is possible to adjust the signal powers in different fiber spans only slightly, such that one span of a highly-nonlinear type may compensate several fiber spans of another type with weaker nonlinearity. This method may be called "one-for-many" (in terms of fiber spans) nonlinearity compensation.

It should be noted that the suitability of compensating nonlinearities among lossy fibers does not exclude the method of translation symmetry from applying to systems with amplifying fibers due to Raman pumping [9, 82, 83, 84, 85] or rare-earth-element doping [10]. The scaled translation-symmetric method applies to these systems equally well, provided that an amplifying fiber is brought into translation symmetry with respect to another fiber with gain. In fact, if two fibers with their intrinsic loss coefficients satisfying the scaling rule of equation (4.38), then the power of the Raman pumps (forward or backward) to them may be adjusted properly to yield effective gain/loss coefficients satisfying the same rule of equation (4.38). In particular, Raman pumped [86, 87, 88] or rare-earth-element-doped [89] DCFs may be conveniently tuned translation-symmetric to Raman pumped or rare-earth-element-doped

transmission fibers. For systems suffering considerable nonlinear penalties originated from long EDFAs [61], the penalties may be largely suppressed by arranging the amplifiers into conjugate pairs with STS about the OPC. The nonlinear and gain coefficients as well as the signal amplitudes in the amplifying fibers should obey the scaling rules. If the dispersions of the amplifying fibers are not negligible, they should be designed to satisfy the scaling rules as well. Finally, it is also necessary to note the limitation of nonlinear compensations using STS. That is, the methods could only compensate the first-order nonlinear interactions among the optical signals. The higher-order nonlinear products are not compensated, nor is the nonlinear mixing between transmitted signals and amplifier noise. The accumulation of uncompensated higher-order nonlinearities and nonlinear signal-noise mixing would eventually upper-bound the amount of signal power permitted in the transmission fibers, so to limit the obtainable signal-to-noise ratio, and ultimately limit the product of data capacity and transmission distance.

4.3 *Dispersion and Nonlinear Compensations w/o OPC*

When there is no optical phase conjugator available, two fiber spans in a translation symmetry may still cancel out their intra-channel nonlinear effects to a large extent, and a proper arrangement of the pairs of translation-symmetric fiber spans could significantly reduce intra-channel nonlinear effects in a long distance transmission line. The intra-channel nonlinear effects, namely, nonlinear interactions among optical pulses within the same wavelength channel, are the dominating nonlinearities in systems with high modulation speeds of 40 Gb/s and above [65], where the nonlinear interactions among different wavelength channels become less-limiting factors. As a result of short pulse width and high data rate, optical pulses within one channel are quickly dispersed and overlap significantly so to interact through the Kerr effect. In the past a few years, intra-channel nonlinearities have been extensively investigated by several research groups [28, 29, 90, 91, 92, 93, 94, 95, 96], and a method has been identified for suppressing the intra-channel nonlinearity-induced jitters in pulse amplitude and timing, using lossless or Raman-pumped transmission lines manifesting a mirror symmetry [28, 29]. As mentioned before, the loss of pump power makes it difficult to maintain a constant gain in a long transmission fiber. Consequently, the significant deviation of signal power variation from a desired mirror-symmetric profile degrades the result of intra-channel nonlinear compensation using mirror symmetry [30]. Nevertheless, we have found that two fiber spans in a STS could cancel out their intra-channel nonlinear effects to a large extent without resorting to OPC, and a sig-

nificant reduction of intra-channel nonlinear effects may be achieved in a multi-span system with translation-symmetric spans suitably arranged.

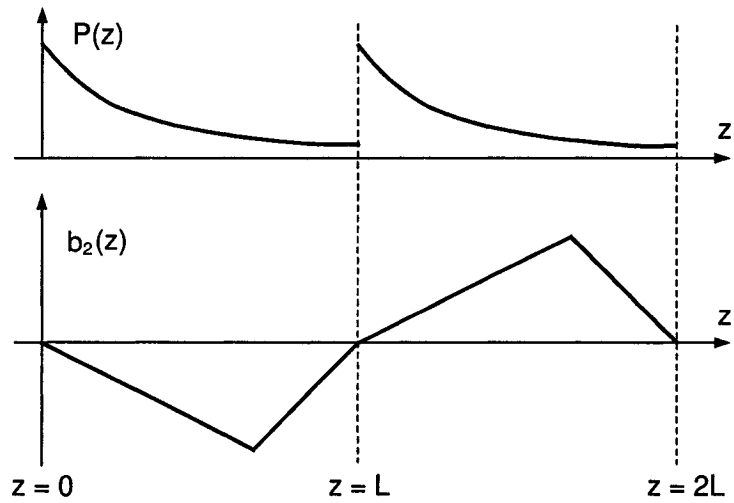

Figure 4.7: The signal power and dispersion maps for a cascade of two fiber spans in scaled translation symmetry with scaling ratio $R = 1$. Top: the variation of signal power along the propagation distance. Bottom: the dispersion map, namely, the variation of accumulated dispersion along the propagation distance.

This time the translation symmetry requires that the corresponding fiber segments have the same sign for the loss/gain coefficients but opposite second- and higher-order dispersions, which are naturally satisfied conditions in conventional fiber transmission systems, where, for example, a transmission fiber may be paired with a DCF as symmetric counterparts. The STS further requires that the fiber parameters should be scaled in proportion and the signal amplitudes should be adjusted to satisfy,

$$\frac{\alpha(z)}{\alpha'(z')} = -\frac{\beta_2(z)}{\beta_2'(z')} = -\frac{\beta_3(z)}{\beta_3'(z')} = \frac{\gamma(z)|A(z,t)|^2}{\gamma'(z')|A'(z',t)|^2} = \frac{z'}{z} = \frac{1}{R}, \tag{4.43}$$

$\forall\ z \in [0, L]$ and $\forall\ t \in (-\infty, +\infty)$, where $\alpha(z)$, $\beta_2(z)$, $\beta_3(z)$, and $\gamma(z)$ denote the loss coefficient, second-order dispersion, third-order dispersion, and Kerr nonlinear coefficient respectively for one fiber stretching from $z = 0$ to $z = L > 0$, while the primed parameters are for the other fiber stretching from $z' = 0$ to $z' = L/R$, $R > 0$ is the scaling ratio, $A(z,t)$ and $A'(z',t)$ are the envelopes of optical amplitude in the two fiber segments respectively, whose initial values at $z = 0$ and $z' = 0$ respectively are required to be complex conjugate,

$$\frac{A^*(z=0,t)}{A'(z'=0,t)} = e^{-i\theta}\left[\frac{\gamma'(z'=0)}{R\gamma(z=0)}\right]^{1/2}, \quad \forall\ t \in (-\infty, +\infty), \tag{4.44}$$

where $\theta \in \mathbf{R}$ is an arbitrary phase. Even though the effect of dispersion slope may be neglected within a single wavelength channel, the inclusion of the β_3-parameters in the scaling rules of equation (4.43) ensures that good dispersion and nonlinear compensations are achieved for each wavelength channel across a wide optical band. When a pair of such fiber segments in STS are cascaded, and the signal power levels are adjusted in accordance with equation (4.43), it may be analytically proved that both the timing jitter and the amplitude fluctuation due to intra-channel nonlinear interactions among overlapping pulses are compensated up to the first-order perturbation of fiber nonlinearity, namely, up to the linear terms of the nonlinear coefficient. Since the dispersive and nonlinear transmission response is invariant under the scaling of fiber parameters and signal amplitudes as in equations (4.43) and (4.44) [13], it is without loss of generality to consider two spans that are in translation symmetry with the ratio $R = 1$ and $\gamma(z = 0) = \gamma'(z' = 0)$. The cascade of such two spans would constitute a transmission line stretching from $z = 0$ to $z = 2L$, with the fiber parameters satisfying,

$$\frac{\alpha(z)}{\alpha(z+L)} = -\frac{\beta_2(z)}{\beta_2(z+L)} = -\frac{\beta_3(z)}{\beta_3(z+L)} = \frac{\gamma(z)}{\gamma(z+L)} = \frac{A^*(0,t)}{A(L,t)} = 1, \tag{4.45}$$

$\forall\, z \in [0, L]$ and $\forall\, t \in (-\infty, +\infty)$. The translation symmetry is illustrated in Fig. 4.7 with plots of signal power and accumulated dispersion along the propagation distance.

It is only necessary to consider the Kerr nonlinearity within one wavelength channel, while the Raman effect may be neglected. The amplitude envelope of a single channel may be represented by a sum of optical pulses, namely, $A(z,t) = \sum_k u_k(z,t)$, where $u_k(z,t)$ denotes the pulse in the kth bit slot and centered at time $t = kT$, with $k \in \mathbf{Z}$ and $T > 0$ being the bit duration. The following NLSE describes the propagation and nonlinear interactions among the pulses [65],

$$\frac{\partial u_k}{\partial z} + \frac{i\beta_2(z)}{2}\frac{\partial^2 u_k}{\partial t^2} + \frac{\alpha(z)}{2}u_k = i\gamma(z)\sum_m\sum_n u_m u_n u^*_{m+n-k}, \quad \forall\, k \in \mathbf{Z}, \tag{4.46}$$

where the right-hand side keeps only those nonlinear products that satisfy the phase-matching condition. The nonlinear mixing terms with either $m = k$ or $n = k$ contribute to self-phase modulation and intra-channel XPM, while the rest with both $m \neq k$ and $n \neq k$ are responsible for intra-channel FWM [65]. It is assumed that all pulses are initially chirp-free or they can be made so by a dispersion compensator, and when chirp-free the pulses $u_k(z = 0, t)$, $k \in \mathbf{Z}$, should all be real-valued. This includes the modulation scheme of binary phase-shift keying, where the relative phases between adjacent pulses are either 0 or π. It is only slightly more general to allow the pulses being modified by arithmetically progressive phase shifts $\phi_k = \phi_0 + k\Delta\phi$,

$k \in \mathbf{Z}$, with $\phi_0, \Delta\phi \in [0, 2\pi)$, because equation (4.46) is invariant under the multiplication of phase factors $\exp(i\phi_k)$ to u_k, $\forall\ k \in \mathbf{Z}$. The linear dependence of ϕ_k on k is in fact equivalent to a readjustment of the frequency and phase of the optical carrier. The pulses may be RZ modulated, and non-return-to-zero (NRZ) modulated as well, for an NRZ signal train is the same as a stream of wide RZ pulses with 100% duty cycle.

Were there no nonlinearity in the fibers, the signal propagation would by fully described by the dispersive transfer function,

$$H(z_1, z_2, \omega) = \exp\left[\frac{i}{2} b_2(z_1, z_2)\omega^2 - \frac{1}{2}\int_{z_1}^{z_2} \alpha(z)dz\right], \tag{4.47}$$

with $z_1, z_2 \in [0, 2L]$ and,

$$b_2(z_1, z_2) \stackrel{\text{def}}{=} \int_{z_1}^{z_2} \beta_2(z)dz, \tag{4.48}$$

or equivalently the corresponding impulse response,

$$h(z_1, z_2, t) = \frac{1}{\sqrt{|b_2(z_1, z_2)|}} \exp\left[-\frac{it^2}{2b_2(z_1, z_2)} - \frac{1}{2}\int_{z_1}^{z_2} \alpha(z)dz\right], \tag{4.49}$$

which is calculated from $\mathsf{F}^{-1}[H(z_1, z_2, \omega)]$ up to a constant phase factor. The impulse response defines a linear propagator $\mathsf{P}(z_1, z_2)$ as in equation (4.18). In reality, the signal evolution is complicated by the Kerr nonlinear effects. Nevertheless, the nonlinearity within each fiber span may be sufficiently weak to justify the application of the first-order perturbation theory:

$$v_k(z, t) = \mathsf{P}(0, z)u_k(0, t), \tag{4.50}$$

$$v'_k(z, t) = i\int_0^z \sum_m \sum_n \mathsf{P}(s, z)\left[\gamma(s)v_m(s, t)v_n(s, t)v^*_{m+n-k}(s, t)\right] ds, \tag{4.51}$$

$\forall\ k \in \mathbf{Z}$, where $u_k(z, t) \approx v_k(z, t)$ is the zeroth-order approximation which neglects the fiber nonlinearity completely, whereas the result of first-order perturbation $u_k(z, t) \approx v_k(z, t) + v'_k(z, t)$ accounts in addition for the nonlinear products integrated over the fiber length. For the moment, it is assumed that both fiber spans are fully dispersion- and loss-compensated to simplify the mathematics. It then follows that $b(0, z + L) = -b(0, z)$, $\int_0^{z+L} \alpha(s)ds = \int_0^z \alpha(s)ds$, $\gamma(z + L) = \gamma(z)$, $\forall\ z \in [0, L]$, and $v_k(L, t) = v_k(2L, t) = u_k(0, t)$, which is real-valued by assumption, $\forall\ k \in \mathbf{Z}$. It further follows that $h(0, z + L, t) = h^*(0, z, t)$, hence $\mathsf{P}(0, z + L) = \mathsf{P}^*(0, z)$ and $\mathsf{P}(z + L, 2L) = \mathsf{P}^*(z, 2L)$, $\forall\ z \in [0, L]$. Consequently, the pulses at z and $z+L$ are complex conjugate, namely, $v_k(z + L, t) = v^*_k(z, t)$, $\forall\ k \in \mathbf{Z}$, $\forall\ z \in [0, L]$. A typical term of nonlinear

mixing,

$$\begin{aligned}
&\int_0^{2L} \mathsf{P}(z,2L)\left[\gamma(z)v_m(z,t)v_n(z,t)v^*_{m+n-k}(z,t)\right]ds \\
&= \int_0^{L} \mathsf{P}(z,2L)\left[\gamma(z)v_m(z,t)v_n(z,t)v^*_{m+n-k}(z,t)\right]ds \\
&\quad + \int_L^{2L} \mathsf{P}(z,2L)\left[\gamma(z)v_m(z,t)v_n(z,t)v^*_{m+n-k}(z,t)\right]ds \\
&= \int_0^{L} \mathsf{P}(z,2L)\left[\gamma(z)v_m(z,t)v_n(z,t)v^*_{m+n-k}(z,t)\right]ds \\
&\quad + \int_0^{L} \mathsf{P}^*(z,2L)\left[\gamma(z)v^*_m(z,t)v^*_n(z,t)v_{m+n-k}(z,t)\right]ds, \qquad (4.52)
\end{aligned}$$

is therefore real-valued. It follows immediately that the first-order nonlinear perturbation $v'_k(2L,t)$ is purely imaginary-valued, which is in quadrature phase with respect to the zeroth-order approximation $v_k(2L,t) = v_k(0,t)$, $\forall\ k \in \mathbf{Z}$. When the span dispersion is not fully compensated, namely, $b_2(0,L) \neq 0$, the input pulses to the first span at $z = 0$ should be pre-chirped by an amount of dispersion equal to $-\frac{1}{2}b_2(0,L)$, so that the input pulses to the second span at $z = L$ are pre-chirped by $\frac{1}{2}b_2(0,L)$ as a consequence. In other words, the input signals to the two spans should be oppositely chirped. Under this condition, the equation $v_k(z+L,t) = v^*_k(z,t)$, $\forall\ z \in [0,L]$, $\forall\ k \in \mathbf{Z}$ is still valid, so are the above argument and the conclusion that v_k and v'_k are real- and imaginary-valued respectively when brought chirp-free.

Mathematically, that v_k and v'_k are in quadrature phase implies $|u_k|^2 = |v_k + v'_k|^2 = |v_k|^2 + |v'_k|^2$, where $|v'_k|^2$ is quadratic, or of second-order, in terms of the Kerr nonlinear coefficient. This fact has significant implications to the performance of a transmission line. Firstly, it avoids pulse amplitude fluctuations due to the in-phase beating between signal pulses and nonlinear products of intra-channel FWM, which could seriously degrade the signal quality if not controlled [28, 65, 91, 96]. The quadrature-phased nonlinear products due to intra-channel FWM lead to the generation of "ghost" pulses in the "ZERO"-slots [90, 93, 94] and the addition of noise power to the "ONE"-bits. As second-order nonlinear perturbations, these effects are less detrimental. Secondly, it eliminates pulse timing jitter due to intra-channel XPM up to the first-order nonlinear perturbation. The (remaining) second-order nonlinear effects may be quantified by estimating the energy of the signals $\{v'_k\}_{k\in\mathbf{Z}}$, which are generated by nonlinear interactions and accumulated through the transmission line. It follows from equation (4.51) that the energy content of a nonlinearly generated pulse at $z = 2L$ is,

$$\int_{-\infty}^{+\infty} |v'_k(2L,t)|^2 dt$$

$$= \int_{-\infty}^{+\infty} \left| \int_0^{2L} \sum_m \sum_n \mathsf{P}(z, 2L) \left[\gamma(z) v_m(z,t) v_n(z,t) v^*_{m+n-k}(z,t) \right] dz \right|^2 dt$$
$$= \gamma_{\max}^2 P_0^3 L^2 T C(0, 2L), \tag{4.53}$$

where $\gamma_{\max} \stackrel{\text{def}}{=} \max\{\gamma(z) \mid 0 \le z \le 2L\}$, P_0 is the average optical power out of the transmitter, and $C(0, 2L)$ is an integration constant,

$$C(0, 2L) \stackrel{\text{def}}{=} \tag{4.54}$$
$$\int_{-\infty}^{+\infty} \left| \int_0^{2L} \sum_m \sum_n \mathsf{P}(z, 2L) \left[\gamma(z) v_m(z,t) v_n(z,t) v^*_{m+n-k}(z,t) \right] \gamma_{\max}^{-1} P_0^{-3/2} L^{-1} dz \right|^2 T^{-1} dt,$$

which depends on the detailed maps of dispersion and loss/gain coefficient of the transmission line under consideration, but is invariant under scaling of pulse power.

Given the dispersion and power maps of a transmission line, the integration constant $C(0, 2L)$ may be evaluated either analytically or numerically, such that the energy of nonlinear pulses may be accurately calculated. To serve our purpose here, it is sufficient to grasp the asymptotic behavior of $\int_{-\infty}^{+\infty} |v'_k(2L, t)|^2 dt$, $k \in \mathbf{Z}$. Using the "big-O" notation [97], (4.53) may be nicely represented as,

$$\int_{-\infty}^{+\infty} |v'_k(2L, t)|^2 dt = P_0 T \times O\left(\gamma_{\max}^2 P_0^2 L^2\right), \quad \forall\, k \in \mathbf{Z}, \tag{4.55}$$

while the energy content of an original pulse is,

$$\int_{-\infty}^{+\infty} |v_l(0, t)|^2 dt = \tfrac{1}{2} P_0 T, \tag{4.56}$$

for any lth data slot that is not empty, so long as the data stream is balanced, namely, the ZERO- and ONE-bits are equal in probability. It is clear from equations (4.55) and (4.56) that the energy of ghost pulses and fluctuations of ONE-bits are second-order infinitesimals comparing to the nominal energy of a ONE-bit, when $\gamma_{\max} P_0 L$ is small. Using the moment method [28, 91], the time of arrival for the center of the kth pulse, if it is a ONE-bit, may be calculated as,

$$\langle t \rangle_k = \frac{\int_{kT-T/2}^{kT+T/2} t |u_k|^2 dt}{\int_{kT-T/2}^{kT+T/2} |u_k|^2 dt} = kT + \frac{\int_{kT-T/2}^{kT+T/2} (t - kT) \left(|v_k|^2 + |v'_k|^2 \right) dt}{\int_{kT-T/2}^{kT+T/2} \left(|v_k|^2 + |v'_k|^2 \right) dt}$$
$$= kT + \frac{\int_{kT-T/2}^{kT+T/2} (t - kT) |v_k|^2 dt + O(T) \int_{kT-T/2}^{kT+T/2} |v'_k|^2 dt}{\left[1 + O\left(\gamma_{\max}^2 P_0^2 L^2\right) \right] \int_{kT-T/2}^{kT+T/2} |v_k|^2 dt}$$
$$= kT + O\left(\gamma_{\max}^2 P_0^2 L^2\right) T, \quad \forall\, k \in \mathbf{Z}. \tag{4.57}$$

The timing jitter $O\left(\gamma_{\max}^2 P_0^2 L^2\right) T$ is a second-order infinitesimal when $\gamma_{\max} P_0 L$ is small. It is noted that the bound of timing jitter in equation (4.57) is derived from energy calculations, which holds true regardless of the pulse shapes of the original and nonlinear signals.

5

Advantages, Limitations, Other Technologies

5.1 *Advantages and Limitations, Comparison to Other Technologies*

Distributed nonlinear compensations are advantaged approaches that are not only theoretically (mathematically) tractable and elegant but also convenient to implement in practice, as the physical requirements may be fulfilled by practical transmission fibers, DCFs, and other specialty fibers. Based on nonlinear Schrödinger equations that describe dispersive and nonlinear signal propagation in optical fibers, it is convenient to analyze the propagation effects of short segments fibers, in particular the compensation of such effects between two segments in conjugation, to identify conditions, and to optimize fiber parameters for best nonlinear compensations. Our methods of distributed nonlinear compensations with scaled symmetries suggest to use recently available specialty fibers with dispersion, dispersion slope or higher order-dispersions, and loss/gain coefficients proportional to those of transmission fibers, where for a mirror symmetry in the scaled sense, a specialty fiber needs to be erbium-doped or Raman pumped to be amplifying and conjugate to a lossy transmission fiber. Apart from the generality of our mathematical derivations ensuring wide applicability, another distinctive feature of our proposals is that the physical implementations are enabled by fiber components and technologies that are either already commercially available, practically installed, or at least becoming available soon. In particular, a translation symmetry in the scaled sense makes it possible to compensate nonlinearity of transmission fibers without requiring an amplifying fiber as conjugate to each lossy transmission fiber. Eliminating the necessity of distributive amplification renders the methods directly applicable to conventional transmission systems consisting of transmission fibers and DCFs. Even without optical phase conjugation, scaled translation symmetries, as well as scaled mirror symmetries, are capable to suppress the so-called intra-channel nonlinear effects.

Distributed nonlinear compensations are rather suitable for new designs and instal-

lations of fiber transmission systems, or upgrading installed systems without DCMs at the sites of optical amplifiers, where types of fibers and their arrangement may be optimally chosen to form proper symmetries in the scaled sense. One major shortcoming of distributed nonlinear compensations is that the applications are inconvenient, or limited, in installed fiber plants with fixed fibers and arrangements that are not configured in accordance with scaled symmetries, where integrated, or lumped compensations may be better suited. Another limitation comes from stochastic and often time-varying polarization variations of optical signals, which lead to PMD, polarization-dependent loss (PDL), and polarization-dependent nonlinear interactions. It should be noted though, that such polarization-related effects are not specific to distributed nonlinear compensations, rather, the same polarization effects also impose challenges to lumped compensators. PMD and PDL are linear effects, which may impose non-negligible limitations to systems using high-speed modulations of 40 Gb/s and above. Fortunately, advanced techniques of fabrication and assembly could drastically reduce such linear polarization-related impairments in fibers, optical amplifiers, optical filters, and optical switches. Furthermore, for systems suffering significant PMD, especially those using legacy fiber plants and high-speed modulations, dynamic (optical) PMD compensators have been developed or are under development [98, 99, 100, 101, 102] to mitigate the effects of pulse broadening and crosstalk due to PMD. By using low-PMD transmission fibers and possibly optical PMD compensators, it may be possible and practical to control the random polarization-dependent effects, such that the differential group delay (DGD) between the two principal states of polarization (PSPs) [103, 104] is always small comparing to the duration of a single optical pulse. Consequently, the two polarization components of each optical pulse stay pretty close to each other, and the optical pulse remains approximately the same as an energy packet. However, nonlinear interactions among optical signals are polarization-discriminating, namely, the nonlinear coupling coefficients for signals with different combinations of polarization states may be different [5, 6, 103, 105]. So the stochastic rotations of polarization states of different wavelength channels due to random fiber birefringence make the nonlinear interactions among optical channels stochastic in nature, and may limit the extent and effectiveness of controlled nonlinear compensations between pairs of fiber spans. Even within one wavelength channel or a few adjacent channels, where the relative polarization states of all signals remain the same, the random birefringence and polarization-dependence of nonlinear coupling generate nonlinear products that are not "parallel" to the original signals in terms of polarization states, which may also limit the effectiveness of controlled nonlinear compensations between pairs of fiber spans. Nonlinear signal propagation and

distributed nonlinear compensations under random birefringence will be discussed in greater details shortly. Here, it may be worthwhile to mention another method of distributed nonlinear compensations proposed by Tsang and Psaltis [106], which tries to compensate fiber nonlinearity and dispersions of all orders by using *spectral* phase conjugation, as opposed to *temporal* phase conjugation used in ours and previous proposals. Specifically, for an optical signal represented by a slow varying envelope $A(z = z_0, t)$ with the corresponding Fourier transform $\tilde{A}(z_0, \omega) \stackrel{\text{def}}{=} \mathsf{F}[A(z_0, t)]$, a temporal phase conjugator at $z = z_0$ transforms the signal into $A^*(z_0, t)$ with the corresponding Fourier transform $\tilde{A}^*(z_0, -\omega)$, whereas a spectral phase conjugator at $z = z_0$ transforms the signal into $A^*(z_0, -t)$ with the corresponding Fourier transform $\tilde{A}^*(z_0, \omega)$. The great advantage of using spectral phase conjugation is that dispersions of any orders, both even and odd, may be compensated simultaneously. One serious drawback is that a spectral phase conjugator is difficult to implement. An operation of spectral phase conjugation, equivalent to time reversal with complex conjugation, is only possible for signals within a finite (usually rather narrow) window of time. A continuous data stream has to be segmented into periodic time slots with guard bands in between, and spectral phase conjugation needs to be performed before optical pulses breach adjacent time windows due to GVD-induced pulse broadening and walk-off among WDM channels. It appears rather difficult to spectrally phase-conjugate multiple WDM channels simultaneously.

Apart from distributed methods, there have been proposals of nonlinear compensations using lumped, or integrated signal processors, which may be either optical, based on fiber and other nonlinear optical devices, or electrical, based on semiconductor IC chips. Watanabe *et al.* [17, 18] have actually built an integrated optical nonlinear compensator consisting of multiple short fiber segments and amplifiers corresponding to a long-distance transmission system based on DSFs. Pare *et al.* [107] proposed to compensate for the dispersion and Kerr nonlinearity using a semiconductor waveguide with a large negative nonlinear coefficient. Gabitov and Lushnikov [108] suggested to compensate the effects of nonlinear transmission fibers using negative nonlinearity generated by a nonlinear optical interferometer. Besides the apparent that lumped compensators use integrated nonlinear devices that do not contribute to the transmission distance, another essential characteristic of lumped nonlinear compensations is that they do not seek to arrange a whole transmission system into any scaled symmetry and to have paired differential fiber segments compensating each other, rather, they attempt to equalize the lumped nonlinear transfer functionals of two sub-systems. In this regard, Minzioni *et al.*'s proposal [109] to optimally place an optical phase conjugator in a fixed transmission line, often not co-located with an

optical amplifier, may be better viewed as a method of lumped nonlinear compensation. However, the proposed optimization is overly constrained by not changing any system configuration and operation condition but only varying the position of the phase conjugator, and thus unable to best equalize the lumped nonlinear transfer functionals. As a consequence, the achievable improvement of transmission performance is only marginal [109]. Recent advancements in digital signal processing (DSP) IC chips have made it possible to digitally process the data stream of a wavelength channel at 10, 20, and even 40 Gb/s, once it is down-converted coherently to the electrical domain or before the data stream is up-converted to the optical domain [110, 111, 112, 113, 114, 115]. Up to now, such semiconductor DSP compensators have mainly demonstrated lumped dispersion compensations, although it is readily conceivable that such DSP approaches may be extended to the realm of nonlinear signal processing, so to achieve lumped nonlinear compensations. To that end, however, the DSP IC chips have to be able to cope with the much increased complexity associated with both dispersive and nonlinear transfer functionals. Furthermore, such complexity grows drastically and rapidly, following a square law, when the essential bandwidth of a data stream increases, due to either an increase of modulation speed or joint signal processing of multiple WDM channels.

A lumped nonlinear compensator, whether optical or electrical, is an integrated device installed at either the transmission or the receiving end of a point-to-point link, which has to be tailor-made for the specific transmission line. The result is a lack of flexibility: an installed nonlinear compensator may cease to work when the corresponding transmission line is altered; it may be prohibitively costly and labor-intensive to design and optimize a special nonlinear compensator for each transmission line. Moreover, an optical lumped nonlinear compensator may be difficult to fabricate: due to the other uncooperative aspect of optical nonlinearity, it is often a challenge to generate enough nonlinearities in a lumped nonlinear compensator using short segments of fibers or other nonlinear waveguides. For electrical lumped nonlinear compensators using DSP IC chips, some flexibility may be accommodated by their programmability. However, it is quite an effort to have such electronics to keep up with the high and increasing speed of optical data. Also, programming the DSP chips for different fiber links, or reprogramming them to accommodate changes of transmission lines or routing paths, could induce extra costs or time delay in network availability. And, an installed electronic processor may become obsolete, when its corresponding channel changes line rate or modulation format. At a fundamental level, lumped nonlinear compensations would require an efficient representation for a lumped nonlinear transfer functional and an efficient algorithm calculating such transfer functional of

a given dispersive and nonlinear system, as well as an efficient method implementing a desired nonlinear transfer functional using a fixed set of operational blocks, which may be either physical such as dispersive components and nonlinear devices for optical compensators, or numerical such as fast Fourier transform (FFT), multiplication of frequency-dependent phase factors, and nonlinear DSP operations, for electronic compensators. Nonlinear transfer functionals may be represented by Volterra series [75, 76], and there have been discussions of using such series to describe the dispersive and nonlinear responses of fiber channels [116, 117, 118, 119]. However, it remains to be a highly complicated computational task to calculate a Volterra series for a given fiber transmission line with known physical parameters. Much worse is to "learn" the nonlinear transfer functional of a "black-box" transmission system with all physical parameters not known, which is a problem of nonlinear system identification. After the transfer functional of a nonlinear system being computed or learned, a following problem is to calculate the best "inverse" transfer functional that should be realized by a lumped compensator for the nonlinear system. Interestingly, the viewpoint of distributed nonlinear compensations may be useful for this problem, that is, a fictitious distributed nonlinear compensator may be constructed mathematically, which forms a scaled symmetry with respect to the system to be compensated and hence optimally undoes the dispersive and nonlinear signal propagation, then a Volterra series may be computed for the fictitious distributed compensator, which would be the best inverse to the lumped transfer functional of the system to be compensated. At last, it has not been addressed, and may be an interesting research topic, to answer questions as what is theoretically the minimum complexity of a nonlinear transfer functional with respect to a given set of operational blocks, and how to practically build a lumped nonlinear compensator using the least number of operational blocks in the given set.

5.2 *Polarization Effects and Vectorial Nonlinear Schrödinger Equations*

In Chapter 3, we have assumed that all optical signals are co-linearly polarized, based on which a scalar slow-varying envelope may be used to represent the signals, and NLSEs of scalar envelopes have been derived to describe the dispersive and nonlinear propagation of signals in fiber transmission lines. The NLSEs serve as the bases of our mathematical derivations and analyses of distributed nonlinear compensations using scaled symmetries. In reality, all input WDM signals may not be co-linearly polarized, even if initially they are, the polarization state of each WDM channel

would rotate randomly (on the so-called Poincaré sphere), and the polarization states of different WDM channels would gradually walk off, due to random birefringence in optical fibers, unless the fibers are polarization-maintaining. Furthermore, different polarization components of the same wavelength channel may travel at different speeds, leading to DGD, which is the lowest order, and often dominating, effect of PMD. Removing the assumption of all signals being co-linearly polarized, and using a two-component slow-varying envelope $(A_x, A_y)^T$ to represent the arbitrarily polarized optical signals, but keeping other assumptions and making the same (or similar) mathematical approximations, one could follow the same procedures in Chapter 3 to derive the following vectorial NLSE [5, 103],

$$\begin{aligned}\frac{\partial A_x}{\partial z} + \beta_{1x}(z)\frac{\partial A_x}{\partial t} - i\mathsf{D}_x(z)A_x + \frac{\alpha_x(z)}{2}A_x - i\kappa(z)A_y\exp[+i\phi(z)] \\ = i\gamma(z)\left(|A_x|^2 + \tfrac{2}{3}|A_y|^2\right)A_x + i\gamma(z)\tfrac{1}{3}A_x^*A_y^2\exp[+i2\phi(z)], \qquad (5.1)\\ \frac{\partial A_y}{\partial z} + \beta_{1y}(z)\frac{\partial A_y}{\partial t} - i\mathsf{D}_y(z)A_y + \frac{\alpha_y(z)}{2}A_y + i\kappa^*(z)A_x\exp[-i\phi(z)] \\ = i\gamma(z)\left(|A_y|^2 + \tfrac{2}{3}|A_x|^2\right)A_y + i\gamma(z)\tfrac{1}{3}A_y^*A_x^2\exp[-i2\phi(z)], \qquad (5.2)\end{aligned}$$

where x and y are orthogonal axes that may be arbitrarily chosen but globally fixed, the α, $\{\beta_k\}_{k\geq 0}$, and D parameters/operators are subscripted by either x or y to indicate the association with the corresponding polarization component, $\kappa(z)$ is a random coefficient of coupling between the two polarization modes,

$$\phi(z) \stackrel{\text{def}}{=} \int^z [\beta_{0y}(\zeta) - \beta_{0x}(\zeta)]d\zeta, \qquad (5.3)$$

is the accumulated phase walk-off between the two polarizations. The vectorial NLSE may be simplified as,

$$\begin{aligned}\frac{\partial A_x}{\partial z} + \beta_{1x}(z)\frac{\partial A_x}{\partial t} - i\mathsf{D}_x(z)A_x + \frac{\alpha(z)}{2}A_x - i\kappa(z)A_y\exp[+i\phi(z)] \\ = i\gamma(z)\left(|A_x|^2 + \tfrac{2}{3}|A_y|^2\right)A_x, \qquad (5.4)\\ \frac{\partial A_y}{\partial z} + \beta_{1y}(z)\frac{\partial A_y}{\partial t} - i\mathsf{D}_y(z)A_y + \frac{\alpha(z)}{2}A_y + i\kappa^*(z)A_x\exp[-i\phi(z)] \\ = i\gamma(z)\left(|A_y|^2 + \tfrac{2}{3}|A_x|^2\right)A_y, \qquad (5.5)\end{aligned}$$

when PDL is negligible so that $\alpha_x(z) = \alpha_y(z) \equiv \alpha(z)$, and the effective length of nonlinear interactions is much longer than the birefringence beat length so that the integration of the last FWM term in (5.1) and (5.2) vanishes [105].

Another model or viewpoint of random fiber birefringence, possibly more pertinent to the physical reality and more suitable for computer simulations, does not take a

globally fixed coordinate (x, y), rather, it assumes that the principle polarization axes of the fiber rotates randomly but continuously and the strength of local birefringence is a random variable. However, the model may employ a rotating coordinate system that follows the continuous rotation of the principle polarization axes of the fiber, such that the local axes appear to be invariant and are always labeled by x and y, and the random fiber birefringence is incorporated by a continuous unitary rotation of the polarization states of signals. For numerical simulations, the model may be discretized and reduces to a split-step model, which mimics a randomly birefringent fiber by repeating the following steps,

A) random but unitary rotation of signal polarization states:

$$\begin{bmatrix} A_x \\ A_y \end{bmatrix} \rightarrow \begin{bmatrix} u & v \\ -v^* & u^* \end{bmatrix} \begin{bmatrix} A_x \\ A_y \end{bmatrix} = \begin{bmatrix} uA_x + vA_y \\ u^*A_y - v^*A_x \end{bmatrix}, \tag{5.6}$$

where u and v are random complex numbers independent of the input polarization state $(A_x, A_y)^T$ and satisfying $|u|^2 + |v|^2 = 1$; for a fiber segment of length Δz and centered at z, u and v may be related to the mode coupling coefficient $\kappa(z)$ in equations (5.4) and (5.5) as $u = [1 - |\kappa(z)\Delta z|^2]^{1/2}$, $v = i\kappa(z)\Delta z$;

B) nonlinear and birefringent propagation:

$$\frac{\partial A_x}{\partial z} + \frac{i\Delta\beta}{2}A_x = i\gamma\left(|A_x|^2 + \tfrac{2}{3}|A_y|^2\right)A_x, \tag{5.7}$$

$$\frac{\partial A_y}{\partial z} - \frac{i\Delta\beta}{2}A_y = i\gamma\left(|A_y|^2 + \tfrac{2}{3}|A_x|^2\right)A_y, \tag{5.8}$$

where $\beta_{0y}(z) - \beta_{0x}(z) \equiv \Delta\beta$, and $\gamma(z) \equiv \gamma$, are constants within each such step;

C) linear dispersive and lossy propagation:

$$\frac{\partial A_x}{\partial z} - i\mathsf{D}_x A_x + \frac{\alpha}{2}A_x = 0, \tag{5.9}$$

$$\frac{\partial A_y}{\partial z} - i\mathsf{D}_y A_y + \frac{\alpha}{2}A_y = 0, \tag{5.10}$$

where $\mathsf{D}_{x,y}(z) \equiv \mathsf{D}_{x,y}$, and $\alpha(z) \equiv \alpha$, are constants within each step.

5.3 *Effectiveness of Nonlinear Compensations under Stochastic Polarization Variations*

When estimating the strength of nonlinear interactions and calculating the amount of nonlinear distortions in a given fiber transmission line, our model of co-linear polarization for all WDM channels leads to a overly pessimistic (upper-bound) estimation [2, 103], as nonlinear interactions are the most efficient when all signals are co-polarized. However, when analyzing the performance of distributed nonlinear compensations, the model of co-linear polarizations tends to be overly optimistic comparing to what is achievable practically, because uncontrollable random birefringence spoils a perfect scaled symmetry between two compensating fiber segments. A straightforward solution to this problem is to use PM fibers throughout a system, and to have PM fibers forming scaled symmetries for matched nonlinear compensations. Such PM transmission systems would not only be amenable to well controlled nonlinear compensations, but also completely solve the problem of PMD-induced random pulse broadening, and further double the capacity per fiber conveniently by means of polarization multiplexing [120, 121, 122, 123, 124, 125, 126].

However, most optical fibers currently available and in use are not of the PM type. Despite all the efforts of maintaining the circular symmetry during the fabrication process, actual non-PM fiber products are always blemished by small but random deviations from an ideal circular waveguide, and often perturbed by random stress and bending. Such deviations and perturbations cause random birefringence hence random coupling between the polarization modes. The manifestations are random rotations of polarization states of different WDM channels and even different frequency components of the same wavelength channel, as well as random walk-offs in time between different polarization components. The resulted linear pulse broadening may be controlled by using low-PMD fibers and and/or installing dynamic PMD compensators [98, 99, 100, 101, 102] along a transmission line. To achieve distributed nonlinear compensations, the DGD between the two PSPs have to be kept always much smaller than the duration of a single optical pulse. Still, the effectiveness of distributed nonlinear compensations may be seriously limited by the stochastic rotations of polarization states due to random fiber birefringence, which in conjunction with the polarization-dependence of fiber nonlinearities [5, 6, 103, 105] makes the nonlinear interactions among optical signals essentially stochastic processes, that might not be well compensated using a fixed, deterministic setup. Nevertheless, our previous formulations and analyses based on the assumption co-linear polarizations should be well applicable to wavelength channels individually and WDM systems with high

modulation speeds and/or wavelength channels widely separated, where intra-channel nonlinear interactions dominate, because the degree of polarization of an individual channel is preserved even after a significant distance of propagation in spite of random rotations, which is more so when soliton transmissions are used [51, 122, 124]. In the model of principle states [102, 103, 127], the first-order and dominating PMD response of a fiber transmission line may be described as the propagation of two orthogonal principle states at different group velocities, where the orthogonality between the two principle states are maintained from the beginning throughout the transmission line. The DGD between the two principle states broadens optical pulses, which however may be controlled using first-order PMD compensators.

It may be expected that distributed nonlinear compensations could perform fairly well even in dense WDM systems based on two considerations. Firstly, the polarization states of adjacent channels with small wavelength separations may rotate synchronously under perturbations of small and random fiber birefringence, such that their relative polarizations, parallel, orthogonal or anything in between, remain the same for a significant transmission distance, beyond which higher-order PMD compensators capable of processing multiple wavelength simultaneously may be employed to readjust the polarization states [98, 101, 102]. Secondly, the polarization-sensitive Kerr nonlinearities among WDM channels, manifested as inter-channel FWM and XPM, die out fast when the channel separation increases, whereas the stimulated Raman coupling between two channels, though strongly polarization-dependent, is effective only if the frequency separation is sufficiently large, much over 1 THz [2, 6]. The relative polarizations of largely separated channels are quickly randomized, such that the Kerr and Raman interactions may be well described by NLSEs with effective (averaged) coefficients [6, 103].

Within one wavelength channel, even though the relative polarization states of all signals remain the same, the random birefringence and polarization-dependence of nonlinear interactions generate nonlinear products that are not parallel to the original signals in terms of polarizations, in contrast to the perfect alignment of the original and nonlinear polarizations predicted by the NLSEs assuming co-linear polarizations and neglecting random fiber birefringence. For two actual fiber segments in a scaled symmetry but each with random and independent birefringence, how well they could match and compensate each other's nonlinear effects may be estimated by a lower-bound of the degree of parallelism between the original and nonlinear polarizations in each segment under random birefringence. In the split-step model discussed previously, the non-parallelism between linear and nonlinear polarizations, also referred as "nonlinear birefringence", is generated in a typical B) step, where a

random input field vector may be,

$$\mathbf{E}(0,t) = \begin{bmatrix} A_x(0,t) \\ A_y(0,t) \end{bmatrix} = A(0,t) \begin{bmatrix} \cos\theta \exp(-i\phi/2) \\ \sin\theta \exp(+i\phi/2) \end{bmatrix}, \tag{5.11}$$

with $\theta \in [0,\pi]$, $\phi \in [0,2\pi)$ being random angles. The statistics of (θ,ϕ) is not of much concern, rather, it is sought to obtain a worst-case estimation of the parallelism between the linear and nonlinear polarizations. The output of the B) step may be approximated as,

$$\begin{aligned} \mathbf{E}(\Delta z,t) &= \mathbf{E}_{\text{lin}}(\Delta z,t) + i\gamma\Delta z\mathbf{E}_{\text{non}}(\Delta z,t) \\ &\stackrel{\text{def}}{=} \begin{bmatrix} A_{0x}(\Delta z,t) \\ A_{0y}(\Delta z,t) \end{bmatrix} + i\gamma\Delta z \begin{bmatrix} A_{1x}(\Delta z,t) \\ A_{1y}(\Delta z,t) \end{bmatrix}, \end{aligned} \tag{5.12}$$

where

$$\mathbf{E}_{\text{lin}}(\Delta z,t) = \begin{bmatrix} A_{0x}(\Delta z,t) \\ A_{0y}(\Delta z,t) \end{bmatrix} = A(0,t) \begin{bmatrix} \cos\theta \exp(-i\varphi/2) \\ \sin\theta \exp(+i\varphi/2) \end{bmatrix}, \tag{5.13}$$

with $\varphi \stackrel{\text{def}}{=} \phi + \Delta\beta\Delta z$, and

$$\begin{aligned} \mathbf{E}_{\text{non}}(\Delta z,t) &= \begin{bmatrix} A_{1x}(\Delta z,t) \\ A_{1y}(\Delta z,t) \end{bmatrix} \\ &= |A(0,t)|^2 A(0,t) \begin{bmatrix} \left(\cos^2\theta + \frac{2}{3}\sin^2\theta\right)\cos\theta\exp(-i\varphi/2) \\ \left(\sin^2\theta + \frac{2}{3}\cos^2\theta\right)\sin\theta\exp(+i\varphi/2) \end{bmatrix} \\ &= |A(0,t)|^2 A(0,t) \begin{bmatrix} \left(\frac{2}{3} + \frac{1}{3}\cos^2\theta\right)\cos\theta\exp(-i\varphi/2) \\ \left(\frac{2}{3} + \frac{1}{3}\sin^2\theta\right)\sin\theta\exp(+i\varphi/2) \end{bmatrix}. \end{aligned} \tag{5.14}$$

The parallelism between $\mathbf{E}_{\text{non}}$ and $\mathbf{E}_{\text{lin}}$ may be quantified by calculating the cosine of the "angle" between the two vectors,

$$\begin{aligned} \cos\angle(\mathbf{E}_{\text{lin}},\mathbf{E}_{\text{non}}) &\stackrel{\text{def}}{=} \frac{\mathbf{E}_{\text{lin}}^{+}\cdot\mathbf{E}_{\text{non}}}{|\mathbf{E}_{\text{lin}}|\cdot|\mathbf{E}_{\text{non}}|} \\ &= \frac{\left(\frac{2}{3} + \frac{1}{3}\cos^2\theta\right)\cos^2\theta + \left(\frac{2}{3} + \frac{1}{3}\sin^2\theta\right)\sin^2\theta}{\sqrt{\left(\frac{2}{3} + \frac{1}{3}\cos^2\theta\right)^2\cos^2\theta + \left(\frac{2}{3} + \frac{1}{3}\sin^2\theta\right)^2\sin^2\theta}} \\ &= \frac{1 - \frac{1}{6}\sin^2 2\theta}{\sqrt{1 - \frac{11}{36}\sin^2 2\theta}}, \end{aligned} \tag{5.15}$$

which is in general less than but always close to 1 as shown in Fig. 5.1, indicating high parallelism. It may be concluded that, for each individual wavelength channel,

so long as the DGD is always controlled well under the bit duration and higher-order PMD effects are negligible, two fiber segments in a scaled symmetry would well compensate each other nonlinearly even under the effect of random birefringence, with the intrinsic error due to nonlinear birefringence upper-bounded by 0.5%. This may explain the experimentally observed excellent performances of distributed nonlinear compensations even under unavoidable random birefringence in actual fibers [17, 18, 20, 24, 25].

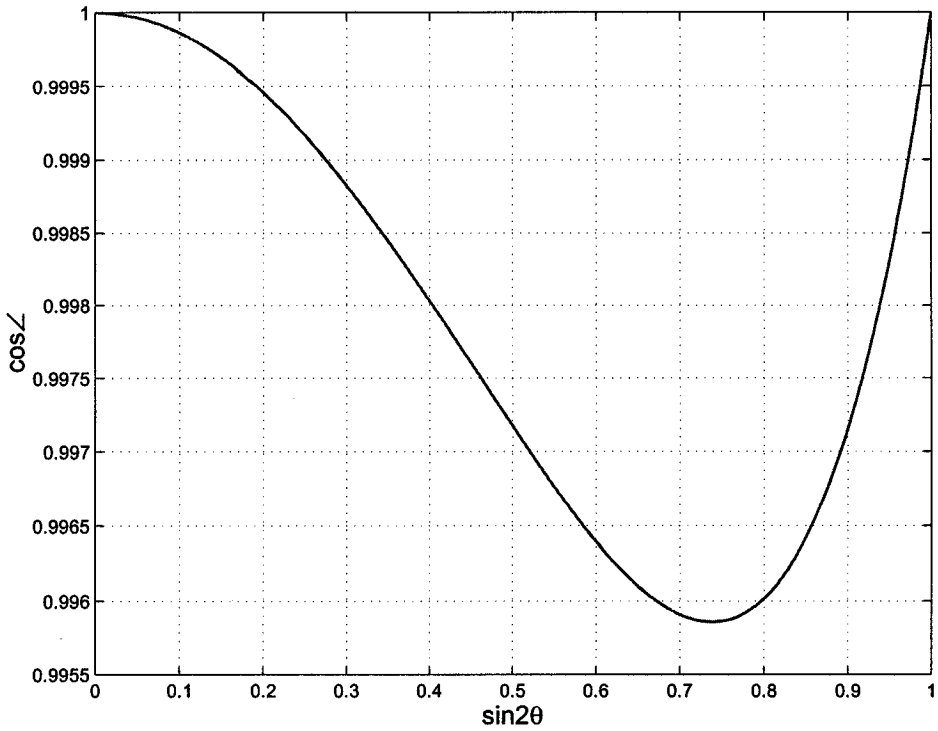

Figure 5.1: Degree of parallelism between $\mathbf{E}_{\text{non}}$ and $\mathbf{E}_{\text{lin}}$ as θ varies.

Part III. Practice: Applications, Implementations, and Verifications

6

Practical Nonlinear Compensation Using STS

6.1 Optimal STS Setups of Fiber Transmission Lines

Having established the basic principles of dispersion equalization and nonlinear compensation using OPC and STS, we shall now discuss practical designs of fiber systems for long-distance transmissions, with realistic (commercially available) DCFs and transmission fibers that are optimally configured according to the basic principles of simultaneous compensation of dispersion and nonlinearity. A long-distance transmission line may consist of many fiber spans, each of which may have transmission and dispersion-compensating fibers. Two fibers with opposite (second-order) dispersions may be tuned translation-symmetric to each other about a phase conjugator. For optimal nonlinear compensation, the fiber parameters and the signal amplitudes should be adjusted to meet the conditions of translation symmetry, often approximately, not exactly, because of the dispersion slopes [13]. In particular, if one fiber span has a positive-dispersion (+D) fiber followed by a negative-dispersion (-D) fiber, then the counterpart span has to place the -D fiber before the +D fiber, in order to achieve an approximate translation symmetry between the two fiber spans. Even though the +D and -D fibers are usually made of similar materials with similar nonlinear susceptibilities, their guided-wave nonlinear coefficients measured in $W^{-1}km^{-1}$ could be quite different due to the wide variation of modal sizes. Unless the ratio of nonlinear coefficients matches the ratio of dispersions, the signal powers in two conjugate fibers may have to differ by several dB as required by the scaling rule of equation (4.42) for STS.

Should it be desired to have a similar level of signal powers into the nonlinearity-compensating +D and -D fibers, one may adjust the signal powers in the +D and -D fibers only slightly, such that one span of a type with stronger nonlinearity generates an amount of nonlinearity that is equivalent to an integral multiple of the amount of nonlinearity generated in one span of another type with weaker nonlinearity. If each span with weaker nonlinearity is dispersion-compensated to have approximately zero accumulated dispersion, then each of several such spans in cascade may indeed induce

approximately the same nonlinear response. And for a reasonably small number of such cascaded spans with weaker nonlinearity, the overall nonlinear response may still be well approximated by a combined first-order perturbation, which is just the sum of the first-order perturbations of individual spans. Then one may take advantage of the additivity of the first-order perturbations and have one span of the type with stronger nonlinearity to compensate several spans of the other type with weaker nonlinearity. This method is called one-for-many nonlinear compensation. More generally, it is possible to have several spans of the type with weaker nonlinearity generating different amounts of nonlinearity, still their combined nonlinearity may be compensated by one span of the type with stronger nonlinearity, so long as all nonlinearities remain perturbative and the first-order perturbation of the span with stronger nonlinearity is equivalent to the sum of the first-order perturbations of the spans with weaker nonlinearity.

When two fiber spans are translation-symmetric about an optical phase conjugator, one span is called the translation conjugate to the other about the OPC. As discussed in Chapter 4, OPC is able to equalize dispersion terms of even orders. So the two parts of a transmission line with OPC in the middle should have the same amount of b_2 and b_4 but exactly opposite b_3, or both have $b_3 = 0$, where the b-parameters are defined as in equation (4.22). In a more restrictive implementation, each fiber span consists of +D and -D fibers with the total dispersion slope compensated to zero. The +D and -D fibers in each span need not to match their dispersions and slopes simultaneously. It is sufficient to fully compensate b_3, while leaving residual even-order terms b_2 and b_4. Two conjugate spans would be configured as +D followed by -D fibers and -D followed by +D fibers respectively. The two conjugate spans may not be exactly the same in length, and they may have different integrated dispersion terms of the even orders. The two types of fiber spans may be mixed and alternated on each side of the OPC, so that the two sides have the same total b_2 and b_4. Transmission lines with such dispersion map are convenient to plan and manage. However, it is worth noting that the present method of simultaneous compensation of dispersion and nonlinearity applies to other dispersion maps as well, where the period of dispersion compensation may be either longer [65] or shorter [128] than the amplifier spacing, or the fiber spans may vary widely in length and configuration. Regardless of the dispersion map, wide-band dispersion compensation could be achieved in a transmission line with middle-span OPC so long as the dispersion terms of the two sides of OPC satisfy equation (4.23), and pairs of conjugate fiber spans could have their nonlinearities canceled up to the first-order perturbation as long as the scaling rules of equations (4.38-4.41) and (4.42) are well observed.

As a result of power loss, the nonlinear response of a long piece of fiber becomes insensitive to the actual fiber length so long as it far exceeds the effective length [2] defined as $L_{\text{eff}} = 1/\alpha$, where α is the loss coefficient in units of km^{-1} (instead of dB/km). So fiber spans consisting of the same types of fibers but with different lengths could contribute the same amount of nonlinearity if the input powers are the same. That all fiber spans contribute the same nonlinearity makes it possible for various spans with different lengths to compensate each other's nonlinear effects. It is straightforward to extend the same argument to fiber spans with scaled parameters and signal powers. The conclusion is that scaled fiber spans could induce approximately the same amount of nonlinear distortion to optical signals, which is insensitive to the varying span lengths, provided that the length of each fiber span is much longer than its own effective length defined by the inverse of the loss coefficient. The main advantage is that the fiber spans may be arbitrarily paired for nonlinear compensation regardless of their actual lengths. This is good news to terrestrial and festoon systems, where the span-distance between repeaters may vary according to the geographical conditions. When the dispersion of each fiber span is not fully compensated, it is desirable to fine-tune (slightly elongate or shorten) the lengths of transmission fibers or DCFs such that all spans have the same amount of residual dispersion. As a consequence, fiber spans of different lengths and possibly consisting of different types of fibers become truly equivalent in two all-important aspects of signal propagation: nonlinearity and accumulated dispersion. Certainly, if the above-mentioned method of one-for-many nonlinear compensation is employed, the residual dispersion of the highly nonlinear span should also be multiplied by the same integer factor. Last but not least, when scaling fiber parameters and signal amplitudes to have two fiber spans inducing the same or compensating nonlinear effects, it is only necessary to make sure that the scaling rules of equations (4.38-4.41) and (4.42) are fulfilled in portions of fibers experiencing high levels of signal power. Elsewhere, the scaling rules may be loosened or neglected when the signal power is low.

Despite the translation symmetry between the constituent fibers of two conjugate spans, it is advantageous to order many conjugate spans in a mirror-symmetric manner about the OPC, especially when all the spans are not identical. The local nonlinearity within each span is usually weak such that the nonlinear perturbations of higher orders than the first may be neglected, even though a strong nonlinearity may be accumulated through many fiber spans. Within the applicability of first-order perturbation for approximating the nonlinearity of each fiber span, it may be argued using mathematical induction that the nonlinearity of multiple spans in cascade is also compensated up to the first-order perturbation, because of the mirror-symmetric

arrangement of fiber spans about the OPC. The spans may be labeled from left to right by $-N, \cdots, -2, -1, 1, 2, \cdots, N$, with OPC located between span -1 and span 1. And one may denote by z_0 and z_0' the beginning and end positions of the section of OPC, while labeling the beginning and end points of span n by z_n and z_n', where $z_n' = z_{n+1}$, $\forall\ n \in [-N, N-1]$. There may be three variations for a mirror-symmetric configuration of pairs of fiber spans in STS, depending upon whether the dispersion in each span is compensated to zero, and if not, how the dispersion is managed. In the first case, all spans are compensated to zero dispersion, as shown in Fig. 6.1 for the case of $N = 3$. It is required that, $\forall\ n \in [1, N]$, spans $-n$ and n should be conjugate, that is translation-symmetric, to each other. The first-order nonlinear perturbations of spans 1 and -1 cancel each other due to the translation symmetry and the OPC, so the optical path from z_{-1} to z_1' is equivalent to an ideal linear transmission line with OPC in the middle, if higher-order nonlinear perturbations are neglected. It follows that the signal input to span 2 at z_2 is approximately the complex conjugate of that input to span -2 at z_{-2}, apart from the nonlinear perturbation due to span -2. So the translation symmetry between spans 2 and -2 about the OPC annihilates their nonlinearities up to the first-order perturbation. Using mathematical induction, assuming that the optical path from z_{-n} to z_n', $1 < n < N$, is equivalent to an ideal linear transmission line with OPC in the middle, then spans $n+1$ and $-n-1$ see input signals at z_{n+1} and z_{-n-1} that are approximately complex conjugate to each other, so their first-order nonlinear effects cancel each other out due to the translation symmetry and OPC. The optical path from z_{-n-1} to z_{n+1}' is linearized and equivalent to an ideal linear transmission line with OPC in the middle. This inductive argument applies as long as the accumulation of nonlinear perturbations of higher-orders than the first is still negligible and the nonlinear mixing of amplifier noise into signal hasn't grown significantly.

In the second case, the fiber spans may have non-zero residual dispersion, as shown in Fig. 6.2 for the case of $N = 3$. It is required that, $\forall\ n \in [1, N]$, spans $-n$ and n should be in a translation symmetry approximately, while the residual dispersion of span $n-1$ should be approximately the same as span $-n$, $\forall\ n \in [2, N]$. Pre- and post-dispersion compensators are employed to equalize the residual dispersion. The pre-dispersion may set the total dispersion to zero immediately before OPC, and a dispersion conditioner at the site of OPC ensures that the signal input to span 1 is approximately the complex conjugate of that input to span -1, apart from the nonlinear perturbation due to span -1. Fig. 6.2 shows a dispersion conditioner placed immediately after OPC, with the amount of dispersion equal to the residual dispersion in span -1. The three thicker line segments in the dispersion map represent

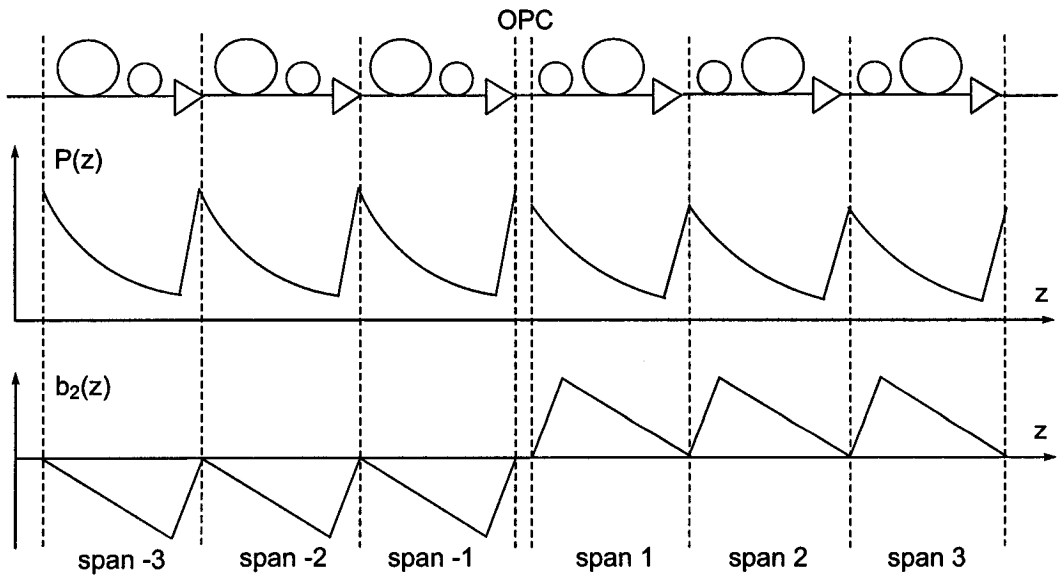

Figure 6.1: A mirror-symmetric configuration of pairs of fiber spans in scaled translational symmetry, with the dispersion in each span compensated to zero. Top: schematic arrangement of fibers and amplifiers with respect to OPC. Middle: map of signal power $P(z)$ along the propagation distance z. Bottom: map of accumulated dispersion $b_2(z)$ along the propagation distance z.

the effects of the pre- and post-dispersion compensators as well as the dispersion conditioner. So the transmission line has been designed such that the accumulated dispersions from z_{-n} to z_n, $n \in [1, N]$, are fully compensated by virtue of OPC, and for each $n \in [1, N]$, the fiber span from z_{-n} to z'_{-n} is translation-symmetric to the fiber span from z_n to z'_n, namely, the parameters of the two fiber spans satisfy the scaling rules of equations (4.38-4.41), at least approximately. Leaving aside the fiber nonlinearity, such dispersion map ensures that the optical signals at z_{-n} and z_n are complex conjugate to each other, then the signal amplitudes may be properly scaled such that equation (4.42) is also satisfied. As a result, all conditions are fulfilled for the fiber spans from z_{-n} to z'_{-n} and from z_n to z'_n to compensate their fiber nonlinearities up to the first-order perturbation, for each $n \in [1, N]$. The first-order nonlinear perturbations of spans 1 and -1 cancel each other due to the translation symmetry and OPC, so the optical path from z_{-1} to z'_1 is equivalent to an ideal linear transmission line with OPC in the middle and some accumulated dispersion at z'_1 due to span 1. Since this amount of dispersion is equal to that of span -2, the signal input to span 2 at z_2 is approximately the complex conjugate of that input to span -2 at z_{-2}, apart from the nonlinear perturbation due to span -2. So the translation symmetry between spans 2 and -2 about the OPC annihilates their nonlinearities

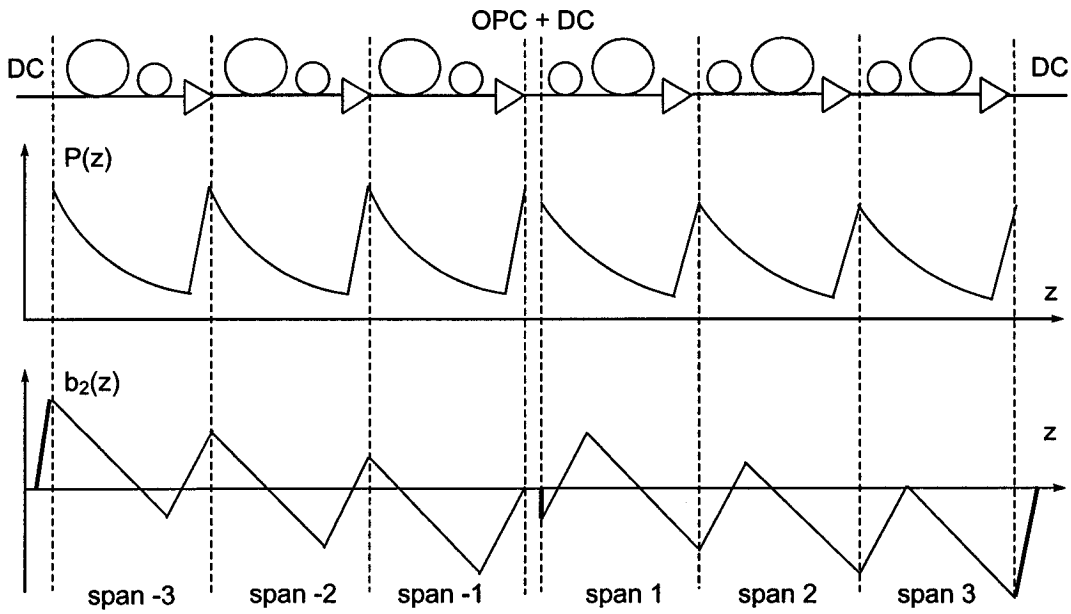

Figure 6.2: A mirror-symmetric configuration of pairs of fiber spans in scaled translational symmetry, with non-zero residual dispersion in the spans. There are pre- and post-dispersion compensators (DCs), as well as a dispersion conditioner immediately after OPC. Top: schematic arrangement of fibers and amplifiers with respect to OPC. Middle: map of signal power $P(z)$ along the propagation distance z. Bottom: map of accumulated dispersion $b_2(z)$ along the propagation distance z.

up to the first-order perturbation. Using mathematical induction, assuming that the optical path from z_{-n} to z'_n, $1 < n < N$, is equivalent to an ideal linear transmission line with OPC in the middle and accumulated dispersion at the right end due to span n, which is the same amount of residual dispersion as of span $-n-1$, then spans $n+1$ and $-n-1$ see input signals at z_{n+1} and z_{-n-1} that are approximately complex conjugate to each other, so their first-order nonlinear effects cancel each other out due to the translation symmetry and OPC. The optical path from z_{-n-1} to z'_{n+1} is linearized and equivalent to an ideal linear transmission line with OPC in the middle and the dispersion of span $n+1$ at the right end. In the third case, the fiber spans still have non-zero residual dispersion, but there is no dispersion conditioner placed immediately before or after OPC to compensate the residual dispersion of span -1. Instead, span 1 may play the role of the dispersion conditioner, and $\forall\, n \in [1, N]$, spans n and $-n$ need to have the same amount of residual dispersion, while spans n and $-n+1$, $\forall\, n \in [2, N]$, should be in an STS approximately to have their nonlinearities compensated up to the first-order perturbation. This is in contrast to the requirement of the second case. The configuration is shown in Fig. 6.3 for the case of $N = 3$, where the two thicker line segments in the dispersion map represent the effects of the pre- and

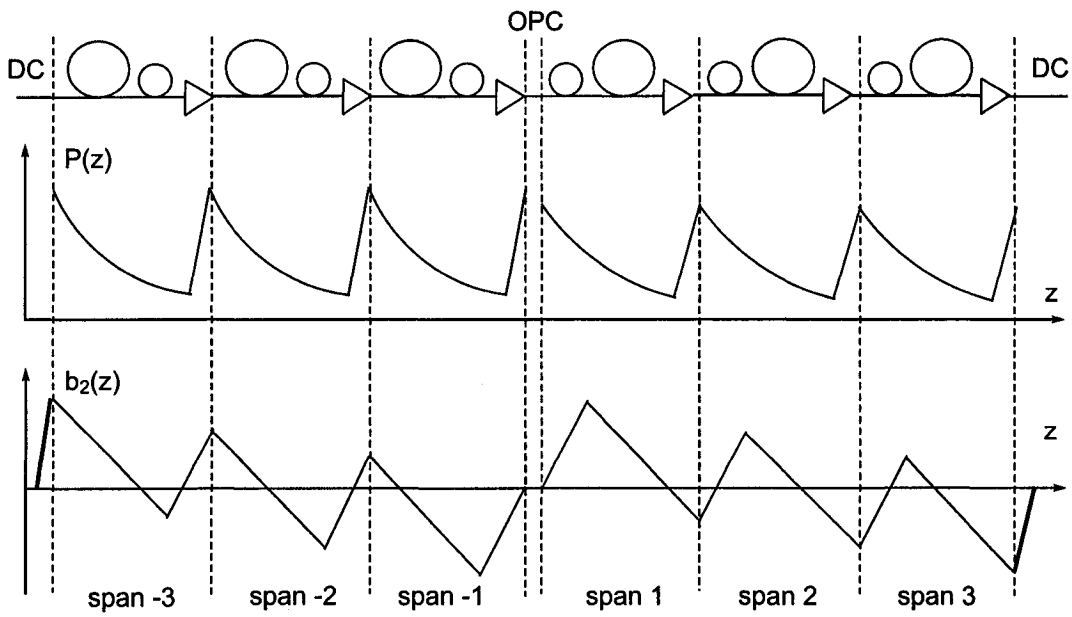

Figure 6.3: A mirror-symmetric configuration of pairs of fiber spans in scaled translational symmetry, with non-zero residual dispersion in the spans. There are pre- and post-dispersion compensators (DCs) but no dispersion conditioner at the site of OPC. Top: schematic arrangement of fibers and amplifiers with respect to OPC. Middle: map of signal power $P(z)$ along the propagation distance z. Bottom: map of accumulated dispersion $b_2(z)$ along the propagation distance z.

post-dispersion compensators. It may be shown using the same inductive argument that the transmission line is largely linearized, except that the nonlinear effects of spans 1 and $-N$, if any, are left uncompensated.

6.2 *Practical Examples of STS Designs Using Commercial Fibers*

DCFs are widely used in modern fiber-optic transmission systems. A DCF may be coiled into a compact module at the amplifier site, or cabled as part of the transmission line. The performance of both types of DCFs has been greatly improved recently. There are now low-loss DCFs capable of (approximately) slope-matched dispersion compensation for various transmission fibers with different ratios of dispersion to dispersion-slope [3, 4], although there are always residual second-order and fourth-order dispersions after the slope is equalized [129, 130, 131]. For SMFs, namely standard single-mode fibers, the ratio of dispersion ($D \approx 16$ ps/nm/km @1550 nm) to dispersion slope ($S \approx 0.055$ ps/nm^2/km @1550 nm) is large, so that the relative change of dispersion is small across the signal band (≈ 40 nm in the C-band). The

so-called RDFs, namely reverse dispersion fibers, are designed to compensate simultaneously the dispersion and dispersion slope of the SMFs. An RDF is not an ideal translation conjugate to an SMF, because their dispersion slopes do not obey the scaling rule of equation (4.39). However, their dispersions satisfy the corresponding scaling rule of equation (4.39) approximately, with only small deviations across the entire signal band (C or L). Therefore, a span having an SMF followed by an RDF on the left side of OPC may be brought into a translation symmetry, approximately, to a span having an RDF followed by an SMF on the right side of OPC, and vice versa. The two types of spans may be denoted by SMF+RDF and RDF+SMF respectively. The indication is that OPC may be installed in the middle of conventional transmission lines with no or minimal modifications to achieve simultaneous wide-band dispersion compensation and nonlinear suppression. The only requirements are that the signal power levels should be properly set in the fiber spans, and the SMFs/RDFs should be suitably arranged, to meet the scaling rules of equations (4.38-4.41) and (4.42) approximately for the translation symmetry between each pair of conjugate fiber spans, and to order the conjugate pairs of spans mirror-symmetrically about the OPC. It is noted that a recent paper [23] has independently proposed the combination of slope-matching DCF and OPC to suppress simultaneously the third-order dispersion and sideband instability due to fiber nonlinearity. However, the work [23] was limited to a single-channel system, considered only the suppression of sideband instability as an intra-channel nonlinear effect, and did not recognize the importance of scaling the nonlinearity (especially the signal power) in different fibers. By contrast, our method applies to wide-band WDM systems as well and is capable of suppressing both intra- and inter-channel nonlinear interactions, being them Kerr- or Raman-originated. Most importantly, we emphasize the importance of the scaling rules of equations (4.38-4.41) and (4.42) for optimal nonlinear compensation.

Several NZDSFs, namely non-zero dispersion-shifted fibers, have also been developed for long-distance high-capacity transmissions. These fibers have reduced but non-zero dispersions across the operating band (C or L). Depending upon the sign of the dispersion (D in units of ps/nm/km), there are positive NZDSFs (+NZDSFs) and negative NZDSFs (-NZDSFs), but their dispersion-slopes are always positive. It becomes possible to bring a +NZDSF and a -NZDSF into a nearly perfect translation symmetry [132], because their oppositely signed dispersions and positively signed dispersion-slopes meet the exact requirements of the scaling rules of equation (4.39). The dispersion-slope of the NZDSFs may be compensated by negative-slope DCFs. The DCFs do not have to (could not indeed) compensate the dispersion and dispersion-slope simultaneously for both the positive and negative NZDSFs. It is suf-

ficient to equalize the accumulated dispersion-slope to zero on each side of the OPC, then the two sides may cancel their accumulated non-zero dispersions of the second and the fourth orders through OPC. To form a nonlinearity-compensating translation symmetry between a +NZDSF span and a -NZDSF span, the accumulated dispersion should be properly managed to ensure that the input signals to the +NZDSF and -NZDSF fibers are complex conjugate to each other, which is a necessary condition for nonlinear cancelation. As long as these requirements are satisfied, there is really no limit as to how much residual (second-order) dispersion may be accumulated in each fiber span as well as on each side of the OPC. It may be difficult to find a fiber translation-symmetric to the slope-compensating DCF, because of its high negative dispersion-slope. However, we note that it is only necessary to have an STS formed between portions of fibers carrying high signal power, elsewhere, such as in the slope-compensating DCFs, the scaling rules may be neglected when the signal power is low and the nonlinearity is insignificant. If the slope-compensating DCFs are cabled, they may be placed near the end of fiber spans where the signal power is low. Or if the DCFs are coiled into modules and co-located with the amplifiers, the signal power inside may be controlled at a low level to avoid nonlinearity. To minimize the noise-figure penalty in such DCF modules, the DCF may be distributively Raman pumped [86, 9, 87, 88], or earth-element doped and distributively pumped [10], or divided into multiple segments and power-repeated by a multi-stage EDFA. The conclusion is that the method of OPC-based simultaneous compensation of dispersion and nonlinearity is perfectly suitable for transmission systems employing NZDSFs, and highly effective nonlinear suppression may be expected in such systems due to the nearly perfect translation symmetry between the +NZDSFs and -NZDSFs. Finally, in the limit of vanishing (second-order) dispersion at the center of the signal band, the +NZDSF and -NZDSF converge to the same DSF, that is dispersion-shifted fiber, which is translation-symmetric to itself. Two identical DSF spans on the two sides of OPC are in perfect translation symmetry to cancel their nonlinearity up to the first-order perturbation. Again the dispersion-slope may be equalized by a DCF with negative dispersion-slope, and the residual second-order dispersion may be arbitrarily valued. Suppressing fiber nonlinearity happens to be highly desired in DSF-based transmission lines, as DSFs are arguably the most susceptible to nonlinear impairments [2].

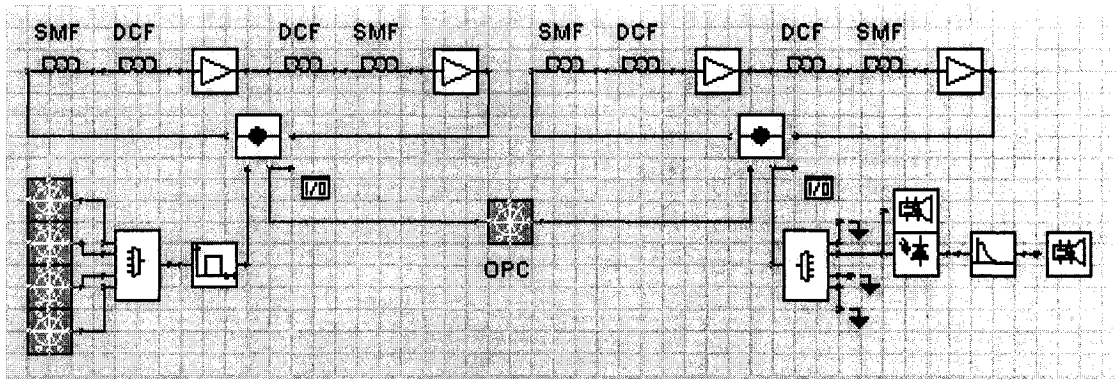

Figure 6.4: A transmission line consisting of SMFs and slope-matching DCFs.

6.3 Simulation Results and Discussions

To verify the proposed method of simultaneous compensation of dispersion and nonlinearity, we have carried out a series of numerical simulations using a commercial transmission simulator (VPItransmissionMaker^{TM}, Virtual Photonics Inc.). Reference [13] has presented an example of SMFs and DCF modules with nearly perfect match of dispersion and slope. Here we consider a practical setup of SMFs and cabled DCFs with residual dispersion, as shown in Fig. 6.4. One type of span consists of 50 km SMF followed by 50 km DCF. The SMF has loss coefficient $\alpha = 0.2$ dB/km, effective mode area $A_{\text{eff}} = 80\ \mu\text{m}^2$, and dispersion parameters $\beta_2 = -20.5$ ps^2/km, $\beta_3 = 0.12$ ps^3/km at 193.1 THz. The corresponding dispersion $D = 16$ ps/nm/km and slope $S = 0.055$ ps/nm^2/km. The DCF mimics a commercial RDF product [131], namely a reverse dispersion fiber, with parameters $(\alpha', A'_{\text{eff}}, \beta'_2, \beta'_3) = (0.2, 30, 18, -0.12)$, in the same units as for the SMF. The Kerr nonlinear index of silica $n_2 = 2.6 \times 10^{-20}$m^2/W. Practical DCFs often have a loss coefficient that is slightly higher than the SMFs, so the optimal design of the DCFs would have a dispersion $|D_{\text{DCF}}|$ slightly higher than $|D_{\text{SMF}}|$ proportionally according to the scaling rules of equations (4.38) and (4.39). The conjugate span has 40 km DCF followed by SMF of the same length. Due to the smaller modal area, a lower power is injected into the DCF to generate the compensating nonlinearity, in accordance with the scaling rule for signal amplitudes in equation (4.42). The shortened span length is to balance the noise figure between the two types of spans. The two span types are also intermixed on each side of the OPC to balance the residual dispersions. Alternatively, all fiber spans may be the same in length, but the signal power injected to the DCF+SMF spans should be 3/8 of that injected to the SMF+DCF spans, and the DCF+SMF spans would add more noise to the optical signal than the SMF+DCF spans. It is noted that the scaling rules are

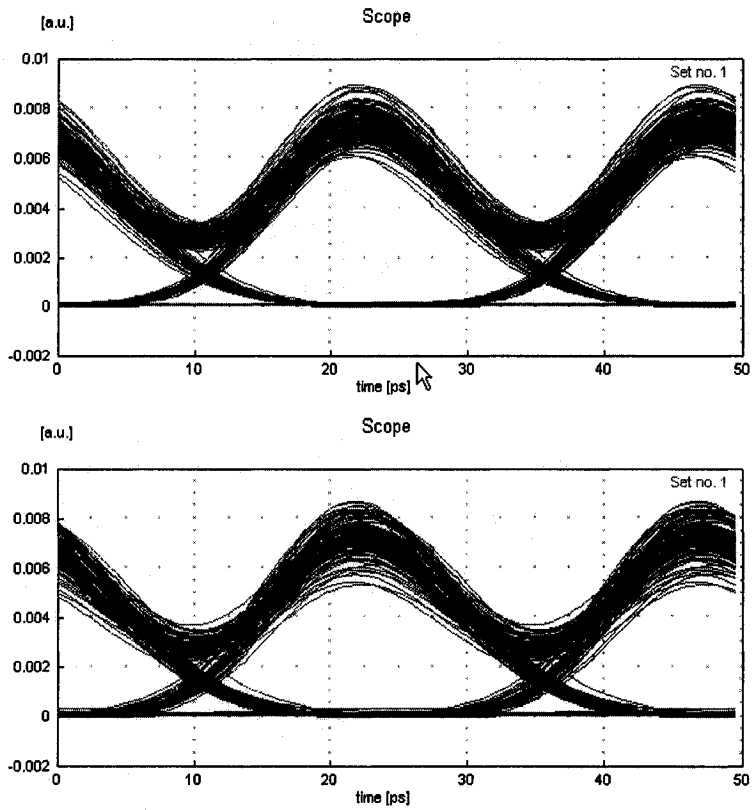

Figure 6.5: Received eye diagrams of the 2nd DEMUX channel using the setup of Fig. 6.4. Top: fiber nonlinearity is OFF, the signal is only impaired by amplifier noise. Bottom: fiber nonlinearity is ON, the signal distortion is only increased slightly.

not obeyed at all in the second part of each span, that is, in the DCFs of SMF+DCF spans and in the SMFs of DCF+SMF spans. Fortunately, the second part of each span experiences low signal power, in which the nonlinear effect is negligible. Back to the setup of Fig. 6.4, where all EDFAs have the same noise figure of 5 dB, each fiber loop recirculates five times, that gives 1000 km worth of fiber transmission on each side of the OPC. The inputs are four 40 Gb/s WDM channels, RZ modulated with peak power 20 mW, channel spacing 200 GHz. The RZ pulses have a duty cycle of 33%, as described in section 4.1.2. The optical multiplexer (MUX) and demultiplexer (DEMUX) consist of Bessel filters of the 7th order with 3dB bandwidth 80 GHz. The input data are simulated by pseudo random binary sequences of order 7, and the simulation time window covers 256 bits. The photo-detector is with responsivity 1.0 A/W and thermal noise 10.0 pA/$\sqrt{\text{Hz}}$. The electrical filter is 3rd order Bessel with 3dB bandwidth 28 GHz. Fig. 6.5 shows the received eye diagrams of the second channel out of the DEMUX. The bottom diagram shows the effect of nonlinear

compensation. For comparison, the top diagram shows the result of a fictitious transmission where no fiber has any nonlinear effect. To confirm that the suppression of nonlinearity is indeed due to the translation symmetry of conjugate spans about the OPC, two diagrams in Fig. 6.6 show simulation results of altered configurations: one setup has the same length of 50 + 50 km and the same input power level to both the SMF+DCF and the DCF+SMF spans, the other has on both sides of OPC identical 100-km SMF+DCF spans carrying the same signal power. Both altered setups suffer from severe nonlinear impairments.

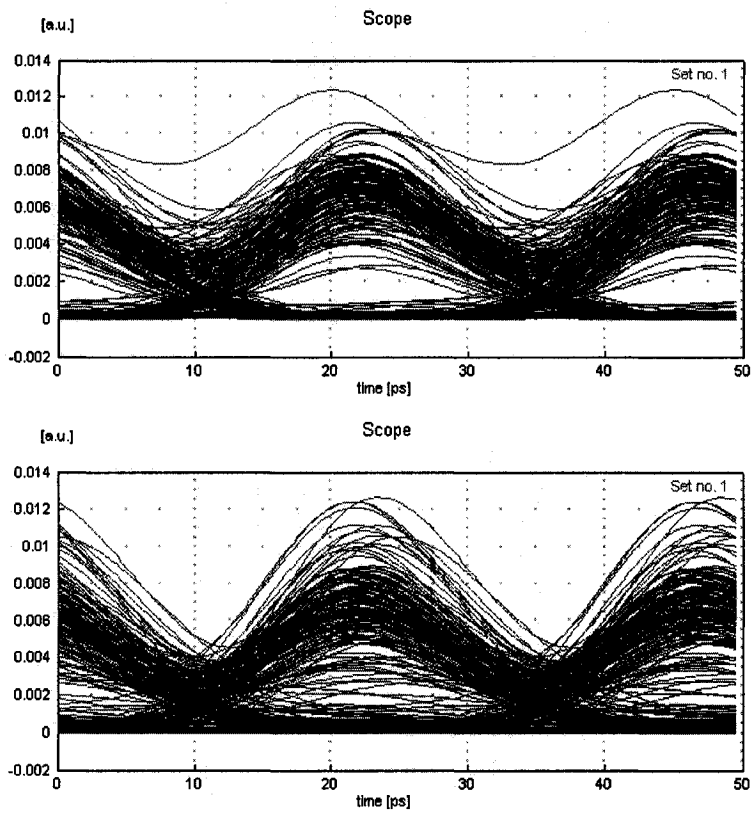

Figure 6.6: Received eye diagrams of the 2nd DEMUX channel when the setup of Fig. 6.4 is modified, and the fiber nonlinearity is always ON. Top: fiber lengths of and input powers to the two types of spans are exactly the same. Bottom: all fiber spans are identical in length and input signal power as well as the ordering of fibers (SMF followed by DCF).

To better quantify the improvement of transmission performance due to STS and OPC, repeated simulations have been carried out for different transmission distances, in order to accumulate data for a plot of the Q value (as discussed in Chapter 2) versus transmission distance for three system configurations. The first system is optimized, having STS and OPC for nonlinear compensation, which is configured as N recirculating loops of (50 km SMF + 50 km DCF + 16 dB EDFA + 40 km DCF +

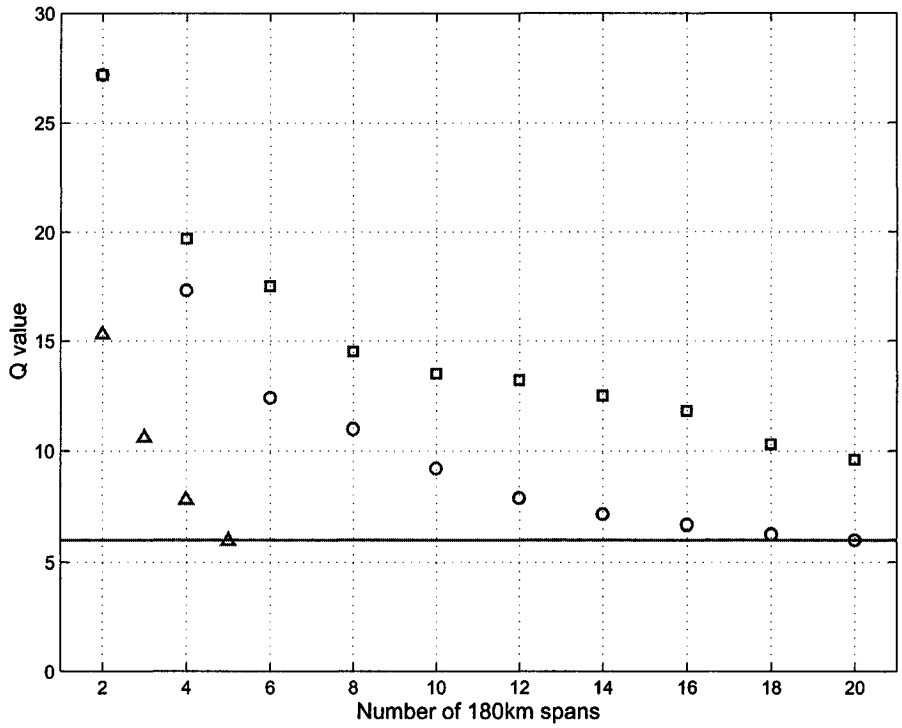

Figure 6.7: The Q value versus transmission distance in number of 180km spans for three system setups: squares - baseline system without fiber nonlinearity; circles - optimized system with STS and OPC; triangles - conventional system without STS and OPC. The solid horizontal line marks the level of $Q = 6$ for BER $\leq 10^{-9}$.

40 km SMF + 20 dB EDFA), followed by OPC, then another N recirculating loops of (50 km SMF + 50 km DCF + 16 dB EDFA + 40 km DCF + 40 km SMF + 20 dB EDFA), with $N = 1, 2, \cdots, 10$. The second system is conventional, without STS and OPC, which is simply configured as M recirculating loops of (45 km SMF + 45 km DCF + 18 dB EDFA + 45 km SMF + 45 km DCF + 18 dB EDFA), with $M = 2, 3, 4, 5$. The third system, serving as a baseline, has the same line configuration as the first system, except that the OPC is removed and nonlinearity is turned off for all fibers. So the baseline system is free of nonlinear impairments, but only subject to signal degradation due to amplifier noise. All parameters of fibers, MUX/DEMUX, transmitters and receivers are the same as in the immediately previous simulations. Fig. 6.7 plots the Q values versus transmission distance in number of 180km spans, where the "square" data points are of the baseline system without fiber nonlinearity, the "circle" data points are of the optimized system with STS and OPC, and the "triangle" data points are of the conventional system without STS and OPC. The solid horizontal line marks the level of $Q = 6$ for BER $\leq 10^{-9}$, which is used to cut off the transmission distance. It is seen that the Q-degradation versus

transmission distance of the optimized nonlinearity-compensating system follows the trend of the baseline system, but always falls under, until reaching $Q \approx 6$ at 20×180 km, which indicates a fairly good nonlinear compensation, with a small amount of nonlinear penalty remaining, possibly due to nonlinearity-mediated signal-noise mixing and other uncompensated nonlinear effects. By contrast, the conventional system without nonlinear compensation suffers a great deal of nonlinear impairments, which barely reaches 5×180 km when $Q \approx 6$. Nonlinear compensation proves to extend the transmission distance by as much as four folds. Furthermore, it may be noted that both the baseline and the optimized systems are disadvantaged in terms of total optical power expenditure and accumulated amplifier noise, comparing to the conventional system. More specifically, the baseline and optimized systems use 30% less optical power than the conventional system ($1.0 + 0.4 = 1.4$ versus $1.0 + 1.0 = 2.0$), while suffers 40% more amplifier noise. To be fair, the optimized system may have the optical power increased 60% everywhere, so to see exactly the same noise figure as the conventional system. The total power expenditure becomes $1.6 + 0.6 = 2.2$, representing a mere 10% increase comparing to $1.0 + 1.0 = 2.0$ needed by the conventional system. With noise figure reduced by a factor of 1.6, the optimized system would perform even better than that shown in Fig. 6.7.

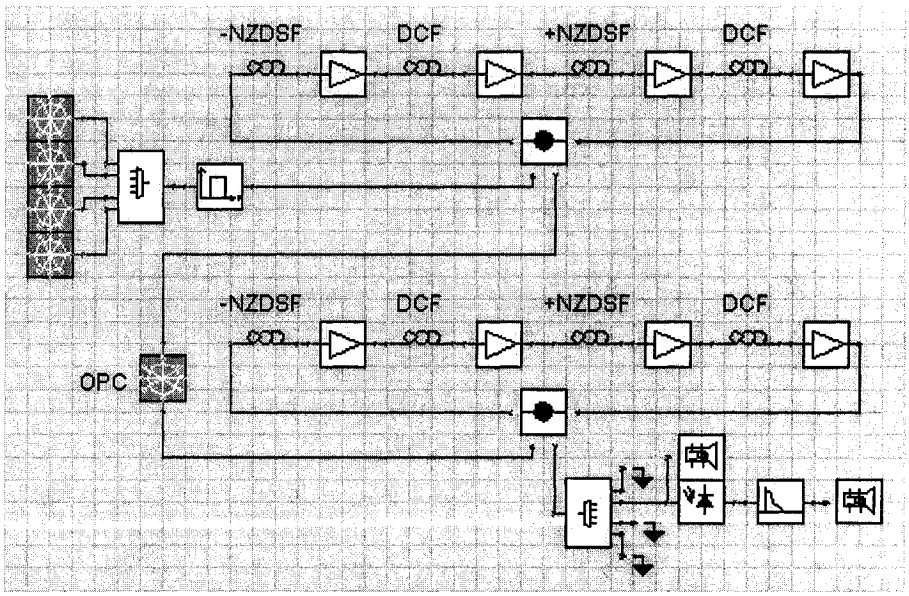

Figure 6.8: A transmission line consisting of +NZDSFs, -NZDSFs, and DCFs compensating the dispersion slope.

For an example system using NZDSFs, we simulated a transmission line consisting of twenty 100-km fiber spans with OPC in the middle, as shown in Fig. 6.8, where

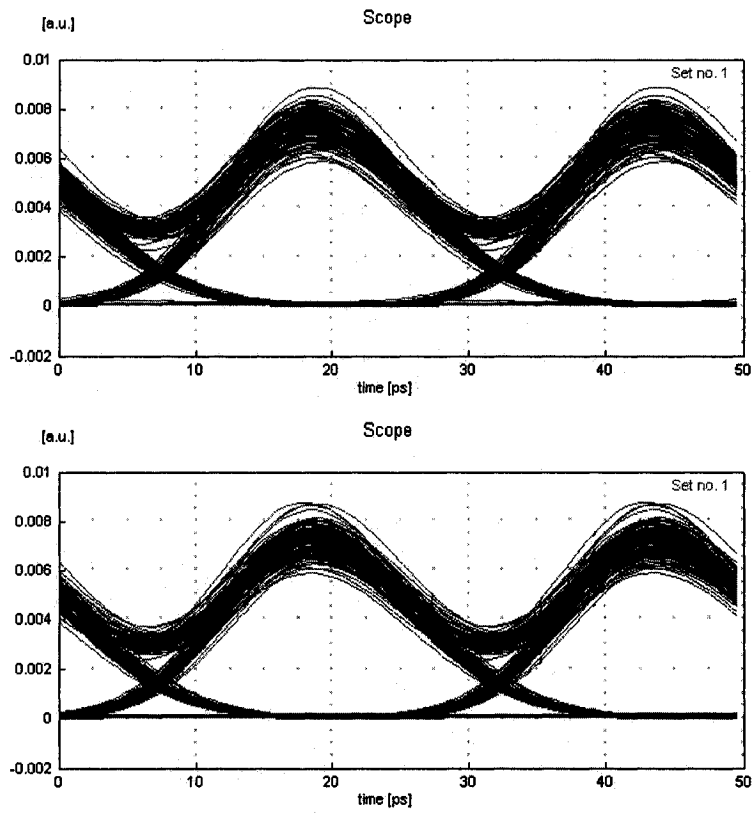

Figure 6.9: Received eye diagrams of the 2nd DEMUX channel using the setup of Fig. 6.8. Top: fiber nonlinearity is OFF, the signal is only impaired by amplifier noise. Bottom: fiber nonlinearity is ON, no extra penalty is visible.

each side of the OPC has a fiber loop circulated five times. In each circulation, the optical signals go through 100 km -NZDSF transmission followed by a two-stage EDFA with 10 km DCF in the middle, then 100 km +NZDSF transmission followed by the same two-stage EDFA and DCF. The +NZDSF has loss coefficient $\alpha = 0.2$ dB/km, dispersion $D = +4$ ps/nm/km and slope $S = 0.11$ ps/nm^2/km at 193.1 THz. The effective mode area is $A_{\text{eff}} = 70$ μm^2. The -NZDSF differs only by $D = -4$ ps/nm/km. The Kerr nonlinear index of silica $n_2 = 2.6 \times 10^{-20}$m^2/W. The two-stage EDFA has $11 + 15 = 26$ dB gain in total to repeat the signal power. The noise figure of each stage is 5 dB. The DCF has $\alpha = 0.6$ dB/km, $D = -40$ ps/nm/km, $S = -1.1$ ps/nm^2/km, $A_{\text{eff}} = 25$ μm^2, but nonlinearity neglected. The transmitting and receiving ends are the same as in the above SMF/DCF transmission. Input to the system are the same four-channel WDM signals, and the peak power of the 40 Gb/s RZ pulses is also the same 20 mW. With their nonlinear effects neglected, the DCFs do not participate directly in nonlinear compensation. Nevertheless, their compensation

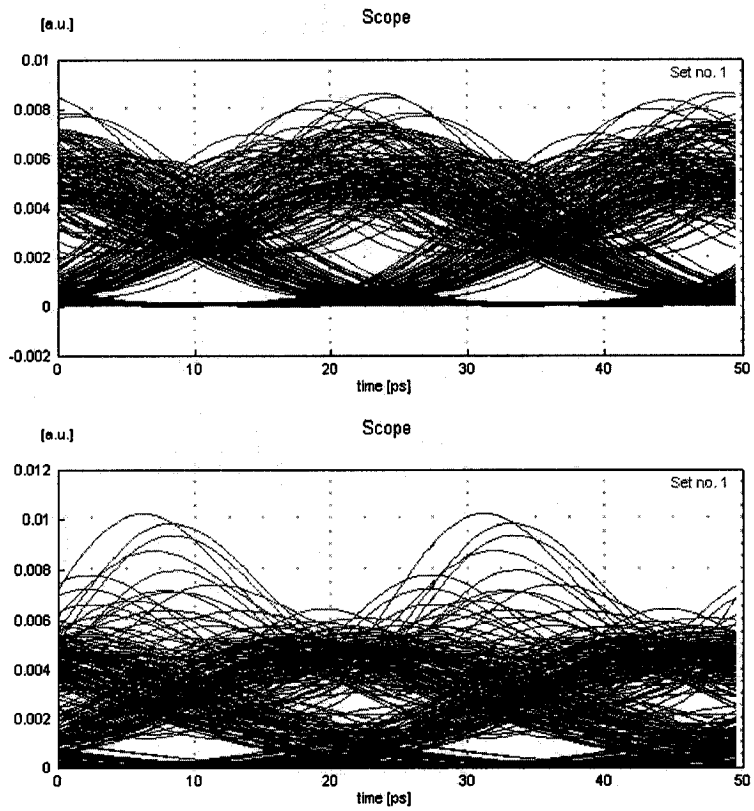

Figure 6.10: Received eye diagrams of the 2nd DEMUX channel when all -NZDSFs are replaced by +NZDSFs in the setup of Fig. 6.8. Top: with OPC. Bottom: without OPC.

of the dispersion-slope of the NZDSFs enables the OPC to effectively compensate the dispersion over a wide frequency band, and helps to condition the optical signals such that the inputs to two conjugate NZDSFs are mutually complex conjugate. Note that the +NZDSF and -NZDSF spans are alternated on each side of the OPC to balance the accumulated dispersion between the two sides. Also note that the first -NZDSF span on the right side of OPC is designed to compensate the nonlinearity of the last +NZDSF span on the left side, and the second span on the right (+NZDSF) is to compensate the second last span (-NZDSF) on the left, so on and so forth. It is important for the +NZDSF spans to be well dispersion-compensated, so to ensure that the input signals to the two conjugate spans of a translation-symmetric pair are complex conjugate to each other, which is a necessary condition for nonlinear cancelation. However, there is no limit as to how much residual dispersion may be in the -NZDSF spans. Alternatively, each fiber span may be a concatenation of + and -NZDSFs. One type of span may have a +NZDSF followed by a -NZDSF, then the conjugate span would consist of the same fibers reversely ordered. Consequently, all spans may

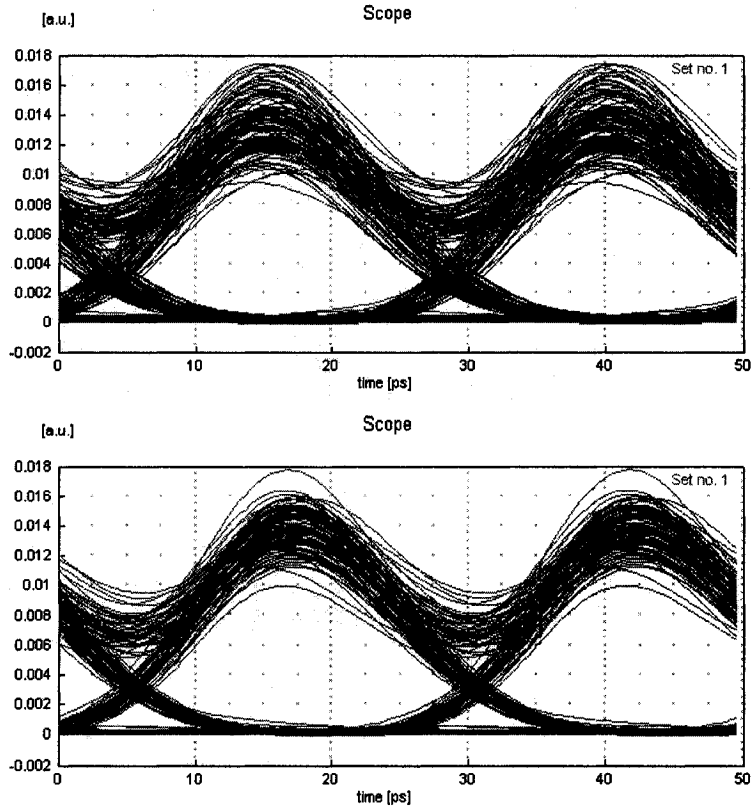

Figure 6.11: Scalability and cascadability of the nonlinearity-suppressed NZDSF transmission line in Fig. 6.8. Top: the number of circulations on each side of OPC is doubled to ten times and the signal power is increased by 3 dB. Bottom: two identical transmission lines as in Fig. 6.8 are in cascade all-optically and the signal power is increased by 3 dB. The eye diagrams are still of the 2nd DEMUX channel.

use the same DCF for slope compensation, and all accumulate the same dispersions of even orders. The received eye diagrams of the second channel out of the DEMUX are displayed in Figs. 6.9 and 6.10, where Fig. 6.9 shows the results of nonlinear transmission and a comparing fictitious transmission without fiber nonlinearity through the setup of Fig. 6.8. The effectiveness of nonlinear compensation is remarkable. By contrast, Fig. 6.10 shows severe degradations in the transmission performance, when all -NZDSFs are replaced by +NZDSFs, so that the transmission line consists of identical +NZDSF spans with DCFs compensating both the dispersion and the dispersion-slope. The highly effective nonlinear compensation is expected as a result of the nearly perfect translation symmetry between the +NZDSF and -NZDSF spans. Furthermore, a nonlinearity-suppressed transmission line should manifest behaviors of a linear system to some extent. Typical linear behaviors include scalability and cascadability. Namely, using the same fiber spans and simply by raising the signal power,

it is possible to further the transmission distance by increasing the number of fiber spans before/after the OPC (scaling up), or by cascading several OPC-compensated transmission lines all-optically (without optical to electrical and electrical to optical signal conversions in the middle). Both the scalability and the cascadability are confirmed via numerical simulations, as shown in Fig. 6.11, where one eye diagram is for a system with the number of spans doubled to 40 in total, and the other diagram is obtained when cascading two identical 20-span transmission lines of Fig. 6.8. The eye diagrams are still of the second channel out of the DEMUX.

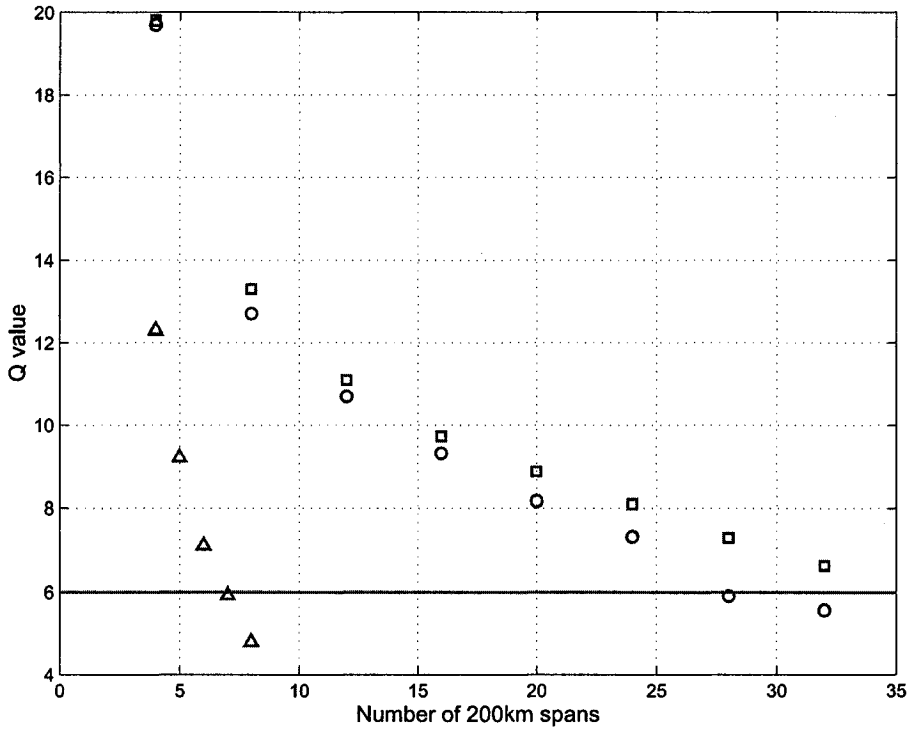

Figure 6.12: The Q value versus transmission distance in number of 200km spans for three system setups: squares - baseline system without fiber nonlinearity; circles - optimized system with STS and OPC; triangles - conventional system without STS and OPC. The solid horizontal line marks the level of $Q = 6$ for BER $\leq 10^{-9}$.

To better quantify the effect of STS-based nonlinear compensation, repeated simulations have been carried out for three systems at different transmission distances in number of 200km spans, to accumulate data of the Q value versus transmission distance. The first system is optimized, having STS and OPC for nonlinear compensation, which is configured as N recirculating loops of (100 km negative NZDSF + 20 dB EDFA + 10 km DCF + 6 dB EDFA + 100 km positive NZDSF + 20 dB EDFA + 10 km DCF + 6 dB EDFA), followed by OPC, then another N recirculating loops of (100 km negative NZDSF + 20 dB EDFA + 10 km DCF + 6 dB EDFA + 100 km pos-

itive NZDSF + 20 dB EDFA + 10 km DCF + 6 dB EDFA), with $N = 2, 4, 6, \cdots, 16$. The second system is conventional, without STS and OPC, which is simply configured as M recirculating loops of (100 km positive NZDSF + 20 dB EDFA + 10 km DCF + 6 dB EDFA + 100 km positive NZDSF + 20 dB EDFA + 10 km DCF + 6 dB EDFA), with $M = 4, 5, 6, 7, 8$. The third system, serving as a baseline, has the same line configuration as the second system, except that nonlinearity is turned off for all fibers, and $M = 4, 8, 12, \cdots, 32$. All parameters of fibers, MUX/DEMUX, transmitters and receivers are the same as in the immediately previous simulations. Fig. 6.12 plots the Q values versus transmission distance in number of 200km spans, where the squares are of the baseline system without fiber nonlinearity, the circles are of the optimized system with STS and OPC, and the triangles are of the conventional system without STS and OPC. The solid horizontal line marks the level of $Q = 6$ for BER $\leq 10^{-9}$, which is used to cut off the transmission distance. It is seen that the Q value of the optimized nonlinearity-compensating system follows closely that of the baseline system, and gets to $Q \approx 6$ at 28×200 km, which indicates an excellent nonlinear compensation. By contrast, the conventional system without nonlinear compensation suffers a large nonlinear penalty, which barely reaches 7×200 km when $Q \approx 6$. An improvement as much as four folds in transmission distance has been achieved by STS-based nonlinear compensation.

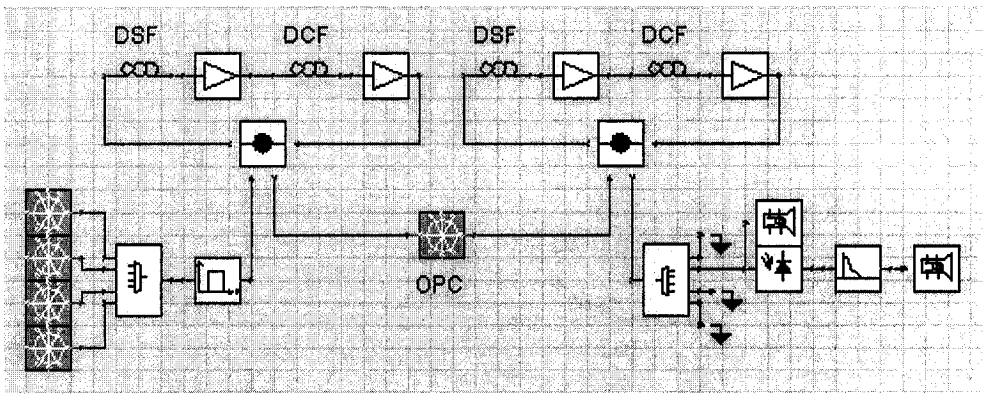

Figure 6.13: A transmission line consisting of ten fiber spans on each side of OPC, each span has 50 km DSF and a slope-compensating DCF.

To test the effectiveness of nonlinear compensation for DSFs, we evaluated numerically a transmission line consisting of twenty 50-km DSF spans with OPC in the middle, as shown in Fig. 6.13. Each span has 50 km DSF and at the end a two-stage EDFA with 5 km DCF in the middle. The DSF has loss $\alpha = 0.2$ dB/km, $D = 0$ ps/nm/km and $S = 0.08$ ps/nm^2/km at the center frequency 193.1 THz, $A_{\text{eff}} = 50$

μm^2. The Kerr nonlinear index of silica is again $n_2 = 2.6 \times 10^{-20}$ m^2/W. The two-stage EDFA has $6+7 = 13$ dB gain in total to repeat the signal power, and the noise figure of each stage is 5 dB. The DCF has $\alpha = 0.6$ dB/km, $D = -100$ ps/nm/km, $S = -0.8$ ps/nm^2/km, $A_{\text{eff}} = 25$ μm^2, but nonlinearity neglected. The transmitting and receiving ends are still the same as in the above SMF/DCF transmission. However, the four channels of 40 Gb/s RZ pulses are transmitted at $(-350, -150, +50, +250)$ GHz off the center frequency, and they are received at $(-250, -50, +150, +350)$ GHz off the center frequency. Note that the channels are assigned asymmetrically about the center frequency to avoid phase-matched FWM, that is four-wave mixing [2]. The channels may also be unequally spaced to further reduce the FWM penalty [133, 134]. But assigning channels with unequal spacing increases the network complexity and may not provide sufficient suppression by itself to the FWM and other nonlinear effects. In particular, it is ineffective to suppress the effect of XPM, that is cross-phase modulation. Nevertheless, when applicable, such legacy methods for nonlinear suppression may be combined with our method of OPC-based nonlinear compensation. The legacy methods may work to enhance the effectiveness of our method, in the sense that they may render weaker nonlinearity in each fiber span, so that the negligence of higher-order nonlinear perturbations becomes a better approximation. Back to the DSF-based transmission system of Fig. 6.13, when the power of the RZ pulses is peaked at 2 mW, Figs. 6.14 and 6.15 show the received eye diagrams of the second channel out of the DEMUX. The top diagram in Fig. 6.14 is obtained when the fiber nonlinearity is turned OFF, so the signal is only impaired by amplifier noise. The bottom diagram in Fig. 6.14 is the received eye when the fiber nonlinearity is turned ON. The increased penalty due to fiber nonlinearity is visible but not too large. The eye diagrams in Fig. 6.15 are obtained when the dispersion of the DCFs changes to $D = 0$ ps/nm/km while the slope remains, with or without OPC in the middle of the link. The good transmission performance shown in the top diagram verifies the insensitivity of our OPC-based method of nonlinear compensation to the amount of residual dispersion in each fiber span, while the bad result in the bottom diagram demonstrates the indispensability of OPC.

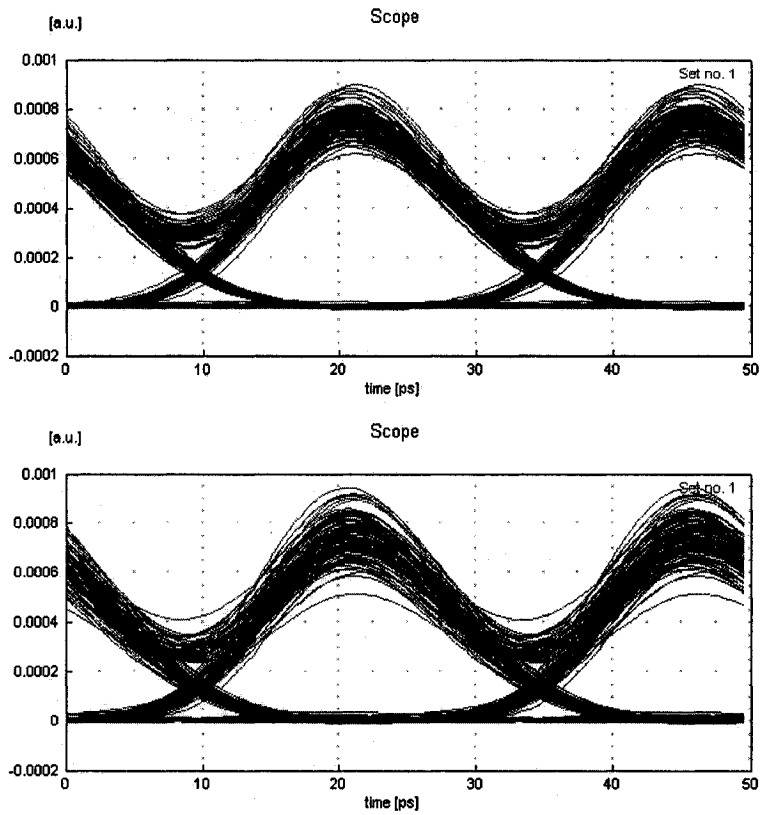

Figure 6.14: Received eye diagrams of the 2nd DEMUX channel using the setup of Fig. 6.13. Top: fiber nonlinearity is OFF, the signal is only impaired by amplifier noise. Bottom: fiber nonlinearity is ON.

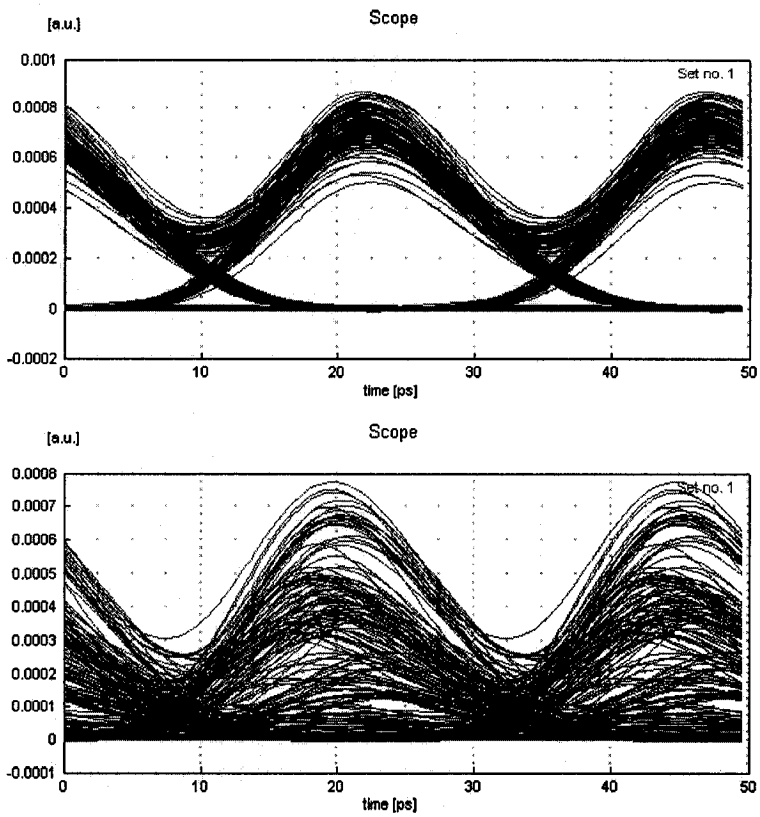

Figure 6.15: Received eye diagrams of the 2nd DEMUX channel when the setup of Fig. 6.13 is modified by setting $D = 0$ ps/nm/km for the DCFs while keeping the dispersion slope. Top: with OPC in the middle of the link. Bottom: when OPC is removed.

7

Practical Nonlinear Suppression without OPC

7.1 *Optimal STS Setups for Intra-channel Nonlinear Compensation*

Fiber spans for intra-channel nonlinear compensation without OPC may be similarly designed and arranged as those described in section 6.1 when OPC is used. A transmission fiber, either SMF or NZDSF, and its corresponding slope-matching DCF [3, 4] are a perfect pair for compensating intra-channel nonlinearities, as their dispersions and slopes of dispersion satisfy the scaling rules of equation (4.43) perfectly, and the signal amplitudes may be easily adjusted to fulfil the corresponding scaling rule. The so-called RDFs [131], as a special type of DCFs, may be suitably cabled into the transmission line and contribute to the transmission distance, since the absolute dispersion value and loss coefficient of RDFs are both comparable to those of the transmission fiber. Only the smaller modal area requires a lower level of signal power for an RDF to compensate the nonlinearity of a transmission fiber. Otherwise the one-for-many compensation scheme may be employed, where the signal power may be slightly adjusted for an RDF to compensate the nonlinearity of multiple transmission fibers. There is usually no power repeater between the transmission fiber and the cabled RDF within one span, so that the signal power decreases monotonically in each fiber span, as shown in Fig. 4.7. Note that one fiber span has a transmission fiber followed by an RDF, while the other span has an RDF followed by a transmission fiber, in accordance with the scaling rules of equation (4.43) for nonlinear compensation. Alternatively, if distributive Raman amplification, especially backward Raman pumping, is used to repeat the signal power, then one span has the transmission fiber Raman pumped in accordance with the RDF being Raman pumped in the other span. The signal power variation in each span may no longer be monotonic, but the power profiles in two compensating spans should still be similar and obey the scaling rules of equation (4.43), especially in portions of fibers that experience high signal power.

For DCFs with absolute dispersion values much higher than the transmission fiber,

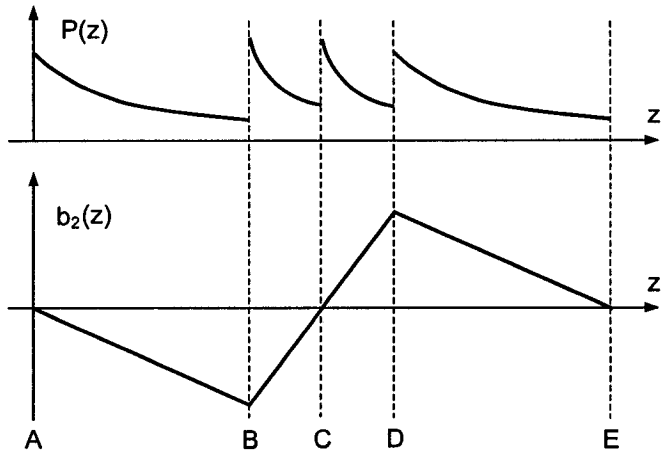

Figure 7.1: The signal power and dispersion maps for a cascade of two fiber spans in STS with lumped dispersion compensators. Top: the variation of signal power along the propagation distance. Bottom: the dispersion map, namely, the variation of accumulated dispersion along the propagation distance.

it is suitable to coil the DCF into a lumped DCM, that is dispersion-compensating module, and integrate the module with a multi-stage optical amplifier at each repeater site. Two fiber spans in STS for intra-channel nonlinear compensation should have oppositely ordered transmission fibers and DCFs. As shown in Fig. 7.1, one span has a piece of transmission fiber from A to B, in which the signal power decreases exponentially, and an optical repeater at the end, in which one stage of a multi-stage optical amplifier boosts the signal power up to a suitable level and feeds the signal into a lumped DCM, where the signal power also decreases exponentially along the length of the DCF from B to C, finally the signal power is boosted by another stage of the optical amplifier. The other span has the same transmission fiber and the same DCM, with the signal power in the DCF from C to D tracing the same decreasing curve. However, this span has the DCM placed before the transmission fiber. Ironically, the efforts of improving the so-called figure-of-merit [1, 4] by DCF vendors have already rendered the loss coefficients of DCFs too low to comply with the scaling rules of equation (4.43). To benefit from nonlinear compensation enabled by STSs, DCFs, at least parts of them carrying high signal power, may be intentionally made more lossy during manufacturing or by means of special packaging to introduce bending losses. As illustrated in Fig. 7.1, the DCFs from B to C and from C to D are arranged in STS to the transmission fibers from D to E and from A to B respectively, such that the transmission fiber from A to B is compensated by the DCF from C to D, and the DCF from B to C compensates the transmission fiber from D to E, for the most detrimental

effects of jittering in pulse amplitude and timing due to intra-channel FWM and XPM. In practice, the DCMs from B to D and the multi-stage optical amplifiers may be integrated into one signal repeater, and the same super-span from A to E may be repeated many times to reach a long-distance, with the resulting transmission line enjoying the effective suppression of intra-channel nonlinear impairments. Again, in case distributive Raman pumping in the transmission fibers is employed to repeat the signal power, the DCFs may also be Raman pumped or erbium-doped for distributive amplification to have similar (scaled) power profiles as that in the transmission fibers for optimal nonlinear compensation.

It should be noted that in regions of fibers carrying lower optical power, the scaling rules of fiber parameters in equation (4.43) may be relaxed without sacrificing the performance of nonlinear compensation, both for systems using cabled DCFs into the transmission lines and for systems using lumped DCMs at the repeater sites. Such relaxation may be done for practical convenience, or to control the accumulated dispersion in a span to a desired value, as well as to reduce the span loss so to reduce the penalty due to optical noise. As an example and a potentially important invention in its own right, a DCM compensating the dispersion and nonlinearity of transmission fibers may be so packaged that the first part of DCF experiencing a high level of signal power may have a higher loss coefficient satisfying the scaling rule of equation (4.43), whereas the second part of DCF may ignore the scaling rule and become less lossy such that the signal power at the end of the DCM is not too low to be significantly impaired by the amplifier noise. In fact, the low-loss part of the DCM may even use optical filters other than DCFs, such as fiber Bragg gratings and photonic integrated circuits. This method of packaging DCMs achieves the capability of nonlinear compensation and good noise performance simultaneously. For instance, it takes 10 km DCF with $D' = -80$ ps/nm/km to compensate 100 km NZDSF with dispersion $D = 8$ ps/nm/km and loss $\alpha = 0.2$ dB/km. The first 4 km of the DCF may be made highly lossy by a special treatment in manufacturing or packaging, with a loss coefficient $\alpha' = 2$ dB/km to form an STS with respect to the first 40 km NZDSF for optimal nonlinear compensation. However, the remaining 6 km DCF may ignore the scaling rules and have a much lower nominal loss $\alpha' = 0.6$ dB/km. The total loss is reduced by 8.4 dB as compared to a DCM that complies strictly with the scaling rules throughout the length of the DCF. Another important parameter of DCFs is the effective modal area, or more directly the nonlinear coefficient. Traditional designs of DCFs have always strived to enlarge the modal area so to reduce the nonlinear effects of DCFs. However, for DCFs used in our method of nonlinear compensation, there exists an optimal range of modal area which should be neither too large nor too small.

According to the scaling rules of equation (4.43), a DCF with a large modal area may require too much signal power to generate sufficient nonlinearity to compensate the nonlinear effects of a transmission fiber, while optical amplifiers may have difficulty to produce that much signal power. On the other hand, when the effective modal area is too small, the scaling rules of equation (4.43) dictate a reduced power level for the optical signal in the DCF, which may be more seriously degraded by optical noise, such as the amplified-spontaneous-emission noise from an amplifier at the end of the DCF.

It is further noted that the nonlinear responses of fiber spans of different lengths may be approximately the same so long as each of them is much longer than the effective length $L_{\text{eff}} = 1/\alpha$. This makes nonlinear compensation possible among spans with different lengths, which are commonly seen in terrestrial and festoon systems, where the span-distance between repeaters may vary according to the geographical conditions. The dispersion of each fiber span may not be always fully compensated, in which case it is desirable to fine-tune the fiber lengths such that any pair of compensating spans have the same amount of residual dispersion. The final note is that two compensating fiber spans are not necessarily located immediately next to each other as drawn in Figs. 4.7 and 7.1. Sometimes, it may be advantageous to order pairs of compensating fiber spans in a mirror-symmetric manner similar to that discussed in section 6.1, especially when all spans are not compensated to zero dispersion. Indeed, it is convenient to have the two spans of any compensating pair accumulating the same amount of total dispersion including the sign. This would be achieved naturally if the two compensating spans consist of exactly the same DCF and transmission fiber of exactly the same lengths, with the only difference being the ordering of the fibers. When a pair of compensating spans are not the same in span distance, the length of either a DCF or a transmission fiber may be fine-tuned, namely slightly elongated or shortened, to make sure that the two spans have the same accumulated dispersion. If the spans of a long-distance transmission line are labeled by $-N, -N+1, \cdots, -2, -1$ and $1, 2, \cdots, N-1, N$ from one end to the other, $N > 1$, a mirror-symmetric arrangement requires that spans $-n$ and n, $n \in [1, N]$ should be paired for nonlinear compensation, that is, their fiber parameters should satisfy the scaling rules of equation (4.43) approximately and their accumulated dispersions should be the same. Note that the scaling rules may only be fulfilled approximately if the two spans have the same non-zero accumulated dispersion. Then pre- and post-dispersion compensators may be employed at the two ends of the transmission line to equalize the total dispersion and importantly, to make sure that the accumulated dispersion from the transmitter to the beginning of span $-n$ is opposite to

the accumulated dispersion from the transmitter to the beginning of span n, for all $n \in [1, N]$, such that the input signals to spans $-n$ and n are complex conjugate, that is oppositely chirped, as required for compensating intra-channel nonlinearities. As an example, when all spans have the same accumulated dispersion b_2, the pre-dispersion compensator should provide $-\left(N - \frac{1}{2}\right) b_2$, while the post-dispersion compensator should contribute $-\left(N + \frac{1}{2}\right) b_2$. Or the amount of post-dispersion compensation may be slightly different from $-\left(N + \frac{1}{2}\right) b_2$, such that the overall dispersion of the transmission line is not zero but within the tolerance of the transmitted pulses. More generally, if the accumulated dispersions of spans $-n$ and n are B_{-n} and B_n respectively, which satisfy the conditions $B_{-n} = B_n$, $\forall\ n \in [1, N]$, while B_m and B_n are not necessarily the same if $m \neq n$, then the pre- and post-dispersion compensators may provide respectively $\frac{1}{2}B_1 - \sum_{n=1}^{N} B_n$ and $-\frac{1}{2}B_1 - \sum_{n=1}^{N} B_n$ worth of dispersion, approximately up to the tolerance of the transmitted pulses. It is worth pointing out that the single-channel nature of intra-channel nonlinear compensation permits the use of channelized pre- and post-dispersion compensators. Namely, at each end of the transmission line, apart from a common pre- or post-dispersion compensator shared by all channels, each individual channel may have a channelized dispersive element, or a short piece of fiber with the length fine-tuned, to compensate the channel-dependence of dispersion if any. Finally, it should be noted that a recent paper [135] proposes to compensate the timing jitter due to intra-channel XPM in a transmission fiber using the nonlinearity of a DCF, which is similar in spirit to our method of intra-channel nonlinear compensation using STS. However, the proposal in [135, 136] is limited to the compensation of timing jitter of RZ pulses that are Gaussian-shaped, whereas our method could compensate both the amplitude fluctuation and timing jitter due to intra-channel nonlinear interactions of arbitrarily shaped pulses, with the only condition for suppressing intra-channel FWM that the signal pulses when chirp-free should be all real-valued upon a suitable choice of frequency and phase for the optical carrier. More importantly, the work presented in [135, 136] did not recognize the significance of scaling the dispersion, loss and nonlinear coefficients of the DCF with respect to the transmission fiber, which is a necessary condition for optimal compensation of nonlinear effects. On the practical side, the proposal in [135, 136] requires fiber Bragg grating dispersion compensators, which are limited in operating bandwidth and may suffer problems as thermal instability and group-delay ripples.

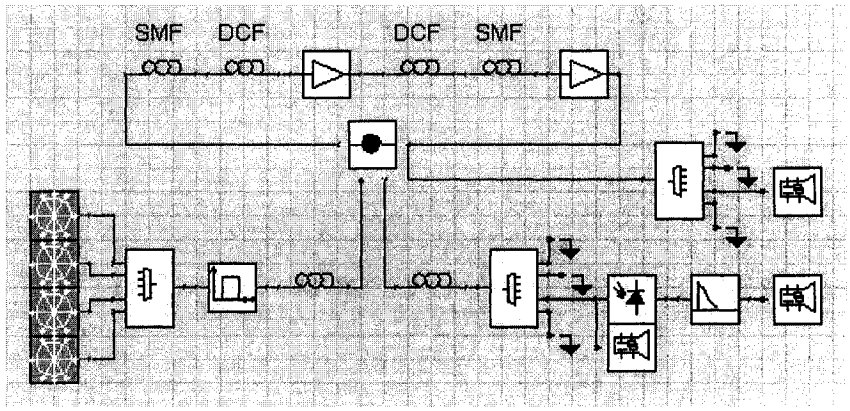

Figure 7.2: A transmission line consists of 6 pairs of fiber spans, with the first span in each pair having 50 km SMF followed by 50 km RDF then 16 dB EDFA gain, and the second span having 40 km RDF followed by 40 km SMF then 20 dB EDFA gain.

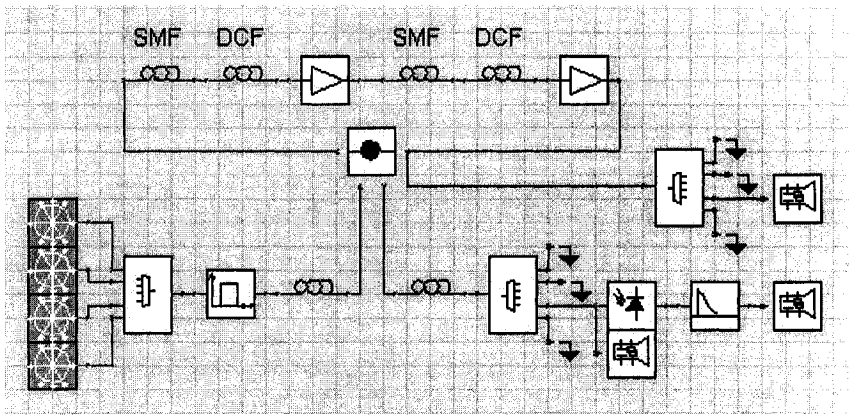

Figure 7.3: A transmission line consists of 6 pairs of fiber spans, with the first span in each pair having 50 km SMF followed by 50 km RDF then 16 dB EDFA gain, and the second span having 40 km SMF followed by 40 km RDF then 20 dB EDFA gain.

7.2 Simulation Results and Discussions

As usual, numerical simulations are carried out to support our theoretical analysis and verify the effectiveness of our method of suppressing intra-channel nonlinearity using STS. In one test system, as depicted in Fig. 7.2, the transmission line consists of 6 pairs of compensating fiber spans totaling a transmission distance of 1080 km. The first span in each pair has 50 km SMF followed by 50 km RDF then an EDFA with gain 16 dB, the second span has 40 km RDF followed by 40 km SMF then an EDFA with gain 20 dB. The other test system consists of the same number of spans with the same span lengths, which are constructed using the same fibers and EDFAs as the first system except that the second span in each span-pair has the 40km

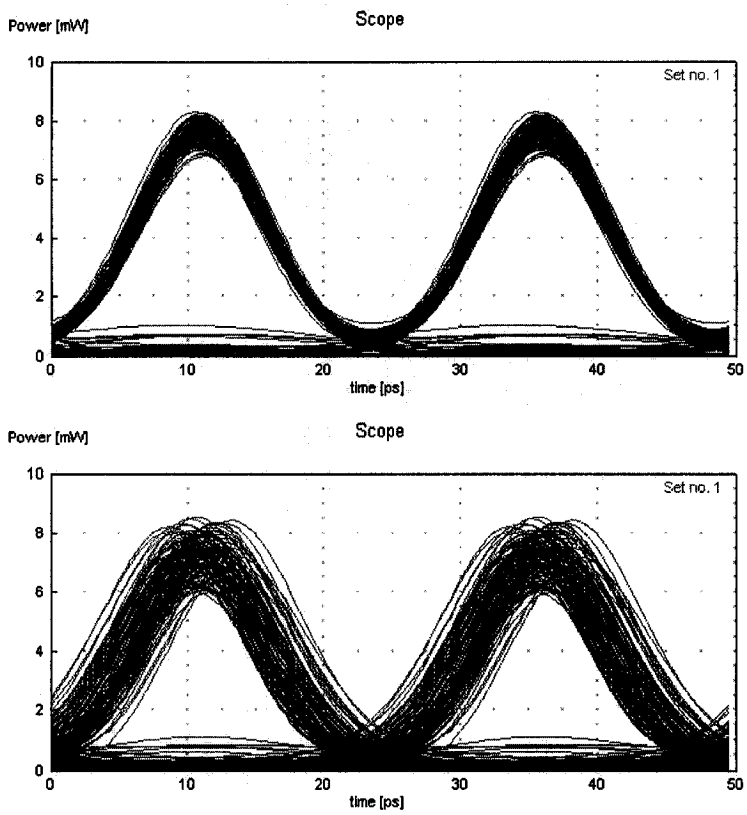

Figure 7.4: The transmission results of the 3rd DEMUX channel with $\delta D = 0$ and amplifier noise turned off to signify the nonlinear effects. Top: received optical eye diagram of the scaled translation-symmetric setup in Fig. 7.2. Bottom: received optical eye diagram of the setup in Fig. 7.3 without STS.

SMF placed before the 40km RDF, as shown in Fig. 7.3. The EDFA noise figure is 4 dB. The SMF has loss $\alpha = 0.2$ dB/km, dispersion $D = 16 + \delta D$ ps/nm/km, and dispersion slope $S = 0.055$ ps/nm^2/km, effective modal area $A_{\text{eff}} = 80$ μm^2, while the RDF has $\alpha = 0.2$ dB/km, $D = -16$ ps/nm/km, $S = -0.055$ ps/nm^2/km, and $A_{\text{eff}} = 30$ μm^2. Fiber-based pre- and post-dispersion compensators equalize 11/24 and 13/24 respectively of the total dispersion accumulated in the transmission line. Both the SMF and the RDF have the same nonlinear index of silica $n_2 = 2.6 \times 10^{-20}$ m^2/W. The transmitter has four 40 Gb/s WDM channels. The center frequency is 193.1 THz, and the channel spacing is 200 GHz. All four channels are co-polarized and RZ-modulated with 33% duty cycle and peak power of 15 mW for the RZ pulses. The MUX and DEMUX filters are Bessel of the 7th order with 3dB-bandwidth 80 GHz. The electrical filter is third-order Bessel with 3dB-bandwidth 28 GHz. The results of four-channel WDM transmissions have been compared with that of single-channel transmissions, with no clearly visible difference observed, which indicates the

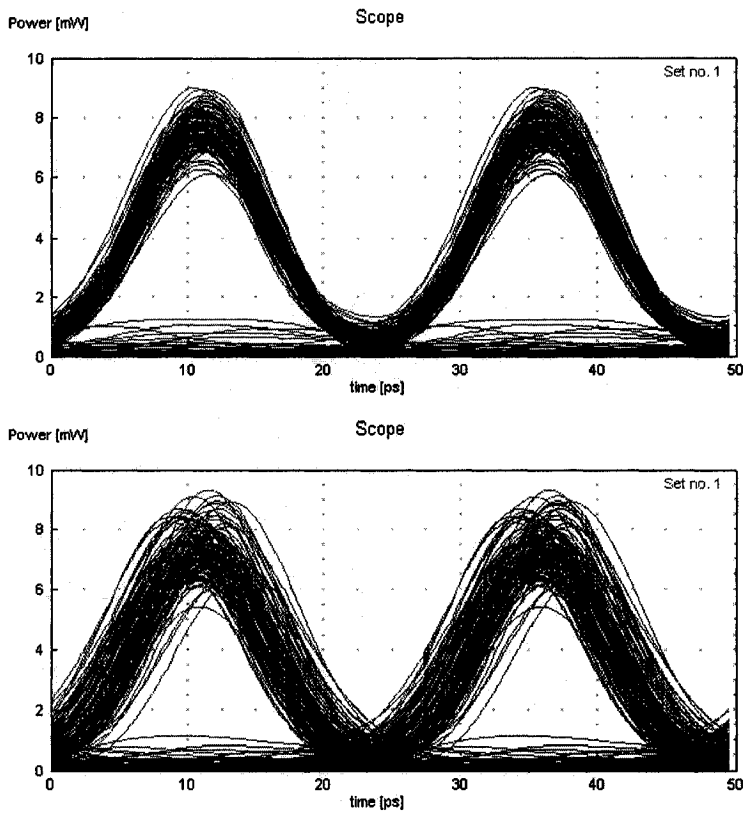

Figure 7.5: The transmission results of the 3rd DEMUX channel with $\delta D = 0$ and amplifier noise turned on. Top: received optical eye diagram of the scaled translation-symmetric setup in Fig. 7.2. Bottom: received optical eye diagram of the setup in Fig. 7.3 without STS.

dominance of intra-channel nonlinearity and the negligibility of inter-channel nonlinear effects. Several trials with various values for δD have been simulated for each test system. The following figures present the eye diagrams of optical pulses of the 3rd DEMUX channel, in order to signify the nonlinear deformation (timing and amplitude jitters) of optical pulses and the generation of ghost-pulses. Fig. 7.4 shows the received optical pulses of $\delta D = 0$ for the two test systems, with the amplifier noise being turned off to signify the nonlinear impairments (bottom diagram) and the effectiveness of nonlinear compensation (top diagram). Clearly shown is the suppression of nonlinear impairments by using STS, and especially visible is the reduction of pulse timing jitter, as seen from the thickness of the rising and falling edges as well as the timing of pulse peaks. In both eye diagrams, there are optical pulses with small but discernable amplitudes above the floor of zero signal power, which could be attributed to ghost-pulse generation [90, 93, 94] due to the uncompensated in-phase components of intra-channel FWM. When the amplifier noise is turned back on, as

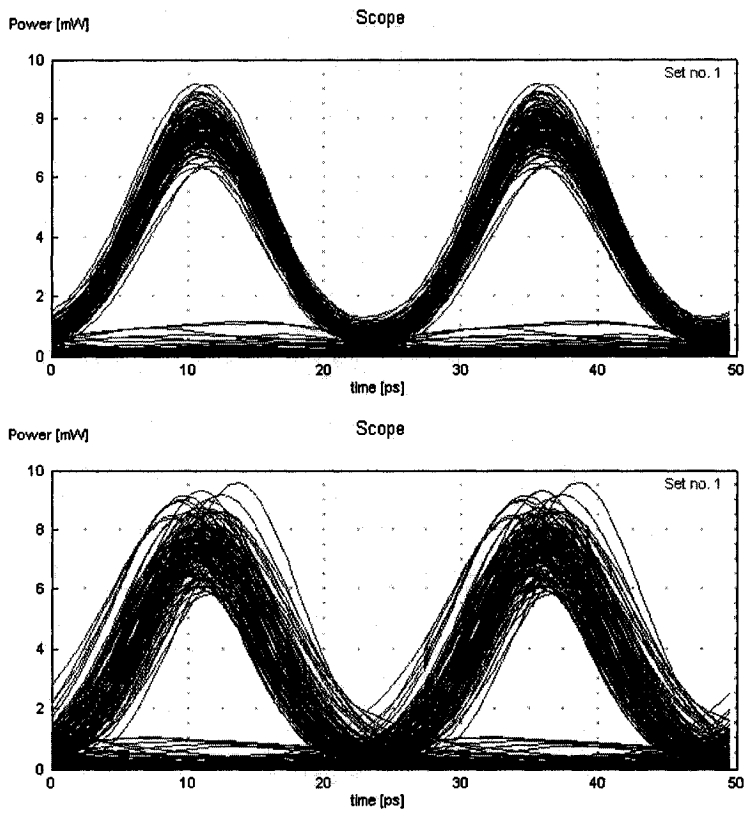

Figure 7.6: The transmission results of the 3rd DEMUX channel with $\delta D = 0.2$ ps/nm/km and amplifier noise turned on. Top: received optical eye diagram of the scaled translation-symmetric setup in Fig. 7.2. Bottom: received optical eye diagram of the setup in Fig. 7.3 without STS.

shown in Fig. 7.5, the received signals become slightly more noisy, but the suppression of nonlinear distortions is still remarkable when there is STS. Then $\delta D = 0.2$ ps/nm/km was set for the two test systems of Fig. 7.2 and Fig. 7.3 respectively, in order to showcase that a mirror-symmetric ordering of pairwise translation-symmetric fiber spans is fairly tolerant to the residual dispersions in individual fiber spans. In this setting, each fiber span has 10 or 8 ps/nm/km worth of residual dispersion, and the accumulated dispersion totals 108 ps/nm/km for the entire transmission line. Importantly, the pre- and post-dispersion compensators are set to compensate $11/24$ and $13/24$ respectively of the total dispersion, ensuring at least approximately the complex conjugateness between the input signals to each pair of spans in STS. The amplifier noise is also turned on. The transmission results, as shown in Fig. 7.6, are very similar to that with $\delta D = 0$, which demonstrates the dispersion tolerance nicely. In a better optimized design to tolerate higher dispersion mismatch $|\delta D|$, either SMFs or RDFs may be slightly elongated or shortened in accordance with the value of δD,

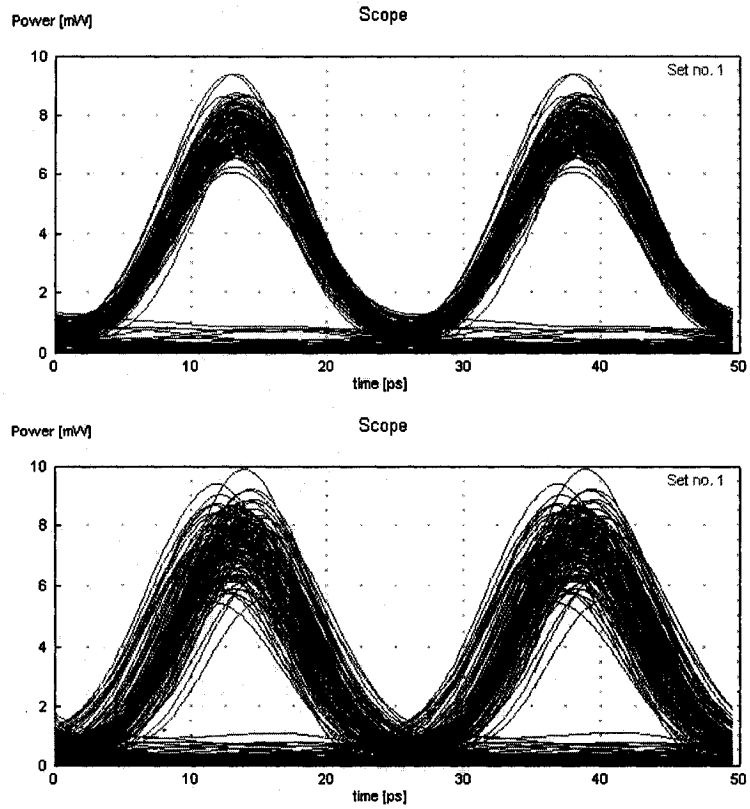

Figure 7.7: The transmission results of the 3rd DEMUX channel with $\delta D = 0.6$ ps/nm/km and amplifier noise turned on. Top: received optical eye diagram of the scaled translation-symmetric setup in Fig. 7.2. Bottom: received optical eye diagram of the setup in Fig. 7.3 without STS.

such that the same residual dispersion is accumulated in all spans. As an example, δD is set to 0.6 ps/nm/km and each 40km SMF is elongated by about 0.4 km, so that all spans have the same residual dispersion of 30 ps/nm/km, and the whole transmission line accumulates 360 ps/nm/km worth of dispersion. The pre- and post-dispersion compensators equalize $360 \times 11/24 = 165$ and $360 \times 13/24 = 195$ ps/nm/km worth of dispersion respectively. The amplifier noise is still on. The transmission results are shown in Fig. 7.7.

To test the applicability and effectiveness of STS-based intra-channel nonlinear compensations to systems using another modulation format and having more WDM channels, we have simulated two comparing systems of multiple WDM channels transmitting NRZ-modulated 40Gb/s signals through recirculating loops. One system has a conventional configuration without STS, as shown in Fig. 7.8, where each loop of recirculation consists of (45 km SMF + 45 km RDF + 18 dB EDFA + 45 km SMF + 45 km RDF + 18 dB EDFA). With 16 co-polarized and 200GHz-spaced WDM chan-

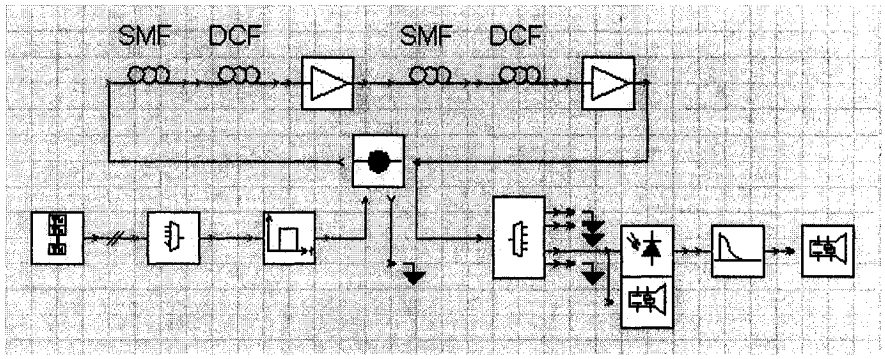

Figure 7.8: A conventional system transmitting multiple NRZ-modulated WDM channels.

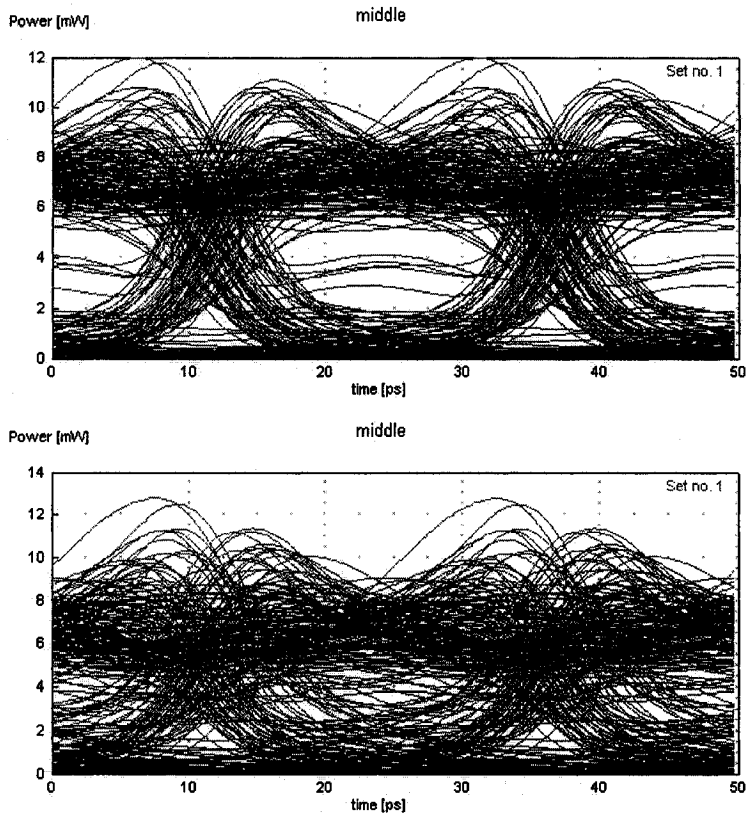

Figure 7.9: Received optical eye diagrams by the 9th channel of the system in Fig. 7.8. Top: after 2 recirculating loops; Bottom: after 3 recirculating loops.

nels input to the system, each channel being NRZ-modulated at 40Gb/s, Fig. 7.9 shows the transmission results of the 9th channel after 2 and 3 recirculating loops. The other system is scaled translation-symmetric, as shown in Fig. 7.10, where each recirculating loop consists of (50 km SMF + 50 km RDF + 16 dB EDFA + 40 km RDF + 40 km SMF + 20 dB EDFA). With the same 16 WDM channels input to

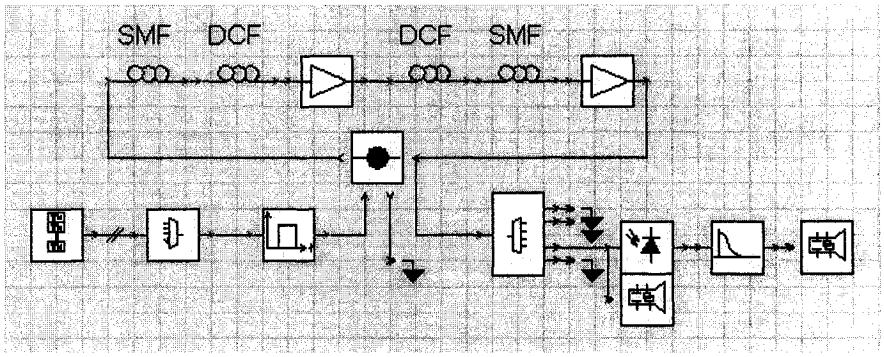

Figure 7.10: A scaled translation-symmetric system transmitting multiple NRZ-modulated WDM channels.

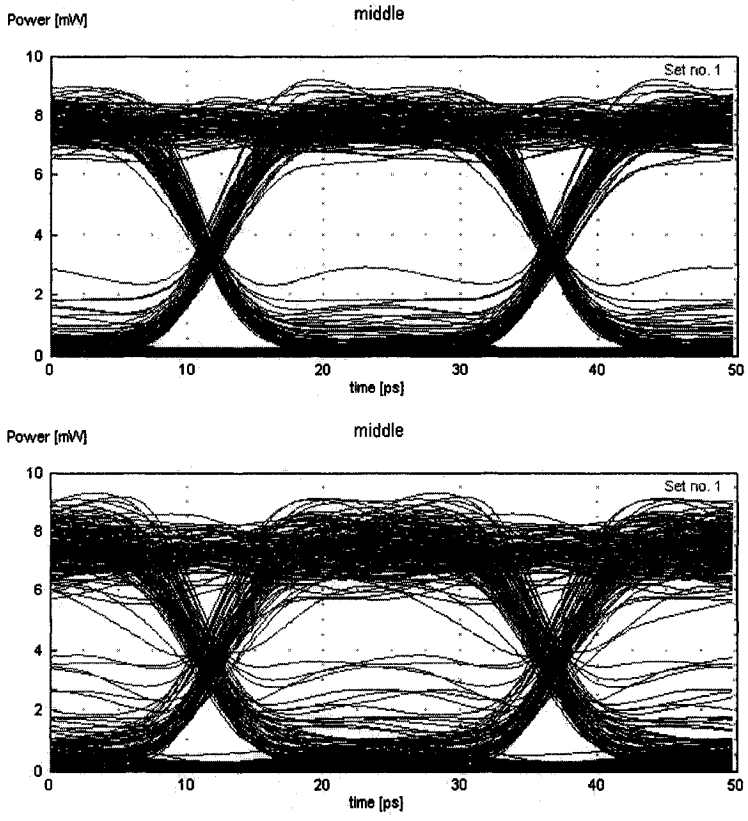

Figure 7.11: Received optical eye diagrams by the 9th channel of the system in Fig. 7.10. Top: after 2 recirculating loops; Bottom: after 3 recirculating loops.

the system, Fig. 7.11 shows the transmission results of the 9th channel after 2 and 3 recirculating loops. Parameters for fibers, amplifiers, and MUX/DEMUX in both systems are the same as in the previous simulations using SMFs and cabled RDFs as DCFs. The pulse power out of the NRZ transmitters is peaked at 8 mW. The rise and

fall time of the NRZ pulses is 6.25 ps, during which the pulse amplitude is between 10% to 90% of its peak value. It is clearly demonstrated that the conventional system without STS suffers a great deal of timing and amplitude jitters, arguably due to nonlinear interactions among signal pulses, whereas the scaled translation-symmetric system manifests significantly reduced jitters in both timing and amplitudes of "ON" pulses. Both systems are also impaired by ghost-pulse generation in "OFF" data slots. With either configuration, it may be noted that NRZ pulses seem to be more severely affected by fiber nonlinearity than RZ pulses. For a comparison, we have carried out another simulation using exactly the same recirculating loop as in Fig. 7.10, but having 16 co-polarized and 200GHz-spaced RZ-modulated WDM channels as input, where the RZ pulses are with 33% duty cycle and peaked at 15 mW. Fig. 7.12 shows the received eye diagram of the 9th channel after 6 recirculating loops, which manifests much improved signal quality even after twice of the transmission distance. This result is consistent with established wisdom that RZ-modulated pulses are more nonlinearity-tolerant than NRZ-modulated ones.

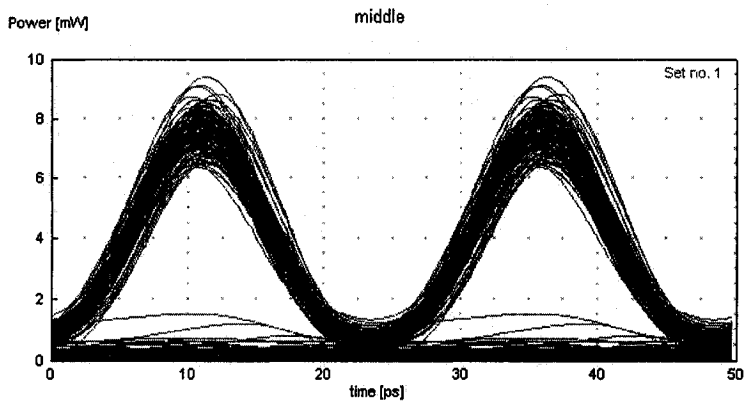

Figure 7.12: Received eye diagram by the 9th channel of 16 RZ-modulated channels after 6 recirculating loops.

7.3 *Reversing intra-channel ghost-pulse generation by mid-way self-phase modulation*

In high-speed long-distance fiber-optic transmissions, a major limitation is imposed by the intra-channel nonlinear effects, such as the pulse amplitude and timing jitters due to intra-channel cross-phase modulation (IXPM) and IFWM (that is intra-channel four-wave mixing) respectively [65]. A method has been proposed to suppress the intra-channel nonlinearities using Raman-pumped transmission lines manifesting

a lossless or mirror-symmetric map of signal power [28, 29]. However, the loss of pump power makes it difficult to maintain a constant gain in a long transmission fiber. Consequently, the significant deviation of signal power profile from a desired mirror-symmetric map degrades the result of intra-channel nonlinear compensation using mirror symmetry [30]. The above has shown that transmission lines designed with translation symmetries in power and dispersion maps could also effectively compensate the IXPM and one aspect of IFWM, so to greatly reduce the timing and amplitude jitters. There have also been recent publications along the similar direction [135, 136]. In particular, our mathematical formulation in the previous section provides a general and unified theory for intra-channel nonlinear compensation using translation or mirror symmetry, and more importantly, it emphasizes the necessity of scaling dispersion, loss coefficient, as well as the product of nonlinear coefficient and signal power in fibers, for optimal nonlinear compensation. The one aspect of IFWM refers to amplitude fluctuation in the "pulse-ON" slots due to coherent superpositions of nonlinearly generated fields onto the original pulses. However, neither the mirror nor the translation symmetry could hold back another aspect of IFWM, namely, the generation of "ghost-pulses" into the "pulse-OFF" slots where there are originally no optical pulses [90, 93, 137, 138]. The growth of ghost-pulses will eventually limit the transmission distance. Here we show that SPM (that is self-phase modulation) in the middle could make the two parts of a long transmission line generating oppositely signed ghost amplitudes, such that the ghost-pulses are annihilated or greatly suppressed at the end.

The amplitude envelope of a single channel may be represented by a sum of optical pulses, namely, $A(z,t) = \sum_k u_k(z,t)$, where $u_k(z,t)$ denotes the pulse in the kth time slot and centered at time $t = kT$, with $k \in \mathbf{Z}$ and $T > 0$ being the duration of one symbol. Again, the following nonlinear Schrödinger equation describes the propagation and nonlinear interactions among the pulses [65],

$$\frac{\partial u_k}{\partial z} + \frac{i\beta_2(z)}{2}\frac{\partial^2 u_k}{\partial t^2} + \frac{\alpha(z)}{2}u_k = i\gamma(z)\sum_m\sum_n u_m u_n u^*_{m+n-k}, \quad \forall\, k \in \mathbf{Z}, \qquad (7.1)$$

where the right-hand side keeps only those nonlinear products that satisfy the phase-matching condition. The nonlinear mixing terms with either $m = k$ or $n = k$ contribute to SPM and IXPM, while the rest with both $m \neq k$ and $n \neq k$ are responsible for IFWM [65]. For a pulse-OFF time slot, for example the kth, the original pulse amplitude $u_k(0,t) = 0$, however the Kerr nonlinearity will generate a ghost amplitude into this slot. In the regime of weak nonlinearity where perturbation theory applies, the ghost amplitude is approximated by a linear accumulation of nonlinear products

over the propagation distance,

$$u_k(z,t) \approx \int_0^z i\gamma(s) \sum_{m\neq k} \sum_{n\neq k} u_m(s,t)u_n(s,t)u^*_{m+n-k}(s,t)ds. \tag{7.2}$$

Consider two transmission lines in cascade, one stretching from $z = 0$ to $z = L$, the other from $z = L$ to $z = L + L'$. Assuming dispersion is compensated in each line such that optical pulses "return" approximately to their original shapes at $z = L$ and $z = L + L'$. Each line may consist of multiple power-repeated and dispersion-equalized fiber spans which are suitably arranged to form a scaled translation or mirror symmetry. Therefore, both lines are effective for suppressing the timing and amplitude jitters in the pulse-ON slots. However, they are not able to prevent the growth of ghost amplitudes in the pulse-OFF slots. The two lines are not necessarily the same, but assumed to generate approximately the same ghost amplitudes, namely,

$$\begin{aligned} &\int_L^{L+L'} i\gamma(z) \sum_{m\neq k} \sum_{n\neq k} u_m(z,t)u_n(z,t)u^*_{m+n-k}(z,t)dz \\ &\approx u_k(L,t) \\ &= \int_0^L i\gamma(z) \sum_{m\neq k} \sum_{n\neq k} u_m(z,t)u_n(z,t)u^*_{m+n-k}(z,t)dz, \end{aligned} \tag{7.3}$$

for all pulse-OFF slots labeled by k. So the ghost amplitude will accumulate into $u_k(L+L',t) = 2u_k(L,t)$ at the end, as long as the perturbation assumption still holds. If the transmission lines become too long, the approximation of linear accumulation of ghost amplitudes will eventually break down. The ghost amplitudes will actually grow exponentially as a result of parametric amplification pumped by the mark pulses. A method of ghost-pulse suppression may need to clean the ghost amplitudes or start reversing their accumulation before they become too strong.

Now consider introducing a self-phase modulator for each wavelength channel in the middle of the two lines at $z = L$, and adjusting the signal power such that the amount of nonlinear phase shift reaches π approximately at the peak of an optical pulse. Fig. 7.13 shows such two transmission lines with channelized SPM in the middle, where each transmission line is STS configured for intra-channel nonlinear compensation. After mid-way SPM, all "originally ON" pulses acquire approximately a π phase shift, while the ghost-pulses in the "originally OFF" time slots experience negligible to small phase shifts due to their low power level. As a consequence, the IFWM products generated in the second line from $z = L$ to $z = L+L'$ would acquire a factor $(-1)^3 = -1$ with respect to when mid-way SPM is absent. For a typical pulse-OFF slot labeled by k, the following calculation gives the ghost amplitude generated

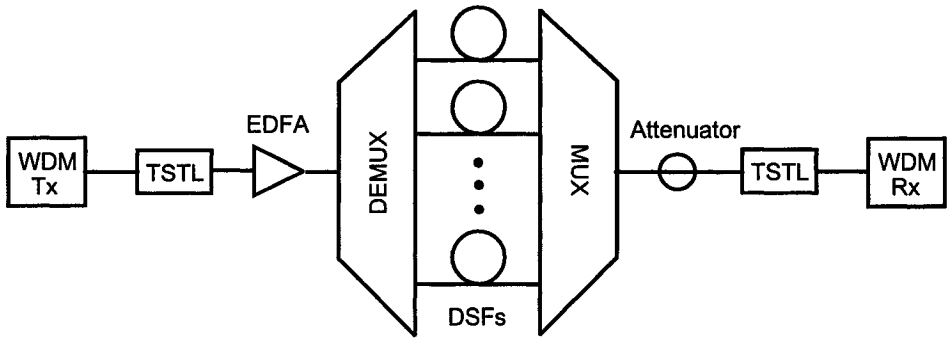

Figure 7.13: Two transmission lines with channelized self-phase modulation in the middle. TSTL: scaled translation-symmetric transmission line. DSF: dispersion-shifted fiber for self-phase modulation.

from start to end through the two transmission lines with SPM in the middle,

$$\begin{aligned}
&\int_0^L i\gamma(z) \sum_{m\neq k} \sum_{n\neq k} u_m(z,t)u_n(z,t)u^*_{m+n-k}(z,t)dz \; + \\
&\int_L^{L+L'} i\gamma(z) \sum_{m\neq k} \sum_{n\neq k} [-u_m(z,t)][-u_n(z,t)][-u_{m+n-k}(z,t)]^* dz \\
&= \int_0^L i\gamma(z) \sum_{m\neq k} \sum_{n\neq k} u_m(z,t)u_n(z,t)u^*_{m+n-k}(z,t)dz \; - \\
&\int_L^{L+L'} i\gamma(z) \sum_{m\neq k} \sum_{n\neq k} u_m(z,t)u_n(z,t)u^*_{m+n-k}(z,t)dz \\
&\approx 0, \qquad (7.4)
\end{aligned}$$

according to equation (7.3). Instead of adding up constructively, the ghost amplitudes generated by the two lines interfere destructively to cancel each other at the end $z = L+L'$. Good transmission performance may be expected from the overall system, as a result of the suppression of amplitude and timing jitters for originally ON pulses and the elimination of ghost-pulses in the originally OFF time slots.

For implementations, the self-phase modulator may be based on the fiber Kerr nonlinearity [6], cascaded $\chi^{(2)}$ in $LiNbO_3$ waveguides [139, 140], the index change induced by carrier density variations in semiconductor optical amplifiers [141], or a combination of a photodiode detecting the optical pulses and electro-optic phase modulator driven by the generated electrical pulses [142, 143]. A fiber-based self-phase modulator may be a better choice than others because of its simplicity and capability of polarization-insensitive operation. Furthermore, a suitable value of fiber dispersion may be chosen such that optical pulses propagate in a soliton-like manner through the nonlinear fiber, in order to reduce the pulse spectral broadening due to SPM [6]. If

SPM is not properly balanced by dispersion, then only the peak of a pulse receives a π phase shift, the rising and falling edges experience less and varying phase shifts, which lead to frequency chirp and spectral broadening. Excessive spectral broadening may cause crosstalk among wavelength channels and decrease the spectral efficiency (rate of data transmission in bit/s over available optical bandwidth in Hz) of transmission systems. A soliton, namely a hyperbolic secant pulse, could propagate invariantly in a lossless fiber given the condition $-\beta_2 = \gamma P_0 T_0^2$, where β_2 and γ are the dispersion and nonlinear coefficients of the fiber, P_0 and T_0 are the peak power and width parameter of the pulse [6]. For actual fibers with loss, strict soliton propagation may not be possible, but the total fiber dispersion may be adjusted so to minimize the frequency chirp of pulses at the end, or to control the chirp at a desired level. An optical filter may also be employed after SPM to limit the spectral width of pulses.

For numerical verifications, we have simulated and compared the performance of three transmission lines, all of which use SMFs with loss $\alpha = 0.2$ dB/km, dispersion $D = 16$ ps/nm/km, effective modal area $A_{\text{eff}} = 80\ \mu\text{m}^2$, and RDFs, namely reverse dispersion fibers, with loss $\alpha' = 0.2$ dB/km, dispersion $D' = -16$ ps/nm/km, effective modal area $A'_{\text{eff}} = 30\ \mu\text{m}^2$, as well as EDFAs with noise figure 4 dB. The first setup is a conventional design consisting of 16 fiber spans, each span has 45 km SMF, followed by 45 km RDF, and a 18 dB EDFA at the end. The second setup is configured to form an STS, having 8 repetitions of (50 km SMF + 50 km RDF + 16 dB EDFA) + (40 km RDF + 40 km SMF + 20 dB EDFA). Note that the EDFA gains are set in a way that the signal powers into the 50km SMF and the 40km RDF are properly scaled. The third system is the same as the second, except for channelized SPM in the middle, using a high-power EDFA, an optical DEMUX/MUX pair, and for each channel a 10km nonlinear fiber with effective modal area $A''_{\text{eff}} = 20\ \mu\text{m}^2$, loss $\alpha'' = 0.3$ dB/km, and dispersion $D'' \approx 3$ ps/nm/km. The optical power is boosted to 80 mW before entering each SPM fiber, and attenuated back to the nominal level for transmissions after the self-phase modulator. All fibers are made of silica glass with nonlinear index $n_2 = 2.6 \times 10^{-20}$ m^2/W. Input to all three systems are four 40 Gb/s channels, spaced by 200 GHz, co-polarized, and return-to-zero modulated with 33% duty and peak power 15 mW. The optical filters are of order 7 with bandwidth 100 GHz for MUX/DEMUX. The transmission results of the 3rd channel are shown in Fig. 7.14. It is evident that the conventional setup suffers a great deal from nonlinearity-induced amplitude and timing jitters, which are greatly reduced in the system with STS, where, however, the ghost-pulse generation imposes a serious limitation. With both STS and mid-way SPM, the third system enjoys a superb signal quality at the end, with small signal fluctuations due to EDFA noise and possibly a

little residual nonlinearity. Again, as discussed in section 6.3, it may be noted that the scaled translation-symmetric systems are disadvantaged in terms of total optical power expenditure and accumulated amplifier noise, comparing to the conventional system. If the optical power is increased hence noise figure is reduced, the scaled translation-symmetric systems should perform even better.

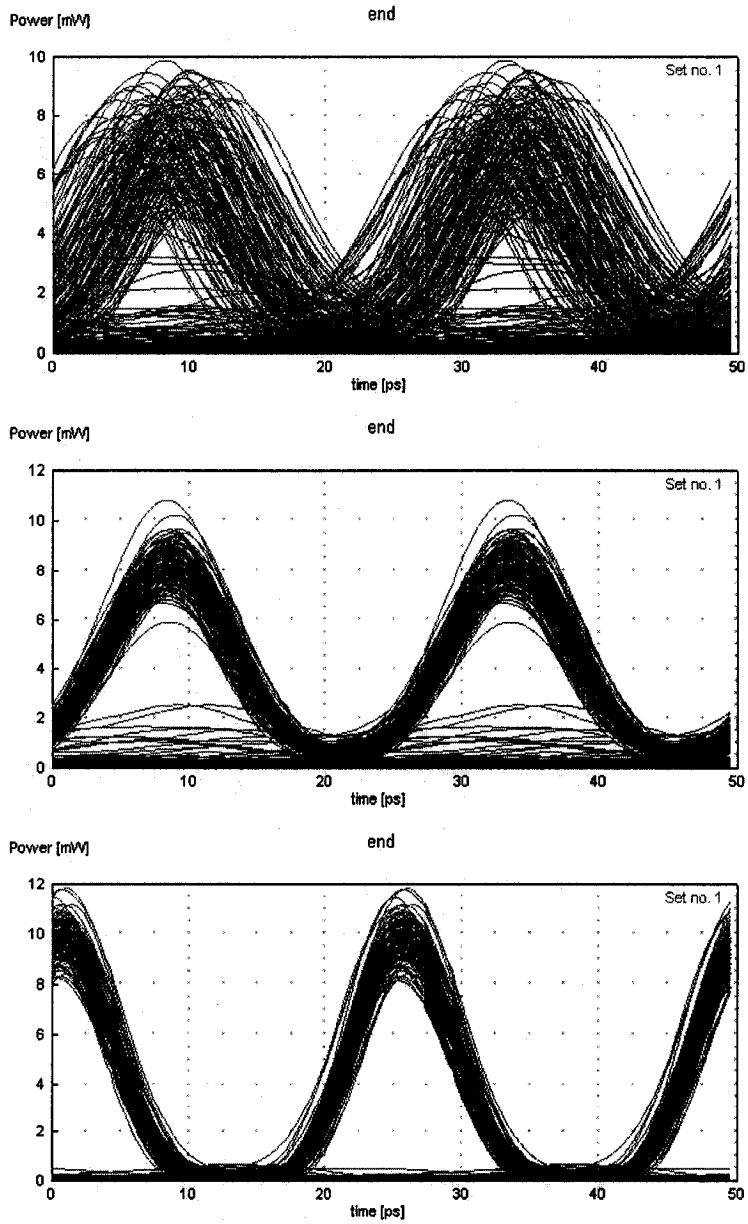

Figure 7.14: Optical eye diagrams of the 3rd channel at the end of transmissions. Top: of a conventional design without STS. Middle: of a system with STS. Bottom: of a system with STS and mid-way SPM.

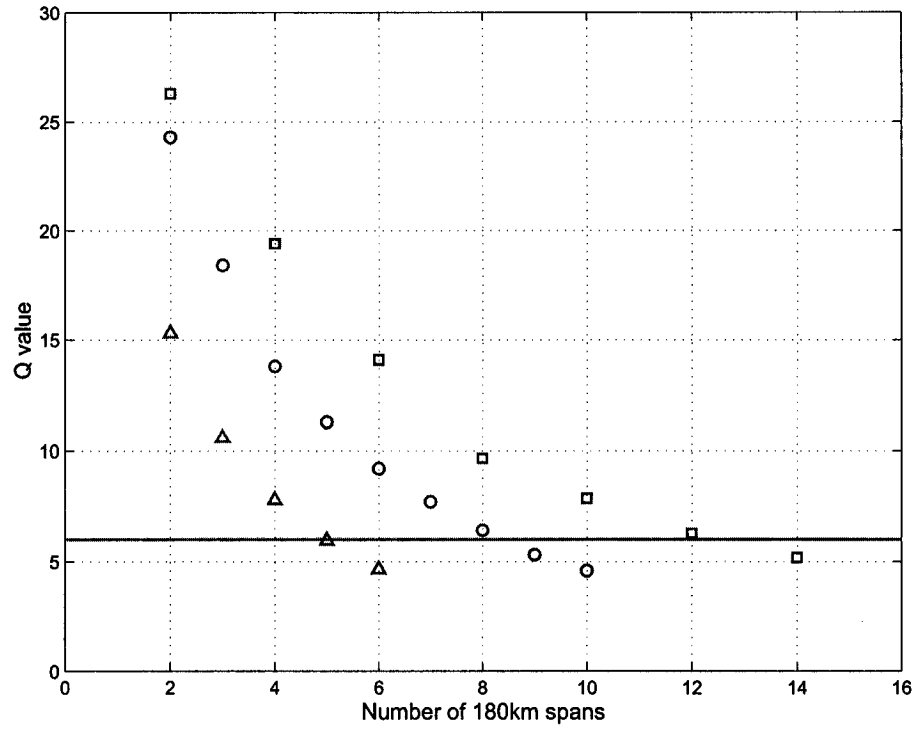

Figure 7.15: The Q value versus transmission distance in number of 180km spans for three system setups: squares - optimized system with STS and mid-way SPM; circles - translation-symmetric system without mid-way SPM; triangles - conventional system without STS nor mid-way SPM. The solid horizontal line marks the level of $Q = 6$ for BER $\leq 10^{-9}$.

To better quantify the improvement of transmission performance due to STS and mid-way SPM, repeated simulations have been carried out for different transmission distances, in order to accumulate data for a plot of the Q value versus transmission distance for the three system configurations, where each system consists of recirculated 180km spans. For the first, conventional setup, each 180km span has (45 km SMF + 45 km RDF + 18 dB EDFA) + (45 km SMF + 45 km RDF + 18 dB EDFA); while for the second, translation-symmetric configuration, each 180km span consists of (50 km SMF + 50 km RDF + 16 dB EDFA) + (40 km RDF + 40 km SMF + 20 dB EDFA). The third, fully optimized system has exactly the same span configuration as the second system, except that it always consists of an even number of 180km spans and employs channelized SPM in the middle. The 3rd channel is monitored, and the simulated signals are used to estimate a Q value. Fig. 7.15 shows the calculated Q values for the three systems as the transmission distances vary from 2 to 14 spans of 180km each, where the "square" data points mark results of the optimized system with STS and mid-way SPM, the "circle" data points indicate results of the translation-symmetric system without mid-way SPM, and the "triangle" data points are for the

conventional system without STS nor mid-way SPM. The solid horizontal line marks the threshold level of $Q = 6$ in order to achieve BER $\leq 10^{-9}$, which is used as the cutoff level to determine the limit of transmission distance. It is seen that the conventional system could barely reach 5 spans of 180km, while the translation-symmetric system without mid-way SPM could readily reach 8 spans of 180km, representing a 60% increase of transmission distance. The addition of mid-way SPM enables the fully optimized system to reach 12 spans, that is another 50% increase of transmission distance. Therefore, the STS and mid-way SPM in combination have more than doubled the transmission distance, comparing to the conventional configuration.

It should be noted that the present method of ghost-pulse suppression by mid-way SPM is not limited to transmission lines with STS. One or both sides, before or/and after the channelized SPM, may be configured in mirror symmetry as well for intra-channel nonlinear compensation [28, 29], and ghost-pulse suppression would be just as effective, provided that the two sides generate nearly the same ghost amplitudes to originally empty data slots. Moreover, one or both sides may be a general transmission line that is not optimally designed for intra-channel nonlinear compensation. In which case, ghost-pulse generations may still be well suppressed due to the cancelation of ghost amplitudes generated by the two sides, however the mark pulses in the originally ON data slots may suffer significant jitters in amplitude and timing, as a result of the transmission system lacking a (scaled) translation or mirror symmetry.

It is interesting to compare the present method of mid-way SPM and signal reshaping based on nonlinear optical loop mirrors (NOLMs) [144, 145], both of which are able to suppress ghost-pulses, and both are channelized solutions suitable for systems with a high modulation speed, because where the number of wavelength channels is less and higher optical power is available in each channel for efficient nonlinear effects. While a NOLM is often regarded as a lumped signal regenerator, mid-way SPM may be viewed as a method of distributive signal regeneration, whose action takes place through an entire transmission line. Practically, mid-way SPM would be more convenient than NOLMs, as the latter require interferometry stability and are sensitive to variations of fiber birefringence [146]. On the other hand, NOLMs are capable of "removing" random optical noise due to amplified spontaneous emission and loss-induced quantum noise [40], while mid-way SPM is not.

8

Practical Implementations: OPC, DCM, & More

When a nonlinear medium is pumped by a strong laser beam, nonlinear interactions can mix the pump laser and a weak signal to generate a phase-conjugated version of the signal. It has been demonstrated that OPC may be employed to compensate the chromatic dispersion and nonlinearity of transmission fibers. It may even serve as a parametric amplifier when the pump is sufficiently intense. Furthermore, nonlinear mixing is capable of phase-conjugating and/or amplifying many WDM signals simultaneously. However, the same nonlinear effect results in parasitic processes by generating inter-mixing terms among the WDM signals. The center frequency of such unwanted mixing terms may coincide with some of the original or conjugated WDM signals to cause significant interference.

In the following, the first section reviews the state-of-the-art of optical phase conjugators, then studies in details the parasitic interference effect by means of theoretical calculations and computer simulations. It will be shown that the coherent interference effect decreases as the PSR (that is pump-power to signal-power ratio) increases. Unfortunately, there could still be strong interference even with a PSR of 20 dB. Some guard-band in the frequency domain may be necessary to avoid such coherent interference: if the total bandwidth of the WDM signals is W, then the nearest signal should be more than W away from the pump frequency.

The second section discusses a method of packaging DCFs which achieves optimal nonlinear compensation and good signal-to-noise ratio simultaneously. An optimally packaged DCM may consist of portions of DCFs with higher and lower loss coefficients. Such optimized DCMs may be paired with transmission fibers to form scaled translation-symmetric lines, which could effectively compensate signal distortions due to dispersion and nonlinearity, with or without OPC.

The third section discusses certain linearity of nonlinear perturbations and applies the property to nonlinear compensations. It proposes and tests (through numerical simulations) methods of one-for-many nonlinear compensations using STS, which realize simultaneous compensations of both dispersion and nonlinearity over a wide optical band. When OPC is employed, a transmission line may consist of many pairs

of compensating fiber spans mirror-symmetrically ordered about the phase conjugator, where each pair may include one fiber span of stronger nonlinearity and several conjugating fiber spans of weaker nonlinearity. First-order nonlinearities are well compensated between spans within each pair, and the mirror-symmetric ordering of conjugating pairs about the phase conjugator helps to prevent the accumulation of nonlinearities over a long transmission distance. When there is no OPC in the middle, a transmission line configured into a one-for-many STS may still suppress the intra-channel nonlinear effects.

8.1 *Inter-channel Crosstalk in FWM-based Phase Conjugators*

OPC proves capable of neutralizing the effect of chromatic dispersion of two fiber lines of the same type, and compensating or at least reducing nonlinearity-induced impairments. When the pump is sufficiently intense, an optical phase conjugator may even serve as a parametric amplifier, boosting the signal level with low, theoretically no additive noise [35, 42]. All these applications beg a good method to physically implement an optical phase conjugator. Recently, there have been a lot of successful lab demonstrations of OPC, most of which employ a Kerr nonlinear medium, such as a highly nonlinear optical fiber [16, 47, 166, 167, 168, 169, 170], a $LiNbO_3$ waveguide [171, 172, 173, 174, 175, 176, 177], a semiconductor optical amplifier [178], or a semiconductor (III-V or silicon) waveguide [179]. There have also been experiments of OPC in transmission systems to fight dispersion and nonlinear impairments [20, 180, 181, 182, 183, 184, 185], as well as efforts to commercialize such phase conjugators [186]. Given the vast number of successful demonstrations and experiments, there is reason to believe that OPC has become an obtainable and deployable technology. What remains may be only further engineering improvements for better performance, higher reliability, and lower cost. It is hoped that this thesis research may add to the list of benefits of employing OPC in transmission systems, so to speed up its adoption in fiber-optic communications.

When a Kerr medium is pumped by a strong laser beam, the $\chi^{(3)}$ nonlinear process manifested as FWM can mix the pump laser and a weak signal, so to generate a phase-conjugated version of the signal. However, the FWM effect results in parasitic processes by generating inter-mixing terms among the WDM signals. The center frequency of such unwanted mixing terms may happen to coincide with the original or the conjugated WDM signals. Because of the coincidence in frequency, the inter-mixing terms are coherently superposed to the desired signals and cause serious

interference [147, 148]. This section studies such interference effect through theoretical calculations and computer simulations, using FWM in a low-dispersion highly nonlinear fiber as an example. Simulation results shall be reported in the form of signal eye diagrams.

It is well known that a zero-dispersion fiber (although the dispersion slope needs not to be zero) with a strong optical pump can perform the OPC operation, by virtue of the FWM effect. For optimal conversion efficiency, the frequency ω_0 of the pump field E_0 should be close to the fiber zero-dispersion frequency, and the pump amplitude should be much larger than all the signal fields $E_1(t)$, $E_2(t)$, ..., $E_N(t)$, which are usually spaced evenly and fall on one side of the pump in the frequency domain. Let the WDM signals be labeled such that the center frequency of $E_n(t)$ is given by $\omega_n = \omega_0 + n\Delta$, where $n > 0$ is an integer, $\Delta \in \mathbf{R}$, and $|\Delta|$ is the channel spacing. The pump power is usually dominating, namely, $P_0 = E_0 E_0^* \gg E_n E_n^* = P_n$, for all $n \neq 0$. The third-order nonlinearity of the fiber generates new terms like $\chi^{(3)} E_l E_m E_n^*$ into the electromagnetic field, which are mixed-product of the signals, hence the name wave mixing [5, 6]. Among the mixed waves, terms of the form $\chi^{(3)} E_n(t) E_0 E_0^*$ and $\chi^{(3)} E_0 E_0 E_n^*(t)$ have the strongest amplitudes. For each $n > 0$, the former term has the center frequency ω_n so to superpose coherently onto the original signal $E_n(t)$, while the latter term generates a new frequency at $\omega_{-n} = \omega_0 - n\Delta$, and the new signal is a phase-conjugated image of $E_n(t)$. Both the original and the phase-conjugated signals start growing in amplitude, the manifestation is of course parametric amplification. The strongest mixed-products are usually the desired terms in applications. There are other mixed-products with weaker amplitudes, which could however coincide with the desired terms in frequency and cause sizable interference to them. Analytical tools are of much help to understand the physics better.

8.1.1 *Mathematical analysis*

FWM is a polarization-sensitive process. In general, the electromagnetic signals should be treated as vectorial fields as all signals may not be co-polarized. A vectorial description is particularly necessary to understand the operation of polarization-insensitive OPC or parametric amplification. For the present study of inter-channel cross-talk, however, it is sufficient to work with a simplified model, in which all signals are co-polarized and may be treated just as scalars. From Maxwell's equations, the following differential equation may be derived for the total electrical field $E(x, y, z, t)$ in the nonlinear medium [5, 6],

$$\nabla^2 E - \frac{1}{c^2}\frac{\partial^2 E}{\partial t^2} - \frac{1}{c^2}\frac{\partial^2}{\partial t^2}\int \mathrm{Re}[\chi^{(1)}(s)]E(t-s)ds = \frac{i}{c^2}\mathrm{Im}[\chi^{(1)}]\frac{\partial^2}{\partial t^2}E + \frac{1}{c^2}\chi^{(3)}\frac{\partial^2}{\partial t^2}E^3, \quad (8.1)$$

where $\chi^{(1)}$ is the linear susceptibility of the medium, whose real and imaginary parts correspond to the dielectric response and signal loss respectively, while $\chi^{(3)}$ is real-valued and represents the Kerr nonlinearity. The Raman nonlinear effect is neglected here. The total electric field may be written as,

$$E(x,y,z,t) = \mathrm{Re}\left[\sum_{n\in\mathbf{Z}} F_n(x,y)A_n(z,t)\exp(i\beta_{n0}z - i\omega_n t)\right], \tag{8.2}$$

where β_{n0} is the optical propagation constant at frequency ω_n, $F_n(x,y)$ is the transverse modal function, and A_n is naturally the slow-varying envelope, of the nth WDM channel [6]. With $n \in \mathbf{Z}$, the set of WDM channels includes the original signals as well as their phase-conjugate images. As discussed in Chapter 3 and detailed in Appendix B, a multi-component NLSE may be obtained by substituting equation (8.2) into equation (8.1) and reducing factors independent of z,

$$\frac{\partial A_n}{\partial z} - i\mathsf{D}_n A_n + \frac{\alpha_n}{2}A_n = i\sum_l\sum_m \gamma_{lmn}A_l A_m A^*_{l+m-n}\exp(i\theta_{lmn}z), \quad \forall\, n \in \mathbf{Z}, \tag{8.3}$$

where

$$\mathsf{D}_n \stackrel{\text{def}}{=} \sum_{k=1}^{+\infty}\frac{\beta_{nk}}{k!}\left(i\frac{\partial}{\partial t}\right)^k - \beta_{01}\left(i\frac{\partial}{\partial t}\right), \tag{8.4}$$

$$\alpha_n \stackrel{\text{def}}{=} \frac{\omega_n^2}{\beta_{n0}c^2}\int \mathrm{Im}[\chi_n^{(1)}(x,y)]|F_n|^2 dxdy, \tag{8.5}$$

$$\beta_{nk} \stackrel{\text{def}}{=} \frac{1}{2\beta_{n0}}\left.\frac{\partial^k\beta^2(\omega)}{\partial\omega^k}\right|_{\omega=\omega_n}, \quad \forall\, k \geq 1, \tag{8.6}$$

$$\gamma_{lmn} \stackrel{\text{def}}{=} \frac{3\omega_n^2}{8\beta_{n0}c^2}\int \chi^{(3)}(x,y)F_l F_m F_n^* F^*_{l+m-n}dxdy, \tag{8.7}$$

$$\theta_{lmn} \stackrel{\text{def}}{=} \beta_{l0} + \beta_{m0} - \beta_{n0} - \beta_{(l+m-n)0}, \tag{8.8}$$

$\forall\, l,m,n \in \mathbf{Z}$. Equation (8.3) is a simpler version of (3.19), and is a fundamental equation governing the propagation of WDM channels and the Kerr nonlinear interactions among them.

Practical implementations often use short low-dispersion fibers, so that dispersion effects, represented by D_n and θ_{lmn}, may be neglected. Constant α and γ may be used as variations of the loss and nonlinear coefficients are often negligible across the channels. Moreover, the PSR is usually high to avoid pump depletion. With these considerations, equation (8.3) may be simplified significantly as,

$$\frac{\partial A_0}{\partial z} + \frac{\alpha}{2}A_0 = i\gamma|A_0|^2A_0, \tag{8.9}$$

$$\frac{\partial A_n}{\partial z} + \frac{\alpha}{2}A_n = i\gamma\sum_l\sum_m A_l A_m A^*_{l+m-n}, \quad \forall\, n \neq 0. \tag{8.10}$$

The right side of equation (8.10) may be written as,

$$i\gamma\left(2|A_0|^2A_n + A_0^2A_{-n}^*\right) + i\gamma\sum_{l\neq 0,n}\left(2A_0A_lA_{l-n}^* + 2A_0^*A_lA_{n-l}\right) + i\gamma\sum_{l\neq 0,\ m\neq 0,\ n\neq l+m} A_lA_mA_{l+m-n}^*, \tag{8.11}$$

which is sorted into three groups according to the signal strength: scaled by $|A_0|^3$, terms in the three groups are on the orders of $(\text{PSR})^{-1/2}$, $(\text{PSR})^{-1}$, and $(\text{PSR})^{-3/2}$ respectively. The first, strongest group happens to contain the desired terms for OPC and parametric amplification. The other two groups are usually unwanted and often cause interference to the desired signals. Increasing the PSR can obviously suppress the unwanted interference. For signal power on the order of mW, which is a common signal level in most applications, it is difficult to have a PSR much higher than 30 dB, because it would then require a pump laser much more intense than one Watt. A reasonable PSR may be around 20 dB, namely, PSR $\approx$ 100. When some of the desired signals are coherently interfered by terms in the third, weakest group, the random amplitude fluctuation would not be much higher than one percent, and may be ignored for most practical purposes. The second group, however, could be a serious source of signal degradation. Even with PSR $\approx$ 100, terms in the second group could result in amplitude fluctuations up to 10%, or equivalently power fluctuations as high as 20% in the desired signals. It is generally necessary to include the mixed-products in the second group. Equation (8.10) may be simplified into,

$$\frac{\partial A_n}{\partial z} + \frac{\alpha}{2}A_n = i\gamma\left(2|A_0|^2A_n + A_0^2A_{-n}^*\right) + i\gamma\sum_{l\neq 0,n}\left(2A_0A_lA_{l-n}^* + 2A_0^*A_lA_{n-l}\right), \quad \forall\, n\neq 0, \tag{8.12}$$

without losing much prediction power of the formulism.

Equations (8.9) and (8.12) are therefore suitable tools for the analysis of FWM-based OPC and parametric amplification of WDM signals. However, the presence of terms in the second group makes it difficult to solve the equations analytically. The problem may be rendered analytically tractable by the perturbation method, which is actually a procedure of stepwise approximation. Firstly, terms of the second group are dropped altogether, and the much simplified equations are solved analytically to provide the familiar result in most theoretical accounts of FWM-based OPC and parametric amplification [6, 16]. Secondly, the solution is used to calculate the terms of the second group in equation (8.12), and the complete differential equations are then integrated again, with terms in the second group regarded as known input drive

signals. Such simple perturbation calculation provides a solution with drastically improved accuracy. It catches nicely the phenomenon of inter-channel cross-talk among the WDM channels. If still higher accuracy is desired, the perturbation procedure may be repeated: substituting the available solution into equation (8.12) to convert terms of the second group into known drive signals, then solving the differential equations, and repeating as desired.

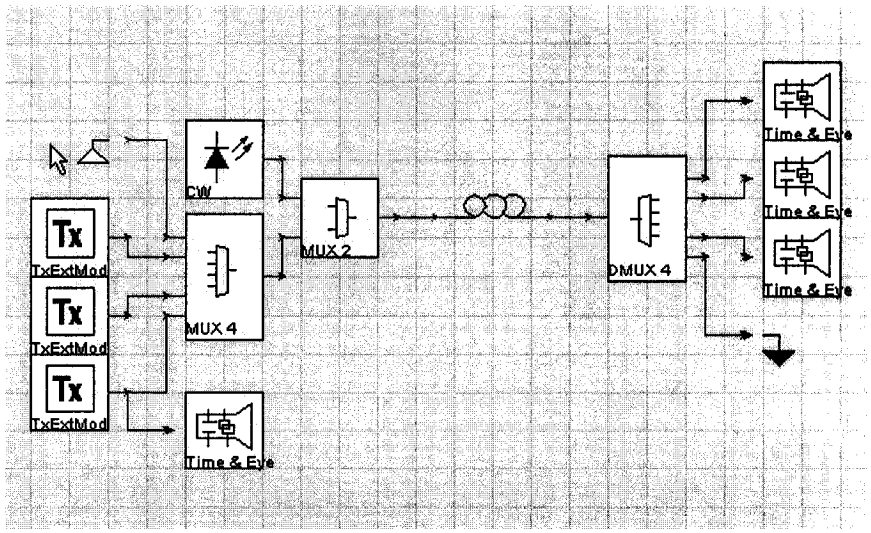

Figure 8.1: The simulation setup of FWM-based OPC.

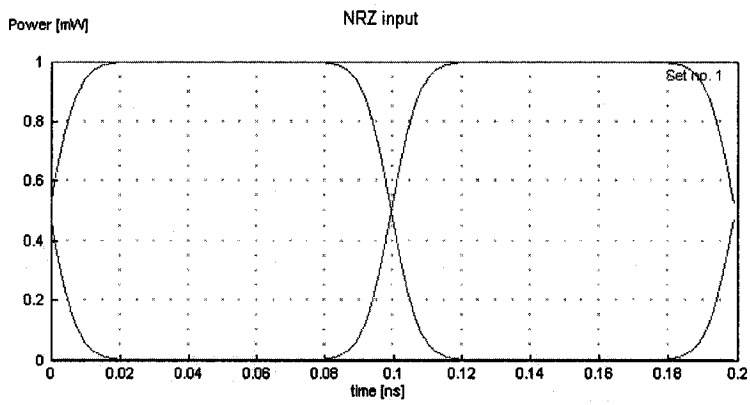

Figure 8.2: The input 10Gb/s NRZ optical signal.

The parametric gain to the signals may be higher or lower, depending upon the intensity of the pump laser, the length and internal loss of the nonlinear fiber. In the case of low parametric gain, the amplitudes of the original signals do not experience much variation apart from the effect of the internal loss of the fiber, and the amplitudes of the phase-conjugated signals are proportional to $A_0^2 A_n^*$, $n > 0$. At the

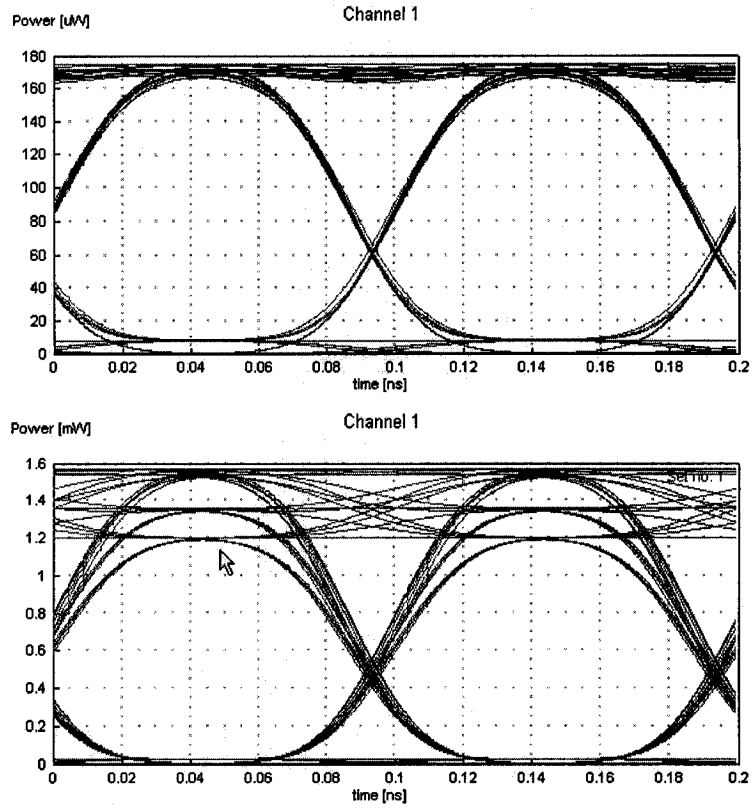

Figure 8.3: The phase-conjugated signals of channel 1, when it is 100 GHz away from the pump frequency.

other extreme of high gain, which is desired for parametric amplification, both the original and the phase-conjugated signals grow substantially, and the amplitudes of the latter are no longer proportional to $A_0^2 A_n^*$, $n > 0$. The perturbation procedure converges very fast and achieves high accuracy in the case of low parametric gain. By contrast, high parametric gain makes the perturbation procedure converge slowly and good accuracy difficult to achieve, it may also aggravate the effect of inter-channel cross-talk. In any case, interference from the mixed-products of the second group could distort the desired signals badly, and should be avoided. One way of preventing such coherent interference is to leave some guard-band in the frequency domain. For applications with a low parametric gain, the interference from the mixed-products $A_0 A_l A_{l-n}^*$ or $A_0^* A_l A_{n-l}$, for all $l > 0$, cause negligible amplitude fluctuation to the original signal A_n, for each $n > 0$. However, the mixed-products $A_0 A_l A_{l+n}^*$, $l > 0$, cause the amplitude of the phase-conjugated signal A_{-n}, for each $n > 0$, to fluctuate considerably. To avoid such interference, it is necessary to make sure that the original signals never occupy the pair of frequencies ω_l and ω_{l+n} simultaneously, for any $l > 0$,

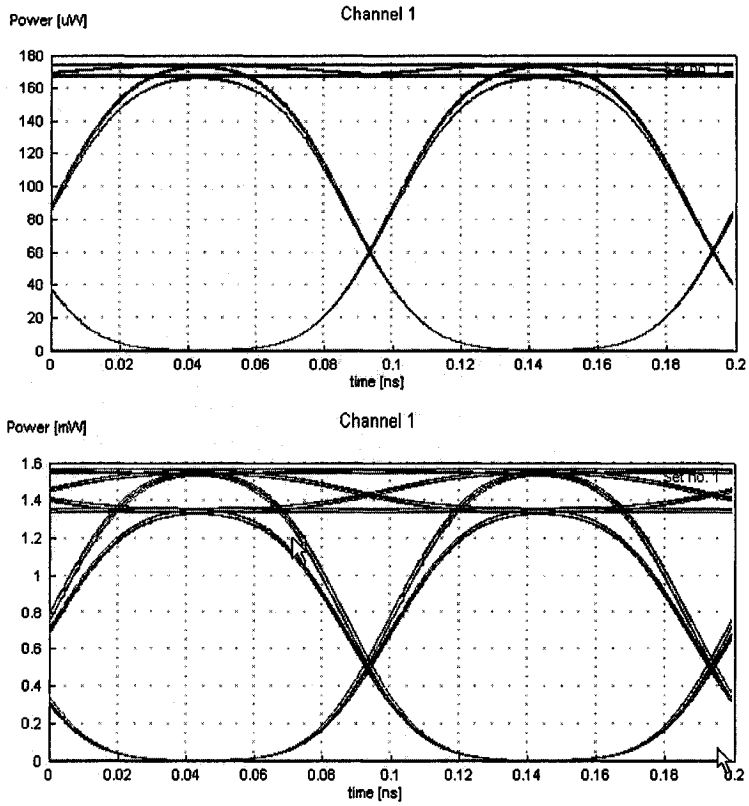

Figure 8.4: The phase-conjugated signals of channel 1, when it is 200 GHz away from the pump frequency.

$n > 0$. If the total bandwidth of the original WDM signals is W, then the nearest channel to the pump should be more than W away from the pump frequency, so that even the mixed product of the pump and the two edge channels of the WDM band will not be able to reach into the band of the phase-conjugated signals. Even with a high parametric gain, the guard-band of W is sufficient to prevent the mixed-products of the pump and two original signals from falling into either the original or the phase-conjugated WDM signal band.

8.1.2 Computer simulations

Computer simulations are carried out using VPItransmissionMaker^{TM}, to visualize the effect of inter-channel cross-talk as well as to demonstrate the effect of a guard-band in avoiding the inter-channel interference. Fig. 8.1 shows the simulation setup of an FWM-based optical phase conjugator, where the Kerr medium is a zero-dispersion fiber with length 1.0 km, material nonlinear index 2.6×10^{-20} m^2/W, core area 25 μm^2. The optical loss is neglected in the fiber. The pump laser is at 193.1 THz,

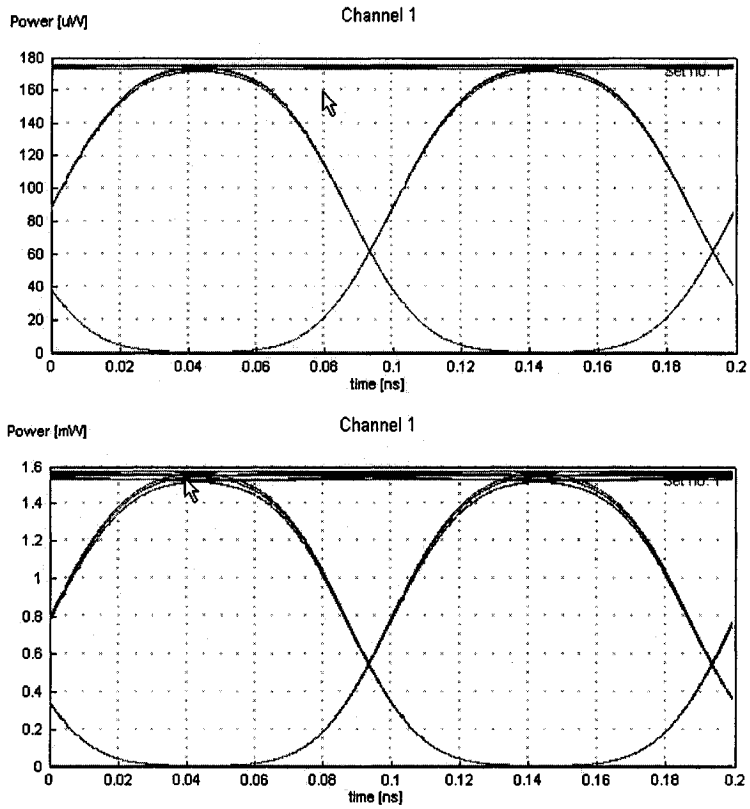

Figure 8.5: The phase-conjugated signals of channel 1, when it is 300 GHz away from the pump frequency.

pump power 100 or 300 mW, corresponding to a low parametric gain and a higher gain of 2 dB approximately. The WDM inputs are three NRZ signals with channel spacing 100 GHz, peak power 1 mW. The original signals are on the left side of the pump, and channel 1 is the nearest. The frequency shift between channel 1 and the pump is set to 100, 200, and 300 GHz respectively. Fig. 8.2 shows a typical input signal NRZ modulated at 10 Gb/s, and figures 8.3, 8.4, 8.5 show the eye diagrams of the phase-conjugated signals of channel 1, with the frequency shift from the pump being set to 100, 200, 300 GHz respectively. The two eye diagrams in each figure are for the cases of lower and higher parametric gain, with the pump power being 100 and 300 mW respectively. The higher parametric gain is clearly seen to aggravate the inter-channel cross-talk, and such interference is obviously prevented by a suitable frequency guard-band.

8.2 *Optimal packaging of dispersion compensating fibers for matched nonlinear compensation and reduced optical noise*

Dispersion compensating fibers have become essential components in high-speed long-distance fiber-optic transmissions. Often they are packaged into compact DCMs and integrated with fiber optical amplifiers at the repeater sites. The loss of signal power in DCFs requires extra gain from optical amplifiers, and amplifiers introduce noise. Because of their small modal area, DCFs could be significant contributors of nonlinearity if the power of signals carried is not limited to a low level. In the past, DCF manufacturers have strived to reduce the loss of DCFs and to lower their nonlinearity by enlarging the modal area [149]. However, reduced DCF nonlinearity does not necessarily translate into improved overall transmission performance. In the above, we have demonstrated that the nonlinear response of DCFs may be taken advantageously to compensate the nonlinearity of transmission fibers (TFs). Simply minimizing the loss in such nonlinearity-compensating DCFs is not necessarily aligned with the best system performance either. Here we propose and analyze a method of packaging DCFs to achieve optimal nonlinear compensation and good SNR simultaneously. Simply stated, an optimally packaged DCM may consist of two (or more) portions of DCFs with higher and lower loss coefficients. In the first portion that experiences high signal power, the loss coefficient may be intentionally increased in proportion to the DCF dispersion with respect to a TF. In another portion where the signal power is low and nonlinearity is negligible, the loss coefficient may be minimized to output stronger signals while compensating the remaining dispersion due to the TF.

Effective nonlinear compensation between DCFs and TFs, with or without OPC, relies on careful arrangements of different types of fibers in a transmission line to form the so-called STS, that is, scaled translation symmetry. The previous has established the analytical theory and numerical simulations verifying nonlinear compensations using translation symmetry. Basically, for two fibers to be matched for a translation symmetry in the scaled sense about an optical phase conjugator, their parameters need to obey the following scaling rules,

$$[\alpha', \beta_2', \beta_3', \gamma' P_0', g'(t) P_0'] = R\,[\alpha, -\beta_2, \beta_3, \gamma P_0, g(t) P_0]\,, \tag{8.13}$$

where α, β_2, β_3, γ, and $g(t)$ are the loss, second-order dispersion, third-order dispersion, Kerr and Raman nonlinear coefficients respectively for one fiber, while the

"primed" parameters are the corresponding parameters of the other fiber, P_0 and P_0' are the signal powers input to the two fibers respectively, $R > 0$ is a scaling factor. Such STS proves to enable nonlinear compensation between the two matched fibers up to the first-order nonlinear perturbation. The seemingly limited compensation capability based on perturbation is in fact quite relevant and powerful in practice, because the nonlinear response of each fiber segment is indeed perturbative in long-distance transmission lines, and matched fiber pairs may be arranged in a mirror-symmetric order to effectively undo the nonlinear distortions that may have accumulated far beyond the regime of perturbations. In the absence of OPC, a DCF and a TF may still be arranged into a translation symmetry in the scaled sense according to the following rules,

$$(\alpha', \beta_2', \beta_3', \gamma' P_0') = R\,(\alpha, -\beta_2, -\beta_3, \gamma P_0)\,, \tag{8.14}$$

where again $(\alpha, \beta_2, \beta_3, \gamma)$ and $(\alpha', \beta_2', \beta_3', \gamma')$ are parameters of the two types of fibers respectively. In both cases of scaling rules of equations (8.13) and (8.14), the requirements for the third-order dispersions may be relaxed, then the two fibers are not in strict translation symmetry across a band of wavelength channels, rather the symmetry and nonlinear compensation between them become approximate. Nevertheless, such approximation is often a good one when the value of $|\beta_2/\beta_3|$ is high, so that the percentage change of β_2 is only small across the band, which is exactly the case for SMFs in the 1550-nm band.

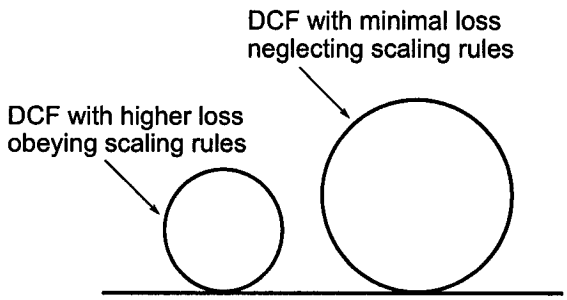

Figure 8.6: Two portions of dispersion-compensating fiber packaged into a compact module or cabled into a transmission line, where the first portion may have an intentionally increased loss coefficient to form an STS with a transmission fiber, while the second portion could have the lowest possible loss coefficient and does not need to satisfy any scaling rule.

In our methods of compensating fiber nonlinearity using translation symmetry with or without optical phase conjugation, dispersion-compensating fibers are brought into STS with respect to TFs such as SMFs and NZDSFs. As noted before, in regions of dispersion-compensating fibers carrying lower optical power, the scaling rules of

fiber parameters in equations (8.13) or (8.14) may be relaxed without sacrificing the performance of nonlinear compensation, both for systems using cabled DCFs into the transmission lines and for systems using lumped DCMs at the repeater sites. Such relaxation may be done for practical convenience, or to control the accumulated dispersion in a span to a desired value, as well as to reduce the span loss so to reduce the penalty due to optical noise. As illustrated in Fig. 8.6, a compact dispersion-compensating module or a dispersion-compensating transmission line may consist of two portions of dispersion-compensating fiber concatenated, where the first portion carrying high-power signals may have an intentionally increased loss coefficient to form an STS with a TF, while the second portion experiencing low signal power could have the minimal loss coefficient and does not need to satisfy any scaling rule. The two portions of DCF with higher and minimal loss coefficients may be of one whole piece of fiber coiled with different radiuses, or differently fabricated DCFs with different loss coefficients and possibly different dispersions, so long as the first fiber is in STS to a target TF. The minimal loss coefficient refers to the lowest fiber loss coefficient that is achievable in practical fabrication of dispersion-compensating fibers. The loss coefficient of the fiber portion on the left side of Fig. 8.6 is higher in the sense that it is intentionally made higher than what is achievable by practical manufacturing processes.

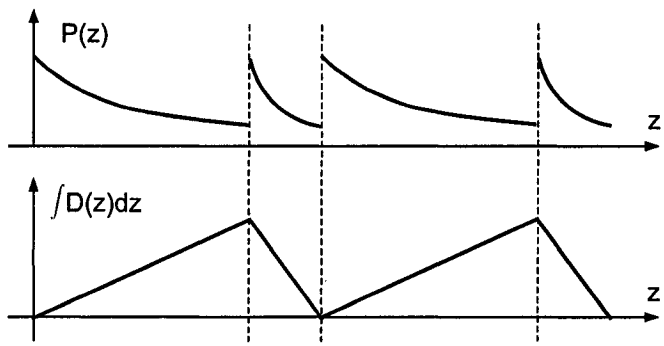

Figure 8.7: The power map and M-type dispersion map over the transmission distance of two traditional fiber spans.

The great advantage of nonlinear compensation using STS is that a pair of matched fiber segments are required to have the same sign for the loss/gain coefficients and opposite dispersions. Such conditions are naturally satisfied in conventional fiber transmission systems, where a TF, for example an SMF, may be paired with a DCF as matched counterparts. However, traditional transmission lines are usually set up with the same configuration for all spans, that is, with a TF followed by a DCF.

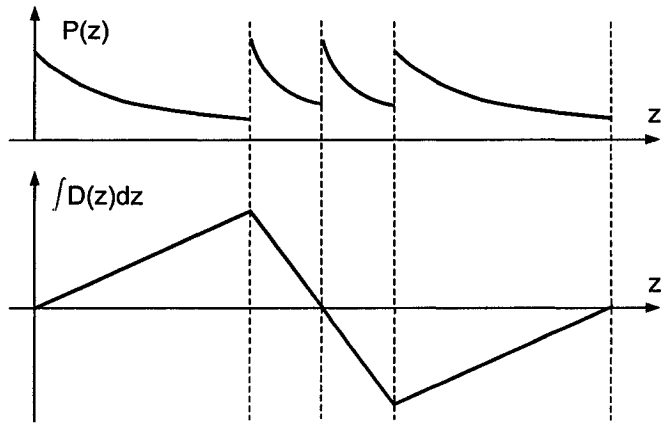

Figure 8.8: The power map and N-type dispersion map over the transmission distance of two matched fiber spans for an STS.

Consequently, the accumulated dispersion in all spans is single-sided, namely, stays always positive or always negative. Such may be called an M-type dispersion map, as shown in Fig. 8.7, where no two spans could form an STS. Our proposal is to simply exchange the ordering of the TF and DCF for some spans, which may be paired with traditional spans to form an N-type dispersion map, where the accumulated dispersion may go both positive and negative and trace an N-like curve, as shown in Fig. 8.8. An STS is formed between two matched fiber spans as in Fig. 8.8, in the sense that the TF of the first span is scaled translation-symmetric to the DCF of the second span, and the DCF of the first span is scaled translation-symmetric to the TF of the second span. Such translation symmetry between two matched spans could cancel some of their intra-channel nonlinearities, or compensate all nonlinearities up to the first-order perturbation if an optical phase conjugator is installed in the middle. Furthermore, many pairs of matched spans may be arranged into a mirror-symmetric order about the point of OPC to form a long-distance transmission line, whose second part could undo the nonlinear distortions due to the first part that may have accumulated far beyond the regime of perturbations.

In traditional transmission lines, each fiber span has a TF and a DCM at the end, which consists of a conventional DCF with a multi-stage EDFA. Many such conventional fiber spans are cascaded to form a line with the M-type dispersion map, as shown on the top of Fig. 8.9, where a conventional DCM is denoted by CDCM_M in short. If the order of TF and DCF is switched for every other span, then an N-type dispersion map is formed, and two adjacent DCFs may be packaged into one DCM, denoted by CDCM_N, as shown in the middle of Fig. 8.9. As a result of the N-type

dispersion map, intra-channel nonlinearities may be suppressed to some extent, and all fiber nonlinearities may be partially compensated at the presence of OPC in the middle of the transmission line. However, the compensation of nonlinearity is not optimal as the scaling rules of equation (8.13) or (8.14) are not satisfied by conventional DCFs paired with TFs. Indeed, DCF manufacturers have succeeded in reducing the loss of DCFs, as it was thought to monotonically improve the performance of transmission systems [149]. The dispersion-to-loss ratio (DLR) of state-of-the-art DCFs is often much larger than that of TFs. From the stand point of matched nonlinear compensation, it would be advantageous to (intentionally) raise the loss of DCFs such that the DLRs of DCFs and TFs are matched to satisfy the scaling rules, at least for portions of fibers carrying high-power signals. On the other hand, in regions of DCFs experiencing low signal power, the nonlinearity is weak and negligible, then the scaling rules may be disregarded and the loss of DCFs may be minimized to enhance the optical SNR at the end of dispersion compensation. Therefore, an optimized DCM (ODCM), as shown at the bottom of Fig. 8.9, may consist of sections of DCFs with higher and lower loss coefficients, as well as multiple EDFA stages to repeat the signal power and regulate the signal power in the lossier portions of DCFs, according to a set of scaling rules with respect to the TFs. Higher DCF loss may be induced by impurity-doping during fiber manufacturing [80, 81] or by bending loss during fiber packaging [70].

Therefore, a DCM compensating the dispersion and nonlinearity of transmission fibers may be so packaged that the first portion of DCF experiencing a high level of signal power may have a higher loss coefficient satisfying the scaling rule in equation (8.13) or (8.14), whereas the second portion of DCF may ignore the scaling rules and become less lossy such that the signal power at the end of the DCM is not too low to be significantly impaired by the amplifier noise. In fact, the low-loss portion of the DCM may even use optical filters other than DCFs, such as fiber Bragg gratings and photonic integrated circuits. This method of packaging DCMs achieves the capability of nonlinear compensation and good noise performance simultaneously. For instance, it takes 10 km DCF with $D' = -80$ ps/nm/km to compensate 100 km NZDSF with dispersion $D = 8$ ps/nm/km and loss $\alpha = 0.2$ dB/km. The first 4 km of the DCF may be made highly lossy by a special treatment in manufacturing or packaging, with a loss coefficient $\alpha' = 2$ dB/km to form an STS with respect to the first 40 km NZDSF for optimal nonlinear compensation. However, the remaining 6 km DCF may ignore the scaling rules and have a much lower nominal loss $\alpha' = 0.6$ dB/km [4]. The total loss is reduced by 8.4 dB as compared to a DCM that complies strictly with the scaling rules throughout the length of the DCF. Another important parameter of DCFs is the

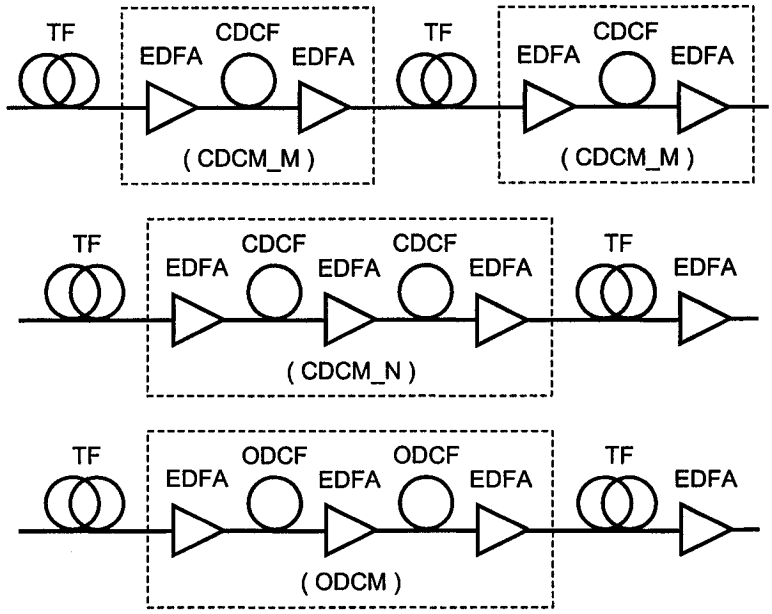

Figure 8.9: Three configurations of transmission lines with different dispersion maps and DCMs. Top: an M-type dispersion map using conventional DCMs; Middle: an N-type dispersion map using conventional DCMs; Bottom: an N-type dispersion map using optimized DCMs. Acronyms: CDCF - conventional DCF, ODCF - optimized DCF, CDCM_M - conventional DCM in an M-type dispersion map, CDCM_N - conventional DCM in an N-type dispersion map, ODCM - optimized DCM.

effective modal area, or more directly the nonlinear coefficient. Traditional designs of DCFs have always strived to enlarge the modal area so to reduce the nonlinear effects of DCFs. However, for DCFs used in our methods of nonlinear compensation, there exists an optimal range of modal area which should be neither too large nor too small. According to the scaling rules of equation (8.13) or (8.14), a DCF with a large modal area may require too much signal power to generate sufficient nonlinearity to compensate the nonlinear effects of a transmission fiber, while optical amplifiers may have difficulty to produce that much signal power. On the other hand, when the effective modal area is too small, the scaling rules of equation (8.13) or (8.14) dictate a reduced power level for the optical signal in the DCF, which may be more seriously degraded by optical noise, such as loss-induced quantum noise [40] and the amplified-spontaneous-emission noise from an amplifier at the end of the DCF.

To give an example of ODCM and test its performance in nonlinear compensation, we simulated (using VPItransmissionMaker^{TM}) and compared three transmission systems as shown in Figs. 8.10, 8.11, and 8.12 respectively, all of which have an optical phase conjugator in the middle and 6 recirculating loops on each side of OPC. For the first system, each recirculating loop consists of two identical spans of 100 km SMF

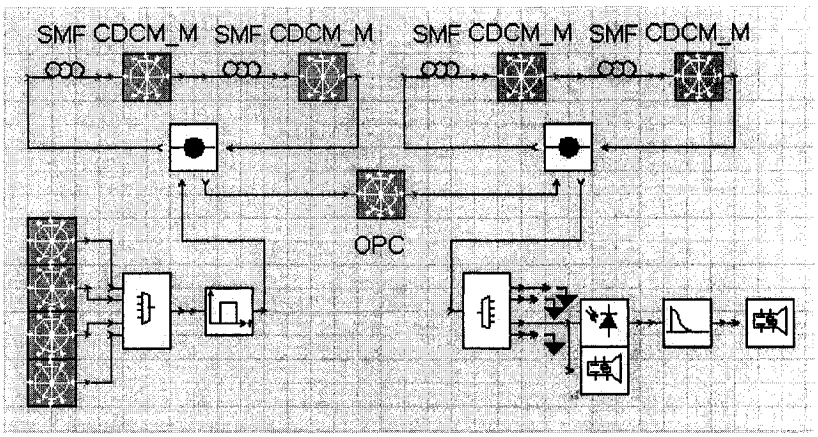

Figure 8.10: A test transmission system consisting of 6 recirculating loops with an M-type dispersion map on the left side, an optical phase conjugator in the middle, then on the right side another 6 loops identical to the ones on the left. Each recirculating loop consists of two identical spans of 100 km SMF followed by a CDCM_M, as shown on the top of Fig. 8.9.

followed by a CDCM_M, as shown on the top of Fig. 8.9. For the second system, each recirculating loop has 100 km SMF followed by a CDCM_N, then 100 km SMF followed by a 20dB EDFA, as shown in the middle of Fig. 8.9. For the third and optimized system, each recirculating loop consists of 100 km SMF followed by an ODCM, then 100 km SMF followed by a 20dB EDFA, as shown at the bottom of Fig. 8.9. Each CDCM_M has a 15dB EDFA, 20 km conventional DCF, then a 15dB EDFA. Each CDCM_N has a 15dB EDFA, 20 km conventional DCF, then another 15dB EDFA, 20 km conventional DCF, and finally a 10dB EDFA. By contrast, each ODCM consists of a 21dB EDFA, 10 km optimized DCF, 10 km conventional DCF, a 15dB EDFA, then 10 km optimized DCF, 10 km conventional DCF, and a 14dB EDFA. Note the adjustment of signal power in the optimized DCFs to fulfil the scaling rules. The SMF has loss $\alpha = 0.2$ dB/km, dispersion $D = 16$ ps/nm/km, dispersion slope $S = 0.055$ ps/nm^2/km, effective modal area $A_{\text{eff}} = 80$ μm^2. The conventional DCF has $(\alpha', D', S', A'_{\text{eff}}) = (0.5, -80, -0.275, 20)$ in the same units. The optimized DCF differs from the conventional one only by the loss coefficient $\alpha'' = 1.0$ dB/km. The same silica nonlinear index $n_2 = 2.6 \times 10^{-20}$ m^2/W is taken for all fibers. All EDFAs have the same noise figure of 4 dB. The center frequency is 193.1 THz. The inputs are four 40Gb/s channels, spaced by 200 GHz, co-polarized and return-to-zero modulated with 33% duty and pulse peak power 15 mW. The eye diagrams of optical signals from the 3rd DEMUX channel at the end of transmissions are shown in Fig. 8.13, where the top diagram displays severe nonlinear distortions for the conventional line with the M-type dispersion map, while the middle diagram shows improved but

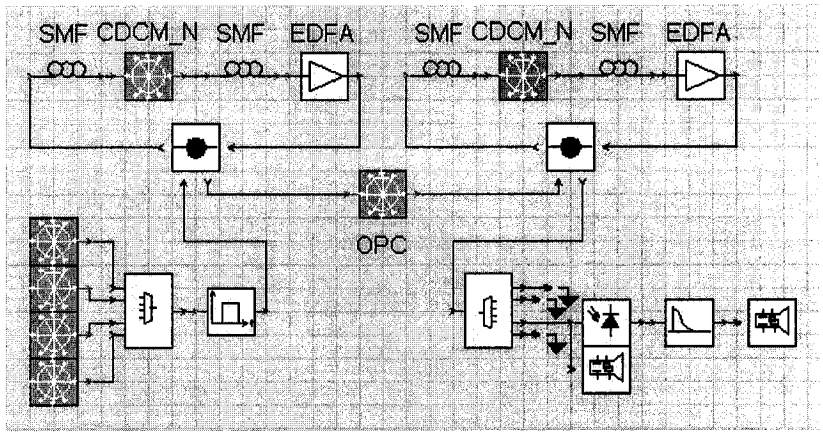

Figure 8.11: A test transmission system consisting of 6 recirculating loops with an N-type dispersion map on the left side, an optical phase conjugator in the middle, then on the right side another 6 loops identical to the ones on the left. Each recirculating loop has 100 km SMF followed by a CDCM_N, then 100 km SMF followed by a 20dB EDFA, as shown in the middle of Fig. 8.9.

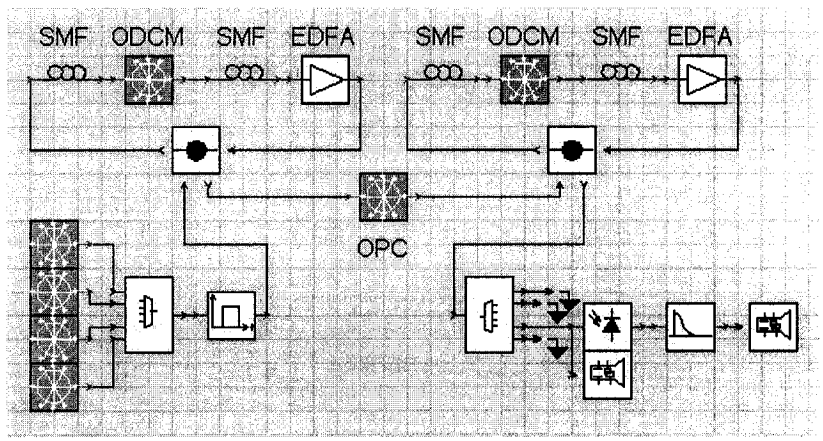

Figure 8.12: A test transmission system consisting of 6 recirculating loops with an optimized N-type dispersion map on the left side, an optical phase conjugator in the middle, then on the right side another 6 loops identical to the ones on the left. Each recirculating loop consists of 100 km SMF followed by an ODCM, then 100 km SMF followed by a 20dB EDFA, as shown at the bottom of Fig. 8.9.

still seriously impaired signals of the line with the N-type dispersion map using conventional DCMs. The bottom diagram demonstrates a significant improvement of signal quality by using optimized DCMs and STS, where the signal distortions are mainly due to EDFA noise and possibly some uncompensated nonlinearity.

Even without OPC, improved transmission performance due to intra-channel nonlinear compensation may be expected in transmission systems manifesting scaled translation symmetries using optimally packaged DCMs for matched nonlinear compensation and reduced optical noise simultaneously. Furthermore, the method of

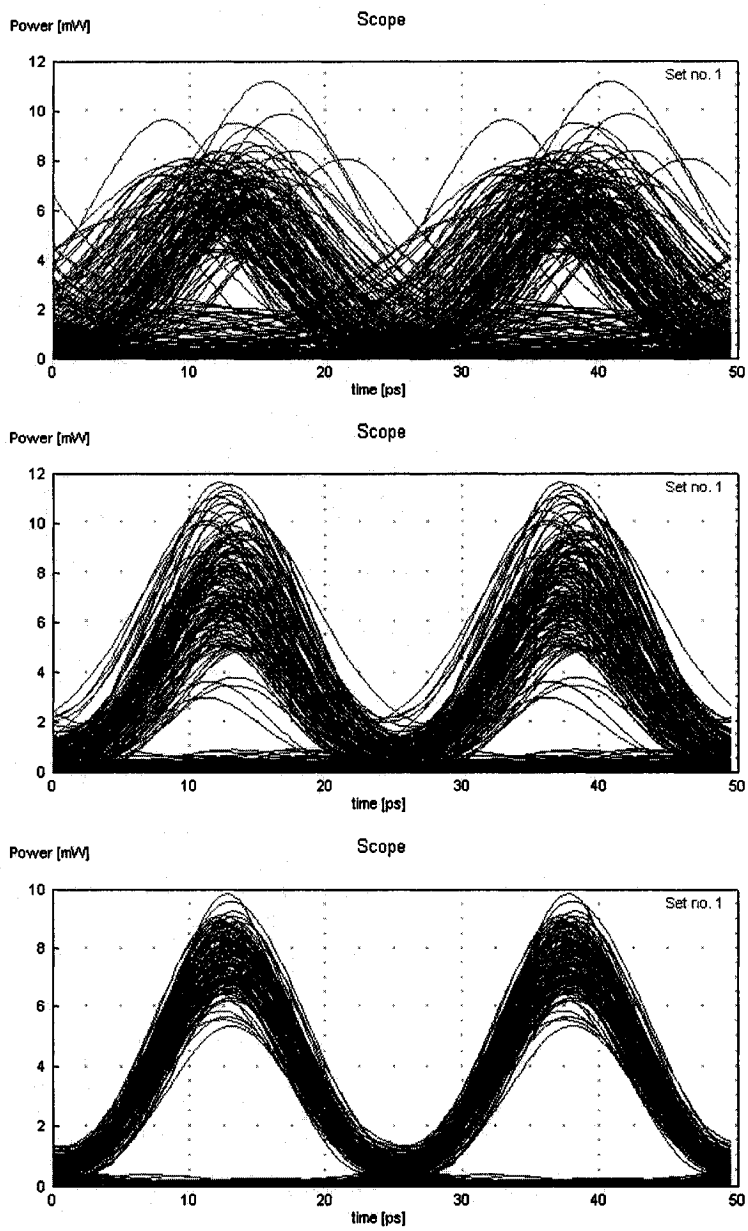

Figure 8.13: Optical eye diagrams of the 3rd DEMUX channel at the end of transmissions. Top: of a conventional line with the M-type dispersion map. Middle: of a line with conventional DCMs in the N-type dispersion map. Bottom: of a system using optimized DCMs and STS.

mid-span SPM discussed previously may be employed in such transmission systems using ODCMs to suppress the generation of ghost-pulses, which are not controlled by scaled translation symmetries alone. Finally, it is noted that the same principle for optimally packaging DCMs, namely, *obeying scaling rules where the signal power is high while disregarding the rules and minimizing the signal loss where the signal*

power is low, may be similarly applied to the design of transmission systems with cabled DCFs. For a piece of DCF cabled into a transmission line, the first portion of the DCF may have a relatively low absolute value of dispersion in proportion to its low loss coefficient, according to the scaling rules of translation symmetry to a transmission fiber as in equation (8.13) or (8.14). Whereas in the second portion of the DCF, where the signal power becomes sufficiently low, the dispersion may be set as high as possible while the loss coefficient should remain minimal, because no scaling rules need to be regarded.

8.3 *Linearity of nonlinear perturbations in fiber transmission lines and its applications to nonlinear compensations*

Our work has helped to recognize the importance of STS for simultaneous compensations of dispersion and nonlinearity in practical transmission systems using conventional fibers and amplifiers [12, 14, 15]. The great advantage of nonlinear compensations using STS is that a pair of matched fiber segments are required to have the same sign for the loss/gain coefficients and opposite dispersions. Such conditions are naturally satisfied in conventional fiber transmission systems using transmission fibers and DCFs with oppositely signed dispersions. An STS between two matched fiber spans could cancel some of their intra-channel nonlinearities [15, 26, 27], or compensate all nonlinear effects up to the first-order perturbation if OPC is performed in the middle [12, 14, 23]. Furthermore, many pairs of matched spans in STS may be arranged into a mirror-symmetric order about a mid-point (with or without OPC) to form a long-distance transmission line, whose second part could undo or compensate the nonlinear distortions due to the first part that may have accumulated far beyond the regime of perturbations [14].

A transmission line designed for nonlinear compensations may choose pairs of fiber segments having linear parameters in proportion with one ratio, *i.e.*,

$$[\alpha'(z'), -\beta_2'(z'), \pm\beta_3'(z')] = R\,[\alpha(z), \beta_2(z), \beta_3(z)]\,, \quad R > 0, \tag{8.15}$$

and nonlinear parameters with another ratio, namely, $\gamma'(z') = Q\gamma(z)$, $Q > 0$, or $[\gamma'(z'), g'(z', t)] = Q\,[\gamma(z), g(z, t)]$ for simultaneous compensations of both Kerr and Raman effects with the help of OPC. The two ratios Q and R may be, and usually are, different. The scaling rules of linear parameters in equation (8.15) between pairs of fiber segments carrying high signal power, in conjunction with proper dispersion

and slope adjustments disregarding the scaling rules in fiber segments experiencing low signal power [14, 15], ensures that the high-power signals flowing in each pair of matched fiber segments are kept proportional and complex conjugate with respect to each other over significant distances along the two fibers. Consequently, the first-order nonlinear terms due to Kerr- or Raman-mediated signal mixing are also proportional and complex conjugate with respect to each other along the two fibers. It becomes possible to adjust the power levels relatively in each pair of matched fibers to make the first-order nonlinear perturbations in the two fibers commensurate, so that the pair compensate each other's nonlinear effects in the presence of OPC, or cancel the most detrimental intra-channel nonlinear effects without OPC.

Although most fibers are made of similar materials with similar nonlinear susceptibilities, their guided-wave nonlinear coefficients measured in $W^{-1}km^{-1}$ could be quite different due to the wide variation of modal sizes. Unless the ratio Q of nonlinear coefficients matches the ratio R of linear parameters, the signal powers in two conjugate fibers may have to differ by several dB as required by the scaling rules for an STS. However, it may be desired to have a similar level of signal power into all fiber spans for a uniform design and similar characteristics of power repeaters as well as simpler system management. Here we discuss an alternative method of scaling and compensating nonlinear effects, which takes advantage of the linear additivity of first-order nonlinear perturbations and adjusts the signal powers in different fiber spans only slightly, such that one span of a type with stronger nonlinearity may compensate several fiber spans of another type with weaker nonlinearity. A span of stronger nonlinearity and a group of spans of weaker nonlinearity corresponding to it are said to form a compensating pair. Through both mathematical analysis and computer simulations, it will be demonstrated that by arranging many compensating pairs mirror-symmetrically about a mid-point of a long transmission line, the two parts of the line, before and after the mid-point, could have their nonlinear effects compensated in a distributive manner, although each part could accumulate much nonlinearity well beyond the regime of perturbations. The nonlinear compensations are especially good when the system has an optical phase conjugator installed at the mid-point. Even without a phase conjugator, the proposed configuration could suppress the so-called intra-channel nonlinear effects.

8.3.1 *Linearity of nonlinear perturbations and one-for-many nonlinear compensations*

As discussed in Section 4.2.1, had there been no nonlinearity, namely $\gamma(z) = g(z,t) \equiv 0$, $z_1 \leq z \leq z_2$, the slow-varying envelope $A(z_2,t)$ of an optical signal output from an optical fiber stretching from $z = z_1$ to $z = z_2 > z_1$, would be readily calculated by applying a linear operator $\mathsf{P}(z_1,z_2)$, often called propagator, to the input signal envelope $A(z_1,t)$. However, the existence of nonlinear terms in an NLSE makes the equation much more difficult to solve. Fortunately, when the signal power is not very high so that the nonlinearity is weak and may be treated as perturbation, the output from a nonlinear fiber line may be represented by a linearly dispersed version of the input, plus nonlinear distortions expanded in power series of the nonlinear coefficients [65, 74]. In practical transmission lines, although the end-to-end response of a long link may be highly nonlinear due to the accumulation of nonlinearity through many fiber spans, the nonlinear perturbation terms of higher orders than the first are usually negligibly small within each fiber span. Up to the first-order perturbation, the signal $A(z_2,t)$ as a result of nonlinear propagation of a signal $A(z_1,t)$ from z_1 to $z_2 \geq z_1$, may be approximated using the following expressions,

$$A_0(z_2,t) = \mathsf{P}(z_1,z_2)A(z_1,t), \tag{8.16}$$

$$\begin{aligned} A_1(z_2,t) = \int_{z_1}^{z_2} \mathsf{P}(z,z_2) \Big\{ & i\gamma(z)|A_0(z,t)|^2 A_0(z,t) \\ & + i\left[g(z,t) \otimes |A_0(z,t)|^2\right] A_0(z,t) \Big\} dz, \end{aligned} \tag{8.17}$$

where $A(z_2,t) \approx A_0(z_2,t)$ amounts to a zeroth-order approximation which neglects the fiber nonlinearity completely, whereas the result of first-order approximation $A(z_2,t) \approx A_0(z_2,t) + A_1(z_2,t)$ accounts in addition for the lowest-order nonlinear products integrated over the fiber length. The term $A_1(z,t)$ is called the first-order perturbation because it is linearly proportional to the nonlinear coefficients $\gamma(z)$ and $g(z,t)$. By linearity of nonlinear perturbations, it is referred to the linear accumulation of first-order nonlinear perturbations as in equation (8.17). Furthermore, the linear additivity of first-order nonlinear perturbations may still hold for a small number of repeated fiber spans.

When a plurality of spans of one type with weaker nonlinearity are scaled symmetric to the same span of another type with stronger nonlinearity according to the following,

$$\left[\alpha^{(n)}(z^{(n)}), -\beta_2^{(n)}(z^{(n)}), \pm\beta_3^{(n)}(z^{(n)})\right] = R^{(n)}\left[\alpha(z), \beta_2(z), \beta_3(z)\right], \quad R^{(n)} > 0, \tag{8.18}$$

$$\left[\gamma^{(n)}(z^{(n)}), g^{(n)}(z^{(n)},t)\right] = Q^{(n)}\left[\gamma(z), g(z,t)\right], \quad Q^{(n)} > 0, \tag{8.19}$$

$$z^{(n)} = z/R^{(n)}, \quad 0 \leq z \leq L, \tag{8.20}$$

$\forall\, n \in [1, N]$, where the scaling rules for the Raman coefficients $\{g^{(n)}(z^{(n)}, t)\}_{n=1}^{N}$ may be omitted when it is not an option to compensate the stimulated Raman effect. The scaling rules of linear parameters in equation (8.18) between pairs of fiber segments carrying high signal power, in conjunction with proper dispersion and slope adjustments disregarding the scaling rules in fiber segments experiencing low signal power, ensures that the high-power signals $\{A_0^{(n)}(z^{(n)} = 0,\ t)\}_{n=1}^{N}$ injected into fiber spans of the first type are kept proportional and complex conjugate with respect to $A_0(z = 0,\ t)$ injected into the span of the second type. According to equation (8.17), the first-order nonlinear terms due to Kerr- or Raman-mediated signal mixing generated in spans of the first type are also proportional and complex conjugate with respect to that generated in the span of the second type, namely,

$$A_1^{(n)}(z^{(n)} = L/R^{(n)},\ t) \ = \ \left[\frac{Q^{(n)}P_0^{(n)}}{R^{(n)}P_0}\right] A_1^*(z = L,\ t), \quad \forall\, n \in [1, N], \tag{8.21}$$

where "$*$" denotes complex conjugation, $P_0^{(n)} = \langle |A_0^{(n)}(0,t)|^2 \rangle$ and $P_0 = \langle |A_0(0,t)|^2 \rangle$ are the average signal powers in the beginning of fiber spans. It becomes possible by choosing the number N and adjusting the power levels $\{P^{(n)}\}_{n=1}^{N}$ and P_0, to render the accumulated first-order nonlinear perturbations of the N spans of the first type commensurate with that of the span of the second type, that is,

$$\sum_{n=1}^{N} A_1^{(n)}(z^{(n)} = L/R^{(n)},\ t) \ = \ A_1^*(z = L,\ t), \tag{8.22}$$

so that the single span of the second type compensates the nonlinear effects of the group of N spans of the first type in the presence of OPC, or cancel the most detrimental intra-channel nonlinear effects without OPC. It is necessary to scale the signal powers as,

$$\sum_{n=1}^{N} \left[\frac{Q^{(n)}}{R^{(n)}}\right] P_0^{(n)} = P_0, \tag{8.23}$$

in addition to the scaling rules of equations (8.18 -8.20). When it is desired to have a similar level of signal power into all fiber spans for a uniform design and similar characteristics of power repeaters as well as simpler system management, it is possible to adjust the signal powers in different fiber spans only slightly from the same nominal power level, and have one span with stronger nonlinearity to compensate several fiber spans with weaker nonlinearity. Such method is called one-for-many (in terms of fiber spans) nonlinear compensations.

Based on the idea of one-for-many nonlinear compensations, a multi-span long-haul transmission line may be designed using two types of fiber spans having relatively stronger and weaker nonlinear responses, where fiber segments in the two types of spans experiencing high-power signals are configured according to the scaling rules of an STS, while fiber segments carrying attenuated signals manage the dispersion and dispersion-slope. In particular, if each span with weaker nonlinearity is dispersion-compensated to have approximately zero accumulated dispersion, and each of several such spans in cascade may indeed induce approximately the same nonlinear response, then for a reasonably small number of such cascaded spans with weaker nonlinearity, the overall nonlinear response may still be well approximated by a combined first-order perturbation, which is just the sum of the first-order perturbations of individual spans. The overall nonlinear response may be compensated by one span with stronger nonlinearity that generates the equivalent amount of nonlinearity. The span of stronger nonlinearity and the corresponding group of spans of weaker nonlinearity are said to form a compensating pair. By arranging many compensating pairs mirror-symmetrically about a mid-point of a long transmission line, the two parts of the line, before and after the mid-point, could have their nonlinear effects compensated in a distributive manner, although each part could accumulate much nonlinearity well beyond the regime of perturbations [14, 15]. The nonlinear compensations are especially good when the system has an optical phase conjugator installed at the mid-point, in which case nonlinear compensations take place distributively between each compensating pair for all nonlinear mixing terms that are proportional to the Kerr or Raman coefficients, both within individual wavelength channels and among different channels. Even without a phase conjugator, the proposed one-for-many configuration in an STS may be able to suppress the so-called intra-channel nonlinear effects, *e.g.*, amplitude and timing jitters due to intra-channel nonlinear effects of IFWM and IXPM, which are often the dominating nonlinear impairments in systems with high modulation speeds of 40 Gb/s and above [65]. With the dominating amplitude and timing jitters due to intra-channel nonlinearities being suppressed, an ON/OFF-keying system may still suffer from IFWM-induced "ghost-pulses" into the "0" slots where there are originally no optical pulses [90, 93, 137, 138]. The growth of ghost-pulses may eventually limit the transmission distance. An interesting method suggests to use channelized SPM in the middle of two parts of a transmission line [31], where each part is designed to suppress the dominating amplitude and timing jitters, and the two parts would generate ghost-pulses at the same level when operating independently. Intriguingly, the mid-way SPM makes the second part of the transmission line generating oppositely signed ghost-pulses with respect to, and hence cancel, the

ghost-pulses generated by the first part.

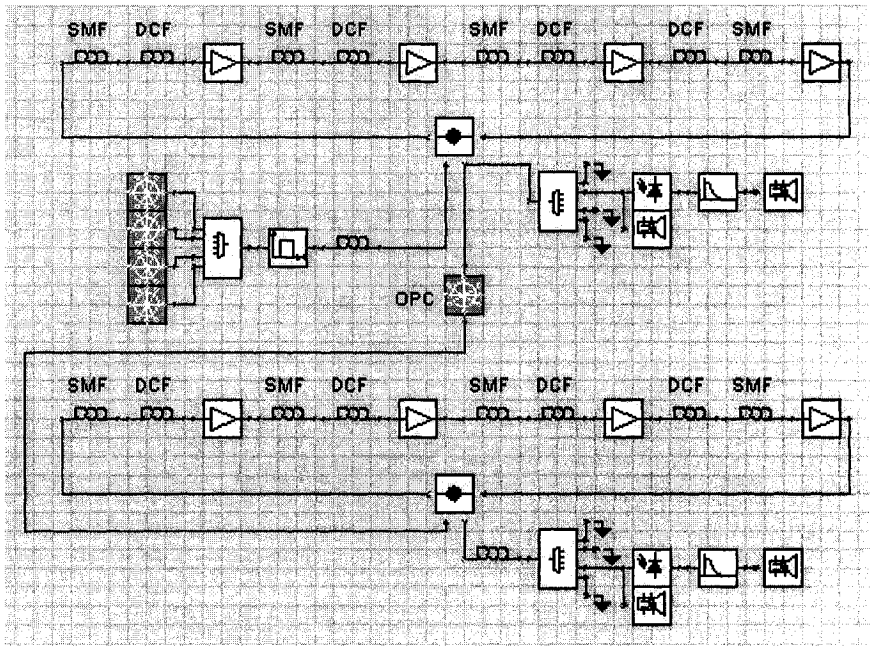

Figure 8.14: A system in one-for-many STS between (RDF + SMF) and (SMF + RDF) spans with OPC in the middle.

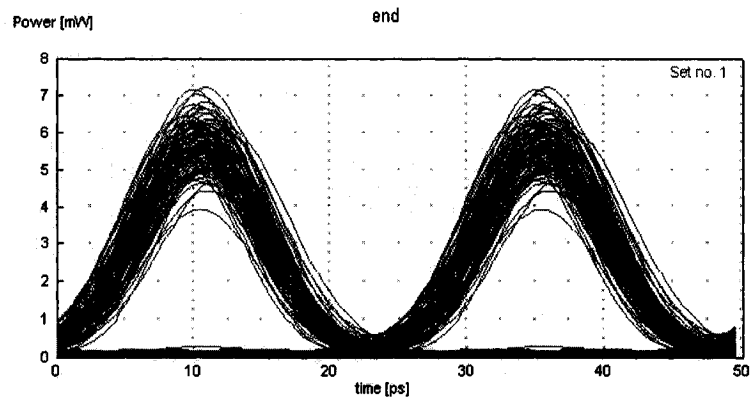

Figure 8.15: Optical eye diagram of the 3rd DEMUX channel received at the end of the one-for-many scaled translation-symmetric system shown in Fig. 8.14.

For a practical example, consider a transmission line using standard SMFs and the so-called RDFs [129, 131], which are arranged into two types of spans: (SMF + RDF) and (RDF + SMF) respectively, where "+" indicates "followed by", so as to achieve simultaneous dispersion and nonlinear compensations. RDFs have loss and dispersion coefficients comparable to those of SMFs, namely, $\alpha_{\text{RDF}} \approx \alpha_{\text{SMF}} \approx 0.2$

dB/km, $D_{\text{RDF}} \approx -D_{\text{SMF}} \approx -16$ ps/nm/km around 1550 nm. But the effective modal area of RDFs is usually small, typically about 30 μm^2, which is far less than that of SMFs, typically about 80 μm^2. As the fiber nonlinear coefficients are inversely proportional to the effective modal area, a typical RDF has Kerr and Raman nonlinear coefficients that are approximately 80/30 times of those of SMFs, namely, $\gamma_{\text{RDF}} \approx 2.7\gamma_{\text{SMF}}$, $g_{\text{RDF}}(\cdot) \approx 2.7 g_{\text{SMF}}(\cdot)$. In which case, one may achieve matched nonlinear compensations by slightly tuning the signal powers injected into the different spans: either raising the input power to the (RDF + SMF) spans (relative to the input power to the (SMF + RDF) spans) by only $0.3/2.7 \approx 10\%$ to have one (RDF + SMF) span generating the equivalent amount of nonlinearity, hence compensating the nonlinear effects, of three (SMF + RDF) spans; or lowering the input power to the (RDF + SMF) spans by just $0.7/2.7 \approx 26\%$ to have one (RDF + SMF) span compensating the nonlinear effects of two (SMF + RDF) spans. Alternatively, if the same level of signal power is injected into the (RDF + SMF) and (SMF + RDF) spans, then one (RDF + SMF) span may compensate approximately 90% of the nonlinear effects due to three (SMF + RDF) spans, leaving a little residue of nonlinearity uncompensated. These are but some examples of using the one-for-many method for nonlinear compensations. It is noted that the same principle and similar fiber arrangements with proper adjustments of signal powers are applicable to systems using other types of fibers, such as dispersion-shifted fibers and non-zero dispersion-shifted fibers, which are known to be suitable for the design of scaled translation-symmetric systems [14].

8.3.2 *Simulation results and discussions*

A series of numerical simulations have been carried out using a commercial transmission simulator (VPItransmissionMaker$^{\text{TM}}$, Virtual Photonics Inc.), to verify the proposed method of simultaneous compensations of dispersion and nonlinearity in one-for-many system configurations. Firstly, we have simulated a transmission system using (SMF + RDF) and (RDF + SMF) spans, as shown in Fig. 8.14, where the DCF is a commercial RDF product. The system has an optical phase conjugator in the middle, and on each side of OPC there is a loop recirculating four times. Each loop consists of three (SMF + RDF) spans each consisting of 40km SMF + 40km DCF + 16dB EDFA, and one (RDF + SMF) span consisting of 40km DCF + 40km SMF + 16dB EDFA. The SMF has loss $\alpha = 0.2$ dB/km, dispersion $D = 16$ ps/nm/km, dispersion-slope $S = 0.055$ ps/nm^2/km, effective modal area $A_{\text{eff}} = 80$ μm^2, and the DCF has $\alpha' = 0.2$ dB/km, $D' = -16$ ps/nm/km, $S' = -0.055$ ps/nm^2/km, $A'_{\text{eff}} = 30$ μm^2. The EDFA has noise figure 4 dB. The inputs are four 40-Gb/s channels, RZ

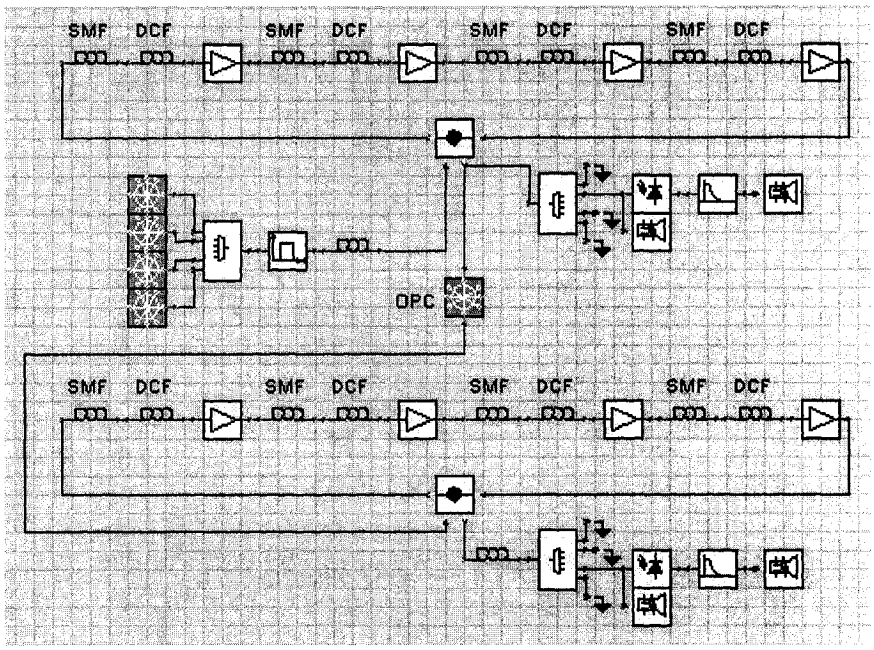

Figure 8.16: A comparative system with no one-for-many STS but with OPC in the middle.

modulated with peak power 10 mW and duty cycle 33%. The channel spacing is 200 GHz. The optical MUX and DEMUX consist of Bessel filters of the 7th order with 3-dB bandwidth 100 GHz. The system is configured such that each (RDF + SMF) span on the left side corresponds to and compensates the nonlinear effects of three (SMF + RDF) spans on the right side, and each (RDF + SMF) span on the right side corresponds to and compensates the nonlinear effects of three (SMF + RDF) spans on the left side. We have tried both a case with all spans being injected exactly the same amount of signal power and a case with the (RDF + SMF) spans being fed with 10% more power comparing to the (SMF + RDF) spans. No observable difference is found in the transmission performance, which indicates robustness of the system design against reasonable parameter deviations. Fig. 8.15 shows the optical eye diagram of the 3rd DEMUX channel at the end of transmission, which demonstrates excellent signal quality after 2560km transmissions. We have also simulated two comparative systems to see how effective is the method of one-for-many nonlinear compensations with STS. One of the comparative systems as shown in Fig. 8.16 has all identical (SMF + RDF) spans on both sides of OPC, the other has neither one-for-many STS nor OPC. Everything else remains the same. Lacking an STS, both comparative systems are seriously impaired by fiber nonlinearities, as shown by the optical eye diagrams of the 3rd DEMUX channel in Fig. 8.17.

For an example of intra-channel nonlinear compensations using one-for-many STS,

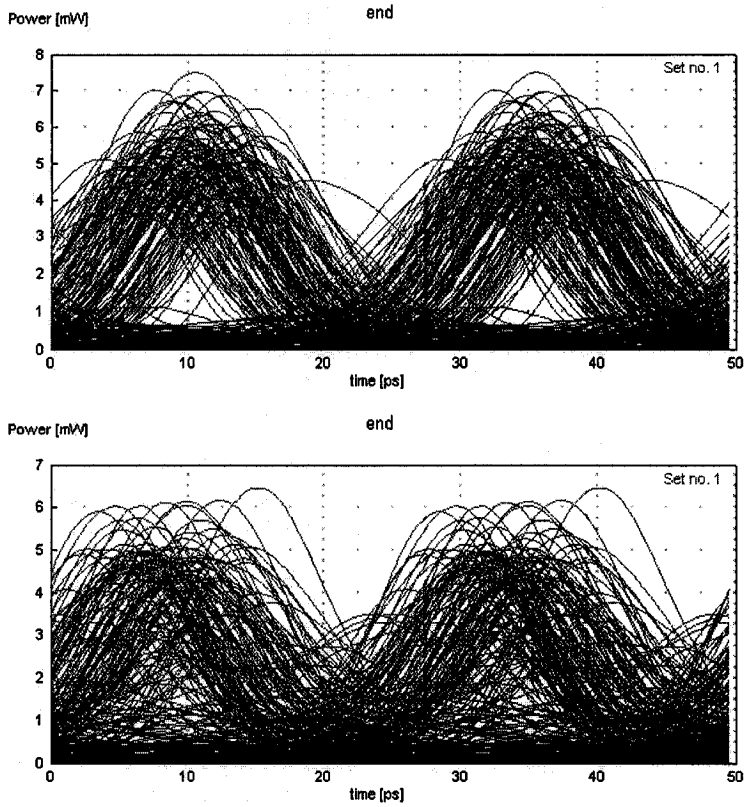

Figure 8.17: Optical eye diagrams of the 3rd DEMUX channel for the two comparative systems. Top: the system with OPC in the middle; Bottom: the system without OPC.

we have simulated an optimized system using (SMF + RDF) and (RDF + SMF) spans as shown in Fig. 8.18, and a comparative system using all (SMF + RDF) spans as shown in Fig. 8.19. Each system is a cascade of two identical transmission lines. Each transmission line has a loop recirculating twice, with each loop consisting of four spans. In the optimized system, each loop consists of three (SMF + RDF) spans having 40km SMF + 40km DCF + 16dB EDFA, and one (RDF + SMF) span having 40km DCF + 40km SMF + 16dB EDFA. Each loop in the comparative system has all four identical (SMF + RDF) spans consisting of 40km SMF + 40km DCF + 16dB EDFA. The parameters of fibers, EDFAs, MUX/DEMUX, and input signals are all the same as in the previous simulations for nonlinear compensations with OPC. Note that the optimized system is configured such that each (RDF + SMF) span corresponds to and compensates the intra-channel nonlinear effects of three (SMF + RDF) spans. The comparative system has no one-for-many STS. Again we have tried both a case with all spans being injected exactly the same amount of signal power and a case with the (RDF + SMF) spans being fed with

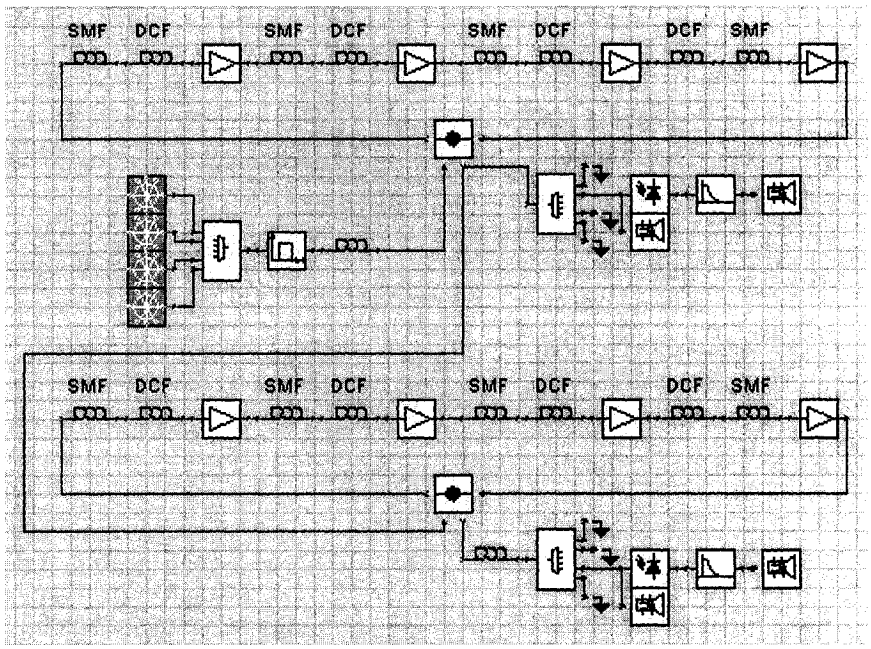

Figure 8.18: An optimized system using SMF+RDF and RDF+SMF spans configured into a one-for-many STS.

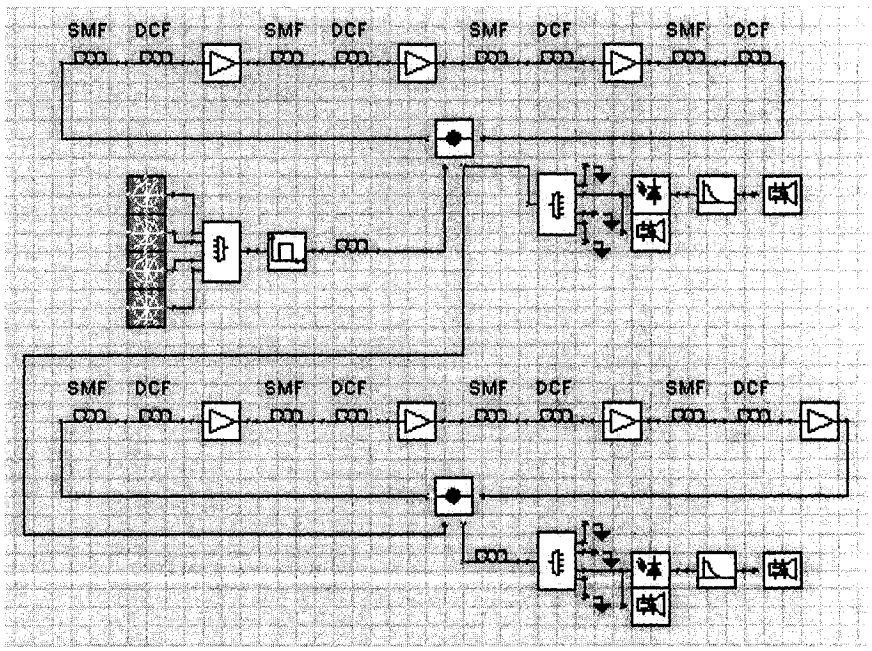

Figure 8.19: A comparative system using all SMF+RDF spans without one-for-many STS.

10% more power comparing to the (SMF + RDF) spans, and found no observable difference. Fig. 8.20 shows the eye diagrams of the 3rd channel at the mid-point of

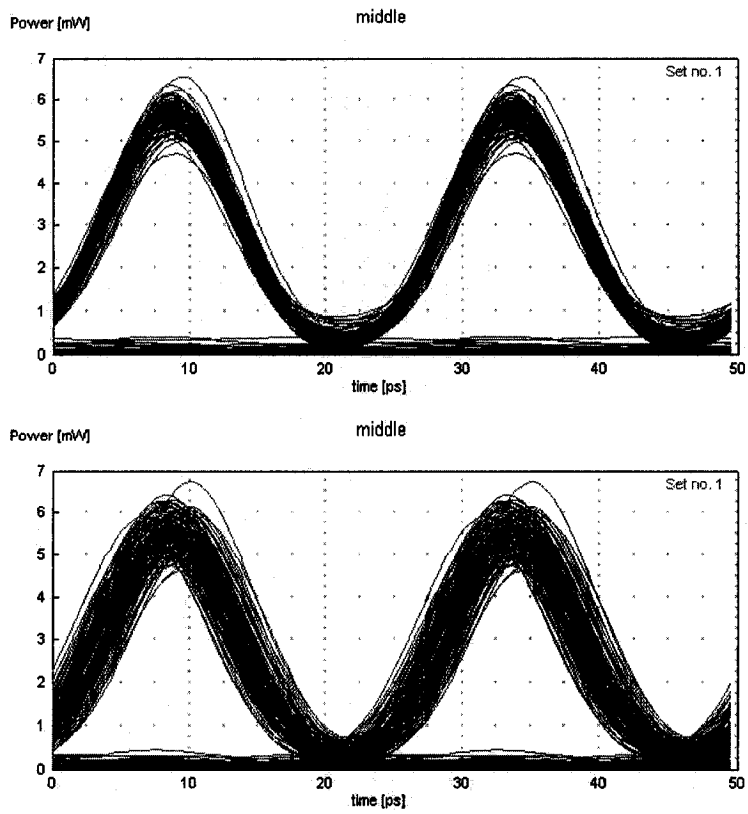

Figure 8.20: Optical eye diagrams of the 3rd channel at the mid-point of transmissions. Top: of the optimized system; Bottom: of the comparative system.

the transmissions, namely, after the first transmission line of 640 km for each system. The eye diagram of the optimized system shows significantly reduced amplitude and timing jitters than the one of the comparative system, which demonstrates the effect of intra-channel nonlinear compensations with a one-for-many STS. At the end of the 1280km transmissions, as shown in Fig. 8.21, the comparative system suffers from significantly more signal degradations than the optimized system, especially in terms of amplitude and timing jitters of the mark pulses. However, it is noted that the optimized system is also penalized by the accumulation of noise energy in the "originally empty" time slots. A good part of the noise energy may be due to the growth of ghost-pulses, which is not suppressed by the one-for-many STS alone. Fortunately, when channelized SPM is introduced in the middle of the optimized system to result a setup as shown in Fig. 8.22, the ghost-pulses may be substantially removed from the signals received at the end of the 1280km transmissions, as shown in Fig. 8.23, in sharp contrast to the top diagram of Fig. 8.21.

To better quantify the improvement of transmission performance due to one-for-

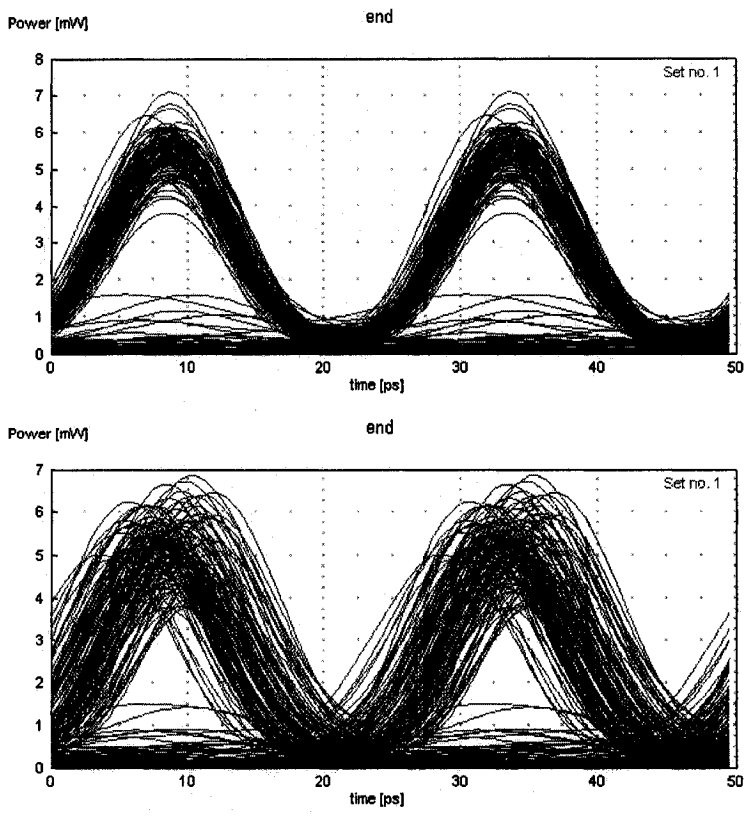

Figure 8.21: Optical eye diagrams of the 3rd channel at the end of transmissions. Top: of the optimized system; Bottom: of the comparative system.

many STS and mid-way SPM, repeated simulations have been carried out for three system configurations at different transmission distances, where each system consists of recirculated 320km spans. For the first, conventional setup, each 320km span has (40 km SMF + 40 km RDF + 16 dB EDFA) repeated four times. The second, one-for-many translation-symmetric configuration, has always an even number of 320km spans, each consists of (40 km SMF + 40 km RDF + 16 dB EDFA) repeated three times and then (40 km RDF + 40 km SMF + 16 dB EDFA). The third, fully optimized system has exactly the same line configuration as the second system, except employing channelized SPM in the middle. The 3rd channel is monitored and Q-quantified. Fig. 8.24 shows the simulated Q values for the three systems as the transmission distance vary from 1 to 8 span(s) of 320km each, where the squares mark results of the optimized system with STS and mid-way SPM, the circles indicate results of the translation-symmetric system without mid-way SPM, and the triangles are for the conventional system without STS nor mid-way SPM. The solid horizontal line marks the threshold level of $Q = 6$ in order to achieve BER $\leq 10^{-9}$, which is used

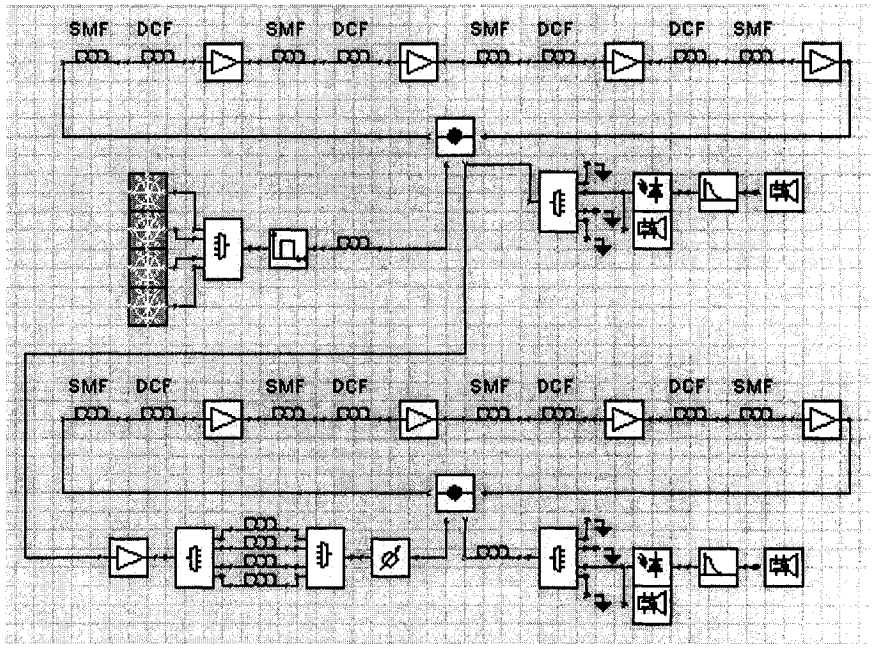

Figure 8.22: An optimized system with one-for-many STS and mid-way SPM.

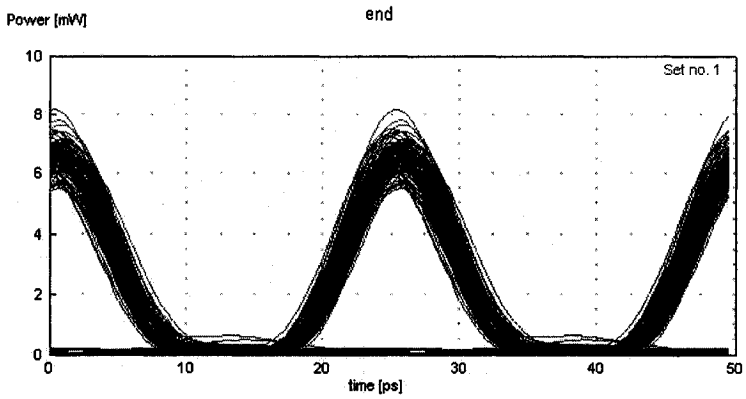

Figure 8.23: Optical eye diagram of the 3rd channel received at the end of the optimized system with one-for-many STS and mid-way SPM.

as the cutoff level to determine the limit of transmission distance. It is seen that the conventional system reaches no more than 3 spans of 320 km, while the translation-symmetric system without mid-way SPM could reach 6 spans of 320 km, and the addition of mid-way SPM further improves the Q value at the same reach distance.

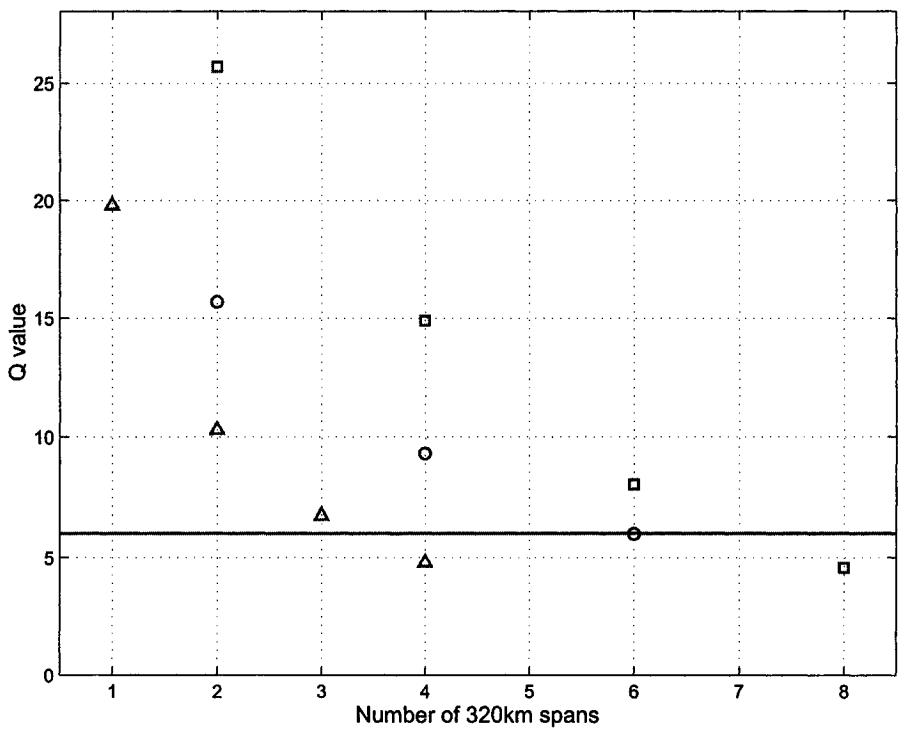

Figure 8.24: The Q value versus transmission distance in number of 320km spans for three system setups: squares - optimized system with one-for-many STS and mid-way SPM; circles - one-for-many translation-symmetric system without mid-way SPM; triangles - conventional system without STS nor mid-way SPM. The solid horizontal line marks the level of $Q = 6$ for BER $\leq 10^{-9}$.

9

Conclusions and Perspectives

In conclusion, it is expected that overcoming nonlinearity could be the next major challenge to optical communications. This thesis has tackled related problems of the fundamental feasibility and practical embodiments to overcome limitations imposed by fiber nonlinearity, from the angle of distributed nonlinear compensations using scaled symmetries in transmission lines. The NLSE formulation has been generalized and used extensively in our analyses of dispersive and nonlinear signal propagation in optical fibers, which provide theoretical guidance in the search, verification, and optimization of two types of methods for distributed nonlinear compensations, using mirror- and translation-symmetric configurations respectively. For each type, we have noted and emphasized the importance of scaled symmetry, in particular, the significance and feasibility of scaling the dispersion slopes of fibers together with their dispersions, loss/gain and nonlinear coefficients. We have shown analytically and verified with computer simulations that practical transmission systems using commercially available fibers may be arranged into nearly perfect mirror or translation symmetries in the scaled sense so to enjoy excellent nonlinear compensations.

Nonlinear compensation using scaled mirror symmetry is based on a simple fact that the nonlinear Schrödinger equation is invariant under parameter scaling, such that a short piece of fiber having properly scaled parameters could subject optical signals to the same dispersive and nonlinear propagation as a long fiber. In principle, OPC and an amplifying specialty fiber could perfectly compensate the nonlinearity of a lossy transmission fiber, except for the ever-existing noise destroying the mirror symmetry. Nevertheless, noise and nonlinearity may be largely separable, because the effect of noise is significant only when the signal power and nonlinearity become weak at the two ends of a link consisting of an amplifying specialty fiber and a lossy transmission fiber with OPC in the middle. A simple but fairly accurate model may assume that optical noise is incurred exclusively at the two extreme ends of the link, while dispersive and nonlinear signal propagation is the only effect of the inner part of the link. Such link is well approximated by a linearized link with additive noise at the ends, and many of such linearized links may be cascaded to reach a longer

transmission distance.

With scaled translation symmetry, it has been shown how OPC may help to achieve simultaneous wide-band compensations of the residual dispersion and the fiber nonlinearities in dispersion-managed fiber transmission lines employing slope-compensating fibers. When the dispersion slope of transmission fibers is equalized by slope-compensating fibers, the residual dispersion and the slope of dispersion slope are compensated by mid-way optical phase conjugation. More importantly, fiber nonlinearity may be largely suppressed by arranging the fibers into conjugate pairs about the phase conjugator, where the two fibers of each pair are in scaled translation symmetry. The translation symmetry is responsible for canceling optical nonlinearities of the two fibers up to the first-order perturbation, then a mirror-symmetric ordering of the fiber pairs about the conjugator linearizes a long transmission line effectively. One noted merit of this dual-compensation method is that it is applicable to a wide variety of transmission fibers and its effectiveness is fairly insensitive to the amount of residual fiber dispersion after the slope compensation. The transmission fibers may be standard SMFs, NZDSFs, or even DSFs, and the slope-compensating fibers may be any DCFs with dispersion slopes opposite to that of the transmission fibers. In view of the recent developments of efficient phase conjugation based on highly nonlinear fibers, $LiNbO_3$ waveguides, or semiconductor optical amplifiers, optical phase conjugators hold the promise of multiple functionalities in fiber-optic transmissions.

Without using optical phase conjugation, it has been demonstrated that two fiber spans in a scaled translation symmetry could cancel out their intra-channel nonlinear effects to a large extent, and a significant reduction of intra-channel nonlinear effects may be achieved in a long-distance transmission line consisting of multiple pairs of translation-symmetric spans arranged into a mirror-symmetric order. It is argued that intra-channel pulse interactions are the dominating nonlinear effects in modern transmission systems with high modulation speeds, in which scaled symmetries could be effective in suppressing amplitude and timing jitters of mark pulses due to nonlinearity, but not for ghost-pulse generation into the empty data slots. For a further method of suppressing ghost-pulse generation into empty data slots, we have proposed and tested a method that uses channelized mid-way self-phase modulation to reverse the generation of ghost-pulses due to intra-channel four-wave mixing.

This thesis has also discussed practical implementations of OPC and DCMs, as well as methods of one-for-many nonlinear compensations using scaled translation symmetries. An example of a Kerr medium pumped by a strong laser beam is showcased as an example for the implementation of OPC, where it is noted that the same FWM effect realizing OPC also results in parasitic processes by generating inter-mixing

terms among WDM signals, that a high pump-power to signal-power ratio and a certain guard-band in the frequency domain may be necessary to reduce such parasitic effect. For optimal packaging of dispersion-compensating fibers, it is explained that a compact dispersion-compensating module or a dispersion-compensating transmission line may better consist of two portions of dispersion-compensating fiber, where the first portion carrying high-power signals may have an intentionally increased loss coefficient to form a scaled translational symmetry with a transmission fiber, while the second portion experiencing low signal power could have the minimal loss coefficient and does not need to satisfy any scaling rule. For methods of one-for-many nonlinear compensations using scaled translation symmetry, it has been proposed and tested that a transmission line may consist of many pairs of compensating fiber spans mirror-symmetrically ordered about the phase conjugator, where each pair may include one fiber span of stronger nonlinearity and several conjugating fiber spans of weaker nonlinearity. It has been demonstrated that such one-for-many configuration achieves simultaneous compensations of both dispersion and nonlinearity over a wide optical band, with or without OPC in the middle.

In summary, this thesis reports mathematical analyses and practical embodiments of nonlinear compensations using scaled symmetries. On the theoretical side, our results provide a constructive and operational paradigm of distributive nonlinear compensations based on scaled mirror or translation symmetries, which shows how nonlinearly mixed signals may be de-mixed and restored, or how the amplitudes of nonlinear signal mixtures may be suppressed. Our paradigm also indicates that nonlinearity does not necessarily or immediately limit the channel capacity, but the nonlinearity-mediated noise-signal inter-mixing, or viewed as parametric amplification of noise pumped by signal power, does impose an ultimate limit to the capacity of a nonlinear channel. On the practical side, many of our proposed methods are readily applicable to practically deployed or designed fiber-optic transmission systems using commercially available transmission and dispersion-compensating fibers, with little or minimum system modification and limited addition of components. For further engineering developments, we have demonstrated the technological feasibilities and optimization criteria for several required components to fully implement transmission systems in scaled symmetries, including specialty fibers, optical phase conjugators, distributed EDFA and Raman amplifiers. In particular, our investigations have recognized several new design metrics and methodologies to optimize optical components and subsystems for better system performance. For example, the dispersion of an RDF may be tuned in proportion to its loss coefficient so to form a scaled translation symmetry to a transmission fiber; the loss coefficient of a packaged DCF may be

set to an optimal value, which is not necessarily minimized, and its core area may be intentionally kept small to enhance nonlinearity, both in considerations of scaled symmetries.

A

Quantum Noise in Optical Communications

Material in this Appendix has been published in reference [40].

A.1 Introductory Quantum Fiber Optics

In modern fiber transmission lines, the optical signals experience alternating loss and gain. The ASE of the in-line amplifiers is usually blamed and considered as the sole source of noise that corrupts the optical signals. However, it should be noted that the fiber propagation loss is a random process along the length of propagation. The stochastic nature of the loss process induces a random fluctuation to the energy of the optical signals, namely, an extra source of noise, which could become comparable to the commonly blamed ASE noise. It is therefore necessary to understand and include this noise in system design and performance evaluation. Fundamentally, the optical noise in random loss/gain has a quantum origin, incurred as a result of the corpuscular nature of electromagnetic radiation. Such quantum noise is often treated in the Heisenberg representation, and interpreted as the result of a Langevin noise operator [39], or vacuum field operators [36, 38], added to the Heisenberg field operator of the signal. Here we adopt the Schrödinger representation, and use a density matrix in the basis of photon number states to describe the signal field, the medium reservoir, and their interactions. When the medium degrees of freedom are traced out, a reduced density matrix is obtained in the diagonal form, which describes the total energy of the optical signal evolving along the propagation distance. Such formulism is sufficient for practical fiber-optic systems with direct intensity detection, because the quantity of concern is indeed the number of photons contained in a signal pulse. Furthermore, our formulism provides a more intuitive interpretation of the quantum-optical noise as the result of a classical Markov process in the space of the photon number states.

To deal with quantum noise, we naturally need the quantum theory of light [38, 150], which was first developed by Dirac in 1927 [151]. The established procedure of the so-called canonical quantization of radiation starts from a set of classical modes of the electromagnetic field, then relates each mode to a quantum-mechanical

harmonic oscillator, and associates to which two operators, named the annihilation and the creation operators respectively. The product of a creation and an annihilation operators has non-negative integers as eigen values. The corresponding eigen states are called the number states, and interpreted as having integer numbers of photons excited in the mode referred. For the problem of signal transmission in an optical fiber, it is convenient to describe the optical signals in terms of the eigen propagation modes of the fiber waveguide. Especially for a single-mode fiber, there is only one guided mode (actually two if counting the different polarizations), optical energy in all other spatial modes are not well-confined in the fiber and eventually get lost into the environment. With a fixed polarization, it is customary to represent an information-carrying optical pulse by [6, 13],

$$E(z,t) = E_0 \mathrm{Re}[A(z,t)\exp(-i\omega_0 t)] = E_0[A_r(z,t)\cos\omega_0 t + A_i(z,t)\sin\omega_0 t], \quad \text{(A.1)}$$

$$H(z,t) = H_0 \mathrm{Im}[A(z,t)\exp(-i\omega_0 t)] = H_0[A_i(z,t)\cos\omega_0 t - A_r(z,t)\sin\omega_0 t], \quad \text{(A.2)}$$

where E and H are the electric and magnetic fields respectively, ω_0 is the center frequency of the optical signal, and $A(z,t) = A_r(z,t) + iA_i(z,t)$ is the so-called slow-varying envelope of the signal pulse, that is, $A(z,t)$ has small derivatives with respect to t. The envelope $A(z,t)$ is found to satisfy an NLSE [6, 13],

$$\frac{\partial A}{\partial z} + \beta_1 \frac{\partial A}{\partial t} + \frac{i}{2}\beta_2 \frac{\partial^2 A}{\partial t^2} = i\beta_0 A + i\gamma |A|^2 A, \quad \text{(A.3)}$$

where β_0 is the propagation constant at the center frequency, β_1 is the inverse of the group-velocity, β_2 is GVD, and γ is the Kerr nonlinear coefficient of the fiber. The term of optical loss in the classical NLSE is not included here, because that term is to be treated quantum-mechanically, and derived from the first principles of light-matter interactions. If neglecting the fiber nonlinearity and the GVD, then the NLSE is solved by a space-invariant envelope of the form $A(z,t) = A'(t - \beta_1 z)\exp(i\beta_0 z)$, for some real-valued function $A'(\tau)$. The fiber nonlinearity may be neglected for the current purpose, because the effect of quantum noise is significant only when the signal power becomes low, and that is when the nonlinearity diminishes. The effect of the GVD is not usually negligible, when the signal modulation speed is high and the propagation distance is long. However, it is believed that the GVD would not alter the characteristics of the quantum noise due to the highly localized light-matter interactions, as the accumulation of GVD over a short length of fiber is too small to change the shape of the signal pulse. We shall proceed to quantize the signal field in a single-mode fiber using the space-invariant mode of pulse propagation. Let

$q(t) = \cos\omega_0 t$, and $p(t) = \sin\omega_0 t$, then the electric and the magnetic fields are represented as,

$$E(z,t) = E_0[A_r(z,t)q(t) + A_i(z,t)p(t)], \tag{A.4}$$

$$H(z,t) = H_0[A_i(z,t)q(t) - A_r(z,t)p(t)]. \tag{A.5}$$

The Hamiltonian, namely the total energy, of the signal field can be calculated as,

$$\mathcal{H} = \frac{1}{2}\int(\epsilon E^2 + \mu H^2)dz = \frac{1}{2}C_1 q^2 + \frac{1}{2}C_2 p^2, \tag{A.6}$$

with

$$C_1 = \int[\epsilon E_0^2 A_r^2(z,t) + \mu H_0^2 A_i^2(z,t)]dz, \tag{A.7}$$

$$C_2 = \int[\epsilon E_0^2 A_i^2(z,t) + \mu H_0^2 A_r^2(z,t))]dz. \tag{A.8}$$

The orthogonality between $A_r(z,t)$ and $A_i(z,t)$ has been used in the derivation. Based on the quadratic form of the Hamiltonian, and the dynamical equations $\dot{q} = -\omega_0 p$, $\dot{p} = \omega_0 q$, we could draw an analogy between the optical mode and a harmonic oscillator, and further the analogy into the quantum world by turning q and p into operators, and introducing commutation relations [151],

$$[q,p] = \frac{i\hbar\omega_0}{\sqrt{C_1 C_2}}, \quad [q,q] = [p,p] = 0. \tag{A.9}$$

It is customary to make a canonical transformation to the annihilation and creation operators,

$$\mathsf{a} = q\sqrt{\frac{C_1}{2\hbar\omega_0}} + ip\sqrt{\frac{C_2}{2\hbar\omega_0}}, \tag{A.10}$$

$$\mathsf{a}^+ = q\sqrt{\frac{C_1}{2\hbar\omega_0}} - ip\sqrt{\frac{C_2}{2\hbar\omega_0}}, \tag{A.11}$$

which satisfy the commutation relations,

$$[\mathsf{a}, \mathsf{a}^+] = 1, \quad [\mathsf{a}, \mathsf{a}] = [\mathsf{a}^+, \mathsf{a}^+] = 0. \tag{A.12}$$

The Hamiltonian of the field becomes,

$$\mathcal{H} = \hbar\omega_0\left(\mathsf{a}^+\mathsf{a} + \frac{1}{2}\right), \tag{A.13}$$

and the electromagnetic fields, now also operators, are represented as,

$$E(z,t) = E_0\sqrt{\frac{\hbar\omega_0}{2}}\left[\left(\frac{A_r(z,t)}{\sqrt{C_1}} - i\frac{A_i(z,t)}{\sqrt{C_2}}\right)\mathsf{a} + \left(\frac{A_r(z,t)}{\sqrt{C_1}} + i\frac{A_i(z,t)}{\sqrt{C_2}}\right)\mathsf{a}^+\right], \tag{A.14}$$

$$H(z,t) = H_0\sqrt{\frac{\hbar\omega_0}{2}}\left[\left(\frac{A_r(z,t)}{\sqrt{C_1}} + i\frac{A_i(z,t)}{\sqrt{C_2}}\right)\mathsf{a} + \left(\frac{A_r(z,t)}{\sqrt{C_1}} - i\frac{A_i(z,t)}{\sqrt{C_2}}\right)\mathsf{a}^+\right], \quad \text{(A.15)}$$

in terms of a and a^+. In the standard quantum theory of light [38, 150, 151], the modal functions are usually time-independent, and often called the normal modes of the field. Here, however, our modal function $A(z,t)$ is time-dependent, albeit slowly. The propagating mode $A(z,t)$ is actually a linear superposition of many normal (time-independent) modes with slightly different oscillation frequencies ω around the center ω_0. By grouping the normal modes together into $A(z,t)$, we have adopted an approximation that neglects the energy variation of $\hbar\omega$ from $\hbar\omega_0$. We shall further assume that all the normal modes participate into the same interactions with the same environment, namely, the same material molecules and unguided modes of the fiber, and the strength of the interactions is approximately the same for all the normal modes. Such approximation enables the concise single-mode quantum description of the optical signal as in equations (A.12) through (A.15), and it should be applicable to practical WDM communication systems, as the modulation bandwidth of the optical signals is usually far less than the center carrier frequency.

The eigen states of $\mathsf{n} \stackrel{\text{def}}{=} \mathsf{a}^+\mathsf{a}$ are the number states $|n\rangle$, $n \in \mathbf{N} = \{0, 1, 2, \cdots\}$, and the following holds,

$$\mathsf{a}|n\rangle = \sqrt{n}\ |n-1\rangle, \quad \forall\ n \in \mathbf{N}, \quad \text{(A.16)}$$

$$\mathsf{a}^+|n\rangle = \sqrt{n+1}\ |n+1\rangle, \quad \forall\ n \in \mathbf{N}. \quad \text{(A.17)}$$

For each $n \in \mathbf{N}$, the state $|n\rangle$ has the physical interpretation of n photons being contained in the single-mode wave packet defined by $A(z,t)$. The wave function of a general wave packet may be expanded in the basis of the number states as,

$$|\psi\rangle = \sum_n c_n|n\rangle, \quad \text{(A.18)}$$

from which the expectation value of an operator Q may be calculated as,

$$\langle\psi|Q|\psi\rangle = \sum_m\sum_n c_m^* c_n \langle m|Q|n\rangle. \quad \text{(A.19)}$$

In particular, the average photon number is calculated as,

$$\langle\psi|\mathsf{n}|\psi\rangle = \langle\psi|\mathsf{a}^+\mathsf{a}|\psi\rangle = \sum_n n|c_n|^2. \quad \text{(A.20)}$$

If the wave packet is probed by a photon counter, for example a photo-detector (which is totally destructive though), $|c_n|^2$ is obviously the probability of n photons being detected.

A.2 Interaction with the Environment

The loss or gain to the wave packet of a single pulse is due to interactions with the environment, including molecules in the waveguide, that may absorb photons from or emit photons to the wave packet, and other optical modes, which signal photons may be scattered into or from. Such interacting molecules and leaky optical modes shall be called interaction centers for convenience. The active molecules and Rayleigh scattering centers [69] are naturally localized in the waveguide material. Light scattering due to waveguide non-uniformities, such as micro-bends and tensile stresses [69], may take place within an extended length of fiber. However, the effect may still be viewed as localized comparing to the long distance of signal transmission. With all interaction centers localized, the following model Hamiltonian [152] may be used to describe the interaction between the signal field and the environment,

$$U = \sum_k \hbar(g_k \mathsf{a}\sigma_k^+ + g_k^* \mathsf{a}^+ \sigma_k^-)\delta(z - z_k), \tag{A.21}$$

where $k \in \mathbf{Z}$ labels the interaction centers, z_k is the location of the kth center, g_k is the coupling strength, σ_k^+ and σ_k^- are operators to change the state of the interaction center after absorbing/emitting a photon respectively. It is assumed that the sequence $\{z_k\}_{k\in\mathbf{Z}}$ is a realization of a generally inhomogeneous Poisson point process [153] with intensity $\lambda(z)$ along the length of the fiber, that is, the probability of having an interaction center inside an interval $[z, z+dz)$ is $\lambda(z)dz$ for an infinitesimal dz. Although not always true, it is often a very good approximation to model each interaction center as a two-state system, because multi-photon processes are usually rare events. A general quantum state of the kth interaction center is $d_k|\downarrow\rangle_k + u_k|\uparrow\rangle_k$, where $|d_k|^2 + |u_k|^2 = 1$, $|\downarrow\rangle_k$ and $|\uparrow\rangle_k$ are the down and up states of the interaction center, which satisfy,

$$\sigma_k^+|\downarrow\rangle_k = |\uparrow\rangle_k, \quad \sigma_k^+|\uparrow\rangle_k = 0, \tag{A.22}$$

$$\sigma_k^-|\uparrow\rangle_k = |\downarrow\rangle_k, \quad \sigma_k^-|\downarrow\rangle_k = 0. \tag{A.23}$$

Despite the simplicity of the signal field and the individual interaction centers, it becomes rather complicated to describe the whole system in a fully quantum-mechanical manner, because of the vast Hilbert space of an interacting many-body system. To shorten the notation, we write the wave function of the whole system in a simplified form,

$$|\Psi(t) = \sum_n \phi_n(t)|n\rangle, \tag{A.24}$$

where $|n\rangle$ is the nth number state of the signal field, and the coefficient $\phi_n(t)$ is Φ-valued, representing the quantum state of all interaction centers entangled with $|n\rangle$ at

time t, Φ is a suitable Hilbert space to accommodate all the possible wave functions of the interaction centers, or simply called the environment. The Schrödinger equation is still of the form,

$$i\frac{\partial}{\partial t}|\Psi(t)\rangle = U|\Psi(t)\rangle = \sum_k (g_k \mathsf{a}\sigma_k^+ + g_k^* \mathsf{a}^+ \sigma_k^-)\delta(z - z_k)|\Psi(t)\rangle, \tag{A.25}$$

in the interaction picture, although the solution is quite involved. Before going further, it is noted that the space-invariance of the wave packet, $A(z,t) = A'(t - \beta_1 z)\exp(i\beta_0 z)$, makes the space and time variables inter-changeable, if the space-time extent of the wave packet is neglected, and the signal pulse is represented by a "point particle" at the center of the packet, $t - \beta_1 z = 0$. With t substituted by $\beta_1 z$, equation (A.25) becomes,

$$i\frac{\partial}{\partial z}|\Psi(z)\rangle = \sum_k \beta_1 (g_k \mathsf{a}\sigma_k^+ + g_k^* \mathsf{a}^+ \sigma_k^-)\delta(z - z_k)|\Psi(z)\rangle, \tag{A.26}$$

which describes a quantum dynamics along the z axis. Equations (A.24) and (A.26) may be combined to get,

$$i\sum_n \dot{\phi}_n(z)|n\rangle = \sum_k \sum_n \beta_1 (g_k \mathsf{a}\sigma_k^+ + g_k^* \mathsf{a}^+ \sigma_k^-)\delta(z - z_k)\phi_n(z)|n\rangle. \tag{A.27}$$

It is difficult in general to solve the whole system quantum-mechanically. Just the initial condition would be hard to specify, with so many interaction centers, each of which is randomly located, and may be at any superposition state of the two levels. However, we note again that the signal field interacts with the interaction centers in a highly localized manner. The signal can interact with only one center at any given time. The interaction centers that the signal has already passed do not interact with the signal any longer in terms of energy exchange. But the spooky quantum entanglement [154] still connects the signal to the past interaction centers. Were not for the quantum entanglement, a much simpler system of the signal field exchanging energy with the immediate interaction center would be separated from the complicated many-body system. One way to extract a collective system from the whole, somewhat forcedly, is to use the density matrix [155] description of the entire system, that is $\rho_{\text{tot}} = |\Psi\rangle\langle\Psi|$, then take the trace over all the unwanted degrees of freedom, leaving only those of the signal field and the single chosen interaction center. The reduced density matrix is then a complete representation of the collective system, although the quantum coherence in the reduced system is also reduced, even totally lost. That is, the system is no longer in a pure quantum state, but a statistically mixed one [155]. This is the familiar yet hard-to-understand phenomenon of decoherence. Fortunately,

decoherence is indeed what happens in reality. In fact, the technique of tracing over the environmental degrees of freedom has been used to explain the mysterious phenomenon of decoherence of open quantum systems in general [156, 157]. Furthermore, the main goal of optical communications is not to perform any delicate experiments of quantum optics where quantum coherence needs to be carefully preserved, but to deliver information encoded in the number of photons for which quantum coherence is not the first concern. Consequently, we shall assume that the vast number of interaction centers and their interactions with the larger environment destroy the quantum coherence in a signal wave packet quickly and completely, so that the reduced density matrix of the signal field has only diagonal terms, that is, $\rho = \sum_n \rho_{nn}|n\rangle\langle n|$, where $\rho_{nn} \geq 0$ is a classical probability of the wave packet being at the number state $|n\rangle$. Note that each $|n\rangle$ is still a pure quantum state, but there is no quantum coherence among the number states. So we need only to consider the reduced system of a wave packet at a number state $|n\rangle$ interacting with a single interaction center, as shown in Fig. A.1, then mix different initial number states statistically according to the input density matrix. An output density matrix is obtained, also in the diagonal form, when taking the trace of the resulted density matrix again over the degrees of freedom of the interaction center. This leads to a classical Markovian model that relates the input/output density matrices.

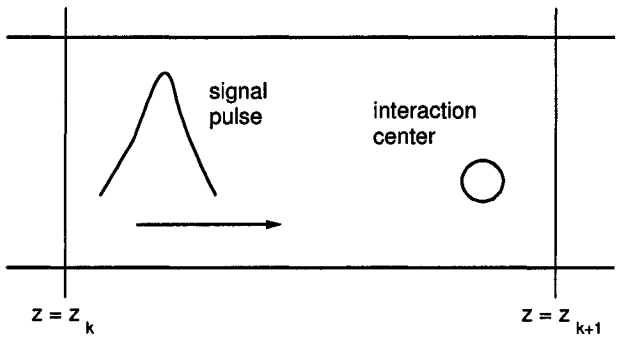

Figure A.1: A signal pulse interacting with an interaction center.

A.3 A Classical Markovian Model

Let us set $z_{k+1} - z_k = 1/\lambda(z_k)$ in Fig. A.1, assume that there is one and only interaction center in the interval, which is at a general quantum state $d_k|\downarrow\rangle + u_k|\uparrow\rangle$, and take $|n\rangle$ as the input state of the signal wave packet. The interaction Hamiltonian is $V_k = \hbar(g_k \mathsf{a}\sigma_k^+ + g_k^* \mathsf{a}^+\sigma_k^-)\delta(z - z_k)$, which transforms the input quantum state

$\Psi_k = d_k|n\rangle|\downarrow\rangle + u_k|n\rangle|\uparrow\rangle$ into,

$$\begin{aligned}\Psi_{k+1} &= \exp[-i\int V(t)dt/\hbar]\,(d_k|n\rangle|\downarrow\rangle + u_k|n\rangle|\uparrow\rangle)\\ &= \exp[-i\beta_1(g_k\mathsf{a}\sigma_k^+ + g_k^*\mathsf{a}^+\sigma_k^-)]\,(d_k|n\rangle|\downarrow\rangle + u_k|n\rangle|\uparrow\rangle)\\ &\approx [1 - i\beta_1(g_k\mathsf{a}\sigma_k^+ + g_k^*\mathsf{a}^+\sigma_k^-)]\,(d_k|n\rangle|\downarrow\rangle + u_k|n\rangle|\uparrow\rangle)\\ &= d_k|n\rangle|\downarrow\rangle + u_k|n\rangle|\uparrow\rangle - i\beta_1 g_k d_k\sqrt{n}\;|n-1\rangle|\uparrow\rangle\\ &\quad -i\beta_1 g_k^* u_k\sqrt{n+1}\;|n+1\rangle|\downarrow\rangle. \end{aligned} \tag{A.28}$$

By tracing $|\Psi_{k+1}\rangle\langle\Psi_{k+1}|$ over the interaction-center degrees of freedom, then neglecting the off-diagonal terms, and renormalizing the coefficients, a reduced density matrix for the signal wave packet is obtained as,

$$\begin{aligned}(1 - n\beta_1^2|g_k|^2 - \beta_1^2|g_k|^2|u_k|^2)\;|n\rangle\langle n| \;+\; n\beta_1^2|g_k|^2|d_k|^2\;|n-1\rangle\langle n-1|\\ +\;(n+1)\beta_1^2|g_k|^2|u_k|^2\;|n+1\rangle\langle n+1|. \end{aligned} \tag{A.29}$$

A mixed state of the signal field $\rho(z_k) = \sum_n \rho_{nn}(z_k)|n\rangle\langle n|$ is therefore converted by the interaction center into another mixed state,

$$\begin{aligned}\rho(z_{k+1}) &= \sum_n (1 - n\beta_1^2|g_k|^2 - \beta_1^2|g_k|^2|u_k|^2)\rho_{nn}(z_k)|n\rangle\langle n|\\ &\quad + \sum_n (n+1)\beta_1^2|g_k|^2|d_k|^2\rho_{n+1,n+1}(z_k)|n\rangle\langle n|\\ &\quad + \sum_n n\beta_1^2|g_k|^2|u_k|^2\rho_{n-1,n-1}(z_k)|n\rangle\langle n|. \end{aligned} \tag{A.30}$$

By definition, $\rho(z_{k+1}) = \sum_n \rho_{nn}(z_{k+1})|n\rangle\langle n|$. So the coefficients of the density matrices are related by,

$$\begin{aligned}\rho_{nn}(z_{k+1}) &= (1 - n\beta_1^2|g_k|^2 - \beta_1^2|g_k|^2|u_k|^2)\rho_{nn}(z_k) + (n+1)\beta_1^2|g_k|^2|d_k|^2\rho_{n+1,n+1}(z_k)\\ &\quad + n\beta_1^2|g_k|^2|u_k|^2\rho_{n-1,n-1}(z_k),\quad \forall\, n \in \mathbf{N}. \end{aligned} \tag{A.31}$$

The dynamics of the reduced density matrix may be interpreted as a discrete Markov chain [158, 159, 160] indexed by $k \in \mathbf{Z}$, with $\mathbf{N} = 0, 1, 2, \cdots$ being the state space, and $[\rho_{00}(z_k), \rho_{11}(z_k), \rho_{22}(z_k), \cdots]$ being the probability distribution vector at "time" k. The compound process of the discrete Markov chain and the Poisson point process of interaction centers is a continuous Markov chain along the z axis, with the transition law for the probability distribution given by a continuous version of equation (A.31),

$$\begin{aligned}\dot{\rho}_{nn}(z) &= -\alpha(z)[n + f(z)]\rho_{nn}(z) + \alpha(z)[1 - f(z)](n+1)\rho_{n+1,n+1}(z)\\ &\quad +\alpha(z)f(z)n\rho_{n-1,n-1}(z),\quad \forall\, n \in \mathbf{N}, \end{aligned} \tag{A.32}$$

where

$$\alpha(z) \stackrel{\text{def}}{=} \lambda(z)\beta_1^2|g(z)|^2, \tag{A.33}$$

$$f(z) \stackrel{\text{def}}{=} |u(z)|^2. \tag{A.34}$$

Obviously, $\alpha(z) \geq 0$ represents a compound interaction strength, which is the spatial density of interaction centers times their quantum coupling strength to the signal field, $0 \leq f(z) \leq 1$ is the fraction of interaction centers at z that are at the excited state, ready to emit a photon. Note that our definition of the interaction centers includes both the actual atomic levels of the active molecules, and the passive light scattering into/from other optical modes due to fiber non-uniformities, micro-bends, and tensile stresses *etc.* Consequently, the parameters $\alpha(z)$ and $f(z)$ should be determined by counting both the active and the passive interaction centers. The effect of the passive interaction centers may become significant in, for example, distributed Raman and erbium-doped fiber amplifiers, where the passive centers could induce a sizable internal loss in the fiber. The commonplace case of a transmission fiber with no amplification in the middle constitutes an extreme in which the passive light scatterers all at the "down state" are the only interaction centers.

So we have derived, from the first-principles of quantum optics, the fundamental equation (A.32) governing the dynamics of photon-number distribution of optical signals propagating in a waveguide with loss and/or gain. The mathematical equation is essentially the same as appeared in precious studies of photon statistics in optical amplifiers [10, 161, 162]. It may be recognized as the forward Kolmogorov equation [159, 160], and can be solved analytically by using the method of probability generating function (PGF) [10, 161, 162]. To simplify the notation, let

$$P_n(z) = \rho_{nn}(z), \quad \forall\, n \in \mathbf{N}, \tag{A.35}$$

$$a(z) = \alpha(z)f(z), \tag{A.36}$$

$$b(z) = \alpha(z)[1 - f(z)], \tag{A.37}$$

then equation (A.32) may be re-written as,

$$\dot{P}_n = a[nP_{n-1} - (n+1)P_n] + b[(n+1)P_{n+1} - nP_n], \tag{A.38}$$

which is in the same form as appeared in previous works [10]. The established formulas [10, 161, 162] can then be adopted with little or no modification. A brief introduction to the PGF method seems to be appropriate here. A PGF $F(x, z)$ for the probability distribution vector $[P_0(z), P_1(z), P_2(z), \cdots]$ is defined as,

$$F(x, z) \stackrel{\text{def}}{=} \sum_n x^n P_n(z). \tag{A.39}$$

And the inverting formula is,

$$P_n(z) = \frac{1}{n!}\left[\frac{\partial^n F(x,z)}{\partial x^n}\right]_{x=0}, \quad \forall\, n \in \mathbf{N}. \tag{A.40}$$

The forward Kolmogorov equation (A.38) may be translated into a differential equation for the PGF,

$$\frac{\partial F}{\partial z} = (ax-b)(x-1)\frac{\partial F}{\partial x} + a(x-1)F, \tag{A.41}$$

with the initial condition,

$$F(x,0) = \sum_n x^n P_n(0). \tag{A.42}$$

The differential equation is analytically solved by [10, 161, 162],

$$F(x,z) = \frac{1}{1+N(1-x)}\sum_n P_n(0)\left[\frac{1+(N-G)(1-x)}{1+N(1-x)}\right]^n, \tag{A.43}$$

where

$$G(z) \stackrel{\text{def}}{=} \exp\left[\int_0^z [a(\zeta)-b(\zeta)]\,d\zeta\right], \tag{A.44}$$

$$N(z) \stackrel{\text{def}}{=} G(z)\int_0^z \frac{a(\zeta)}{G(\zeta)}d\zeta. \tag{A.45}$$

The physical interpretation of $G(z)$ is the overall gain/loss from 0 to z, whereas $N(z)$ may be interpreted as the ASE due to the presence of interaction centers that are at the "up state".

A.4 Applications and a Numerical Example

Our Markovian model is derived rigorously from the first principles of quantum optics, and the model is applicable to a wide range of guided-wave systems with arbitrary distributions of gain/loss media along the length of the waveguide. The existence of analytical solutions enhances further the appeal and prediction power of the established model. We expect the model to find many applications in quantifying the quantum noise in fiber-optic systems, such as transmission fibers without gain, doped fiber amplifiers, and Raman amplifiers. As an example, we shall work out the quantum noise induced by the pure loss of a transmission fiber. This example is chosen not just because of its simplicity, but more importantly due to the fact that such noise has largely been neglected by the fiber-optic engineering community.

Optical signals usually start with a high initial power level and high SNR in order to reach a long transmission distance. For all practical purposes, the noise of the laser transmitter may be neglected, and the starting signal may be modeled by a pure

number state $|m\rangle$, which is of course noise-free if detected by an ideal photo-detector. The photon number m corresponds to the total energy of a pulse. For example, in a 10 Gb/s system, the peak optical power is often set to approximately 0 dBm, or 1 mW, so a binary "one" is represented by an energy packet of 1 mW $\times$ 100 ps $= 10^{-13}$ J, or approximately 10^6 photons at 1.55 μm. So the input state of the pulse may be set to the number stat $|m\rangle$ with $m = 10^6$. The average photon number will be reduced to about 10^4 after a 100-km fiber propagation with 20 dB loss. Because of the random nature of the loss process, the actual photon number at the end will fluctuate around 10^4, even though the signal starts with exactly 10^6 photons. We resort to equation (A.43) for an exact solution to the probability distribution of the number of signal photons at the output of the transmission fiber. There is only loss in this case, $G = 0.01$ and $N = 0$, therefore,

$$F(x) = \sum_n P_n(0)\left[(1-G) + Gx\right]^n = \left[(1-G) + Gx\right]^m, \tag{A.46}$$

which corresponds to the well-known binomial distribution,

$$P_n = \begin{pmatrix} m \\ n \end{pmatrix} (1-G)^{m-n} G^n, \quad \forall\, n \in [0, m], \tag{A.47}$$

here $m = 1,000,000$ is a very large number. This result agrees exactly with that obtained using a Langevin noise operator in the Heisenberg representation [39]. The probability distribution is plotted in Fig. A.2, where the horizontal axis is the deviation of the photon number n from the mean $mG = 10,000$, and the vertical axis is the normalized probability P_n. Graphically, the signal photon number is seen to fluctuate on the order of ± 100 with large probability. To quantify the effect of the quantum noise, it is found that the probability distribution is excellently fitted by a Gaussian distribution,

$$P_n \approx P(n) = P_{\max} \exp\left[-\frac{(n-mG)^2}{2mG(1-G)}\right], \tag{A.48}$$

here $G = 0.01$ and $mG = 10,000$. Indeed, it can be proved by using Stirling's formula that $\log P(n)$ is the Taylor expansion of $\log P_n$ in power series of $(n - mG)/\sqrt{mG(1-G)}$ up to the quadratic term [163]. When the attenuated optical signals are converted into electrical current by an ideal photo-detector, the level of the "1" bits is Gaussian distributed as given above, while that of the "0" bits is free of fluctuations, so the Q factor is [39],

$$Q \stackrel{\text{def}}{=} \frac{\langle n\rangle_1 - \langle n\rangle_0}{\sigma_1 + \sigma_0} = \frac{\langle n\rangle_1}{\sigma_1} = \frac{mG}{\sqrt{mG(1-G)}} = \sqrt{\frac{mG}{1-G}}. \tag{A.49}$$

For the current example, it predicts $Q \approx 100$ after one span of 100-km fiber. However, the Q factor will decrease quickly as the transmission distance increases. Even if the attenuated signal were boosted back to the 1mW power level by a noiseless amplifier, and such amplified fiber span were repeated M times to reach a long-distance of $M \times 100$ km, the Q would be degraded to $\sqrt{mG/M(1-G)}$, based on a model assuming that the "effective Gaussian noise" at the end of each fiber span is independent and additive. The independency assumption is only natural, while the additivity should be a good approximation so long as the accumulated noise remains much lower than the signal level. If taking $M = 25$ for a 2500km transmission line, the Q would not be much better than 20 at the end, even completely neglecting the noise contribution of the repeating amplifiers! The problem gets worse when the signal modulation speed goes to 40 Gb/s and higher. If the signal power level is fixed, then the number of photons contained in one pulse is inversely proportional to the modulation speed. Consequently, the Q is inversely proportional to the square-root of the modulation speed, so $Q \leq 10$ for 40 Gb/s, and $Q \leq 5$ for 160 Gb/s, at the end of 25 fiber spans of 20 dB loss. The Q factor needs to be higher than 6 in order to guarantee a BER below 10^{-9} [39]. Clearly, the quantum noise due to fiber loss could amount to a significant source of noise that should be seriously considered in practical fiber transmission systems, especially in those with modulation speed of 40 Gb/s and above.

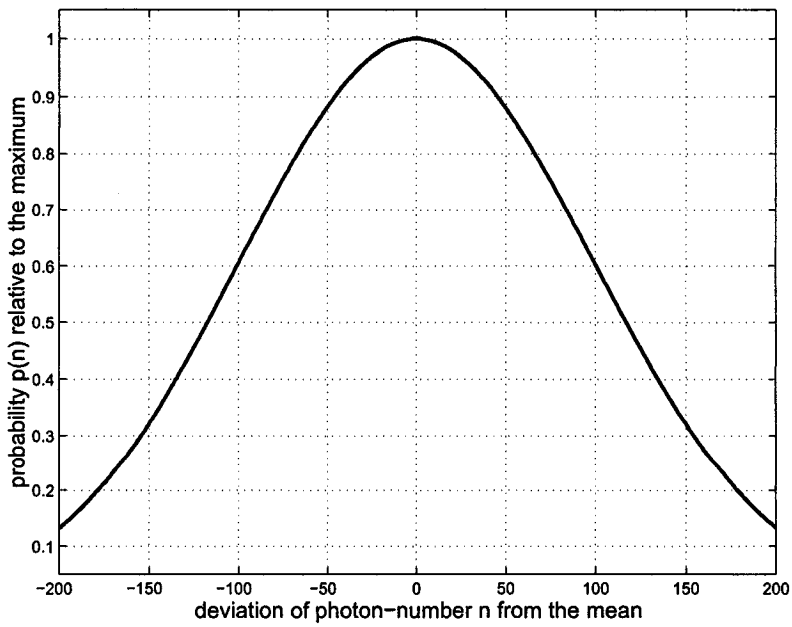

Figure A.2: Probability distribution of the number of photons after 100km fiber transmission.

B

Fundamentals of Nonlinear Fiber Optics

Due to the material nonlinear effects, a fiber-optic transmission line is a nonlinear channel. In state-of-the-art transmission systems, a single-mode optical fiber may carry tens even more wavelength channels. Each wavelength carries 10Gb/s or higher data rate, and the signal may travel several thousand of kilometers in the fiber. With such long transmission distance at such high data rate, the optical nonlinearity of the fiber becomes significant. Indeed, fiber nonlinearity has become one of the major limiting factors in practical transmission system [2, 60]. The theory of nonlinear guided-wave optics, in particular nonlinear fiber optics, has played and should continue to play an important role in understanding fiber-optic signal transmissions, the generation and propagation of ultra-fast laser pulses in optical fibers, and fiber Raman amplifiers, to name just a few. The available formulations in the literature often use a single-component representation of the optical signals, treat the effect of GVD up to the dispersion slope, and usually neglect the variations of the optical loss, the transverse mode function etc. across the signal frequency band [5, 6]. Although these approximations simplify the equations and offer some convenience, they may have already been or will soon be broken down by the rapid growth of the signal bandwidth. Indeed, modern transmission systems have already been carrying several tens of WDM channels across an optical bandwidth in excess of 30 nm. Some pioneering systems have even operated with a bandwidth close to 100 nm. With such a wide bandwidth and so many WDM channels, it is rather inconvenient to use a single-component equation to describe the dynamics of all signals, and the higher-order GVD effects start to play important roles in the dynamics of signal propagations, especially the nonlinear interaction among the signals. Recent advancements in fiber technologies have produced DCFs that are capable of compensating simultaneously the dispersion and the slope of transmission fibers, leaving the residual dispersion dominated by the higher-order derivatives of GVD [3, 87, 130, 131, 164, 165].

This Appendix will derive a set of nonlinear differential equations from the first principles, namely the Maxwell's equations and the material responses to electromagnetic excitations. The derivation retains the mathematical exactitude down to

details. Each approximation is justified and the scope of its applicability is discussed. Still in compact and convenient forms, the final equations include the effect of GVD down to an arbitrary order, and take into account the frequency variations of the optical loss as well as the transverse modal function. Also established is a new formulation of multi-component nonlinear differential equations, in which the total electromagnetic field is represented as a sum of signals with different center frequencies. The multi-component formulation is especially suitable for the study of wide-band wavelength-division multiplexed systems of optical communications.

In dielectric optical waveguides, *e.g.* silica glass fibers, there is no source of electric charge, nor source of current, that is able to excite electromagnetic waves at the optical frequency. The magnetic response of most dielectrics is negligible at optical frequencies. The optics of dielectric waveguides is governed by Maxwell's equations [71],

$$\nabla \times \mathbf{E} = -\mu_0 \frac{\partial \mathbf{H}}{\partial t}, \tag{B.1}$$

$$\nabla \times \mathbf{H} = \epsilon_0 \frac{\partial \mathbf{E}}{\partial t} + \frac{\partial \mathbf{P}}{\partial t}, \tag{B.2}$$

$$\nabla \cdot (\epsilon_0 \mathbf{E} + \mathbf{P}) = 0, \tag{B.3}$$

$$\nabla \cdot \mathbf{H} = 0, \tag{B.4}$$

and the material equation [5, 6],

$$\begin{aligned} \mathbf{P}(\mathbf{r},t) = \epsilon_0 \int \chi^{(1)}(\mathbf{r},s)\mathbf{E}(\mathbf{r},t-s)ds \\ + \epsilon_0 \int \chi^{(3)}(\mathbf{r},t_1,t_2,t_3)\vdots\mathbf{E}(\mathbf{r},t-t_1)\mathbf{E}(\mathbf{r},t-t_2)\mathbf{E}(\mathbf{r},t-t_3)dt_1dt_2dt_3, \end{aligned} \tag{B.5}$$

where $\chi^{(1)}$ and $\chi^{(3)}$ are the linear and the third-order nonlinear susceptibilities of the dielectric material respectively. Although Maxwell's equations describe the optical phenomena with the highest accuracy, they seem to be rather complicated when directly applied to optical waveguides, which usually consist of regions with different dielectric properties. Within each region, however, the material is often uniform and isotropic, so that the vector $\mathbf{P}$ is always proportional and parallel to $\mathbf{E}$, if neglecting the nonlinear polarization for the moment. Then equation (B.3) is reduced to $\nabla \cdot \mathbf{E} = 0$. By applying $\nabla\times$ to (B.1), using (B.2) and the identity,

$$\nabla \times \nabla \times \mathbf{E} = \nabla(\nabla \cdot \mathbf{E}) - \nabla^2 \mathbf{E} = -\nabla^2 \mathbf{E}, \tag{B.6}$$

it is obtained,

$$\nabla^2 \mathbf{E}(\mathbf{r},t) = \frac{1}{c^2}\frac{\partial^2}{\partial t^2}\mathbf{E}(\mathbf{r},t) + \mu_0 \frac{\partial^2}{\partial t^2}\mathbf{P}, \tag{B.7}$$

with $1/c^2 = \epsilon_0\mu_0$. Both $\chi^{(1)}$ and $\chi^{(3)}$ may be complex quantities. The real part of $\chi^{(1)}$ represents the position- and frequency-dependent dielectric constant, while the imaginary part reflects the optical loss or gain in the materials, which may be regarded as frequency-independent, as the total signal bandwidth W is usually much smaller than the center optical frequency ω_0 of the band. The imaginary part of $\chi^{(3)}$ represents the two-photon absorption effect, which is negligible in fibers of silica glass. The real part of $\chi^{(3)}$ comes from two contributions, $\text{Re}[\chi^{(3)}] = \chi_K^{(3)} + \chi_R^{(3)}$, where $\chi_K^{(3)}$ is responsible for the optical Kerr effect, which may be regarded as an instantaneous one, while $\chi_R^{(3)}$ is tied to the Raman scattering effect, which is a time-delayed process [5, 6]. So the material equation (B.5) may be simplified as,

$$\begin{aligned}\mathbf{P}(\mathbf{r},t) = \epsilon_0 \int \text{Re}[\chi^{(1)}(\mathbf{r},s)]\mathbf{E}(\mathbf{r},t-s)ds + i\epsilon_0\text{Im}[\chi^{(1)}(\mathbf{r})]\mathbf{E}(\mathbf{r},t) \\ + \epsilon_0\chi_K^{(3)}(\mathbf{r})\vdots\mathbf{E}(\mathbf{r},t)\mathbf{E}(\mathbf{r},t)\mathbf{E}(\mathbf{r},t) \\ + \epsilon_0 \int \chi_R^{(3)}(\mathbf{r},s)\vdots\mathbf{E}(\mathbf{r},t-s)\mathbf{E}(\mathbf{r},t-s)\mathbf{E}(\mathbf{r},t)ds. \qquad \text{(B.8)}\end{aligned}$$

Now the guided-wave optics is described fairly accurately by equations (B.7) and (B.8), in addition to the proper boundary conditions [71] connecting the fields in different dielectric materials. But there is still too much complexity, due to the vectorial nature of the electromagnetic field and the involved boundary conditions. Fortunately, optical fibers are designed to guide a few discrete modes, even just one mode, and the difference in the dielectric constant is small between the core and the cladding, which makes the guided modes very close to linearly polarized [69]. In most fibers, the optical birefringence is either vanishingly weak to avoid the effect of PMD, or sufficiently strong to render the fiber polarization maintaining. For mathematical simplicity, it is assumed that all signals are co-linearly polarized when entering an optical fiber, and coupled into one polarization eigen state when the fiber is polarization maintaining. In case the signals are not co-linearly polarized, the mathematical description should be slightly modified to deal with the complication. However, the same physics remains to govern the nonlinear signal propagation in optical fibers. With the linear polarization representation $\mathbf{E}(\mathbf{r},t) = E(\mathbf{r},t)\mathbf{e}_1$, equations (B.7) and (B.8) are simplified and combined as,

$$\begin{aligned}\nabla^2 E - \frac{1}{c^2}\frac{\partial^2 E}{\partial t^2} - \frac{1}{c^2}\frac{\partial^2}{\partial t^2}\int \text{Re}[\chi^{(1)}(s)]E(t-s)ds = \frac{i}{c^2}\text{Im}[\chi^{(1)}]\frac{\partial^2}{\partial t^2}E + \\ \frac{1}{c^2}\chi_K^{(3)}\frac{\partial^2}{\partial t^2}E^3 + \frac{1}{c^2}\frac{\partial^2}{\partial t^2}\int \chi_R^{(3)}(s)E^2(t-s)E(t)ds. \qquad \text{(B.9)}\end{aligned}$$

When the total signal bandwidth W is not much more than a few THz, it satisfies the condition $W \ll \omega_0$, as $\omega_0 \approx 200$ THz. The frequency dependence of the transverse

modal function may be neglected, so that a trial solution,

$$E(\mathbf{r},t) = \mathrm{Re}[F(x,y)A(z,t)\exp(i\beta_0 z - i\omega_0 t)], \tag{B.10}$$

with β_0 being the optical propagation constant at ω_0, may be substituted into (B.9) to derive a differential equation for the envelope function $A(z,t)$. Since the fast variation is absorbed by the factor $\exp(i\beta_0 z - i\omega_0 t)$, the signal envelope $A(z,t)$ is expected to be slow-varying in both z and t. The transverse modal function $F(x,y)$ is determined by substituting $F(x,y)A(z,\omega-\omega_0)\exp(i\beta_0 z)$ into the Fourier transform of (B.9) with the right side set to zero. $F(x,y)$ is found to solve the eigen-value equation,

$$\left(\frac{\partial^2}{\partial x^2}+\frac{\partial^2}{\partial y^2}\right)F(x,y)+\frac{\omega^2}{c^2}F(x,y)+\frac{\omega^2}{c^2}\mathrm{Re}[\chi^{(1)}(x,y,\omega)]F(x,y)=\beta^2(\omega)F(x,y). \tag{B.11}$$

Note that the eigen-value β^2 is ω-dependent, which may be expanded into Taylor series,

$$\beta^2(\omega)=\beta_0^2+2\beta_0\sum_{k=1}^{+\infty}\frac{\beta_k}{k!}(\omega-\omega_0)^k, \quad \text{with} \quad \beta_k \stackrel{\text{def}}{=} \frac{1}{2\beta_0}\left.\frac{d^k\beta^2(\omega)}{d\omega^k}\right|_{\omega=\omega_0}. \tag{B.12}$$

When transformed back into the time domain, equation (B.11) leads to,

$$\frac{\partial^2 E}{\partial x^2}+\frac{\partial^2 E}{\partial y^2}-\frac{1}{c^2}\frac{\partial^2 E}{\partial t^2}-\frac{1}{c^2}\frac{\partial^2}{\partial t^2}\int \mathrm{Re}[\chi^{(1)}(s)]E(t-s)ds = \beta_0^2 E+2\beta_0 F(x,y)\exp(i\beta_0 z-i\omega_0 t)\mathsf{B}A(z,t), \tag{B.13}$$

where B is a differential operator defined as,

$$\mathsf{B}\stackrel{\text{def}}{=}\sum_{k=1}^{+\infty}\frac{\beta_k}{k!}\left(i\frac{\partial}{\partial t}\right)^k. \tag{B.14}$$

Substituting (B.10) and (B.13) into equation (B.9) in full, and multiplying both sides by $F^*(x,y)$ then integrating over the transverse plane, it is obtained the NLSE, which governs the propagation dynamics of the signal envelope in optical fibers,

$$\frac{\partial A}{\partial z}-i\mathsf{B}A+\frac{\alpha}{2}A=i\gamma|A|^2A+i(g\otimes|A|^2)A, \tag{B.15}$$

where

$$\alpha \stackrel{\text{def}}{=} \frac{\omega_0^2}{\beta_0 c^2}\int \mathrm{Im}[\chi^{(1)}(x,y)]|F(x,y)|^2dxdy, \tag{B.16}$$

$$\gamma \stackrel{\text{def}}{=} \frac{3\omega_0^2}{8\beta_0 c^2}\int \chi_K^{(3)}(x,y)|F(x,y)|^4dxdy, \tag{B.17}$$

$$g(s) \stackrel{\text{def}}{=} \frac{\omega_0^2}{4\beta_0 c^2}\int \chi_R^{(3)}(x,y,s)|F(x,y)|^4dxdy, \tag{B.18}$$

assuming that $F(x,y)$ is normalized, and $\otimes$ denotes the convolution operator such that,

$$\left[g \otimes |A|^2\right](z,t) \stackrel{\text{def}}{=} \int g(s)|A(z,t-s)|^2 ds. \tag{B.19}$$

In deriving equation (B.15), nonlinear products out of the signal band around ω_0, and the Raman term involving $A^2(z,t-s)A^*(z,t)$, are dropped because the corresponding nonlinear processes are prevented by large phase-mismatches, the term $\partial^2 A/\partial z^2$ is neglected in view of the slow-varying nature of $A(z,t)$ in z, also neglected are terms involving the time-derivatives of $A(z,t)$ multiplied by $\text{Im}[\chi^{(1)}]$, $\chi_K^{(3)}$, or $\chi_R^{(3)}$, hence the name slow-varying envelope approximation. A long transmission link may use fibers of different types. Sometimes the fiber parameters may vary along a single piece of waveguide. So the quantities $(\mathsf{B}, \alpha, \gamma, g)$ are z-dependent in general. However, the corresponding derivatives with respect to z may be neglected, as the z-dependence is usually step-wise, or extremely slow if continuous. A more general NLSE reads,

$$\frac{\partial A}{\partial z} - i\mathsf{B}(z)A + \frac{\alpha(z)}{2}A = i\gamma(z)|A|^2 A + i\left[g(z) \otimes |A|^2\right]A. \tag{B.20}$$

With a change of variables,

$$z = z', \tag{B.21}$$

$$t = t' + \int^{z'} \beta_1(\zeta)d\zeta, \tag{B.22}$$

such that,

$$\begin{bmatrix} \frac{\partial}{\partial z} \\ \frac{\partial}{\partial t} \end{bmatrix} = \begin{bmatrix} \frac{\partial z'}{\partial z} & \frac{\partial t'}{\partial z} \\ \frac{\partial z'}{\partial t} & \frac{\partial t'}{\partial t} \end{bmatrix} \begin{bmatrix} \frac{\partial}{\partial z'} \\ \frac{\partial}{\partial t'} \end{bmatrix} = \begin{bmatrix} 1 & -\beta_1(z) \\ 0 & 1 \end{bmatrix} \begin{bmatrix} \frac{\partial}{\partial z'} \\ \frac{\partial}{\partial t'} \end{bmatrix}, \tag{B.23}$$

equation (B.20) takes a simpler form in the so-called "retarded frame" [6], which after the primes in the variables being dropped reads,

$$\frac{\partial A}{\partial z} - i\mathsf{D}(z)A + \frac{\alpha(z)}{2}A = i\gamma(z)|A|^2 A + i\left[g(z) \otimes |A|^2\right]A, \tag{B.24}$$

with

$$\mathsf{D}(z) \stackrel{\text{def}}{=} \sum_{k=2}^{+\infty} \frac{\beta_k(z)}{k!}\left(i\frac{\partial}{\partial t}\right)^k. \tag{B.25}$$

When the bandwidth of the optical signals becomes too large, it may violate the ω-independent assumptions for the transverse modal function $F(x,y)$ and the loss or gain coefficient $\text{Im}[\chi^{(1)}]$. However, the huge bandwidth is usually shared by many WDM channels, each of which, labelled by $n \in \mathbf{Z}$, is narrow-band around its own center frequency ω_n. Within each WDM channel, the transverse modal function

$F_n(x,y)$ and the loss or gain coefficient $\mathrm{Im}[\chi_n^{(1)}]$, both subscripted by n, are regarded as frequency-independent and valued at ω_n. So the trial solution would be,

$$E(\mathbf{r},t) = \mathrm{Re}\left\{\sum_n F_n(x,y,z)A_n(z,t)\exp\left[i\int^z \beta_{n0}(\zeta)d\zeta - i\omega_n t\right]\right\}, \tag{B.26}$$

where $\beta_{n0}(z) \stackrel{\text{def}}{=} \beta(z,\omega_n)$ is the optical propagation constant at frequency ω_n and position z, A_n is naturally the slow-varying envelope of the nth channel. The transverse modes $F_n(x,y)$, $n \in \mathbf{Z}$, are determined by the eigenvalue equations,

$$\left(\frac{\partial^2}{\partial x^2} + \frac{\partial^2}{\partial y^2}\right)F_n(x,y) + \frac{\omega_n^2}{c^2}F_n(x,y) + \frac{\omega_n^2}{c^2}\mathrm{Re}[\chi^{(1)}(x,y,\omega_n)]F_n(x,y) = \beta^2(\omega)F_n(x,y), \quad \forall\, n \in \mathbf{Z}, \tag{B.27}$$

whose time-domain equivalents are,

$$\frac{\partial^2 E_n}{\partial x^2} + \frac{\partial^2 E_n}{\partial y^2} - \frac{1}{c^2}\frac{\partial^2 E_n}{\partial t^2} - \frac{1}{c^2}\frac{\partial^2}{\partial t^2}\int \mathrm{Re}[\chi^{(1)}(s)]E_n(t-s)ds = \beta_{n0}^2 E_n + 2\beta_{n0}F_n(x,y)\exp\left[i\int^z \beta_{n0}(\zeta)d\zeta - i\omega_n t\right]\mathsf{B}_n A_n(z,t), \quad \forall\, n \in \mathbf{Z}, \tag{B.28}$$

where

$$E_n(\mathbf{r},t) = F_n(x,y,z)A_n(z,t)\exp\left[i\int^z \beta_{n0}(\zeta)d\zeta - i\omega_n t\right], \quad \forall\, n \in \mathbf{Z}, \tag{B.29}$$

and

$$\mathsf{B}_n(z) \stackrel{\text{def}}{=} \sum_{k=1}^{+\infty}\frac{\beta_{nk}(z)}{k!}\left(i\frac{\partial}{\partial t}\right)^k, \quad \text{with } \beta_{nk}(z) \stackrel{\text{def}}{=} \frac{1}{2\beta_{n0}(z)}\left.\frac{\partial^k \beta^2(z,\omega)}{\partial \omega^k}\right|_{\omega=\omega_n}, \tag{B.30}$$

$\forall\, k \geq 1$, $\forall\, n \in \mathbf{Z}$. Substituting (B.26) and (B.28) into (B.9), projecting the field into individual transverse modes $F_n(x,y)$, $n \in \mathbf{Z}$, and similarly, dropping the nonlinear products suffering from large phase-mismatches, neglecting $\partial^2 A/\partial z^2$ and the terms involving the time-derivatives of $A(z,t)$ multiplied by $\mathrm{Im}[\chi^{(1)}]$, $\chi_K^{(3)}$, or $\chi_R^{(3)}$, disregarding the z-derivatives of the fiber parameters and F_n, $\forall\, n \in \mathbf{Z}$, a multi-component NLSE is obtained,

$$\frac{\partial A_n}{\partial z} - i\mathsf{B}_n(z)A_n + \frac{\alpha_n(z)}{2}A_n = i\sum_l\sum_m \gamma_{lmn}(z)A_l A_m A_p^* \exp[i\theta_{lmn}(z)] - \sum_l\sum_m g_{lmn}(z)A_l A_m A_p^* \exp[i\theta_{lmn}(z)], \quad \forall\, n \in \mathbf{Z}, \tag{B.31}$$

where p is determined by the condition,

$$\omega_p = \omega_l + \omega_m - \omega_n, \tag{B.32}$$

and

$$\alpha_n(z) \stackrel{\text{def}}{=} \frac{\omega_n^2}{\beta_{n0}(z)c^2} \int \text{Im}[\chi_n^{(1)}(\mathbf{r})]|F_n(x,y)|^2 dxdy, \tag{B.33}$$

$$\gamma_{lmn}(z) \stackrel{\text{def}}{=} \frac{\omega_n^2}{8\beta_{n0}(z)c^2} \int [3\chi_K^{(3)}(\mathbf{r}) + 2G_r(\mathbf{r}, \omega_n - \omega_l)] F_l F_m F_n^* F_p^* dxdy, \tag{B.34}$$

$$\theta_{lmn}(z) \stackrel{\text{def}}{=} \int^z [\beta_{l0}(\zeta) + \beta_{m0}(\zeta) - \beta_{n0}(\zeta) - \beta_{p0}(\zeta)] d\zeta, \tag{B.35}$$

$$g_{lmn}(z) \stackrel{\text{def}}{=} \frac{\omega_n^2}{4\beta_{n0}(z)c^2} \int G_i(\mathbf{r}, \omega_n - \omega_l) F_l F_m F_n^* F_p^* dxdy, \tag{B.36}$$

$\forall\ l, m, n \in \mathbf{Z}$, with

$$\beta_{nk}(z) \stackrel{\text{def}}{=} \frac{1}{2\beta_{n0}(z)} \left. \frac{\partial^k \beta^2(z,\omega)}{\partial \omega^k} \right|_{\omega=\omega_n}, \ \forall\ k \geq 1, \ \forall\ n \in \mathbf{Z}, \tag{B.37}$$

$$G_r(\mathbf{r}, \omega) \stackrel{\text{def}}{=} \text{Re}\left[\int \chi_R^{(3)}(\mathbf{r}, t) \exp(\omega s) dt\right], \tag{B.38}$$

$$G_i(\mathbf{r}, \omega) \stackrel{\text{def}}{=} \text{Im}\left[\int \chi_R^{(3)}(\mathbf{r}, t) \exp(\omega s) dt\right]. \tag{B.39}$$

As the Fourier transform of $\chi_R^{(3)}(t)$, $G_r(\omega) + iG_i(\omega)$ is basically the Raman gain spectrum. Because $\chi_R^{(3)}$ is real valued, G_r and G_i are even and odd functions of ω respectively, namely, $G_r(-\omega) = G_r(\omega)$, $G_i(-\omega) = -G_i(\omega)$. By a change of variables $(z,t) \rightarrow (z, t + \int^z \beta_{01}(\zeta)d\zeta)$, (B.31) may be rewritten as,

$$\begin{aligned} \frac{\partial A_n}{\partial z} - i\mathsf{D}_n(z)A_n + \frac{\alpha_n(z)}{2}A_n = i\sum_l \sum_m \gamma_{lmn}(z) A_l A_m A_p^* \exp[i\theta_{lmn}(z)] \\ - \sum_l \sum_m g_{lmn}(z) A_l A_m A_p^* \exp[i\theta_{lmn}(z)], \ \forall\ n \in \mathbf{Z}, \end{aligned} \tag{B.40}$$

with

$$\mathsf{D}_n(z) \stackrel{\text{def}}{=} \sum_{k=1}^{+\infty} \frac{\beta_{nk}(z)}{k!} \left(i\frac{\partial}{\partial t}\right)^k - \beta_{01}(z)\left(i\frac{\partial}{\partial t}\right), \ \forall\ n \in \mathbf{Z}. \tag{B.41}$$

After some tedious mathematical derivations, it is rather satisfying to see that the complicated phenomena of group-velocity dispersion and nonlinear interactions among optical signals are fully captured by the NLSE (B.24) or (B.40) in a simple and appealing form. At this point, it may be beneficial to highlight the theoretical model and analytical tools by recapping the assumptions and mathematical approximations being made in the above derivations. Such highlight should help to identify the applicability of the NLSEs as well as their limitations.

Assumptions

1) First of all, the optical field is believed to obey Maxwell's equations (B.1-B.4);

2) The waveguide material is assumed to display third-order nonlinearity, with the electric response given by (B.5);

3) The waveguide material is step-wise uniform and isotropic; Namely, the waveguide consists of domains of uniform and isotropic materials, such that the polarization $\mathbf{P}$ (linear response) is always a scalar constant times the electric field $\mathbf{E}$ within each domain;

4) The third-order nonlinearity consists of an instantaneous (Kerr) response and a time-delayed (Raman) scattering effect;

5) All signals are assumed co-linearly polarized when entering an optical fiber, and coupled into one polarization eigen state when the fiber is polarization maintaining;

6) The fiber parameters may be z-dependent, but their derivatives with respect to z are always negligible.

These assumptions are responsible for distilling the first-principle equations (B.1 - B.4) and the material property (B.5) into the single scalar equation (B.9). Then the following approximations have been made in order to derive the single-component NLSE (B.24):

Approximations for the single-component NLSE

S1) The optical loss or gain in the materials is regarded as frequency-independent;

S2) The two-photon absorption effect is neglected in fibers of silica glass;

S3) The frequency dependence is neglected for the transverse modal function;

S4) The guided modes are treated as linearly polarized;

S5) Nonlinear products out of the signal band are neglected;

S6) The Raman term involving $A^2(z,t-s)A^*(z,t)$ is dropped because of a large phase-mismatch;

S7) The term $\partial^2 A/\partial z^2$ is neglected in view of the slow-varying nature of $A(z,t)$ in z;

S8) Also neglected are terms involving time-derivatives of $A(z,t)$ multiplied by $\mathrm{Im}[\chi^{(1)}]$ and the nonlinear coefficients $\chi_K^{(3)}$, $\chi_R^{(3)}$;

The above approximations S1) and S3) are good when the total optical bandwidth W is less than or on the order of a few THz. For systems with an optical bandwidth well exceeding the THz bandwidth limit, a channelized representation (B.26) may be used for the optical signals, and the following approximations may be made to derive a multi-component NLSE (B.40):

Approximations for the multi-component NLSE

M1) The optical loss or gain in the materials may vary for different channels, however they are treated as frequency-independent within each channel;

M2) The two-photon absorption effect is again neglected in fibers of silica glass;

M3) The transverse modal function may depend on the center frequency of the channels, however no frequency dependence is considered within each channel;

M4) The guided modes are treated again as linearly polarized;

M5) Nonlinear products out of the total signal band are neglected;

M6) The Raman terms involving $A_m^2(z,t-s)A_n^*(z,t)$, $\forall\ m,n \in \mathbf{Z}$ are dropped due to large phase-mismatches;

M7) The terms $\partial^2 A_n/\partial z^2$, $\forall\ n \in \mathbf{Z}$, are neglected in view of the slow-varying nature of $A_n(z,t)$ in z;

M8) Also neglected are terms involving the time-derivatives of $A_n(z,t)$, $\forall\ n \in \mathbf{Z}$, multiplied by $\mathrm{Im}[\chi^{(1)}]$, $\chi_K^{(3)}$, or $\chi_R^{(3)}$.

C

Fiber Parameters

Using the D and S parameters carelessly could lead to confusion. For instance, the values $D = 16$ ps/nm/km and $S = 0.08$ ps/nm^2/km are often cited for the standard single-mode fiber. We note that it is necessary to use the D and S values at the same wavelength for the same fiber to avoid confusion. At 1550 nm, the SMF has $D \approx 16$ ps/nm/km and $S \approx 0.055$ ps/nm^2/km instead of 0.08 ps/nm^2/km, which is the approximate dispersion slope at 1310 nm. Regarding the use of D and S in simulations, our scaling rules are for β_2 and β_3, not directly D and S. The relations are given by,

$$D \stackrel{\text{def}}{=} \frac{d\beta_1}{d\lambda} = \frac{d\omega}{d\lambda}\frac{d\beta_1}{d\omega} = -\frac{2\pi c\beta_2}{\lambda^2} = -\frac{2\pi f^2\beta_2}{c}, \tag{C.1}$$

$$S \stackrel{\text{def}}{=} \frac{dD}{d\lambda} = \frac{4\pi c\beta_2}{\lambda^3} + \frac{4\pi^2 c^2\beta_3}{\lambda^4} = \frac{4\pi f^3\beta_2}{c^2} + \frac{4\pi^2 f^4\beta_3}{c^2}. \tag{C.2}$$

Conversely,

$$\beta_2 = -\frac{cD}{2\pi f^2}, \tag{C.3}$$

$$\beta_3 = \frac{c^2 S}{4\pi^2 f^4} - \frac{\beta_2}{\pi f} = \frac{c^2 S}{4\pi^2 f^4} + \frac{cD}{2\pi^2 f^3}. \tag{C.4}$$

The speed of light $c = 2.9979 \times 10^8$ m/s. For the optical frequency $f = 193.1$ THz, $\lambda = c/f = 1552.5$ nm. The standard single-mode fiber has,

$$D = 16 \text{ ps/nm/km} = 16 \times 10^{-6} \text{ s/m}^2, \tag{C.5}$$

$$S = 0.055 \text{ ps/nm}^2\text{/km} = 0.055 \times 10^3 \text{ s/m}^3, \tag{C.6}$$

therefore,

$$\begin{aligned}\beta_2 &= -\frac{2.9979 \times 10^8 \times 16 \times 10^{-6}}{2 \times 3.14159 \times 1.931^2 \times 10^{28}} \text{ s}^2\text{/m} \\ &= -2.047 \times 10^{-26} \text{ s}^2\text{/m} \\ &= -20.47 \text{ ps}^2\text{/km},\end{aligned} \tag{C.7}$$

and,

$$\begin{aligned}\beta_3 &= \frac{2.9979^2 \times 10^{16} \times 0.055 \times 10^3}{4 \times 3.14159^2 \times 1.931^4 \times 10^{56}} + \frac{2.047 \times 10^{-26}}{3.14159 \times 1.931 \times 10^{14}} \text{ s}^3/\text{m} \\ &= 0.09006 \times 10^{-39} + 0.03374 \times 10^{-39} \text{ s}^3/\text{m} \\ &= 0.1238 \text{ ps}^3/\text{km}. \end{aligned} \tag{C.8}$$

For convenience, the parameters (D, S) and (β_2, β_3) may be converted numerically as,

$$D = -0.78163\ \beta_2, \tag{C.9}$$

$$S = 0.610704\ \beta_3 + 0.0010066\ \beta_2, \tag{C.10}$$

and conversely,

$$\beta_2 = -1.279375\ D\ , \tag{C.11}$$

$$\beta_3 = 1.637455\ S + 0.00210875\ D, \tag{C.12}$$

where D, S, β_2, β_3 are in units of ps/nm/km, ps/nm^2/km, ps^2/km, ps^3/km respectively.

With a scaling factor $R = 1$, a mirror-symmetric compensating fiber would have,

$$\beta_2' = \beta_2 = -20.47 \text{ ps}^2/\text{km}, \tag{C.13}$$

$$\beta_3' = -\beta_3 = -0.1238 \text{ ps}^3/\text{km}, \tag{C.14}$$

correspondingly,

$$D' = -\frac{2\pi f^2 \beta_2'}{c} = -\frac{2\pi f^2 \beta_2}{c} = D = 16 \text{ ps/nm/km}, \tag{C.15}$$

$$\begin{aligned} S' &= \frac{4\pi f^3 \beta_2'}{c^2} + \frac{4\pi^2 f^4 \beta_3'}{c^2} = \frac{4\pi f^3 \beta_2}{c^2} - \frac{4\pi^2 f^4 \beta_3}{c^2} \\ &= S - \frac{8\pi^2 f^4 \beta_3}{c^2} = S - \frac{8\pi^2 f^4}{c^2}\left(\frac{c^2 S}{4\pi^2 f^4} + \frac{cD}{2\pi^2 f^3}\right) \\ &= -S - \frac{4fD}{c} = -0.055 \times 10^3 - 0.04122 \times 10^3 \text{ s/m}^3 \\ &= -0.09622 \text{ ps/nm}^2/\text{km}, \end{aligned} \tag{C.16}$$

whereas a compensating fiber in translational symmetry would have,

$$\beta_2'' = -\beta_2 = 20.47 \text{ ps}^2/\text{km}, \tag{C.17}$$

$$\beta_3'' = \beta_3 = 0.1238 \text{ ps}^3/\text{km}, \tag{C.18}$$

correspondingly,

$$D'' = -\frac{2\pi f^2 \beta_2''}{c} = \frac{2\pi f^2 \beta_2}{c} = -D = -16 \text{ ps/nm/km}, \tag{C.19}$$

$$S'' = \frac{4\pi f^3 \beta_2''}{c^2} + \frac{4\pi^2 f^4 \beta_3''}{c^2} = -\frac{4\pi f^3 \beta_2}{c^2} + \frac{4\pi^2 f^4 \beta_3}{c^2} = -\left(\frac{4\pi f^3 \beta_2}{c^2} - \frac{4\pi^2 f^4 \beta_3}{c^2}\right)$$
$$= S + \frac{4fD}{c} = 0.09622 \text{ ps/nm}^2\text{/km}. \tag{C.20}$$

By contrast, for perfect direct (without OPC) dispersion compensation, the compensating fiber should have parameters $-(\beta_2, \beta_3)$, and correspondingly $-(D, S)$. When the scaling factor is not one, the parameters of the compensating fibers should multiply whatever the ratio $R > 0$, for all the three cases.

Another important parameter is the effective modal area A_{eff}, often specified alternatively by the modal field diameter (MFD). The MFD is defined as the diameter of the circle where the optical intensity decays to $1/e$ of the peak value. If the modal field is approximated as Gaussian, then there is the relation,

$$A_{\text{eff}} \stackrel{\text{def}}{=} \int_0^\infty \exp[-4r^2/(\text{MFD})^2] 2\pi r dr = \pi(\text{MFD})^2/4. \tag{C.21}$$

BIBLIOGRAPHY

[1] A. H. Gnauck and R. M. Jopson, "Dispersion compensation for optical fiber systems," in *Optical Fiber Telecommunications III A*, I. P. Kaminow and T. L. Koch, eds. Academic Press, San Diego, 1997.

[2] F. Forghieri, R. W. Tkach and A. R. Chraplyvy, "Fiber nonlinearities and their impact on transmission systems," in *Optical Fiber Telecommunications III A*, I. P. Kaminow and T. L. Koch, eds. Academic Press, San Diego, 1997.

[3] V. Srikant, "Broadband dispersion and dispersion slope compensation in high bit rate and ultra long haul systems," *OFC'01*, paper TuH1, Anaheim, CA, March 17-22, 2001.

[4] M. J. Li, "Recent progress in fiber dispersion compensators," *ECOC'01*, paper Th.M.1.1, Amsterdam, The Netherlands, September 30 - October 4, 2001.

[5] Y. R. Shen, *The Principles of Nonlinear Optics.* John Wiley & Sons, New York, 1984.

[6] G. P. Agrawal, *Nonlinear Fiber Optics*, 2nd ed. Academic Press, San Diego, 1995.

[7] A. Yariv, D. Fekete, and D. M. Pepper, "Compensation for channel dispersion by nonlinear optical phase conjugation," *Opt. Lett.*, vol. 4, pp. 52-54, 1979.

[8] D. M. Pepper and A. Yariv, "Compensation for phase distortions in nonlinear media by phase conjugation," *Opt. Lett.*, vol. 5, pp. 59-60, 1980.

[9] K. Rottwitt and A. J. Stentz, "Raman amplification in lightwave communication systems," in *Optical Fiber Telecommunications IV A: Components*, I. P. Kaminow and T. Li, eds. Academic Press, San Diego, 2002.

[10] E. Desurvire, *Erbium-Doped Fiber Amplifiers: Principles and Applications.* John Wiley & Sons, New York, 1994.

[11] H. Wei and D. V. Plant, "On the capacity of nonlinear fiber channels," arXiv:physics/0307020 at http://arxiv.org/.

[12] H. Wei and D. V. Plant, "Two means of compensating fiber nonlinearity using optical phase conjugation," arXiv:physics/0307022 at http://arxiv.org/.

[13] H. Wei and D. V. Plant, "Fundamental equations of nonlinear fiber optics," in *Optical Modeling and Performance Predictions*, M. A. Kahan, ed., *Proc. SPIE*, vol. 5178, pp. 255-266, 2003.

[14] H. Wei and D. V. Plant, "Simultaneous nonlinearity suppression and wide-band dispersion compensation using optical phase conjugation," *Opt. Exp.*, vol. 12, no. 9, pp. 1938-1958, 3 May 2004.

[15] H. Wei and D. V. Plant, "Intra-channel nonlinearity compensation with scaled translational symmetry," *Opt. Exp.*, vol. 12, no. 18, pp. 4282-4296, 6 September 2004.

[16] S. Watanabe, G. Ishikawa, T. Naito, and T. Chikama, "Generation of optical phase-conjugate waves and compensation for pulse shape distortion in a single-mode fiber," *J. Lightwave Technol.*, vol. 12, no. 12, pp. 2139-2146, 1994.

[17] S. Watanabe and M. Shirasaki, "Exact compensation for both chromatic dispersion and Kerr effect in a transmission fiber using optical phase conjugation," *J. Lightwave Technol.*, vol. 14, no. 3, pp. 243-248, 1996.

[18] S. Watanabe, S. Kaneko, G. Ishikawa, A. Sugata, H. Ooi, and T. Chikama, "20 Gb/s fiber transmission experiment over 3000 km by waveform pre-compensation using fiber compensator and optical phase conjugator," *Proc. Int. Conf. Integr. Opt. Opt. Fiber Commun. (IOOC'95)*, paper PD2-6, Hong Kong, June 26-30, 1995.

[19] A. G. Grandpierre, D. N. Christodoulides, and J. Toulouse, "Theory of stimulated Raman scattering cancellation in wavelength-division-multiplexed systems via spectral inversion," *IEEE Photon. Technol. Lett.*, vol. 11, no. 10, pp. 1271-1273, 1999.

[20] I. Brener, B. Mikkelsen, K. Rottwitt, W. Burkett, G. Raybon, J. B. Stark, K. Parameswaran, M. H. Chou, M. M. Fejer, E. E. Chaban, R. Harel, D. L. Philen, and S. Kosinski, "Cancellation of all Kerr nonlinearities in long fiber spans using a $LiNbO_3$ phase conjugator and Raman amplification," *OFC'00*, paper PD33, Baltimore, Maryland, March 7-10, 2000.

[21] H. Yu and K.-P. Ho, "Limitation of stimulated Raman scattering cancellation in WDM systems via spectral inversion," *IEEE Photon. Technol. Lett.*, vol. 12, no. 8, pp. 998-1000, 2000.

[22] M. E. Marhic, N. Kagi, T.-K. Chiang, and L. G. Kazovsky, "Cancellation of third-order nonlinear effects in amplified fiber links by dispersion compensation, phase conjugation, and alternating dispersion," *Opt. Lett.*, vol. 20, no. 8, pp. 863-865, 1995.

[23] P. Kaewplung, T. Angkaew, and K. Kikuchi, "Simultaneous suppression of third-order dispersion and sideband instability in single-channel optical fiber transmission by midway optical phase conjugation employing higher order dispersion management," *J. Lightwave Technol.*, vol. 21, no. 6, pp. 1465-1473, June 2003.

[24] A. Chowdhury and Rene-Jean Essiambre, "Optical phase conjugation and pseudolinear transmission," *Opt. Lett.*, vol. 29, no. 10, pp. 1105-1107, May 15, 2004.

[25] A. Chowdhury, G. Raybon, R.-J. Essiambre, J. Sinsky, A. Adamiecki, J. Leuthold, C. R. Doerr, and S. Chandrasekhar, "Compensation of intra-channel nonlinearities in 40 Gb/s pseudo-linear systems using optical phase conjugation," *OFC'04*, paper PDP32, Los Angeles, CA, February 22-27, 2004.

[26] A. G. Striegler and B. Schmauss, "Compensation of intrachannel effects in symmetric dispersion-managed transmission systems," *J. Lightwave Technol.*, vol. 22, no. 8, 1877-1882, August 2004.

[27] A. G. Striegler and B. Schmauss, "Fiber-based compensation of IXPM-induced timing jitter," *IEEE Photon. Technol. Lett.*, vol. 16, no. 11, pp. 2574-2576, November 2004.

[28] A. Mecozzi, C. B. Clausen, M. Shtaif, S.-G. Park, and A. H. Gnauck, "Cancellation of timing and amplitude jitter in symmetric links using highly dispersed pulses," *IEEE Photon. Technol. Lett.*, vol. 13, no. 5, pp. 445-447, 2001.

[29] T. Hirooka and M. J. Ablowitz, "Suppression of intrachannel dispersion-managed pulse interactions by distributed amplification," *IEEE Photon. Technol. Lett.*, vol. 14, no. 3, pp. 316-318, 2002.

[30] R. Hainberger, T. Hoshita, T. Terahara, and H. Onaka, "Comparison of span configurations of Raman-amplified dispersion-managed fibers," *IEEE Photon. Technol. Lett.*. vol. 14, no. 4, pp. 471-473, 2002.

[31] H. Wei and D. V. Plant, "Reversing intrachannel ghost-pulse generation by midspan self-phase modulation," *Opt. Lett.*, vol. 30, no. 18, pp. 2366-2368, 2005. Also appeared in *Virtual Journal of Ultrafast Science*, vol. 4, no. 10, Oct. 2005.

[32] H. Wei and D. V. Plant, "Optimal packaging of dispersion-compensating fibers for matched nonlinear compensation and reduced optical noise," *Opt. Lett.*, vol. 30, no. 18, pp. 2369-2371, 2005.

[33] X. Qi, X. Zhang, H. Wei, and D. V. Plant, "Linearity of nonlinear perturbations in fiber transmission lines and its applications to nonlinear compensations," submitted for journal publication.

[34] H. Wei and D. V. Plant, "Compensability of fiber nonlinearities under stochastic polarization variations," in preparation.

[35] C. M. Caves, "Quantum limits on noise in linear amplifiers," *Phys. Rev. D*, vol. 26, no. 8, pp. 1817-1839, 1982.

[36] J. R. Jeffers, N. Imoto, and R. Loudon, "Quantum optics of traveling-wave attenuators and amplifiers," *Phys. Rev. A*, vol. 47, no. 4, pp. 3346-3359, 1993.

[37] L. Mandel and E. Wolf, *Optical Coherence and Quantum Optics.* Cambridge University Press, 1995.

[38] R. Loudon, *The Quantum Theory of Light*, 3rd ed. Oxford University Press, 2000.

[39] H. A. Haus, *Electromagnetic Noise and Quantum Optical Measurements.* Springer-Verlag, Berlin, 2000.

[40] H. Wei and D. V. Plant, "Quantum noise in optical communication systems," in *Optical Modeling and Performance Predictions*, M. A. Kahan, ed., *Proc. SPIE*, vol. 5178, pp. 139-147, 2003.

[41] G. P. Agrawal, *Fiber-Optic Communication Systems*, 2nd. Ed. John Wiley & Sons, 1997.

[42] G. Bartolini, R.-D. Li, P. Kumar, W. Riha, and K. V. Reddy, "1.5 μm phase-sensitive amplifier for ultrahigh-speed communications," *OFC'94*, paper ThF4, 1994.

[43] J. A. Levenson, I. Abram, Th. Rivera, and Ph. Grangier, "Reduction of quantum noise in optical parametric amplification," *J. Opt. Soc. Am. B*, vol. 10, no. 11, pp. 2233-2238, 1993.

[44] A. Takada and W. Imajuku, "Amplitude noise suppression using a high gain phase sensitive amplifier as a limiting amplifier," *Electron. Lett.*, vol. 32, no. 7, pp. 677-679, 1996.

[45] S.-K. Choi, M. Vasilyev, and P. Kumar, "Noiseless optical amplification of images," *Phys. Rev. Lett.*, vol. 83, no. 10, pp. 1938-1941, 1999.

[46] J. L. Blows and S. E. French, "Low-noise-figure optical parametric amplifier with a continuous-wave frequency-modulated pump," *Opt. Lett.*, vol. 27, no. 7, pp. 491-493, 2002.

[47] K. K. Y. Wong, K. Shimizu, M. E. Marhic, K. Uesaka, G. Kalogerakis, and L. G. Kazovsky, "Continuous-wave fiber optical parametric wavelength converter with +40-dB conversion efficiency and a 3.8-dB noise figure," *Opt. Lett.*, vol. 28, no. 9, pp. 692-694, 2003.

[48] W. Imajuku and A. Takada, "Reduction of fiber-nonlinearity-enhanced amplifier noise by means of phase-sensitive amplifiers," *Opt. Lett.*, vol. 22, no. 1, pp. 31-33, 1997.

[49] J. Santhanam and G. P. Agrawal, "Reduced timing jitter in dispersion-managed light-wave systems through parametric amplification," *J. Opt. Soc. Am. B*, vol. 20, no. 2, pp. 284-291, 2003.

[50] N. S. Bergano, "Undersea amplified lightwave systems design," in *Optical Fiber Telecommunications III A*, I. P. Kaminow and T. L. Koch, eds. Academic Press, San Diego, 1997.

[51] L. F. Mollenauer, J. P. Gordon, and P. V. Mamyshev, "Solitons in high bit-rate, long-distance transmission," in *Optical Fiber Telecommunications III A*, I. P. Kaminow and T. L. Koch, eds. Academic Press, San Diego, 1997.

[52] D. Marcuse, "Derivation of analytical expressions for the bit-error probability in lightwave systems with optical amplifiers," *J. Lightwave Technol.*, vol. 8, no. 12, pp. 1816-1823, 1990.

[53] P. A. Humblet and M. Azizoglu, "On the bit error rate of lightwave systems with optical amplifiers," *J. Lightwave Technol.*, vol. 9, no. 11, pp. 1576-1582, 1991.

[54] N. S. Bergano, "Ultra long distance submarine DWDM systems," *ECOC'00*, paper 2.2.1, Munich, Germany, September 3-7, 2000.

[55] J. Hecht, "Raman amplifiers boost system margins at high speed," *Laser Focus World*, June 2001.

[56] The International Engineering Consortium, "Raman amplification design in WDM systems," http://www.iec.org/online/tutorials/raman/index.html.

[57] T. Okuno, T. Tsuzaki, and M. Nishimura, "Novel lossless optical transmission line with distributed Raman amplification," *ECOC'00*, paper 4.4.3, Munich, Germany, September 3-7, 2000.

[58] P. B. Hansen, L. Eskildsen, A. J. Stentz, T. A. Strasser, J. Judkins, J. J. DeMarco, R. Pedrazzani, and D. J. DiGiovanni, "Rayleigh scattering limitations in distributed Raman pre-amplifiers," *IEEE Photon. Technol. Lett.*, vol. 10, no. 1, pp. 159-161, 1998.

[59] M. Nissov, K. Rottwitt, H. D. Kidorf, and M. X. Ma, "Rayleigh crosstalk in long cascades of distributed unsaturated Raman amplifiers," *Electron. Lett.*, vol. 35, no. 12, pp. 997-998, 1999.

[60] P. P. Mitra and J. B. Stark, "Nonlinear limits to the information capacity of optical fiber communications," *Nature*, vol. 411, pp. 1027-1030, June 2001.

[61] M. Eiselt, M. Shtaif, R. W. Tkach, F. A. Flood, S. Ten, and D. Butler, "Cross-phase modulation in an L-band EDFA," *IEEE Photon. Technol. Lett.*, vol. 11, no. 12, pp. 1575-1577, 1999.

[62] G. J. Pendock, S. Y. Park, A. K. Srivastava, S. Radic, J. W. Sulhoff, C. L. Wolf, K. Kantor, and Y. Sun, "The contribution to cross-phase modulation in L-band WDM systems from erbium-doped fiber amplifiers," *IEEE Photon. Technol. Lett.*, vol. 11, no. 12, pp. 1578-1580, 1999.

[63] V. E. Perlin and H. G. Winful, "On trade-off between noise and nonlinearity in WDM systems with distributed Raman amplification," *OFC'02*, paper WB1, Anaheim, CA, March 17-22, 2002.

[64] B. E. A. Saleh and M. C. Teich, *Fundamentals of Photonics.* John Wiley & Sons, New York, 1991.

[65] R.-J. Essiambre, G. Raybon, and B. Mikkelson, "Pseudo-linear transmission of high-speed TDM signals: 40 and 160 Gb/s," in *Optical Fiber Telecommunications IV B: Systems and Impairments*, I. P. Kaminow and T. Li, eds. Academic Press, San Diego, 2002.

[66] J. Tang, "The Shannon channel capacity of dispersion-free nonlinear optical fiber transmission," *J. Lightwave Technol.*, Vol. 19, No. 8, pp. 1104-1109, 2001.

[67] J. Tang, "The multispan effects of Kerr nonlinearity and amplifier noises on Shannon channel capacity of a dispersion-free nonlinear optical fiber," *J. Lightwave Technol.*, Vol. 19, No. 8, pp. 1110-1115, 2001.

[68] K. S. Turitsyn, S. A. Derevyanko, I. V. Yurkevich, and S. K. Turitsyn, "Information capacity of optical fiber channels with zero average dispersion," *Phys. Rev. Lett.*, vo. 91, no. 20, 203901, 2003.

[69] A. W. Snyder and J. D. Love, *Optical Waveguide Theory.* Chapman and Hall, Now York, 1983.

[70] J. A. Buck, *Fundamentals of Optical Fibers.* John Wiley & Sons, New York, 1995.

[71] M. Born and E. Wolf, *Principles of Optics: Electromagnetic Theory of Propagation, Interference and Diffraction of Light*, 7th ed. Cambridge University Press, 1999.

[72] C. E. Shannon, "A mathematical theory of communication," *Bell Syst. Tech. J.*, vol. 27, pp. 379-423, pp. 623-656, 1948.

[73] K.-J. Engel and R. Nagel, *One-Parameter Semigroups for Linear Evolution Equations.* Springer-Verlag, New York, 2000.

[74] E. E. Narimanov and P. Mitra, "The channel capacity of a fiber optics communication system: perturbation theory," *J. Lightwave Technol.*, vol. 20, pp. 530-537, 2002.

[75] V. Volterra, *Theory of Functionals and of Integral and Integro-Differential Equations.* Dover Publications, Inc., New York, 1959.

[76] M. Schetzen, *The Volterra and Wiener Theories of Nonlinear Systems.* Krieger Publishing Company, Malabar, Florida, 1989.

[77] A. Yariv, *Optical Electronics in Modern Communications*, 5th ed., Chapter 3. Oxford University Press, 1997.

[78] At any position z, the Kerr coefficient $\gamma(z)$ has a well-defined sign, which is by convention positive for most physical materials. However, the Raman coefficient $g(z,t)$ is usually an oscillating function in the time delay t, as shown in reference [79]. Nevertheless, one may still call a Raman impulse response $g(z,t)$ "positive" or "negative" depending upon whether its first peak with the least time delay is positive- or negative-valued.

[79] R. H. Stolen, J. P. Gordon, W. J. Tomlinson, and H. A. Haus, "Raman response function of silica-core fibers," *J. Opt. Soc. Am. B*, vol. 6, no. 6, pp. 1159-1166 (1989).

[80] K. Nouchi, E. Matsuyama, Y. Morishita, and G. Tanimoto, "Ultra-wideband response in Co^{2+}-doped fiber attenuators," *ECOC'01*, paper P.2, Amsterdam, The Netherlands, September 30 - October 4, 2001.

[81] D. J. DiGiovanni, S. K. Das, L. L. Blyler, W. White, R. K. Boncek, and S. E. Golowich, "Design of optical fibers for communications systems," in *Optical Fiber Telecommunications IV A: Components*, I. P. Kaminow and T. Li, eds. Academic Press, San Diego, 2002.

[82] M. Vasilyev, B. Szalabofka, S. Tsuda, J. M. Grochocinski, and A. F. Evans, "Reduction of Raman MPI and noise figure in dispersion-managed fiber," *Electron. Lett.*, vol. 38, no. 6, pp. 271-272, 2002.

[83] J.-C. Bouteiller, K. Brar, and C. Headley, "Quasi-constant signal power transmission," *ECOC'02*, paper S3.04, Copenhagen, Denmark, September 8-12, 2002.

[84] M. Vasilyev, "Raman-assisted transmission: toward ideal distributed amplification," *OFC'03*, paper WB1, Atlanta, Georgia, March 23-28, 2003.

[85] C. Rasmussen, T. Fjelde, J. Bennike, F. Liu, S. Dey, B. Mikkelsen, P. Mamyshev, P. Serbe, P. van der Wagt, Y. Akasaka, D. Harris, D. Gapontsev, V. Ivshin, P. Reeves-Hall, "DWDM 40G transmission over trans-Pacific distance (10,000 km) using CSRZ-DPSK, enhanced FEC and all-Raman amplified 100 km UltraWave™ fiber spans," *OFC'03*, paper PD18, Atlanta, Georgia, March 23-28, 2003.

[86] S. A. E. Lewis, S. V. Chernikov, and J. R. Taylor, "Broadband high gain dispersion compensating raman amplifier," *OFC'00*, paper TuA2, Baltimore, Maryland, March 7-10, 2000.

[87] L. Gruner-Nielsen, Y. Qian, B. Palsdottir, P. B. Gaarde, S. Dyrbol, T. Veng, Y. Qian, R. Boncek, and R. Lingle, "Module for simultaneous C + L-band dispersion compensation and Raman amplification," *OFC'02*, paper TuJ6, Anaheim, CA, March 17-22, 2002.

[88] T. Miyamoto, T. Tsuzaki, T. Okuno, M. Kakui, M. Hirano, M. Onishi, and M. Shigematsu, "Raman amplification over 100nm bandwidth with dispersion and dispersion slope compensation for conventional single mode fiber," *OFC'02*, paper TuJ7, Anaheim, CA, March 17-22, 2002.

[89] J. Maury, J. L. Auguste, S. Fevrier, J. M. Blondy, B. Dussardier, and G. Monnom, "Conception and characterization of a dual-concentric-core erbium-doped dispersion-compensating fiber," *Opt. Lett.*, vol. 29, no. 7, pp. 700-702, April, 2004.

[90] P. V. Mamyshev and N. A. Mamysheva, "Pulse-overlapped dispersion-managed data transmission and intrachannel four-wave mixing," *Opt. Lett.*, vol. 24, no. 21, pp. 1454-1456, 1999.

[91] A. Mecozzi, C. B. Clausen, and M. Shtaif, "Analysis of intrachannel nonlinear effects in highly dispersed optical pulse transmission," *IEEE Photon. Technol. Lett.*, vol. 12, no. 4, pp. 392-394, 2000.

[92] J. Martensson, A. Berntson, M. Westlund, A. Danielsson, P. Johannisson, D. Anderson, and M. Lisak, "Timing jitter owing to intrachannel pulse interactions in dispersion-managed transmission systems," *Opt. Lett.*, vol. 26, no. 2, pp. 55-57, 2001.

[93] P. Johannisson, D. Anderson, A. Berntson, and J. Martensson, "Generation and dynamics of ghost pulses in strongly dispersion-managed fiber-optic communication systems," *Opt. Lett.*, vol. 26, no. 16, pp. 1227-1229, 2001.

[94] M. J. Ablowitz and T. Hirooka, "Resonant nonlinear intrachannel interactions in strongly dispersion-managed transmission systems," *Opt. Lett.*, vol. 25, no. 24, pp. 1750-1752, 2000.

[95] M. J. Ablowitz and T. Hirooka, "Intrachannel pulse interactions in dispersion-managed transmission systems: timing shifts," *Opt. Lett.*, vol. 26, no. 23, pp. 1846-1848, 2001.

[96] M. J. Ablowitz and T. Hirooka, "Intrachannel pulse interactions in dispersion-managed transmission systems: energy transfer," *Opt. Lett.*, vol. 27, no. 3, pp. 203-205, 2002.

[97] A. Erdelyi, *Asymptotic Expansions.* Dover Publications, Inc., New York, 1956.

[98] L. Moller, "Filter synthesis for broad-band PMD compensation in WDM systems," *IEEE Photon. Technol. Lett.*, vol. 12, no. 9, pp. 1258-1260, September 2000.

[99] D. Penninckx and S. Lanne, "Reducing PMD impairments," *OFC'01*, paper TuP1, Anaheim, CA, March 17-22, 2001.

[100] M. Karlsson, "Polarization mode dispersion mitigation performance of various approaches," *OFC'02*, paper WI1, Anaheim, CA, March 17-22, 2002.

[101] S. Kim, "Schemes for complete compensation for polarization mode dispersion up to second order," *Opt. Lett.*, vol. 27, no. 8, pp. 577-579, 2002.

[102] H. Kogelnik, R. M. Jopson, and L. E. Nelson, "Polarization-mode dispersion," in *Optical Fiber Telecommunications IV B: Systems and Impairments*, I. P. Kaminow and T. Li, eds. Academic Press, San Diego, 2002.

[103] E. Iannone, F. Matera, A. Mecozzi, and M. Settembre, *Nonlinear Optical Communication Networks.* John Wiley & Sons, 1998.

[104] J. P. Gordon and H. Kogelnik, "PMD fundamentals: Polarization mode dispersion in optical fibers," *Proc. National Academy of Sciences*, vol. 97, no. 9, pp. 4541-4550, April 25, 2000.

[105] K. Inoue, "Polarization effect on four-wave mixing efficiency in a single-mode fiber," *IEEE J. Quantum Electron.*, vol. 28, no. 4, pp. 883-894, April 1992.

[106] M. Tsang and D. Psaltis, "Dispersion and nonlinearity compensation by spectral phase conjugation," *Opt. Lett.*, vol. 28, no. 17, pp. 1558-1560, September 1, 2003.

[107] C. Pare, A. Villeneuve, P.-A. Belanger, and N. J. Doran, "Compensating for dispersion and the nonlinear Kerr effect without phase conjugation," *Opt. Lett.*, vol. 21, no. 7, pp. 459-461, April 1, 1996.

[108] I. R. Gabitov and P. M. Lushnikov, "Nonlinearity management in a dispersion-managed system," *Opt. Lett.*, vol. 27, no. 2, pp. 113-115, January 15, 2002.

[109] P. Minzioni, F. Alberti, and A. Schiffini, "Optimized link design for nonlinearity cancellation by optical phase conjugation," *IEEE Photon. Technol. Lett.*, vol. 16, no. 3, pp. 813-815, March 2004.

[110] P. J. Winzer, F. Fidler, M. J.Matthews, L. E. Nelson, S. Chandrasekhar, L. L. Buhl, M. Winter, and D. Castagnozzi, "Electronic equalization and FEC enable bidirectional CWDM capacities of 9.6 Tb/s-km," *OFC'04*, paper PDP7, Los Angeles, CA, Feb. 22-27, 2004.

[111] D.-S. Ly-Gagnon, K. Katoh, and K. Kikuchi, "Unrepeatered optical transmission of 20 Gbit/s quadrature phase-shift keying signals over 210km using homodyne phase-diversity receiver and digital signal processing," *Electron. Lett.*, vol. 41, no. 4, pp. 206-207, Feb. 17, 2005.

[112] D. McGhan, C. Laperle, A. Savchenko, C. Li, G. Mak, and M. O'Sullivan, "5120 km RZ-DPSK transmission over G652 fiber at 10 Gb/s with no optical dispersion compensation," *OFC'05*, paper PDP27, Anaheim, CA, March 6-11, 2005.

[113] S. Chandrasekhar, C. R. Doerr, L. L. Buhl, D. Mahgerefteh, Y. Matsui, B. Johnson, C. Liao, X. Zheng, K. McCallion, Z. Fan, and P. Tayebati, "Flexible transport at 10-Gb/s from 0 to 675km (11,500ps/nm) using a chirp-managed laser, no DCF, and a dynamically adjustable dispersion-compensating receiver," *OFC'05*, paper PDP30, Anaheim, CA, March 6-11, 2005.

[114] R. I. Killey, P. M. Watts, V. Mikhailov, M. Glick, and P. Bayvel, "Electronic dispersion compensation by signal predistortion using digital processing and a

dual-drive MachZehnder modulator," *IEEE Photon. Technol. Lett.*, vol. 17, no. 3, pp. 714-716, March 2005.

[115] R. Noe, "PLL-free synchronous QPSK polarization multiplex/diversity receiver concept with digital I&Q baseband processing," *IEEE Photon. Technol. Lett.*, vol. 17, no. 4, pp. 887-889, April 2005.

[116] K. V. Peddanarappagari and M. Brandt-Pearce, "Volterra series transfer function of single-mode fibers," *J. Lightwave Technol.*, vol. 15, no. 12, pp. 2232-2241, December 1997.

[117] K. V. Peddanarappagari and M. Brandt-Pearce, "Volterra series approach for optimizing fiber-optic communications system designs," *J. Lightwave Technol.*, vol. 16, no. 11, pp. 2046-2055, November 1998.

[118] B. Xu and M. Brandt-Pearce, "Modified volterra series transfer function method," *IEEE Photon. Technol. Lett.*, vol. 14, no. 1, pp. 47-49, January 2002.

[119] A. Vannucci, P. Serena, and A. Bononi, "The RP method: a new tool for the iterative solution of the nonlinear Schrödinger equation," *J. Lightwave Technol.*, pp. 1102-1112, vol. 20, no. 7, July 2002.

[120] E. Dietrich, B. Enning, R. Gross, and H. Knupke, "Heterodyne transmission of a 560Mbit/s optical signal by means of polarisation shift keying," *Electron. Lett.*, vol. 23, pp. 421-422, 1987.

[121] R. Calvani, R. Caponi, and F. Cisternino, "Polarisation phase-shift keying: a coherent transmission technique with differential heterodyne detection," *Electron. Lett.*, vol. 24, no. 10, pp. 642-643, 1988.

[122] S. G. Evangelides Jr., L. F. Mollenauer, J. P. Gordon, and N. S. Bergano, "Polarization multiplexing with solitons," *J. Lightwave Technol.*, vol. 10, no. 1, pp. 28-35, January 1992.

[123] S. Benedetto and P. Poggiolini, "Theory of polarization shift keying modulation," *IEEE Trans. Commun.*, vol. 40, no. 4, pp. 708-721, April 1992.

[124] L. F. Mollenauer, J. P. Gordon, and F. Heismann, "Polarization scattering by soliton-soliton collisions," *Opt. Lett.*, vol. 20, no. 20, pp. 2060-2062, 15 October 1995.

[125] S. Benedetto, R. Gaudino, and P. Poggiolini, "Polarization recovery in optical polarization shift-keying systems," *IEEE Trans. Commun.*, vol. 45, no. 10, pp. 1269-1279, October 1997.

[126] M. I. Hayee, M. C. Cardakli, A. B. Sahin, and A. E. Willner, "Doubling of bandwidth utilization using two orthogonal polarizations and power unbalancing in a polarization-division-multiplexing scheme," *IEEE Photon. Technol. Lett.*, vol. 13, no. 8, pp. 881-883, August 2001.

[127] C. D. Poole and R. E. Wagner, "Phenomenological approach to polarisation dispersion in long single-mode fibres," *Electron. Lett.*, vol. 22, pp. 1029-1030, 1986.

[128] H. S. Chung, S. K. Shin, D. W. Lee, D. W. Kim, and Y. C. Chung, "640Gbit/s (32×20Gbit/s) WDM transmission with 0.4(bit/s)/Hz spectral efficiency using short-period dispersion-managed fiber," *Electron. Lett.*, vol. 37, no. 10, pp. 618-620, 2001.

[129] S. N. Knudsen and T. Veng, "Large effective area dispersion compensating fiber for cabled compensation of standard single mode fiber," *OFC'00*, paper TuG5, Baltimore, Maryland, March 7-10, 2000.

[130] Q. L. N.T., T. Veng, and L. Gruner-Nielsen, "New dispersion compensating module for compensation of dispersion and dispersion slope of non-zero dispersion fibres in the C-band," *OFC'01*, paper TuH5, Anaheim, CA, March 17-22, 2001.

[131] K. Mukasa, H. Moridaira, T. Yagi, and K. Kokura, "New type of dispersion management transmission line with MDFSD for long-haul 40 Gb/s transmission," *OFC'02*, paper ThGG2, Anaheim, CA, March 17-22, 2002.

[132] For example, a nearly perfect translation symmetry could be well formed between Corning's LEAF, a +NZDSF with $D \approx 4$ ps/nm/km, $S \approx 0.1$ ps/nm^2/km, and its Vascade LEAF, a -NZDSF with $D \approx -4$ ps/nm/km, $S \approx 0.1$ ps/nm^2/km in the C band. The fiber parameters are available at http://www.corning.com/opticalfiber.

[133] F. Forghieri, R. W. Tkach, A. R. Chraplyvy, and D. Marcuse, "Reduction of four-wave mixing crosstalk in WDM systems using unequally spaced channels," *IEEE Photon. Technol. Lett.*, vol. 6, no. 6, pp. 754-756, 1994.

[134] F. Forghieri, R. W. Tkach, and A. R. Chraplyvy, "WDM systems with unequally spaced channels," *J. Lightwave Technol.*, vol. 13, no. 5, pp. 889-897, 1995.

[135] A. Striegler, A. Wietfeld, and B. Schmauss, "Fiber based compensation of IXPM induced timing jitter," *OFC'04*, paper MF72, Los Angeles, CA, February 24-26, 2004.

[136] A. G. Striegler and B. Schmauss, "Compensation of intrachannel effects in symmetric dispersion-managed transmission systems," *J. Lightwave Technol.*, vol. 22, no. 8, 1877-1882, August 2004.

[137] R.-J. Essiambre, B. Mikkelsen, and G. Raybon, "Intra-channel cross-phase modulation and four-wave mixing in high-speed TDM systems," *Electron. Lett.*, vol. 35, no. 18, pp. 1576-1578, 1999.

[138] F. Merlaud and S. K. Turitsyn, "Intra-channel four wave mixing and ghost pulses generation: time domain approach," *ECOC'00*, paper 7.2.4, Munich, Germany, September 3-7, 2000.

[139] P. Vidakovic, D. J. Lovering, J. A. Levenson, J. Webjrn, and P. St.J. Russell, "Large nonlinear phase shift owing to cascaded $\chi^{(2)}$ in quasi-phase-matched bulk $LiNbO_3$," *Opt. Lett.*, vol. 22, no. 5, pp. 277-279, March 1997.

[140] X. Liu, X. Wei, R. E. Slusher, and C. J. McKinstrie, "Improving transmission performance in differential phase-shift-keyed systems by use of lumped nonlinear phase-shift compensation," *Opt. Lett.*, vol. 27, no. 18, pp. 1616-1618, September 2002.

[141] G. P. Agrawal and N. A. Olsson, "Self-phase modulation and spectral broadening of optical pulses in semiconductor laser amplifiers," *IEEE J. Quantum Electron.*, vol. 25, no. 11, pp. 2297-2306, November 1989.

[142] C. Xu and X. Liu, "Postnonlinearity compensation with data-driven phase modulators in phase-shift keying transmission," *Opt. Lett.*, vol. 27, no. 18, pp. 1619-1621, September 2002.

[143] J. Hansryd, J. van Howe, and C. Xu, "Experimental demonstration of nonlinear phase jitter compensation in DPSK modulated fiber links," *IEEE Photon. Technol. Lett.*, vol. 17, no. 1, pp. 232-234, January 2005.

[144] N. J. Doran and D. Wood, "Nonlinear optical loop mirror," *Opt. Lett.*, vol. 13, no. 1, pp. 56-58, 1988.

[145] Z. Huang, A. Gray, I. Khrushchev, and I. Bennion, "10-Gb/s transmission over 100 Mm of standard fiber using 2R regeneration in an optical loop mirror," *IEEE Photon. Technol. Lett.*, vol. 16, no. 11, pp. 2526-2528, November 2004.

[146] D. B. Mortimore, "Fiber loop reflectors," *J. Lightwave Technol.*, vol. 6, no. 7, pp. 1217-1224, 1988.

[147] K. Krastev and J. Rothman, "Crosstalk in fiber parametric amplifier," *ECOC'01*, paper We.L.3.5, Amsterdam, The Netherlands, September 30 - October 4, 2001.

[148] H. Wei, X. Xue, and D. V. Plant, "Inter-channel cross-talk in FWM-based phase conjugators," in *Nonlinear Frequency Generation and Conversion: Materials, Devices, and Applications II*, K. L. Schepler, D. D. Lowenthal, and J. W. Pierce, eds., *Proc. SPIE*, vol. 4972, pp. 158-163, 2003.

[149] T. Kato, M. Hirano, K. Fukuda, A. Tada, M. Onishi, and M. Nishimura, "Design optimization of dispersion compensating fiber for NZ-DSF considering nonlinearity and packaging performance," *OFC'01*, paper TuS6, Anaheim, CA, March 17-22, 2001.

[150] W. Heitler, *The Quantum Theory of Radiation*, 3rd ed. Clarendon Press, Oxford, 1954.

[151] P. A. M. Dirac, "The quantum theory of the emission and absorption of radiation," *Proc. Roy. Soc. Lond. A*, vol. 114, pp. 243-265, 1927.

[152] M. O. Scully and M. S. Zubairy, *Quantum Optics.* Cambridge University Press, Cambridge, 1997.

[153] J. F. C. Kingman, *Poisson Processes.* Clarendon Press, Oxford, 1993.

[154] A. D. Aczel, *Entanglement: The Greatest Mystery in Physics.* Four Walls Eight Windows, New York, 2001.

[155] K. Blum, *Density Matrix Theory and Applications*, 2nd ed. Plenum Press, New York, 1996.

[156] W. H. Zurek, "Decoherence and the transition from quantum to classical," *Physics Today*, vol. 44, pp. 36-44, 1991.

[157] R. Omnes, *The Interpretation of Quantum Mechanics.* Princeton University Press, Princeton, NJ, 1994.

[158] D. Freedman, *Markov Chains.* Springer-Verlag, New York, 1983.

[159] S. Karlin and H. M. Taylor, *A First Course in Stochastic Processes*, 2d ed. Academic Press, San Diego, 1975.

[160] S. Karlin and H. M. Taylor, *A Second Course in Stochastic Processes.* Academic Press, New York, 1981.

[161] K. Shimoda, H. Takahasi, C. H. Townes, "Fluctuations in amplification of quanta with application to maser amplifiers," *J. Phys. Soc. Japan*, vol. 12, no. 6, pp. 686-700, 1957.

[162] P. Diament and M. C. Teich, "Evolution of the statistical properties of photons passed through a traveling-wave laser amplifier," *IEEE J. Quantum Electron.*, vol. 28, no. 5, pp. 1325-1334, 1992.

[163] E. W. Weisstein, "Binomial Distribution." From MathWorld – A Wolfram Web Resource, http://mathworld.wolfram.com/BinomialDistribution.html.

[164] M. Hirano, A. Tada, T. Kato, M. Onishi, Y. Makio, M. Nishimura, "Dispersion compensating fiber over 140nm bandwidth," *ECOC'01*, paper Th.M.1.4, Amsterdam, The Netherlands, September 30 - October 4, 2001.

[165] M. Wandel, P. Kristensen, T. Veng, Y. Qian, Q. Le, L. Gruner-Nielsen, "Dispersion compensating fibers for non-zero dispersion fibers," *OFC'02*, paper WU1, Anaheim, CA, March 17-22, 2002.

[166] A. H. Gnauck, R. M. Jopson, and R. M. Derosier, "Compensating the compensator: a demonstration of nonlinearity cancelation in a WDM system," *IEEE Photon. Technol. Lett.*, vol. 7, no. 5, pp. 582-584, May 1995.

[167] J. M. Chavez Boggio, P. Dainese, F. Karlsson, and H. L. Fragnito, "Broadband 88% efficient two-pump fiber optical parametric amplifier," *IEEE Photon. Technol. Lett.*, vol. 15, no. 11, pp. 1528-1530, November 2003.

[168] T. Torounidis, B.-E. Olsson, H. Sunnerud, M. Karlsson, and P. A. Andrekson, "Fiber-optic parametric amplifier in a loop mirror configuration," *IEEE Photon. Technol. Lett.*, vol. 17, no. 2, pp. 321-323, February 2005.

[169] K. K. Chow, C. Shu, C. Lin, and A. Bjarklev, "Polarization-insensitive widely tunable wavelength converter based on four-wave mixing in a dispersion-flattened nonlinear photonic crystal fiber," *IEEE Photon. Technol. Lett.*, vol. 17, no. 3, pp. 624-626, March 2005.

[170] J. H. Lee, T. Nagashima, T. Hasegawa, S. Ohara, N. Sugimoto, T. Tanemura, and K. Kikuchi, "Wavelength conversion of 40-Gbit/s NRZ signal using four-wave mixing in 40-cm-long bismuth oxide based highly-nonlinear optical fiber," *OFC'05*, paper PDP23, Anaheim, CA, March 6-11, 2005.

[171] M. H. Chou, I. Brener, M. M. Fejer, E. E. Chaban, and S. B. Christman, "1.5-μm-band wavelength conversion based on cascaded second-order nonlinearity in $LiNbO_3$ waveguides," *IEEE Photon. Technol. Lett.*, vol. 11, no. 6, pp. 653-655, 1999.

[172] I. Brener, M. H. Chou, E. Chaban, K. R. Parameswaran, M. M. Fejer, and S. Kosinski, "Polarization-insensitive parametric wavelength converter based on cascaded nonlinearities in $LiNbO_3$ waveguides," *OFC'00*, paper TuF1, Baltimore, Maryland, March 7-10, 2000.

[173] M.-S. Chou, K. Parameswaran, M. M. Fejer, and I. Brener, "Optical frequency mixers for WDM and TDM applications," *OFC'00*, paper FB1, Baltimore, Maryland, March 7-10, 2000.

[174] O. Tadanaga, M. Asobe, H. Miyazawa, Y. Nishida, and H. Suzuki,, "A 1-THz optical frequency shifter using quasi-phase-matched $LiNbO_3$ wavelength converters," *OFC'02*, paper ThDD1, Anaheim, CA, March 17-22, 2002.

[175] B. Chen, C.-Q. Xu, B. Zhou, Y. Nihei, and A. Harada, "All optical variable-in variable-out wavelength converters based on MgO doped $LiNbO_3$ quasi-phase matched waveguides," *OFC'02*, paper ThDD2, Anaheim, CA, March 17-22, 2002.

[176] F. Carbone, L. Socci, M. Romagnoli, I. Cristiani, and V. Degiorgio, "Polarization-insensitive wavelength conversion in a lithium niobate waveguide by the cascading technique," *OFC'02*, paper ThGG83, Anaheim, CA, March 17-22, 2002.

[177] Y. L. Lee, B.-A. Yu, C. Jung, Y.-C. Noh, J. Lee, and D.-K. Ko, "All-optical wavelength conversion and tuning by the cascaded sum- and difference fre-

quency generation (cSFG/DFG) in a temperature gradient controlled Ti:PPLN channel waveguide," *Opt. Exp.*, vol. 13, no. 8, pp. 2988-2993, 18 April 2005.

[178] Y. Hong, P. S. Spencer, and K. A. Shore, "Wide-band polarization-free wavelength conversion based on four-wave-mixing in semiconductor optical amplifiers," *IEEE J. Quantum Electron.*, vol. 40, no. 2, pp. 152-156, February 2004.

[179] M. A. Foster, A. C. Turner, J. E. Sharping, B. S. Schmidt, M. Lipson, and A. L. Gaeta, "Broad-band optical parametric gain on a silicon photonic chip," *Nature*, vol. 441, pp. 960-963, 22 June 2006.

[180] D. Kunimatsu, C. Q. Xu, M. D. Pelusi, X. Wang, K. Kikuchi, and A. Suzuki, "Femtosecond optical pulse transmission over 144 km using midspan spectral inversion with a $LiNbO_3$ waveguide," *ECOC'00*, paper 8.3.1, Munich, Germany, September 3-7, 2000.

[181] S. Radic, R. M. Jopson, C. J. McKinstrie, A. H. Gnauck, S. Chandrasekhar, and J. C. Centanni, "Wavelength division multiplexed transmission over standard single mode fiber using polarization insensitive signal conjugation in highly nonlinear optical fiber," *OFC'03*, paper PD12, Atlanta, Georgia, March 23-28, 2003.

[182] S. L. Jansen, S. Spalter, G.-D. Khoe, H. de Waardt, H. E. Escobar, L. Marshall, and M. Sher, "16×40 Gb/s over 800 km of SSMF using mid-link spectral inversion," *IEEE Photon. Technol. Lett.*, vol. 16, no. 7, pp. 1763-1765, July 2004.

[183] A. Chowdhury, G. Raybon, R.-J. Essiambre, J. H. Sinsky, A. Adamiecki, J. Leuthold, C. R. Doerr, and S. Chandrasekhar, "Compensation of intrachannel nonlinearities in 40-Gb/s pseudolinear systems using optical-phase conjugation," *J. Lightwave Technol.*, vol. 23, no. 1, pp. 172-177, January 2005.

[184] A. Chowdhury, G. Raybon, R.-J. Essiambre, and C. R. Doerr, "WDM CSRZ 40 Gbit/s pseudo-linear transmission over 4800km using optical phase conjugation," *Electron. Lett.*, vol. 41, no. 3, pp. 151-152, February 2005.

[185] S. L. Jansen, D. van den Borne, C. Climent, M. Serbay, C.-J. Weiske, H. Suche, P. M. Krummrich, S. Spalter, S. Calabro, N. Hecker-Denschlag, P. Leisching, W. Rosenkranz, W. Sohler, G. D. Khoe, T. Koonen, and H. de Waardt, "10,200km

22×2×10Gbit/s RZ-DQPSK dense WDM transmission without inline dispersion compensation through optical phase conjugation," *OFC'05*, paper PDP28, Anaheim, CA, March 6-11, 2005.

[186] W. C. Holton, "Post-deadline papers show commercial edge," *Laser Focus World*, June 2003. (The "all-optical 2R regenerator" of Lightbit, Inc. is actually a $LiNbO_3$-based optical phase conjugator.)